AN INVESTIGATION INTO THE APPLICABILITY OF NMR FOR CURE MONITORING OF COMPOSITES

by

ANGELA LOIS NEWBURY

A thesis submitted to the University of Plymouth
in partial fulfilment for the degree of

DOCTOR OF PHILOSOPHY

School of Manufacturing, Materials and Mechanical Engineering
Faculty of Technology

In collaboration with Oxford Instruments,
Industrial Analysis Group

February 1994

AN INVESTIGATION INTO THE APPLICABILITY OF NMR FOR CURE MONITORING OF COMPOSITES

Angela L. Newbury

ABSTRACT

Fibre–reinforced polymer–matrix composite materials have highly attractive physical properties which justify the present rapid increase in applications within industry. However, composite materials suffer, like every structural material, from a failure to achieve their design properties. Therefore this research project has investigated the processing of resin used in composite materials.

Initially the research programme has been concerned with the cure of epoxy resins (specifically Araldite MY750 epoxy resin system), the behaviour of the resin as it cures and how the extent of cure can affect the mechanical properties of components. Therefore, investigations have been carried out into how resin cure can be monitored by the NMR spectra and the relaxation time properties. There were four methods of analysing the data investigated, overall transverse relaxation time (T_2) and free induction decay data (FID) data using the Oxford QP NMR analyser, transverse relaxation time data and spectral changes for the individual chemical environments using the Jeol EX270 NMR spectrometer, curemeter investigations using the vibrating needle curemeter (VNC) and finally Barcol hardness investigations during the later part of the cure cycle.

Both the Jeol NMR spectrometer and the Oxford QP NMR analyser are designed for use primarily with liquid–state experimentation, however for the spectral, relaxation time, and FID investigations results were obtained far longer in the cure than expected. Also for the T_2 investigations a transition period was noticed in the data obtained that corresponded to the gel of the resin as determined by known viscosity data for that resin mix at that cure temperature.

The use of NMR as a curemeter technique was verified by repeating the analysis of the resin cure at 40, 60, 80 and 100^{0}C. This data was then compared to known viscosity data and cure profiles obtained by the VNC curemeter and Barcol hardness readings on similar sized samples.

DECLARATION

The contents of the final permanently bound thesis are identical to the version submitted for examination (except where amendments have been made to meet the requirements of the examiners).

CONTENTS

LIST OF FIGURES

SUBJECT CODE: T

ORDER NO: 621483

PRICE PER COPY: —

TOTAL COST: —

NO. OF COPIES/VOLS: 1

GIFT (Y/~~N~~):

RECOMMENDER:

DEPT:

LOAN PERIOD:

Reserve: 905

Thesis

store

LIST OF TABLES

ACKNOWLEDGEMENTS

I am grateful to the University of Plymouth, School of Manufacturing, Materials and Mechanical Engineering and Department of Environmental Science for the use of their facilities throughout this research project. I would like to thank my three supervisors Mr. David Short, Dr. Roy Lowry and Dr. John Summerscales for their advice and continuous support and for proving to me that it takes people of different character to make a good team.

I am grateful to Oxford Instruments, Industrial Analysis Group for granting me time on the QP at what was a very busy time for the company. I would like to thank Dr. Andrew Crookell and Mr. Claudius Van Wyk for their advice and support.

My thanks also to the following staff of the University of Plymouth, Colin Stansbury, Terry Richards, Mike Sloman and Roger Evens, who have helped with advice, support and tea-breaks.

Finally I would like to thank my parents and brothers for their support and making sure that once I had started I would finish. I would like to thank my father for proof reading the thesis.

AUTHOR'S DECLARATION

At no time during the registration for the degree of Doctor of Philosophy has the author been registered for any other University award.

This study was financed with the aid of a CASE studentship from the Science and Engineering Research Council, and carried out in collaboration with Oxford Instruments, Industrial Analysis Group.

A programme of advanced study was undertaken, which included attendance on the Advanced Composites Manufacturing Centre (ACMC) short courses in composite manufacture and cure monitoring.

Relevant scientific seminars and conferences were regularly attended at which work was often presented; external institutions were visited for consultation purposes, and papers prepared for publication.

Presentations and Conferences Attended:

12th International European Chapter Conference of the Society of Advancement of Materials and Process Engineering, Maastricht, The Netherlands, May 28–30 1991

ICAC 1991, The Hague, 15–17 October 1991.

External Contacts:
Peter Meadows, Jeol (U.K.) Ltd.,
Keith Scott, RAPRA.

Signed..A. L. Newbury.....
Date..1st March 1994..

1.0 INTRODUCTION

1.1 General Background

Polymer composite materials have highly attractive physical properties (e.g. strength–to–weight ratio) which justify the present rapid increase in applications within industry. However composite materials suffer, like every structural material, from a failure to achieve their design properties (strength, environmental adaptability) which can arise from:

- defects or flaws initiated during production (preparation of prepreg, lay–up, cure or structural component assembly) and revealed at the final quality inspection;

- local damage in–service, due to excess loading by mishap, impact, fatigue or from environmental hazards (moisture, ozone, ultraviolet light).

Therefore, to take full advantage of these materials proper quality management and non–destructive examination (NDE) techniques are needed to ensure the manufacture of cost effective, reliable composite structures [1].

NDE techniques can be used to determine multiple defects within a polymer composite. The most important being:

1. under or over cure, cure monitoring [2];
2. porosity [3];
3. voids [4];
4. fibre orientation, stacking sequence and volume fraction, V_f [5];
5. location and extent of impact damage and other cracking [3];
6. environmental degradation (due to moisture, chemicals, ozone, ultra violet (u.v.) light, etc.) [5, 3].

Although NDE methods are available they have not been widely used due to the expense of the equipment and a general lack of knowledge regarding composite

failure and NDE techniques. As a consequence they are not fully developed. Defects such as the above are usually monitored by quality control during manufacture by destructive testing of specimens produced at the same time as the structure. At present the total examination of a sample requires the use of several NDE techniques. It would be beneficial to detect and evaluate all various defects in polymer composites using one single technique.

Conventional NDE techniques have been adapted for polymer composites, principally X–radiography [6] and computer tomography [6, 7], penetrant enhanced X–radiography (PEXR) [6, 7], ultrasonic methods [6, 7, 8] and infrared thermography [6, 8, 11]. New techniques include variations on the coin–tap test [9], shearography [10], neutron radiography [1] and holography [11, 12]. For cure monitoring techniques include: dielectric spectroscopy [13, 14], viscosity measurements [15, 16] and thermal analysis [17, 18]. One technique recently adapted from research and medical usage has immense potential to provide more comprehensive information on cure monitoring and defect detection. This is pulsed nuclear magnetic resonance (NMR) spectroscopy and imaging which will be discussed in greater depth later in this chapter.

The present technology of NDE enables a wide range of defects to be detected. However, the knowledge which would allow a decision on the type and extent of defect is scarce. A recent survey [19] demonstrates that at this moment in time industry tends to follow the attitude stated by R. B. Pipes in reference 20.

"If there is a defect of any size , the component is scrapped, just in case the defect should lead to failure".

Of all the properties of the polymer composite that need to be monitored during production it is the extent of cure that will affect all other properties (e.g. tensile strength, environmental degradation etc.). NMR is capable of investigating the liquid resin at the molecular level and in some respects the liquid / solid interface between resin and fibre as the resin cures.

1.2. Technical Background of Pulsed NMR

Many atomic nuclei (e.g. C^{13} or H^{1}) possess spin or angular momentum in addition to charge and mass. Since a spinning charge generates a magnetic field, there is associated with this angular momentum, a magnetic moment, μ, [21]. The spin ($\pm$ 1/2) generates, in a magnetic field, two energy levels.

When placed in a magnetic field, B_0, the spinning nuclei will either align (lower energy configuration) or oppose (higher energy configuration) their magnetic moments to the field direction. The energy states are separated by an amount, ΔE, which is field dependent, $\Delta E = h\gamma B_o/2\pi$, where h is Planck's constant and γ is the magnetogyric ratio, the constant of proportionality between the nuclear angular momentum and the magnetic moment. It is this constant that determines the resonant frequency of the nucleus. However, like gyroscopes in a gravitational field, their spin axes undergo precession about the field direction , see figure 1.1. This precession is called the Larmor precession and is $\omega = \gamma B_o$ in radians per second or $\upsilon = \gamma B_o/2\pi$ in Hertz (Hz). Increasing B_0 will cause their spin axes to precess faster.

The spinning nuclei will only flip between energy configurations when a second pulsed radio-frequency (r.f.) magnetic field, B_1, is applied at right angles to the original magnetic field and causing this second field to rotate at the precession frequency . Resonance occurs when μ and B_1 precess at the precession frequency. At a characteristic r.f. resonance occurs and the nuclear moments align causing the nuclei to emit or absorb energy. Lower energy nuclei absorb radiation and undergo a transition from being aligned to the field to being opposed, while at the same time higher energy nuclei are stimulated to emit energy when they change their opposed orientation and become aligned with the field [22]. The net absorption of r.f. by a sample only arises because there exists an excess of nuclei in the lower energy state.

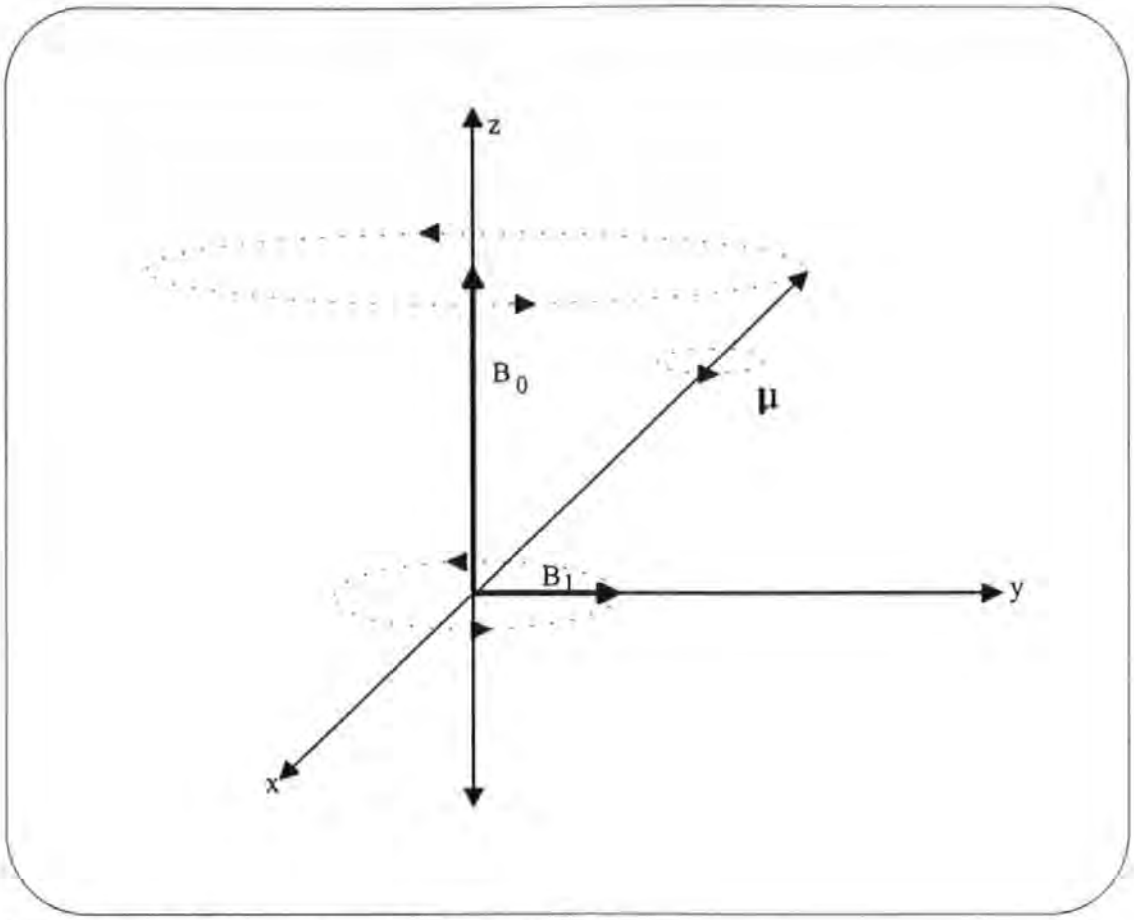

Figure 1.1. Nuclear moment in magnetic field.

1.2.1. Chemical Shift

It could easily be assumed from what has been discussed so far that at a particular frequency all nuclei of a given species resonate at the same value of B_0. However, if this were the case NMR would be of little interest. The characteristic resonant frequency of a nucleus is dependent to a small, but measurable, extent upon its chemical environment. This characteristic chemical shift is measured in parts per million (ppm). It was found [21] that the protons of water do not absorb at quite the same frequency as those of mineral oil, the difference is only a few ppm. For heavier nuclei, much larger effects are noted – up to 2% for certain metals.

The origin of this variation in resonant field strength is the cloud of electrons about each nuclei. When a molecule is placed in a magnetic field B_o, orbital currents are induced in the unpaired electron clouds, and these give rise to small, local magnetic fields, which are always proportional to B_o but opposite in direction. Each nucleus is,

in effect, partially shielded from B_0 by the electrons and requires a slightly higher value of B_0 to achieve resonance. This can be expressed as [21]:

$$B_{IOC} = B_0(1-\sigma)$$

where B_{IOC} is the actual local field experienced by the nucleus and σ is the *screening constant*, expressing the reduction in the effective field. Since σ is independent of B_0 but highly dependent on the chemical structure then the above equation can be modified to [21]:

$$h\nu_0 = \mu B_0(1-\sigma)/I$$

Therefore the effect of nuclear screening is to decrease the spacing of the nuclear magnetic energy levels. At a constant r.f. field strength and an increase in σ i.e. an increase in the magnetic shielding of the nucleus results in B_0 having to increase to reach resonance. Thus if resonance peak positions are expressed on a scale of magnetic field strengths increasing from left to right (as the universal case) the peaks for the more shielded nuclei will appear on the right hand side of the spectrum.

The chemical shifts of many species shows a significant temperature dependence, which may affect resonances of interest.

1.2.2. Relaxation Phenomena

Free Induction Decay: If the input of r.f. energy is in excess then the populations of the two states will become equal and there will be no further net absorption of r.f., i.e. the system is saturated. Due to this saturation, the NMR absorption signal will only be restored if the nuclei relax back to their original energy distribution, giving off a characteristic signal. This decaying signal is called the free induction decay (FID): *free* of the influence of the radio frequency, *induced* in the instrument coil and *decaying* back to the Boltzmann distribution [94]. The signal is also a transient because it decays after excitation. The FID is a characteristic of a particular type of

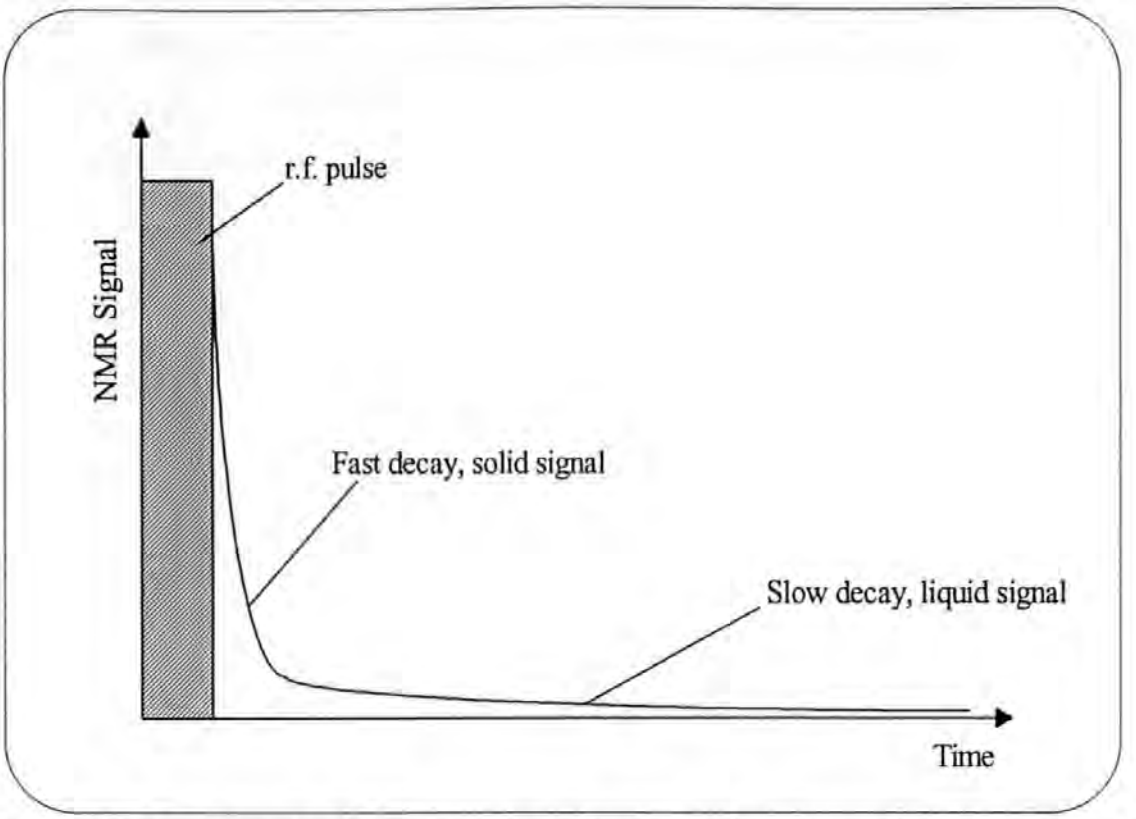

Figure 1.2. An example of a an FID for a liquid / solid mixture (only envelope of signal is shown).

nucleus and its chemical environment. With Fourier transform techniques the frequency-domain high resolution spectrum can be obtained more rapidly than the conventional NMR plot of frequencies.

Since the FID is characteristic of the chemical environment of the nucleus it is also characteristic of the different phases within a sample i.e. liquid or solid (see figure 1.2.). The different phases decay at different rates and by examining the shape of the decay envelope the different phases can be distinguished. The envelope is defined by the individual echo maxima.

Spin-Lattice (or Longitudinal) Relaxation, T_1 : The relaxation process implies a loss of energy from the system of nuclear spins. Some of this energy is re-emitted as r.f. but much is lost by radiationless transfer to surrounding nuclei within the sample. Transfer of energy from the spins to the lattice requires that there be a magnetic field

at the nucleus fluctuating at the Larmor precession frequency in order to induce an NMR transition.

The random tumbling of molecules and vibration of bonds sets up many transient dipoles. A proportion will be of an appropriate frequency to interact with the higher energy nuclei. This results in a transfer of the spin energy to the surrounding nuclei, hence the term spin–lattice relaxation. This is also termed longitudinal relaxation as a reminder that it is the behaviour of the z–component of magnetisation that is being considered. If the magnetisation is moved away from the z–axis, we may assume that it will tend to return there exponentially with the time constant T_1 [23].

Spin–Spin (or Transverse) Relaxation, T_2 : In contrast to T_1 interactions, the T_2 interactions do not involve exchange of energy with the lattice, but are concerned with the exchange of energy between the nuclei themselves, via flip–flop type mechanisms [24].

From the Heisenberg Uncertainty Principle, if T_1 and T_2 are both long (i.e. their spin state life times are long) then the change in energy for NMR absorption can be measured with high accuracy, and the frequency line–width will be narrow. Any factor which shortens the spin state lifetimes and leads to more rapid relaxation processes will lead to broader NMR signals. T_1 is equal to or longer than T_2 and can range from a few microseconds in non–viscous liquids (mobile systems) to hours in solids (immobile systems) whereas T_2 will be microseconds in solids.

1.2.3. Theory of Relaxation Time Measurements

In principle T_2 is obtained simply by measuring the signal width at half-height, which is theoretically given by $1/(\pi T_2)$(Hz) [23]. However, owing to insufficient homogeneity of the B_o magnetic field, the measured line-widths will yield the effective relaxation time, T_2^*, which is defined by:

$$1/T_2^* = 1/T_2 + 1/T_2(B_o) \qquad (1.1)$$

where $1/T_2(B_o)$ is the instrumental broadening which obscures the effect of the natural relaxation rate $1/T_2$. In fact as slightly different values of the static magnetic field, B_o, are experienced in different parts of the sample, magnetisation isochromats can be defined. These are characterised by slightly different resonant frequencies. As a result of this dispersion of resonance frequencies the isochromats* rapidly lose their phase coherence – after a pulse excitation for instance. Such a source of dephasing accelerates the fanning out of the transverse, spin-spin, component of the magnetisation vector. However, the dephasing of spin isochromats which results from field homogeneities is reversible, and refocussing is possible under appropriate conditions. In this way echoes are formed when repetitive pulses are applied at intervals longer than the effective relaxation time T_2^* but smaller than the transverse relaxation time T_2.

1.2.3.1. The Carr-Purcell method for measuring T_2

The Carr-Purcell sequence can be written [25]:

$$\left[\frac{\pi}{2} - \tau - \pi'_x - \tau_{echo} - \tau - \pi'_x - \tau_{echo} - \tau \ldots \pi'_x - \tau_{echo} - A_t - D\right]_n$$

Where τ is the time interval between pulses, A_t is the acquisition time, D is the delay between repetitions and n is the number of repetitions.

* *Isochromats – destructive interference from different regions of the sample because of non-uniformity of* B_o.

The above pulse sequence describes the following experimental method: A $\pi/2$ pulse is used to tip the magnetisation vector M along the y' axis in the rotating frame ** (see figure 1.3.a.). Due to the field homogeneity effects, the spin isochromats rapidly dephase during the interval τ since some move more slowly (S) while others move more rapidly (R) with respect to the nominal resonance frequency (see figure 1.3.b.). At time τ_1 a π–pulse is applied along the x' axis (figure 1.3.c.). The slow and fast spin isochromats, which continue to rotate, now move towards each other. Complete refocussing is reached at time 2τ and a maximum spin–spin magnetisation or spin–echo being obtained at figure 1.3.d. After this echo, the spin isochromats dephase again (figure 1.3.e.), while another π–pulse applied at time 3τ in the x' direction (figure 1.3.f.) allows a second echo to be observed at time 4τ (figure 1.3.g.) and so repetitive π–pulses produce echoes at $6\tau, 8\tau$ etc. As

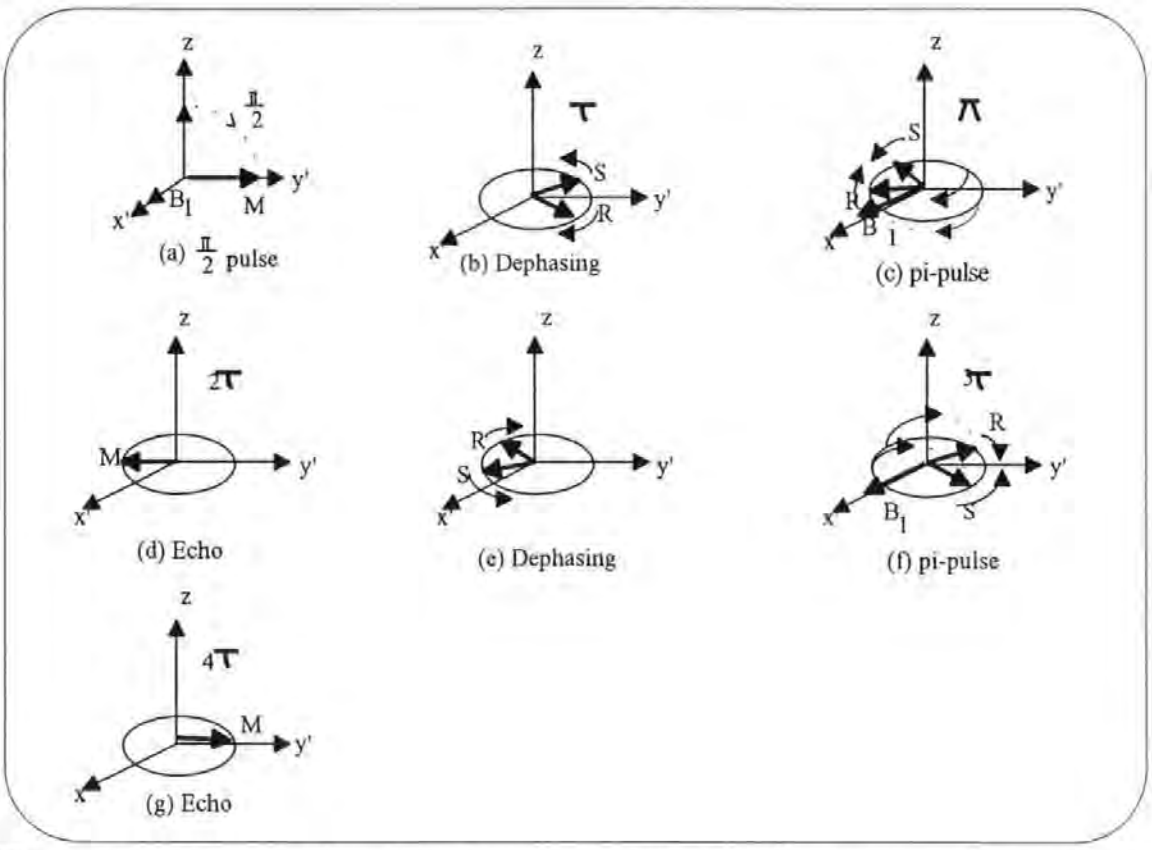

Figure 1.3. Magnetisation behaviour in a Carr–Purcell sequence. The pulse is assumed to be applied exactly at the top of the resonance. [Extract from M. L. Martin, "Practical NMR Spectroscopy," Heydon and Son Ltd., (1980)].

** a set of co–ordinates that rotate along with the nuclear precession [25] denoted by x'y'z.

the refocussing process eliminates the field inhomogeneity effects, the amplitude of the successive echoes is expected to decay exponentially with the natural relaxation rate, $1/\tau_2$. This assumes that the pulse interval is short enough (<100ms) for any decay due to diffusion of spin isochromats for different regions of the sample to be negligible. However, if the spin–spin relaxation times are long then numerous π–pulses must be applied to properly define the decay and any mis–settings in the pulse angle introduces a cumulative deviation of the magnetisation vector with respect to the x'y' plane. Thus imperfect refocussing results from large τ values. The problem is circumvented in the Meiboom–Gill variant of the Carr–Purcell sequence.

1.2.3.2. Carr–Purcell–Meiboom–Gill (CPMG) sequence

To avoid cumulative errors resulting from a slight mis–adjustment of the flip angle it is preferable to apply the π–pulse in the y' direction instead of the x' direction [25].

$$\left[\frac{\pi}{2} - \tau - \pi'_y - \tau_{echo} - \tau - \pi'_y - \tau_{echo} - \tau \ldots \pi'_y - \tau_{echo} - A_t - D\right]_n$$

Consider the example of a pulse, θ, slightly shorter than π and directed along the y' axis (figure 1.4.). This pulse interchanges the orders of rotation of the slow and fast magnetisation isochromats (figure 1.4.c.) and leaves them slightly above the x'0y' plane. Then refocussing occurs normally at time 2τ but takes place above the y' axis in the z0y' plane (figure 1.4.d.). After the dephasing period τ (figure 1.4.e.) the second θ pulse rotates the isochromats exactly back into the x'0y' plane where they are refocussed at time 4τ (figure 1.4.g.). Thus all even–numbered echoes are produced along the right direction, y', whereas the odd–numbered echoes are slightly displaced by a constant angle.

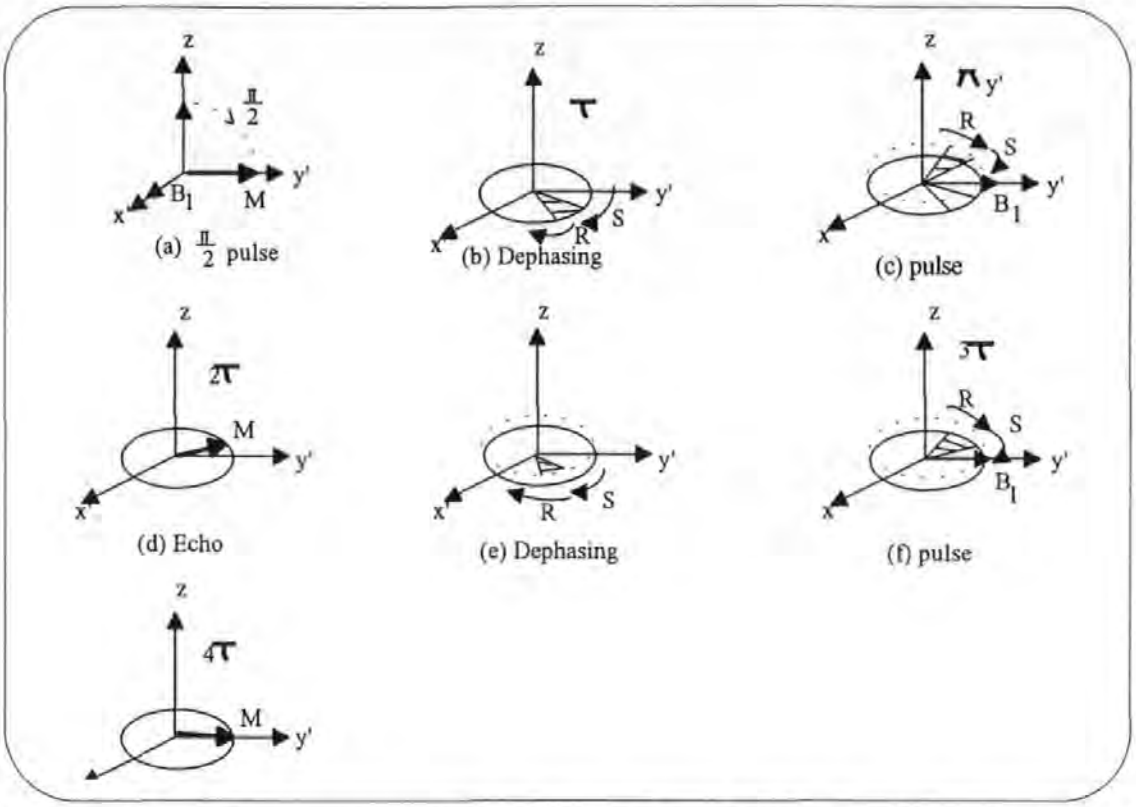

Figure 1.4. The compensating effect of the Meiboom–Gill variant of the Carr–Purcell method. The frequency of the rotating frame was set at a slower Larmor frequency. [Extract from: M. L. Martin et al; "Practical NMR Spectroscopy", Heydon and Son Ltd., (1980)].

1.2.4. Solid–State NMR

There are three main reasons why the production of high–resolution NMR spectra from solids is technically difficult: sensitivity of many important nuclei is poor; NMR signals from solids are inherently broader than those for liquids; relaxation times can be long, leading to unacceptably long spectrum–accumulation periods.

NMR broadening mechanisms include:

i) magnetic dipolar coupling (homonuclear and heteronuclear);
ii) chemical shift (isotropic and anisotropic);
iii) magnetic susceptibility.

Spin–lattice relaxation certainly contributes to the effect of intrinsic broadening. Extrinsic broadening from the inhomogeneity of the static field can also be included in this list.

The problem can be solved using a combination of techniques: sensitivity can be improved by using higher–field super–conducting magnets for studying isotropically dilute nuclei such as ^{13}C and ^{29}Si ; lines can be narrowed by "magic angle spinning" (MAS) and heterodipolar decoupling (for dilute spins) or homonuclear decoupling (for abundant spins); relaxation times can be shortened by cross–polarisation (CP) techniques or by the deliberate introduction of paramagnetic species into the sample.

Magic angle spinning (MAS) : Chemical Shift Anisotropy (CSA) causes broadening of the NMR signal and is due to the chemical shift of a particular carbon atom being directional, depending on the orientation of the molecule with respect to the magnetic field.

In the mathematical analysis of shielding in an applied field [22], the term $(3\cos^2\theta - 1)$ arises, where the angle, θ, determines the orientation of the molecule with respect to B_o . Theory shows that the chemical shift anisotropy falls to zero when $(3\cos^2\theta - 1)$ falls to zero and this occurs when θ=54.7°, the *MAGIC ANGLE*. The sample is thus spun around the axes orientated at the magic angle. The spinning rate must be comparable to the CSA. For MAS a high magnetic field is a disadvantage since it would increase the CSA.

Cross polarisation (CP) : This method takes advantage of the fact that the proton spin diffusion generally causes all the protons in a solid to have the same spin–lattice relaxation time, T_1 . Also the proton T_1 is shorter than the carbon T_1 .

CP works by effectively forcing an overlap of proton (H) and carbon (C) energies (these concepts can apply to the polarisation between any abundant spin and a rare

spin). This method was first demonstrated by Hartmann and Hahn in 1962. Energy transfers between nuclei with widely differing Larmor frequencies (the frequency of precession in a magnetic field of particles possessing magnetic moments) can be made to occur when:

$$\gamma_C B_{1C} = \gamma_H B_{1H}$$ Hartmann–Hahn Condition

where γ = magnetogyric ratio.

1.2.5. NMR Imaging (NMRI)

NMRI computer tomography has also been termed zeugmatography, from zeugma meaning "that which is used for joining" i.e. the matching of the r.f. field to the magnetic field to create resonance conditions.

The ability to obtain information as a function of spatial position within the sample makes NMRI an important technique for the NDE of composite materials. The major limitation to the direct application of NMRI to the study of solid materials is that NMR line–widths are three to five orders of magnitude greater than those observed for liquids. The increased line–width causes two problems [26]:

1. There is a decrease in the spatial resolution for given imaging parameters;
2. There is a decrease in the signal–to–noise ratio.

NMRI techniques have recently been utilised for the spatially localised ^{1}H NMR measurement of moisture gradients in components such as concrete bridges [27].

In the solid state, however uniform the magnetic field, local magnetic fields due to varying environments in the material cause T_2 to be very short, while a lack of motion–induced relaxation may give rise to a very long T_1. Therefore there is still

the possibility for solid-state (short T_2) imaging technology to make NMRI a feasible technique to use on composite components.

1.3. Experimentation Techniques

Cure monitoring techniques have greatly improved over the years and this section will now give an introduction to the type of techniques currently available. It will then proceed to discuss the recent advances which have greatly expanded the potential of NMR spectroscopy and tomography for applications outside the laboratory. The main area of study is the investigation concerning moisture uptake in composites. Other studies have the specimen boiled in water before examination to allow water to ingress into near-surface defects [28] so that liquid-state NMR can be utilised to resolve the voids via the free protons in the water. Studies have included surface and matrix studies [29, 30], and structural investigations [31].

Other research has been undertaken on the location and identification of glass fibre using ^{29}Si NMR [29], quantitative determination of fibre integrity and volume fraction [32], interfacial effects [29], prepreg ageing [33] and thermal degradation [32].

1.3.1. Cure Monitoring Techniques

Dielectric Spectroscopy: There are few techniques available that can monitor the amount of cross-linking taking place in a polymer both in the liquid and the solid states. Dielectric measurement techniques have been widely used to study the cure characteristics of thermosets since this method can follow the cure from liquid resin to glassy solid.

There are four major properties that are reported during dielectric analysis:

– Permittivity or dielectric constant,
– loss factor,
– dissipation factor, and
– ionic conductivity.

Dielectric analysis measures the capacitive and conductive nature of the sample. Typically the sample is placed between two electrodes and subjected to a dynamic or static thermal profile, while having a sinusoidal voltage applied. An alternating field is created that produces polarisation in the sample which oscillates at the same frequency as the electric field, but undergoes a phase angle shift. This phase shift can then be measured [34] in terms of capacitive and conductive components of the sample. From these the permittivity of the sample, also called the *Dielectric Constant* can be found since it is proportional to capacitance while the loss factor is proportional to conductance.

Dielectric analysis can be undertaken using dielectric thermal analysis (DETA) or under isothermal conditions depending on what data is required. DETA can be used to monitor the following viscoelastic events for an uncured thermoset [34]:

– Glass transition temperature, T_g (if the DETA is initially cooled below the T_g of the resin);
– resin flow (as the resin softens above T_g);
– temperature of minimum viscosity;
– onset of cure.

It must be mentioned that the gel point temperature is not noted by the DETA since this is a mechanical event rather than an electrical event.

When analysis using uncured thermosets is undertaken under isothermal conditions the following viscoelastic events can be observed [34]:

– the point of minimum viscosity (occurs near time equals zero);

- the onset of cure (observed as a drop in the ionic conductivity);
- vitrification may or may not be observed, depending on the characteristics of the given resin;
- complete cure

Note that not all resin systems will show the vitrification event under isothermal conditions. Although prepregs may show a dielectric response which is similar to that of unreacted neat resin, the data may contain effects due to the presence of the fibres.

Whetton et al [35] have studied the benefits of DETA against dynamic mechanical thermal analysis (DMTA). They found that although DETA could be used for on–line monitoring it was only applicable for short cure times. Also at higher temperatures the conductivity background causes too much interference for successful measurements to be undertaken.

Gotro et al [36, 13] have undertaken similar studies with DETA and viscosity measurements. The object of the work was to develop a method to simultaneously measure the dynamic mechanical and dielectric properties during various cure schedules. For these experiments a small dielectric sensor was embedded into the lower plate of a rheometer. Tests were carried out on three different types of prepreg systems.

Gotro concluded that dynamic dielectric and dynamic mechanical analysis had verified that particular dielectric events may be correlated with physical transitions. Careful heating rate studies demonstrated the following:

1. The loss factor may be correlated to the viscosity during various heating schedules to 175°C and subsequent isothermal hold.
2. For a thermosetting resin with an ultimate T_g well below the cure temperature, the loss factor was found to retain a high value after the maximum, and full cure could be determined when the slope [d(log(loss factor))]/dt equals zero.

Bidstrup et al [14] used microdielectric techniques to monitor the cure of composite matrix resins. The initial results were for neat resins and the relationship between its conductivity and corresponding changes in the T_g during cure. This was then taken further to incorporate the study of cure for glass and carbon fibre composites. It was found that the technique proved to be a good cure monitoring technique and that good reproducibility was obtained. (See also reference 37).

Nass et al [38] developed a mathematical relationship between the experimentally obtained signals and the physical state of the polymer during isothermal and dynamic cure. Experimental results for a model epoxy / amine system were predicted with the developed methodology for isothermal cure at 140 °C, 150 °C, 160 °C and 170 °C and cure under dynamic heating conditions at 1 °C per minute. The model was successful in predicting isothermal data using parameters obtained at 20kHz. The model provided good description at high frequency for non–isothermal cure conditions.

Bidstrup et al [39] undertook experimentation to correlate the dielectric properties directly with the network structure and so developed a comprehensive model relating conductivity with the extent of reaction and cure temperature. At specific states in the cure, small samples were quenched and then analysed for T_g and the degree of cross–linking using DSC (see thermal analysis section and references 40 to 43).

Kranbuehl et al [44] have undertaken experiments with dielectric impedance measurement (DIM) techniques for the process monitoring of properties in several high performance thermoplastics. It has been shown that DIM can be used to monitor viscosity, T_g, crystal melting, recrystallisation, and residual solvent content and evolution. These processing properties can be used to help define the optimum process conditions and to thus monitor the polymer as it polymerises in the mould (see also reference 45).

Thermal analysis: There are two complementary techniques to dielectric analysis: differential scanning calorimetry (DSC) and dynamic mechanical thermal analysis (DMTA). These are two valuable techniques for the characterisation of composite prepregs and laminates. Properties which can be determined by the use of both techniques include gel points, T_g, reaction rates and kinetics, extent of cure, moisture and end–use properties.

DSC can be defined as the difference in energy inputs into a substance and reference material when measured as a function of time or temperature whilst subjected to a controlled temperature programme [17]. DMTA is a complementary technique (not just for DSC but it can also prove useful with DETA analysis) that can provide valuable information for the optimising of process control.

Gramelt et al [18] have used DSC and thermogravimetry (TG) to investigate performance problems with fibre–glass reinforced plastic components. These simple techniques can also be used, so they suggest, during production development to pick the curing agents and cure cycle for complete cure at minimum cost. Gramelt and colleagues concentrated on polyester cure and during the course of the experiments they assumed the following: that there is no resin decomposition of the specimen during cure completion in the DSC nor is there any styrene loss during DSC scans; that there is no material lost during transfer from the DSC to the TG module and that the heat of reaction is constant throughout the cure.

Acoustic emission and acousto–ultrasonic techniques: The curing process for composite components involves the application of heating, pressurisation and cooling cycles which can induce residual stresses into the component for a number of reasons [46]. These reasons may be as a result of: a mismatch in thermal expansion between the reinforcement and the matrix, the application of pressure to consolidate the laminate, the cooling cycle being too quick or removal of the component too early from the mould.

The acoustic emission (AE) activity can be monitored once pressure is applied to the laminate and corresponds to fibre fretting and friction caused by the consolidation of the laminate being too strong and "pushing" out some of the resin. Finally during the cooling part of the cycle changing the cooling rates can affect the amount of AE activity. It is the microcracking caused by the relieving of the residual stresses that can be monitored at this time. At a slow cool there is little stress relief and therefore little AE activity. These laminates that have a high level of unrelieved stress are liable to subsequent dimensional instability.

In conventional AE it is the high frequency sound produced in response to a change in environment that is being monitored. The acousto–ultrasonic (AU) technique [46] is a symbiosis between AE and ultrasonics in that it involves the injection of an ultrasonic signal into the test specimen. Since AU is essentially a method for measuring relative attenuation it can be used to detect local anomalies.

During the cure of a composite the main variable controlling the ultrasonic attenuation is the state of the resin. During the initial heat–up period, as the resin starts to melt and flow the mechanical strength and stress wave factor start to fall. Then as the resin starts to cross–link and the polymer starts to form an extended network, the mechanical strength and stress wave factor both start to rise.

Saliba et al [47] have used AU to investigate the effects on the acoustic response curve with the following: moisture; vacuum; laminate thickness; prepreg to bleeder ratio; ply orientation sequence; and degree of prepreg advancement. They found that the vacuum release during a run shifted the response curve down, but did not alter the general shape of the curve. The addition of plies lowered the response curve without altering the time required to reach minimum viscosity. Prepreg bleeder ratio and ply orientation sequence had no effect on the response curve. Saliba et al also developed a general correlation relating the actual viscosity to the acoustic reading and degree of cure (obtained by DSC) to the acoustic signal.

Curemeters: Instruments for measuring the cure of rubbers have been used in the industry for more than fifty years [48]. The older types work on the principle of oscillating disks. Due to the evolution of curemeter design it is not always possible to directly compare cure profiles from different meters

The Vibrating Needle Curemeter (VNC) is designed to monitor the cure of liquid polymer formulations. It is not only capable of giving a complete cure profile for liquid polymers but also for large composite mouldings.

The VNC [15] monitors the increase in the viscosity of curing specimens before gelation and subsequent changes in the stiffness can also be measured. This is achieved by suspending a needle into the curing resin. The needle vibrates vertically by the use of a small electro-dynamic vibrator and resistance to its movement is recorded. The shape of the trace obtained is dependent on the frequency at which the needle vibrates.

Scott [16, 49] has investigated the use of the VNC to monitor the cure of polyurethanes. By monitoring the cure of liquid polymers the effect of the various components in a given formulation can be assessed. Scott used the VNC to monitor delay in cure, changes in the cure profile and property development of polyurethane elastomers. It was demonstrated that the VNC was capable of: continuous monitoring of the cure of liquid systems; detecting changes in the curing formulation after the gel point; monitoring the effect of small changes in the formulation of polyurethanes (e.g. catalyst type, isocyanate index and chain extender content) and possible in-mould cure monitoring.

Optical techniques: Davies et al [50 and 51] have investigated the use of opto-ultrasonics for cure monitoring of resin fibre composite structures. Opto-ultrasonics combines ultrasound generated either by laser or piezoelectric transducer with fibre optic sensing. The high power laser beam that is used to generate ultrasound can also be delivered by an optical fibre or fibre bundle. The generation of ultrasound takes place on the surface or within the specimen and this

can apply to the detection of the ultrasonic waves as well. The waves are modified as they travel through the material. Davies suggests that the distinct advantage of this technique is that it can be used for cure monitoring during fabrication and then serve as a strain and damage sensing system during the remaining component life. At present further signal processing and an improved signal–to–noise ratio are required.

Liu et al [92] introduced in this paper an opto–ultrasonic approach to cure monitoring which employs fibre optic sensors for the detection of ultrasound generated by either laser or piezoelectric transducer. As cross–linking bonds between polymer chains form, the epoxy resin changes its state from a viscoelastic liquid to a viscoelastic solid. The viscoelastic moduli (both bulk and shear moduli) of the material change accordingly, which in turn produces a change in the acoustic properties of the material, yielding a good indicator of the state of cure.

Levey et al [52] have investigated the use of fluorescence–based fibre–optic sensors (FOCS) for cure monitoring of carbon–epoxy composites. These cure sensors have been designed to be integrated into the composite component during manufacture. The sensor generates two characteristic signal profiles which reflect the chemorheological events of the process and permit autoclave control. These signals continue to change during the late stage of the cure. Additional refinements to the "optrode–laminate" interface are required (see also references 53 and 54).

1.3.2. NMRI Experimentation

Moisture content: Shuford et al [55] suggested that absorbed moisture causes the matrix to swell, lowers the glass transition temperature of the resin, induces residual stresses and microcracking in the composite and can irreversibly degrade the fibre / matrix interface. In addition moisture in prepregs can change the curing behaviour during cure and hence degrade the physical and mechanical properties of the fabricated component.

Matzkanin [56 to 58] investigated the feasibility of using NMRI to examine non-destructively the amount of moisture in organic matrix composites (by measuring the free hydrogen content) and the extent of moisture-induced mechanical degradation. In some cases moisture levels of 0.2% could be detected and variations of less than 0.1% could be resolved. Absorbed moisture NMR signal components were found to be readily distinguishable from the signal component arising from the chemically bound structural hydrogen atoms. The distinct components of the absorbed moisture NMR signal may be associated with the moisture absorbed along the fibre / matrix interface and the moisture absorbed into the matrix. In addition, certain features of the NMR signals may be useful in providing information on moisture in different physical states within the composite. Such measurements could be related to potential mechanical damage and ultimately be instrumental in assessing the remaining useful service life of structures.

Imaging of voids: Jackson et al [28] carried out experiments where the specimen was boiled in water to allow water to ingress into the defects. The defects are therefore easier to detect since the signal can be selected for the ingressed water only. The problem with this approach is that only defects close or connected to the surface, i.e. where water can ingress, can be detected. The detection of wholly internal voids requires the alternative approach of direct imaging of the polymer matrix.

Investigations into jet fuel ingress into carbon fibre reinforced poly(ether ether ketone) (PEEK) have also been carried out by Jackson et al [59]. Simple wide-lined NMR gives a two component spectrum, with a broad component due to the polymer matrix and a narrow component due to the ingressed fuel. This difference is due to the much longer T_2 of the more mobile fuel components. The difference in relaxation times can be exploited to generate images of the distribution of jet fuel in polymers, without observing signals from the protons in the more rigid matrix.

Imaging of solids: Jezzard et al [60] have obtained a series of images of solid polymers using standard spin–echo imaging pulse sequences. This was achieved by raising the temperature of the sample above the glass transition temperature by a small amount. This increases thermal motion sufficiently to partly average out the large dipolar and chemical shift anisotropies, which are characteristic of solid polymers at ambient temperatures.

Jezzard et al [91] suggested that NMR imaging can be used to provide a map of the spatial distribution of surface–connected voids. This technique need not be restricted to flat sheets and can provide a fully quantitative map of the distribution of ingressed water. Each composite sample was boiled overnight in water before commencing the NMR experiment, this allows water to penetrate into any surface connected voids present in the sample and provides the mobile liquid which was subsequently imaged. Loss of the liquid during imaging was minimised by wrapping the samples in cellulose film. Care was taken when comparing the measured weight uptake of water during the boiling process with the amount of water observed in the NMR images. This is because the water taken up in the polymer composite can exist in two states: interstitial water contained in void spaces, generally having a T_2 value of many milliseconds, and bound water, which is strongly associated with the polymer matrix and has a very short T_2 value. In the NMR images presented by Jezzard only the signal from the interstitial water is observed, since the T_2 relaxation time of the bound water is much shorter than the spin–echo time used. Jezzard states that because the polymer matrices studied were ultra–high density and so the absolute amount of bound water which diffuses into them is quite small.

Lind [90] investigated the use of NMR techniques for the inspection and evaluation of organic matrix composite materials. The emphasis of the experimental work was to evaluate the usefulness of the NMR technique to determine nuclear level information in polymeric and ceramic materials that can be linked to macroscopic material properties. There was a particular focus on the imaging capabilities of NMR in these materials.

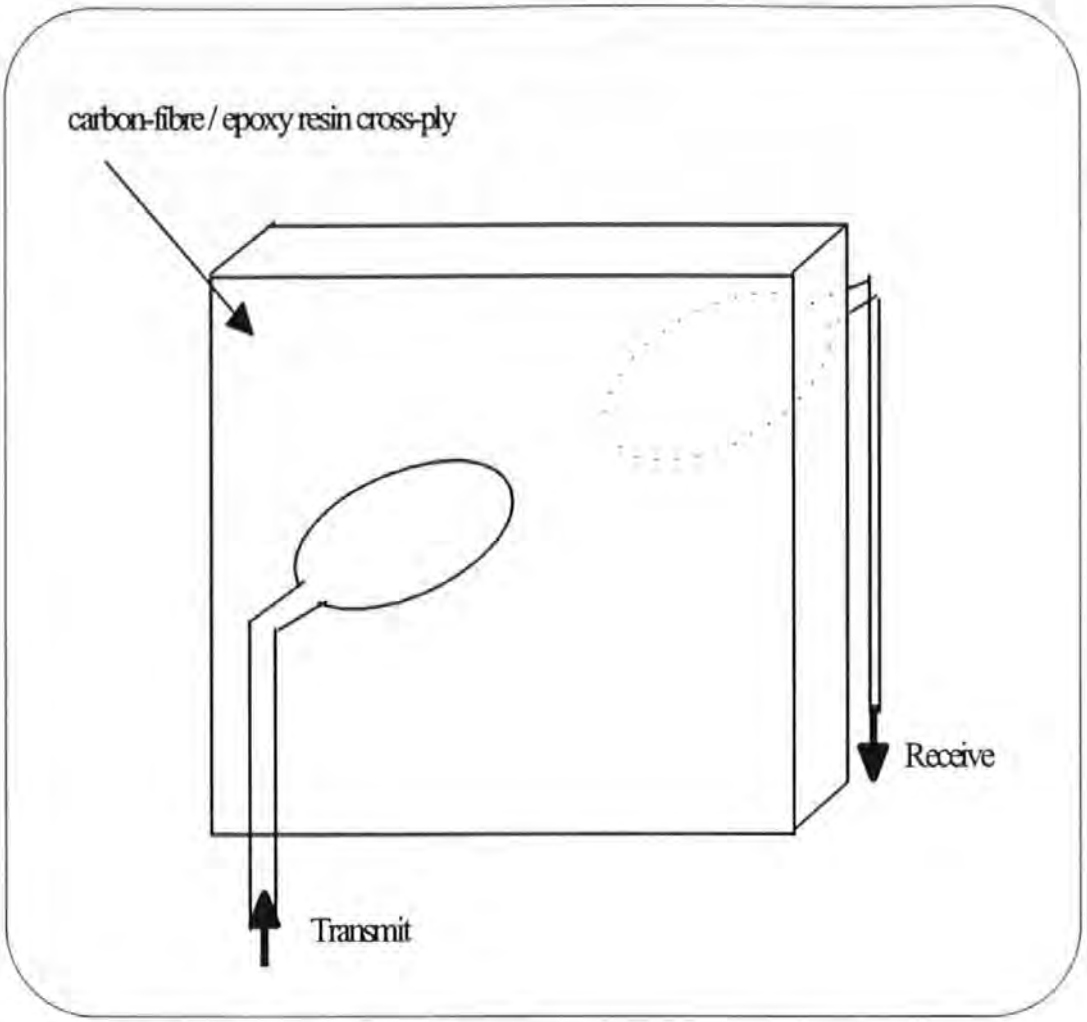

Figure 1.5. Schematic of use of surface coils.

Lind used surface coils to analyse larger components. With the surface coil parallel to the surface of the cross-ply of the organic matrix composite panel and nearly touching the surface, as shown in figure 1.5, the static magnetic field was normal to the plies, and the radio frequency magnetic field was parallel to the plies. The NMR images obtained of rubber band phantoms mounted on the surface of cardboard as a reference, mounted on the surface of the cross-ply panel, and located 0.25, 0.5, 1.0 and 2.0mm below the surface of the cross-ply panel. The reference image was obtained with a 25μs, $\pi/2$ r.f. pulse using a transmitter power of 21W. For all measurements, the radio frequency pulse length and transmitter power were adjusted to produce $\pi/2$ and π pulses needed for the imaging experiment with the transmitter power ranging from 21 to 94W. An image of the sample at 2mm depth could not be obtained because of the large r.f. attenuation at this depth.

A similar experiment was also carried out with the surface coils normal to the surface of a cross-ply sample. This sample was 8mm thick and had an oil phantom which extended from the centre to one edge of the panel and was located between the two centre plies of the panel. This panel was well consolidated and no ply separation occurred except in the immediate vicinity of the phantom. The transmitter power was held constant at 2.25kW, and a series of images were obtained as the pulse length was incrementally increased. The length of the $\pi/2$pulse in the absence of the carbon-fibre sample was 30μs. The static magnetic field was orientated normal to the plies and the r.f. magnetic field was parallel to the plies. Field directions here are the same as in the above experiments. However, in these experiments a surface coil was used at the location of the phantom beneath the surface and the r.f. field propagated inward and normal to the plies. The phantom was 4mm away from the surface therefore the propagation inward and normal to the plies experiences very large attenuations, and propagation that is observed instead comes in from the panel edge parallel to the plies.

Due to bad cross-ply consolidation and transmitter power requirements the NMR and NMR imaging of features at depths ≥3mm in the carbon-fibre cross-ply (and similarly chopped fibre) composites at frequencies greater than or equal to 10MHz (0.235T) is not feasible when the r.f. must propagate normal to the plies. Even if technical advances are made in experimental design of probes only a small amount of improvement seems possible according to Lind.

Also for flaws such as delaminations and broken fibres where the eddy current pathways are broken, the radio frequency must first reach the area of the flaw. Unless the delaminations or broken fibres propagate from close to the surface, r.f. attenuation will prevent detection as it does with other features. Therefore nominal NMR and NMR imaging do not appear to be viable NDE techniques for the inspection of large scale carbon-fibre composite pieces such as wing-skins.

^{13}C Imaging: Lind [90] investigated ^{13}C imaging and said the important aspects of these experiments was that it took 2 hours to obtain a one-dimensional image, containing a resolution of ≥300μs. In assessing the future viability of ^{13}C NMR

imaging of solids, it is important to predict the time needed to turn the 2 hour experiment into one which would achieve 100 x 100 μm resolution within a 100 μm slice. Lind concluded that practical, high-resolution, three-dimensional NMR imaging of solid-state materials using ^{13}C may never be achievable.

Prepreg ageing: Koller et al [33] have used NMR imaging and spectroscopy techniques to characterise the cross-link state after exposure at room and at an elevated (50 °C) temperature. It is believed that the resulting mechanical properties of the cured components are strongly influenced by the ageing state of the prepregs. The technique can also show the influence of moisture content on the ageing process. The NMR technique has the advantage over DSC or dielectric techniques because there is no influence of the sample volume and geometry.

Equipment advances: Research into making NMRI more feasible for solids and large volume components has led to various suggestions, e.g. Magic-Angle NMRI (De Luca et al [61] and Cory et al [62]) NMRI by Multiple-Quantum Resonance (Garroway et al [63]) plus variations on the MREV-8 pulse sequence *.

However the main advances have been with the use of surface coils (Miller et al [64]). Since there is a limitation on the r.f. power available there is a severe restriction on the size of the r.f. coil that can be used in the probe. If the sample is compelled to fit inside the r.f. coil, the sample volume is severely constrained. One solution is to use a surface coil which will generate a sufficiently large B_1 field in a small region of the sample. For this application Miller used a 16 pulse pre-sequence of π-pulses with the narrow-line capabilities of the MREV-8 sequence. This gave a resolution of 1mm and a depth of signal of 8mm, which corresponds to the outer diameter of the coil divided by four.

Another step forward has been the use of liquid-state technology to image solids with spin-spin relaxation times as short as 0.5ms. Carpenter et al [65] have demonstrated that with a modified gradient system, standard NMR hardware

designed for the liquid-state can be used to image solid materials using liquid-state pulse sequences.

1.3.3. NMR Spectroscopy Experimentation

Bound and free moisture investigations: Ward et al [67] have examined how to distinguish between water available to the surroundings and that which was bound within the lattice. Most studies were carried out with Triaminotrinitrobenzene (TATB) which exhibits a broad 40kHz "Pake" doublet with a superimposed narrow "water" peak. Under high resolution the water peak can often be resolved into two peaks.

* *MREV-8: A multiple-pulse line narrowing technique [66]. These sequences utilise the fact that, when applied with suitable widths and delays, a series of pulses can average the dipolar interactions by re-orientating the spins. To a simple approximation, the sequences produce an averaging of the spin vectors in the rotating frame to the magic angle with respect to the applied field. The two most widely used sequences are a four-pulse sequence known as WAHUHA (after WAugh, HUber, and HAberlen) and an eight-pulse sequence known as MREV-8 (after Mansfield, Rhim, Ellerman and Vaughan). The WAHUHA sequence is :*

$$\left[t_D - \left(\frac{\pi}{2}\right)_x - t_D - \left(\frac{\pi}{2}\right)_{-y} - 2t_D - \left(\frac{\pi}{2}\right)_y - t_D - \left(\frac{\pi}{2}\right)_{-x} - t_D \right]$$

The cycle of four pulses separated by delays of t_D or $2t_D$ is repeated throughout the acquisition time, and the individual time domain data points are collected during one of the $2t_D$ delays. The spectral width is determined by the cycle time $6t_D$. The MREV-8 sequence uses pairs of WAHUHA cycles with phase shifts which serve to reduce sensitivity of the experiment to errors in pulse width, pulse phase, and radio frequency field inhomogeneity.

Matis et al [68] undertook experiments on wet samples of organic polymers. The results of the experimental investigation of a moist organic composite by high–resolution NMR and differential thermal analysis (DTA) indicate a change in the structure of the water, due to an interaction between the water molecules and the macromolecules when water is absorbed by the organic polymer. A percentage of the absorbed water molecules are strongly bound to the macromolecules but their mobility is very low and is not recorded by the NMR. As the moisture content of the composite increases, a signal due to water appears, the mobility of which is intermediate between strongly bound and free water molecules in the macrospace. This proportion of the molecules is represented in the NMR spectrum by a broadened and shifted line.

Batra and Graham [69] have suggested NMR as a means to non–destructively estimate quantitatively the moisture content in composite samples. Since the number of nuclei is proportional to the area under the NMR absorption curve, the moisture content in a given sample can be measured from the NMR spectra. A plot of NMR intensity versus moisture content can be used as a calibration curve

Jeong et al [70] have proposed that NMR detection of absorbed water may be a feasible method of detecting and locating impact damage in glass reinforced polymer (GRP) structures. GRP is difficult to inspect for damage since generally the damaged region occurs on the rear of the impacted component where it is least accessible. However, it has been noticed that the damaged regions absorb more water from a humid atmosphere than the undamaged regions.

With the practical case of a receiver coil on the front side and damage on the inaccessible back side, the spin signal is attenuated through the GRP. The measurements here show a broad maximum in sensitivity as a function of frequency.

Structural investigations: Cholli et al [31] using ^{13}C NMR spectra have characterised the different regions of composites. Studies have been carried out with coupling agents on the silica surfaces, and on the matrix by looking at the curing of epoxy resins with curing agents at elevated temperatures. Surface studies give an indication of the extent of the hydrolysis reaction. An experimental curve can be obtained, the deviation from the ideal decreasing as the extent of the reaction proceeds and approaches the ideal behaviour. One possible explanation for the deviation from the ideal are the changes in the physical state of the system during curing.

Tzou et al [71] have studied the structural development of high-speed poly(ethylene terephthalate) fibres using line-shape simulation of ^{13}C NMR. See also reference 72.

Relaxation phenomena and characterisation of cure: Cholli et al [31] also investigated relaxation phenomena. Solid-state ^{13}C NMR relaxation studies ($^{13}C\ T_{1\rho}$) indicate the effect of the presence of fibre on the ^{13}C relaxation times of the matrix. In principle, the $^{13}C\ T_{1\rho}$ measurements should distinguish between regions of different motional character in the composite polymeric materials. The shortening of the NMR relaxation times in the composite shows the presence of molecules that are highly constrained in their range of motions on or near to the surface.

Gasilova et al [73] have investigated the use of spectral and relaxation methods to provide information on the chemical reactions in the system, the phase structure, the molecular mobility of the components and the density and homogeneity of the network of cross-linked composites.

Composite properties: Weeding et al [29] have used an interpenetrating network theory, an extension of the chemical bonding theory, that states that the matrix can diffuse into the coupling agent interphase to form an entangled network. A detailed knowledge of chemical and structural changes that occur in the composite, especially the interface region, is of interest for the optimisation of composite

properties. Solid-state NMR is ideally suited to this task since it allows NDE of the environments of specific nuclei in the matrix and on the surface of the filler, i.e. in the interfacial region.

Weeding et al [30] have also investigated the effect on ^{13}C spectra of poly-amide-6 composite on the addition of fillers. It concluded that the ^{13}C MAS NMR spectra of the two composites are the same and do not contain signals from the additive.

Thermal degradation: The effects of thermal degradation have been studied using Celion 6000 carbon fibres in polyamide resin. The isothermal weight loss of the resin was correlated to changes observed in the spectra obtained by FT-IR and NMR spectroscopy. Intermediate oxidation products were not detected in the composite. After 1200 hours thermal degradation began with an associated weight loss [32].

1.3.4. NMR for Cure Monitoring

Jackson [74] has taken the work discussed in section 1.2.6.2. further by monitoring the cure of carbon-fibre reinforced epoxy resin. Experiments were carried out on a 20 ply {0, 90} sample made up from 10mm x 7mm sections and rolled samples made up from a 10mm wide strip, with the fibre direction parallel to the x-axis of the formed 10mm diameter cylinder.

The multi-laminate sample was slowly heated to 90 °C, the sample was allowed to equilibriate and then images were taken as a function of time. A series of images were taken for approximately 3 minutes and 42 seconds.

The rolled sample was heated to 90 °C and again allowed to equilibriate before images were taken every 2 to 4 minutes to follow the progression of the cure. After 90 minutes no further images could be obtained.

Jackson then went on to conclude that the preliminary results indicated the great potential of NMR imaging with regard to the study of curing epoxy systems. Investigations are now to be carried out by Jackson to include temperatures up to 200 °C , pressures up to 5kg/cm^2 and an increased sample size of 200mm x 100mm x 5mm by using wide bore magnet technology. Such an increase in sample size will allow the mechanical properties of test samples to be investigated.

Jackson et al [75] have investigated the cure of carbon fibre composites. At room temperature, the epoxy used has a T_2 value too short to allow imaging. On raising the measurement temperature from 20 °C to 100 °C, the T_2 is found to increase from 160μs to 25ms. By performing T_2 measurements in the first five minutes after reaching the appropriate temperature it is possible to neglect the influence of reactive cross-linking on the results. During this early part of the cure cycle, the polymer viscosity is determined only by the temperature of the sample, and the increasing T_2 reflects the decreasing viscosity of the sample as the temperature is raised. Therefore since the polymer viscosity is known at particular temperatures it is also possible to relate the polymer T_2 to viscosity. See also reference 76.

Haw et al [77] have used NMR with magic-angle spinning (MAS) to study in-situ cure of an epoxy resin. Since MAS is a solid-state technique the sample can be monitored well into the cure. The study demonstrates that MAS can be used throughout the entire curing process without loss of material or rotor instabilities. With such a strategy, the loss of signal caused by the progression of the resin from a "solution" to a "solid" may be compensated for (in part) by a switch from NMR excitation techniques appropriate for solutions to techniques used in the study of solid samples e.g. CP. This study also underscores several important limitations of NMR studies of the curing process in thermosetting resins and suggests experimental strategies for overcoming these limitations. The spectra obtained in this preliminary study provide little, if any, insight into the details of the curing process, largely due to inadequate resolution and signal-to-noise ratio per unit time. This technique can only be used on small samples and so could not strictly speaking

be an on–line process but could be used for quality control on test samples. See also references 32, 78 and 79.

Lizak [80] applied NMR to non–destructively examine advanced materials. The main aim of the project was to follow the cure of epoxy resin and carbon fibre / epoxy prepreg. In this way improperly cured materials could be removed from any production process. T_2^* and T_{1D} (relaxation time for dipolar order) were found to be the most effective way of monitoring cure. This technique can also be used with low–field magnets therefore it is easily transferable to a factory setting especially since the magnetic field homogeneity requirements are modest.

Bergmann et al [79] have made an investigation of the hardening process in unsaturated polyester resins with the aid of NMR measurements. Three kinds of protons could easily be distinguished: strongly mobile which could be attributed primarily to the styrene not yet included in the polymerisation; more weakly mobile, which corresponds essentially to the uncross–linked; and non mobile, which corresponds to regions already cross–linked, solidified and glass–like. For the specimens that were studied that had a T_g above room temperature, 7–18% of the protons are still mobile after hardening at room temperature. The mobile portion falls as a result of post–curing at an elevated temperature to a content of 3–7%, so that the mechanical strength of the sample has increased. However, if T_g lies below room temperature, then the mobile portion is considerably greater and a post–hardening process causes practically no change.

2.0. EXPERIMENTAL METHODS

2.1. Introduction

The main aim of the experimental programme was to investigate whether a low–field NMR analyser could be used as a curemeter. This was to be accomplished by comparing the NMR data to that obtained from a standard laboratory high–field NMR spectrometer and also that from a vibrating needle curemeter. The extent of cure that the above mentioned techniques could monitor was validated with Barcol hardness measurements.

2.2. The NMR Hardware

The basic NMR hardware consists of a set of field gradient coils mounted inside the bore of the magnet and inside these sits the NMR probe. The probe contains the apparatus for transmitting pulses to the sample and receiving the NMR signals they produce. For a more detailed explanation see reference 23.

The experimentation required the use of two different types of analytical NMR techniques: an NMR analyser designed to perform routine quality control tasks within industry which can also be programmable (the Oxford QP) and an NMR spectrometer designed for research and capable of a variety of pre–programmed experiments (the Jeol EX270 NMR spectrometer).

2.2.1. The Oxford QP (Low–Field NMR Analyser)

The QP is constructed with a thermally stabilised (at 40 °C) permanent magnet with a 0.47 Tesla field which observes protons at 20MHz (see specification in Appendix 1.0, section 1.1.).

The QP has been designed in such a way that by adding a personal computer with some extra software it will function in a similar way to a high-resolution NMR spectrometer. However, no spectral information is given and data derived by this method, e.g. relaxation time data, is for the overall sample and not, as is usually the case, for individual chemical environments. The QP has its own pulse-programming language and data manipulation tools. Applications developed in this way can be installed on the QP as menu items for routine use. A range of specialised routines are included in the software these include T_1 relaxation times by inversion recovery [66] and T_2 relaxation times by spin-echoes [23] (including CPMG see section 5.2.) or solid echoes [81].

2.2.2. The Jeol EX270 NMR Spectrometer (High-Field Analyser)

The EX270 NMR spectrometer contains a liquid helium cooled super-conducting magnet which generates a field of 6.34 Tesla which causes ^{1}H nuclei to resonate at 270 MHz and ^{13}C nuclei to resonate at 68 MHz (see appendix 1.0., section 1.2.). The EX270 has a multi-nuclear facility for observing nuclei such as ^{29}Si and ^{31}P. Standard research measurement modes have been incorporated into the software which include T_1 and T_2 relaxation time measurements, INEPT, DEPT, difference NOE, 2D NMR ^{1}H-^{1}H or ^{1}H-^{13}C shift correlation, ^{1}H-^{1}H or ^{1}H-^{13}C J-spectroscopy and ^{1}H-^{1}H NOE correlation (for definitions of these techniques see reference 23).

2.3. The Curemeter Hardware

Viscosity is probably the physical property most widely monitored for the study of the cure of resin mixes. A traditional parallel plate rheometer can only monitor the initial stages of the cure since the resin needs to be removed from the rheometer before it gels. Therefore a curemeter has been used to monitor the cure of the initially free-flowing resin mix. However, a curing resin mix develops elasticity as

the molecular network builds up. Therefore, a simple viscometer cannot monitor the extent of cure reliably beyond the earliest stages.

Due to this a complete cure profile, such as that that can be obtained for vulcanised rubber, could be difficult to obtain since the early curemeters were not designed to handle a free– flowing liquid mix. Initially the first commercial curemeters were of the oscillating disk type the disks oscillating at 3 cycles per minute [48].

2.3.1. Vibrating needle curemeter (VNC)

The VNC monitors the increase in the viscosity of curing formulations before gelation; subsequent changes in the stiffness of the gelled formulation can also be measured. This is achieved by suspending a steel needle into the formulation. The needle is vibrated vertically by a small electro–dynamic vibrator driven by a low power amplifier oscillator (see figure 2.1.). Resistance to the needle's movement is ultimately recorded in the software or on a chart recorder. The VNC can be operated at a wide variety of frequencies however the shape of the trace is dependent on the frequency (see appendix 1.0., section 1.3.).

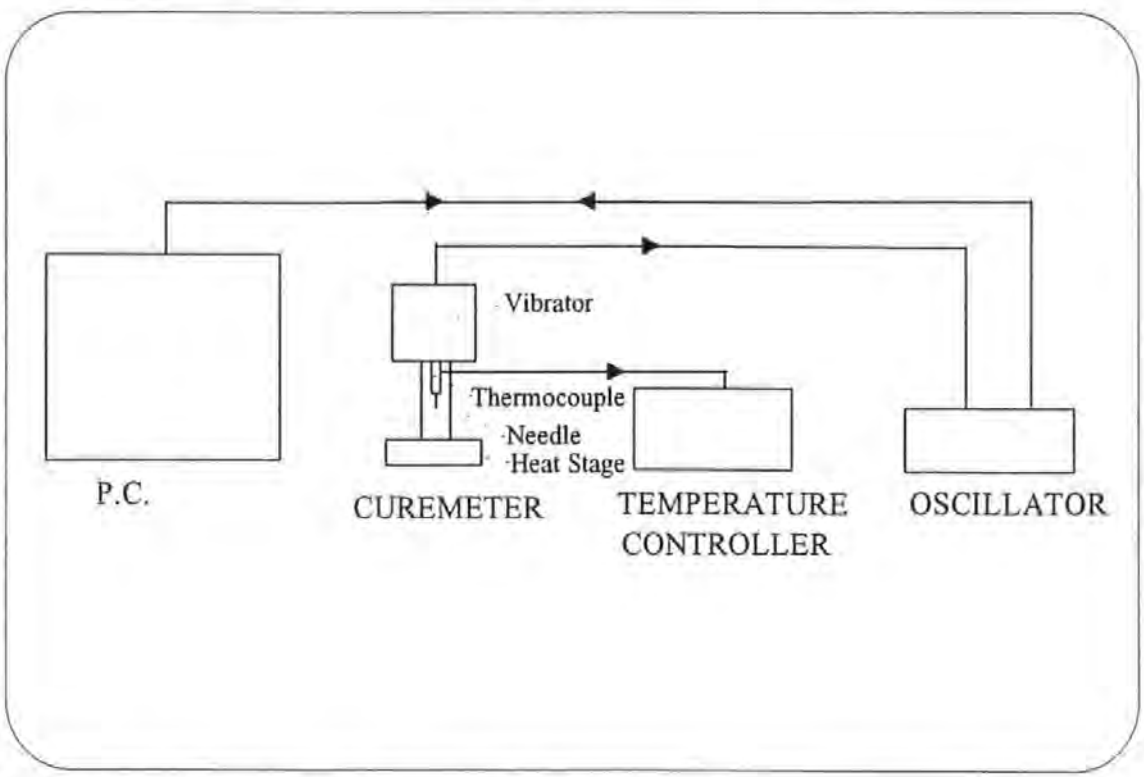

Figure 2.1. Schematic of vibrating needle curemeter.

2.4. Physical Properties Testing

The physical properties of the resin and resin / fibre mix can be most easily measured by use of a hardness test. For this a hand held Barcol hardness test device was used. (Manufactured by Barber Colman Company). The readings obtained from the device were verified using calibration disks as supplied by the manufacturer.

2.4.1. Barcol hardness

The Barcol hardness impressor is a hand held device and is designed to be used on fabricated parts and individual test specimens for production control purposes (see appendix 1.0. section 1.4.) The apparatus consists of the following parts [82] (see figure 2.2.):

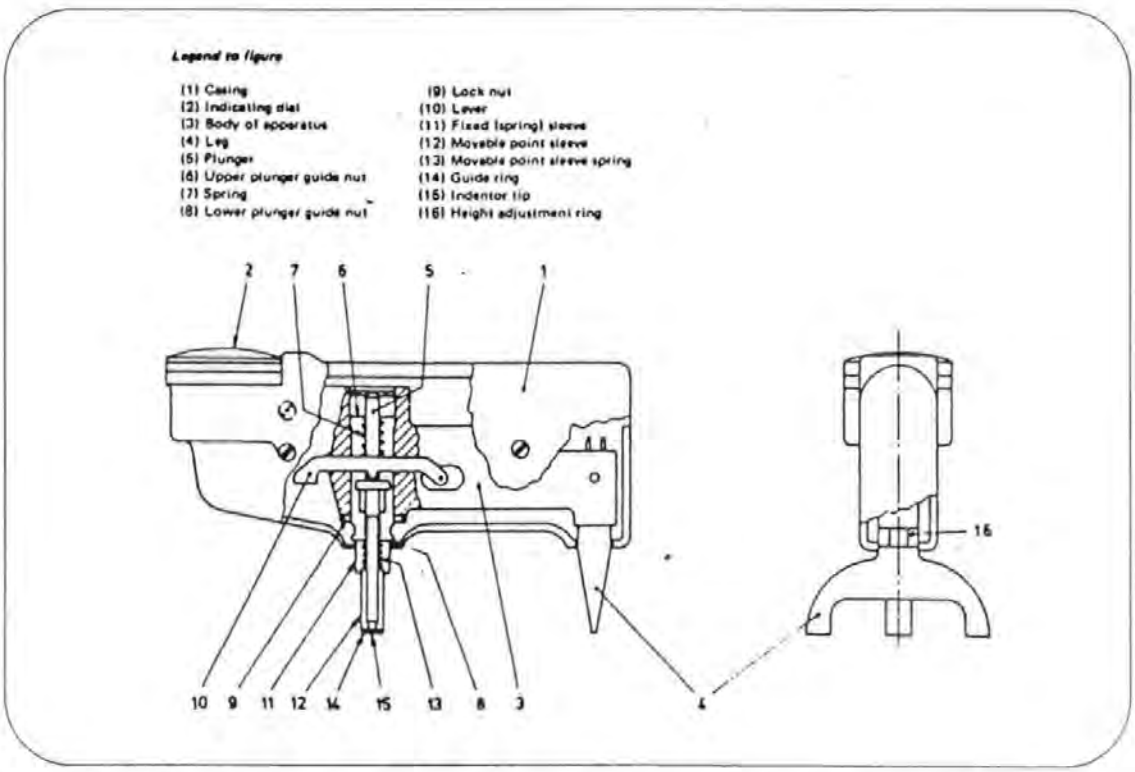

Figure 2.2. General construction of Barcol impressor. (Extract from BS 2782: part 10: Method 1001: 1977 EN99).

1. Indentor: This consists of a hardened steel truncated cone having an angle of 26° with a flat tip of diameter 0.157mm. This fits into a hollow spindle and is held down by a spring-loaded plunger.
2. Indicating device: The indicating dial has 100 divisions, each representing a penetration depth of 0.0076mm. The dial reads directly in Barcol hardness units, the higher the reading the harder the material.

The dimensions of the test specimens need to be at least 1.5mm thick and large enough to ensure a minimum distance of 3mm in any direction from the indentor tip to the edge of the specimen or to another earlier test position.

2.4.2 Burn-off Test

Burn-off tests were carried out in order to establish the actual volume fraction of resin used during the volume fraction experimentation on the Oxford QP NMR analyser and the vibrating needle curemeter, The actual volume fraction used is termed V_{f-expt}.

Samples were placed in a crucible of known weight and then weighed . They were then placed in a furnace at 550°C for approximately 30 minutes until there was no further weight change and then allowed to cool in the furnace. The crucible and remaining glass fibre were then re-weighed.

The volume fraction can then be derived as follows:

$$\text{Actual volume fraction, } V_{f-expt} = \frac{\text{weight of glass fibre/density of glass fibre}}{\text{volume of sample}} \times 100$$

This simple test was carried out for all composite samples for the Oxford QP NMR analyser and VNC volume fraction experimentation.

2.5. Methodology

A Ciba–Geigy – Araldite MY750 resin system was chosen due to its importance in the aerospace industry. This is a system that will gel between room temperature and 100 °C, the gel time reducing as the temperature rises.

MY750 is a liquid epoxy resin (Bisphenol–A–Epichlorohydrin) of medium viscosity, which is mixed with HY917 a low viscosity liquid hardener (methyltetrahydrophthalic anhydride). The latter is required to produce the cross–linking in the final resin. To adjust the balance between usable life and cure time a small quantity of DY070 a catalyst, commonly called an accelerator, (1–methylimidazole) is usually added.

The experimental programme can be divided into six sections:

1. Analysis of components of resin – for familiarisation of individual component spectra obtained by NMR and infra–red (IR.) spectroscopy (a Perkin Elmer Fourier Transform Infra–red (FT–IR) spectrometer (model 1720) was used) and to ascertain the cross–linking reaction that takes place.

2. Analysis of NMR spectra during cure – A sample of resin was allowed to cure at 40 °C while the resin was monitored every 10 minutes using high–field NMR.

3. Analysis of NMR relaxation times – Relaxation times during a 40 °C gel and cure were monitored by the QP (which gave relaxation times for the system as a whole) and the Jeol EX270 (which gives relaxation times for each individual component). The relaxation times were then compared to the cure profile (see item 5.

4. Analysis of free induction decay data – various cure schedules for resin and resin / fibre samples were monitored on the QP.

5. Analysis of cure profile – using the VNC to gain cure profiles for various cure

schedules for resin and resin / fibre samples.

6. Analysis of hardness of resin from "point of cure" – resin samples of the same dimensions as those cured during the QP experimentation, were hardness tested to ascertain the mechanical properties of the resin throughout cure.

7. The above six experiments were then repeated for 60°C, 80°C and where possible 100°C cure cycles

So that the data from each of these experiments could be reliably compared it was required that the sample geometry should be the same when ever possible. It should be noted that the Jeol EX270 did require much smaller diameter sample tubes and therefore the volume of resin monitored was different. However the experiments performed using the QP, VNC and Barcol hardness impressor all used the same volume and geometry. The largest sample tube for the QP was used and therefore this defined the sample size for other experiments. The sample diameter was 18mm and the length of the column of resin required was 40mm. To create this sample size for the VNC a brass mould was manufactured. At 40 °C the heat conduction through the brass mould from the VNC heat plate underneath was sufficient to maintain a uniform temperature distribution. However at 80 °C or 100 °C this was not found to be sufficient and so the addition of a heating coil (fitting directly to the outside of the brass mould) was required.

The Oxford QP was used to take FID and CPMG acquisitions at the start of cure and every subsequent 30 minutes at 40 °C, every 15 minutes for the 60 °C and 80 °C test runs and every 10 minutes for the 100 °C run. To facilitate this a programme was written (see appendix 2).

For the QP tests carried out at temperatures above 40 °C two or three samples were placed in an oven (heated to the required temperature) and then placed in the QP alternately for the 1 minute data acquisition.

2.6. Experimental Error

The term error signifies a deviation of the result from some "true" value. Often the true value is not known and only estimates of the errors inherent in the experiment can be considered. A repetition of the experiment may give results that differ from the first set. This difference can be expressed as a discrepancy between the two results. The fact that a discrepancy arises is due to results being determined with a given uncertainty.

Experimental error could have arisen from a number of areas due to human and instrumental error:

1. Temperature control. Oven varied by approximately ±5°C,
2. Errors in statistical analysis using the SPSS PC+ and Origin packages, required best fit by eye
3. Errors in the curemeter software.

The samples for the Oxford QP NMR analyser tests were heated in an oven and only transferred to the QP for the duration of the data acquisition i.e. 40 seconds. During the experiment the temperature of the oven varied by approximately ±5°C. The variation of the temperature will affect the rate of cure that is taking place and the shape of the FID. This will of course also affect the percentage solid which was calculated from the FID data.

The variation in oven temperature would also have affected the hardness tests at 40 °C, 60 °C, 80 °C and 100 °C. In the case of the Barcol hardness the temperature of the specimen when it was tested would also effect the readings. Barcol hardness testing requires the specimen to be at room temperature. Therefore each specimen was cooled in cold water before testing took place.

On weighing the resin components, hardener and accelerator percentages varied by ±2% and ±0.1% respectively. Too much hardener would give an excess of hardener in the cured component, while too little hardener would have meant that not all of the cross-linking sites would have been utilised. However, too much accelerator

would actually increase the rate of cure for all cure temperatures, while too little accelerator would have had the effect that the resin had cured more slowly.

The effects of accelerator content and oven temperature can be seen in figure 2.3. As the temperature increases the time for the resin to gel decreases. While as the accelerator content increases to 2% so does the gel time. The effect of an accelerator content that is more than 2% is not shown in the current data.

The curemeter software reproduced the cure profile and from this calculated the times for 10%, 80%, 95% and 100% cured and the voltages at 10% and 95% cured . However for cure temperatures of 60°C or more the resin viscosity decreased initially which confused the software into thinking this was the part of the graph that calculations were required. For these cases the calculations were done by hand, see figure 2.4b. Therefore errors will have occurred throughout this process and so it is unlikely that the VNC cure percentages correspond exactly to the QP data. The times to 10%, 80%, 95% and 100% cure can be calculated as shown in figure 2.5.

To calculate the transverse relaxation times from the CPMG data the statistical package SPSS PC+ was used. A graph of the natural logarithm of the signal intensity versus time was plotted which gave a gradient equal to the following:

$$\text{Gradient} = -\frac{1}{T_2}$$

giving a T_2 value for a specific time in the cure. The standard error limits (σ) for these T_2 values were also calculated.

A plot of $\ln(T_2)$ vs time of cure could then be plotted incorporating into these error limits of (2σ), meaning that there was a 95% chance for the point to lie within 2σ [83 and 84] of the calculated point (see figure 2.6).

The standard error limits are calculated with respect to the number of initial points giving a straight line to calculate the gradient and the number of further points that are not used for this calculation. As the relaxation time became quicker fewer points

Accelerator content varied by 2pbw, 1pbw, 0.5pbw.

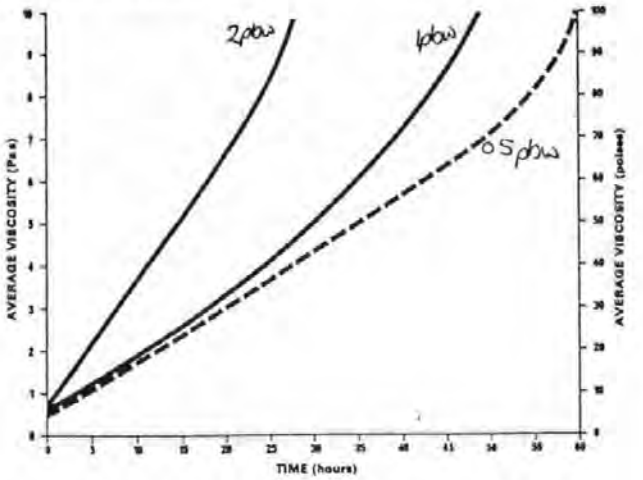

a) Viscosity vs. time at 25 °C

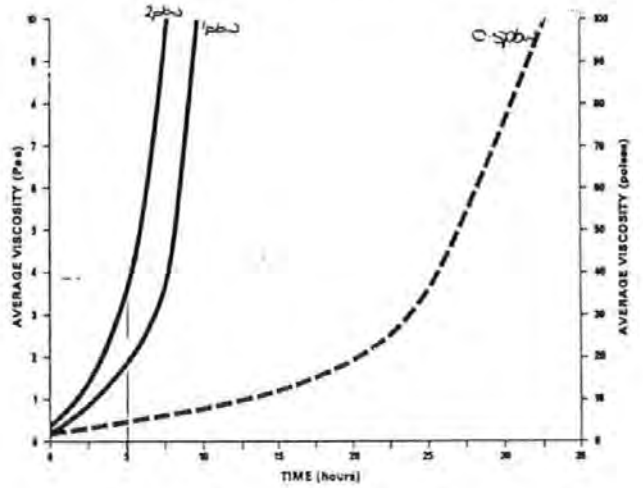

b) Viscosity vs. time at 40 °C

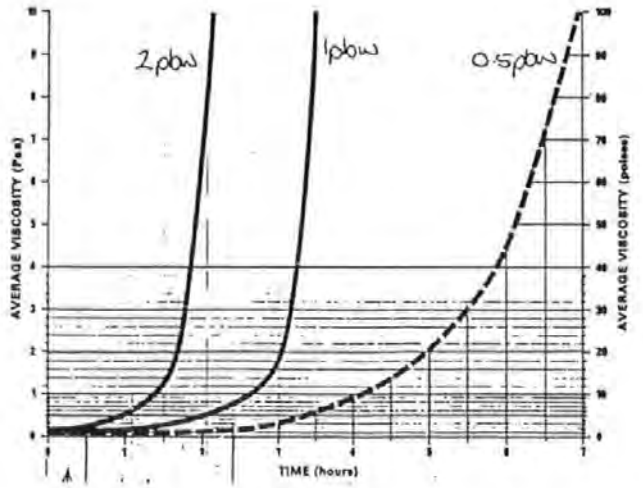

c) Viscosity vs. time at 60 °C

Figure 2.3. The effects of cure temperature and accelerator content on the viscosity of the resin mix. Extract from Ciba-Geigy Instruction Sheet number C.36b. The quantities used for the viscosity data were 500gm, larger volumes and an exothermic reaction would give steeper viscosity curves.

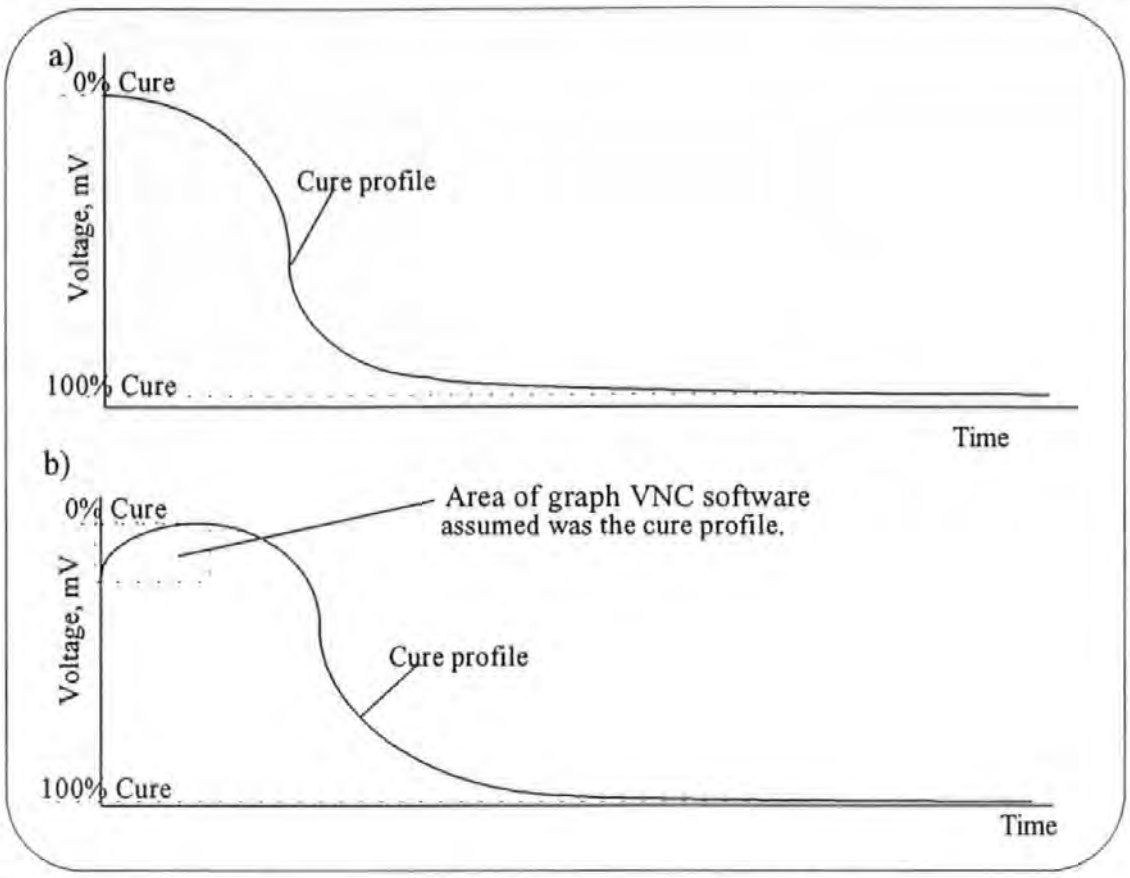

Figure 2.4. Examples of cure profiles as obtained with the VNC.

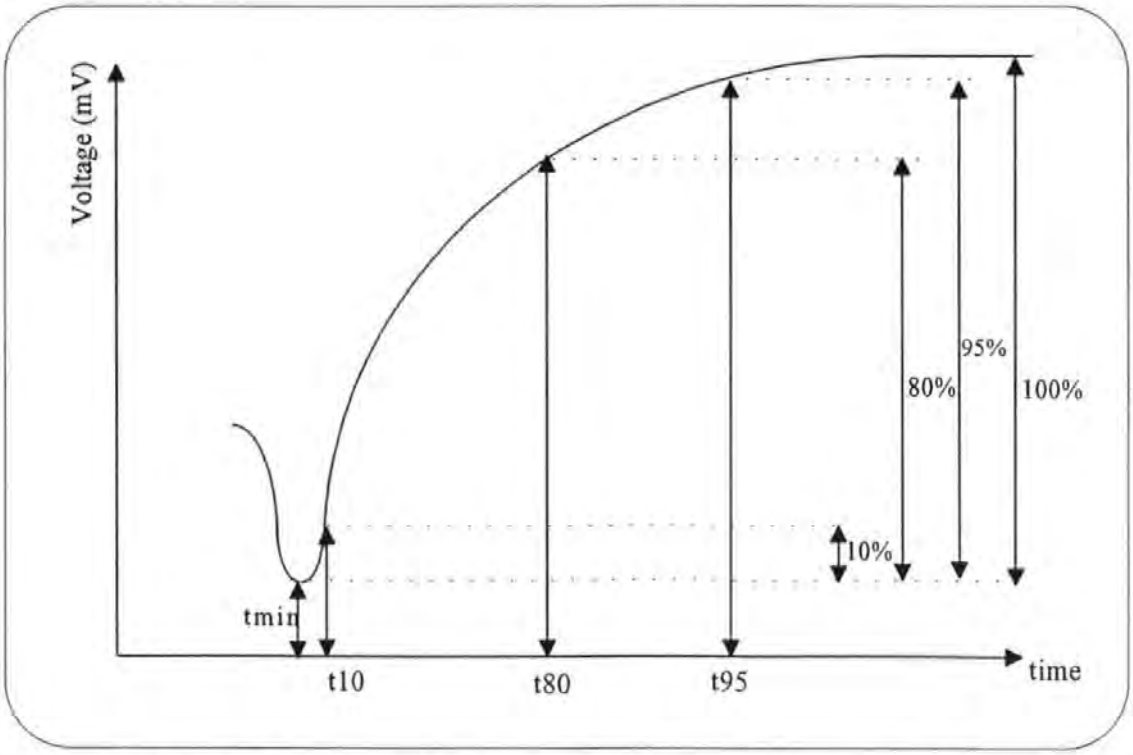

Figure 2.5. A typical VNC trace to demonstrate times for 10%, 80%, 95% and 100% cured.

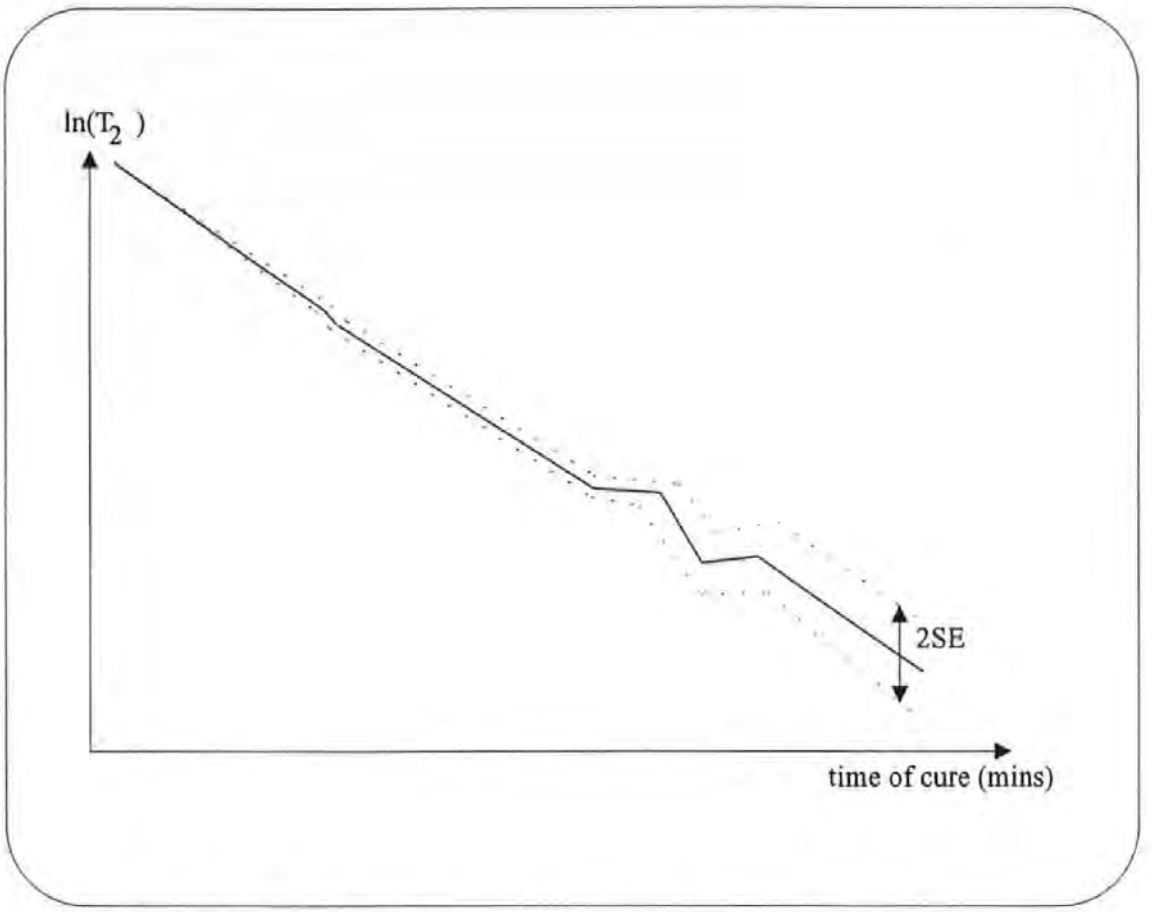

Figure 2.6. Example of $\ln(T_2)$ vs time of cure curve illustrating error limits used.

constituted the straight line the gradient was calculated from, and so the standard error limits increased.

The experimental results will be presented in chapters 4 to 9 while chapters 3 and 4 will discuss resin chemistry and the reaction steps undertaken during the curing process.

3.0. GENERAL RESIN CURE CHEMISTRY

3.1. Introduction

The term *RESIN* is taken to refer to any material whose molecules are polymers, however originally the term was restricted to natural secretions usually from coniferous trees which were used mainly in surface coatings. Later similar synthetic substances were included. Generally the term is now used to indicate a forerunner to a cross–linked polymeric material, e.g. epoxy or phenolic resin.

A great variety of polymeric materials of many different types are used in countless technological applications. These materials are commonly classified as adhesives, paints, plastics and rubbers. The common link between the applications is that all the polymers are of a high molecular weight. It is the molecular weight that determines the physical properties of the individual polymeric material e.g. strength of intermolecular forces, regularity of polymer structure and flexibility of the polymer molecule.

This chapter will now give a brief introduction to general resin chemistry for the following three resin types epoxy, polyester and phenolic.

3.2. Epoxy Resin Chemistry

3.2.1. Components

Epoxies are defined as cross–linking polymers in which the cross–linking is derived from reactions of the epoxy group

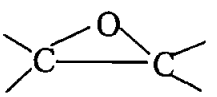

Despite their relatively high cost compared to other resins, epoxies are now firmly established in a number of significant industrial applications. They are primarily used in surface coatings, encapsulation of electronic components, adhesives, castings and laminates. The interest in epoxy resins originated due to the wide variety of chemical reactions that can be used for curing and the many different properties that result [85]. The chemistry is unique among thermosetting resins. No volatiles are given off during cure therefore minimum pressures are required for fabrication techniques. There is little shrinkage therefore reducing stresses in the final part.

The majority of commercial epoxy resins are prepared by condensing 2,2–bis(4–hydroxyphenyl)propane (bisphenol A) with epichlorhydrin [86, 87]. These are mixed at 60 °C without stirring and solid sodium hydroxide is added. Since the reaction is exothermic cooling is required to keep the temperature at 60 °C. Excess epichlorhydrin can then be distilled off leaving behind epoxy resin with sodium chloride. The latter can easily be removed by filtration once toluene has been added to facilitate this. The toluene is removed by distillation under reduced pressure and then the resin is heated to 150 °C at 5 mm Hg of pressure to remove traces of volatile matter. The final step is important since the presence of volatiles may lead to bubble formation when the resin is used. The resin can be clarified by passage through a fine filter.

For more "solid" epoxy resins the above process is modified slightly by making the reaction temperature 100 °C and slowly adding aqueous sodium hydroxide with vigorous stirring. When the reaction is complete an emulsion of approximately 30% water in resin rises to the top of the reaction mixture. The lower layer of brine is removed and the resinous layer is coagulated and washed with hot water. The resin is heated at 150 °C under reduced pressure to remove water, clarified by passage through a filter and then allowed to solidify.

The general reaction for an epoxy resin based on bisphenol A and epichlorhydrin is as follows:

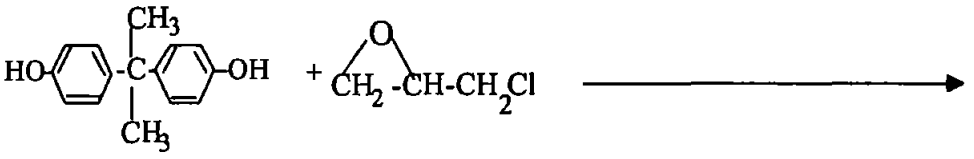

Bisphenol A Epichlorhydrin

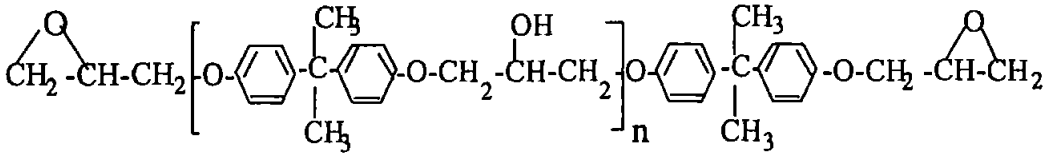

Compounds such as this are also called diglycidyl ethers since they contain two glycidyl ether groups per molecule which are:

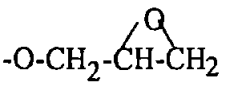

The value of n is determined by the molar ratio of the reactants; the nearer the ratio is to unity the higher the molecular weight of the product.

3.2.2. Cross-linking agents (Hardeners)

The bisphenol A-epichlorhydrin resins produced by the method described previously cannot be cross-linked at a reasonable rate by heat alone therefore a cross-linking agent or hardener is added. Most of the hardeners in common use can be classified into three groups which are tertiary amines, polyfunctional amines and acid anhydrides.

Tertiary Amines: The reaction between an epoxy resin and a tertiary amine (R_3N) is thought to proceed by the following steps:

1

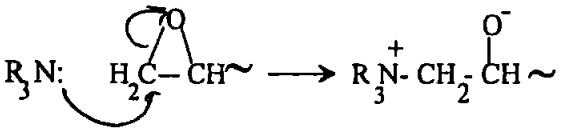

2

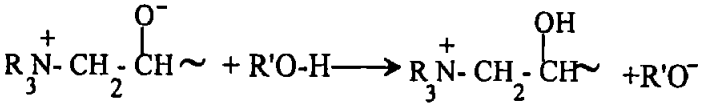

or

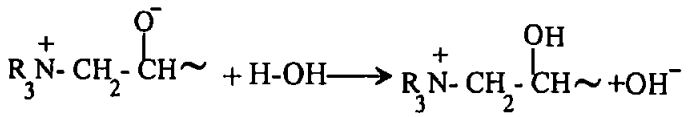

The proton donor may either be the curing agent itself or water present as an impurity. As shown above, the resulting by-product anion will initiate polymerisation through the epoxy groups as follows.

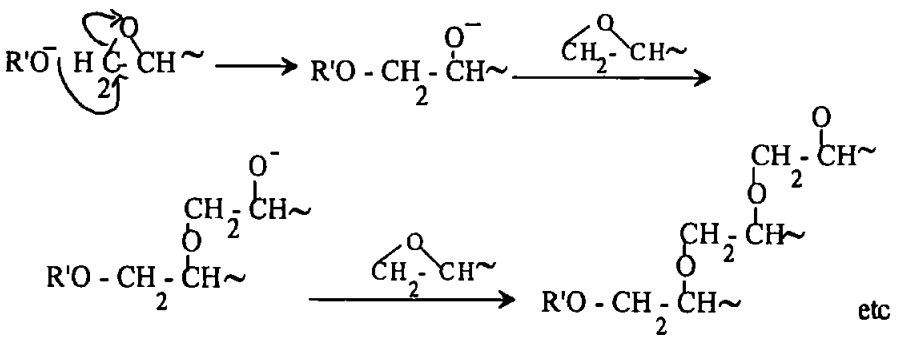

Since bisphenol A-epichlorhydrin resins have epoxy groups at each end of the polymer the above scheme results in the formation of a cross-linked polymeric structure.

Tertiary amines are commonly referred to as "catalytic" curing agents because they cause cross-linking directly through the epoxy groups as opposed to other hardeners that function by providing intervening groups through which epoxy groups are linked to one another.

Polyfunctional Amines: Aliphatic and aromatic compounds have at least three active hydrogen atoms present in primary and/or secondary amine groups and are used as curing agents for epoxy resins. The reaction between an epoxy resin and a primary amine (RNH_2) may be written simply as:

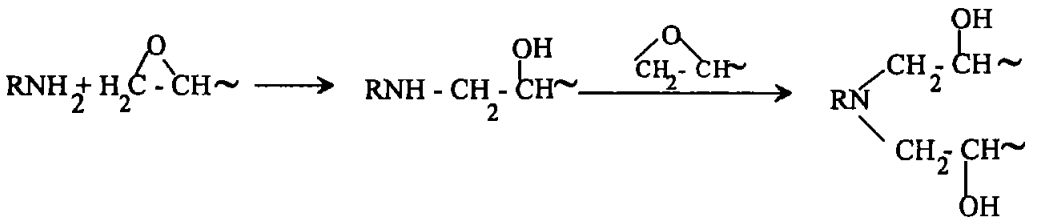

There is evidence to suggest that the reaction requires the presence of a proton–donor, either hydroxy groups present in the resin or traces of water [86]. These compounds aid the opening of the epoxy ring.

Aliphatic amines provide fast cures and are effective at room temperature. The aromatic amines are less reactive and give products with higher heat distortion temperatures. Polyfunctional amines are widely used in adhesive, casting and laminating applications.

Acid Anhydrides: The relation between an acid anhydride and an epoxy resin is complex and several different reactions could be involved, the relative extent of which may be affected by the conditions of the cure.

The cross linking reaction that takes place during cure can be divided into two types of reactions [86]: reactions of the anhydride group and reactions of the epoxy group.

Reactions of the anhydride group

The anhydride ring may be opened to produce one or two carboxy groups by reacting with: water (since the anhydride is hydroscopic there may be traces present) or hydroxy groups, present as pendant groups in the original resin.

1.a.

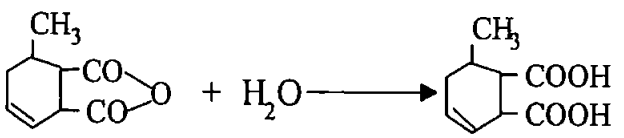

1.b. 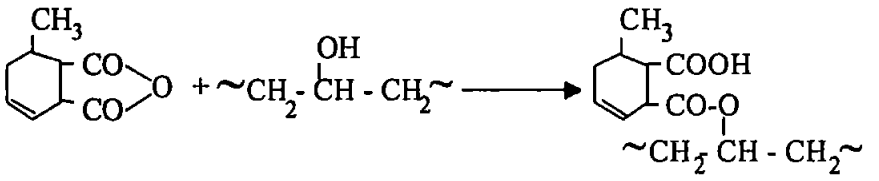

The reaction between an epoxy resin and an acid anhydride will be discussed in more detail in the next chapter.

Reactions of the Epoxy Group

The epoxy ring may be opened with:

a. carboxy groups formed by reactions 1a or 1b above, or
b. hydroxy groups (which may be present in the original resin or produced by reaction 2.a. below.

2a 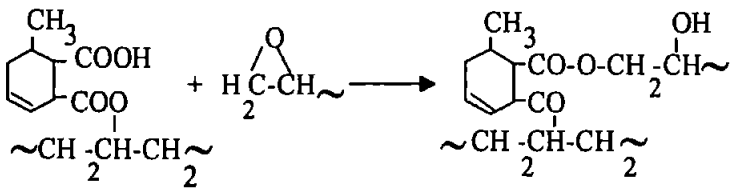

2b 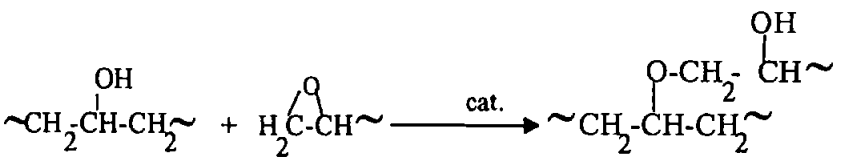

where the catalyst is a proton donor, H^+.

3.3 Polyester Resin Chemistry

3.3.1. Components

Polyester resins are commonly produced from a phthalic acid (isophthalic or orthophthalic) the chemical formulae for which are as follows

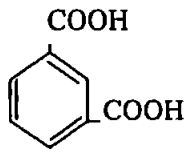

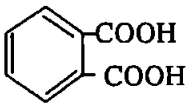

isophthalic acid
(1,3–benzene dicarboxylic acid)

orthophthalic acid
(1,2–benzene dicarboxylic acid)

Either of these compounds will form an ester by reacting with a diol e.g. propylene glycol (1,2–dihydroxyglycol), as seen below.

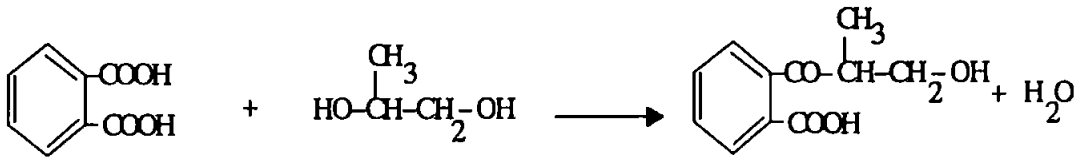

Therefore the reaction to give a saturated linear polyester is as follows.

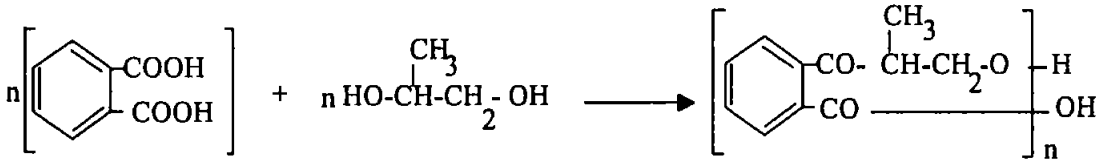

It is possible to cross–link saturated linear polyester chains directly to one another, however this is slow and a low degree of cross–linking is achieved. These limitations are overcome by the introduction of a cross–linking agent.

3.3.2. Cross–linking agents (Hardeners)

The materials most commonly used to cross–link unsaturated linear polyesters are vinyl monomers (e.g. styrene (ethylene benzene)). The addition of the liquid vinyl monomer to the polymer leads to a reduction in viscosity and this facilitates the impregnation of glass–fibre in the preparation of laminates.

Cross–linking takes place at the unsaturated sites on the polyester molecule. The reaction is a free radical reaction and requires the use of an initiating system to start.

The initiating systems that are effective at room temperature are normally mixtures of a peroxy compound and a catalyst (accelerator). In the presence of the catalyst the peroxy compound rapidly decomposes, without the application of heat, into free radicals.

The peroxy material commonly used is methyl ethyl ketone peroxide (MEKP). This material is not a single compound and has a variable composition which is dependent on its manufacture. The main compounds of commercial MEKP are the following.

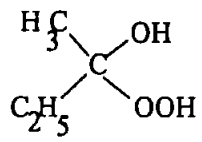

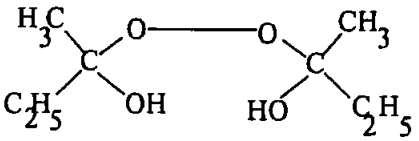

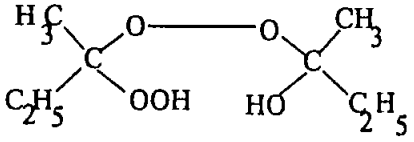

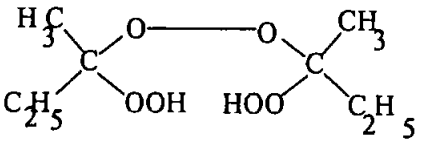

The most common accelerators for MEKP are salts of metals which exhibit more than one valency. The most widely used metal of this kind is Cobalt (Co). In order to be effective as an accelerator a metal salt (e.g. cobalt napthalene) must be soluble in the polyester resin. The decomposition of a hydroperoxide (ROOH) by such a salt to give free radicals proceeds according to the following reaction.

$$ROOH + Co^{++} \longrightarrow RO\cdot + OH^{-} + Co^{+++}$$

$$ROOH + Co^{+++} \longrightarrow ROO\cdot + H^{+} + Co^{++}$$

Where RO•and ROO• are the free radicals.

This cycle is repeated until all the hydroperoxide has been decomposed. Cobalt naphthalene – methyl ethyl ketone peroxide systems are extensively used in the

production of large glass fibre laminates made by hand lay–up and cured at room temperature.

3.4. Phenolic Resin Chemistry

3.4.1. Raw Materials

Phenolic resin is produced by the reaction of a phenol and an aldehyde in the presence of an acid or a base. The nature of the product is greatly dependent on the type of catalyst and the mole ratio of the reactants. Cresols (methylphenols) are used for the production of acid–resistant grades of resin, cresol has the following structure and can be ortho, meta or para.

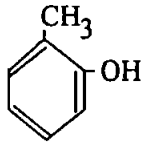

ortho–cresol

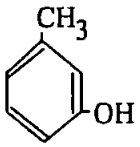

meta–cresol

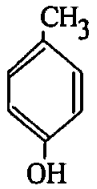

para–cresol

The initial step in the reaction between phenol and an aldehyde (e.g. formaldehyde) is the formation of addition compounds known as methylol derivatives, the reaction taking place at the ortho or para position, see below. These products may be considered the monomers for subsequent polymerisation. The best conditions for this reaction to take place are neutral or alkaline environments.

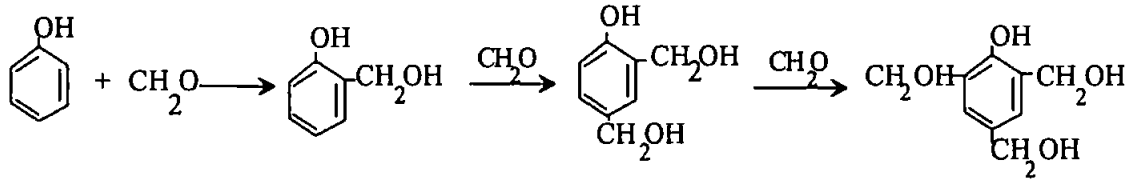

In the presence of acid catalysts, and with the molar ratio of formaldehyde to phenol less than one, the methylol derivatives condense with phenol to form firstly

dihydroxydiphenol methane and then on further condensation and methylene bridge formation, linear low polymers (called novolacs) with the following structure are formed. Ortho and para links occur at random.

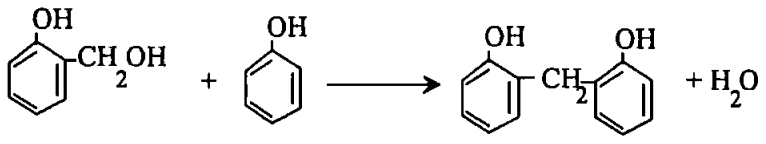

dihydroxydiphenol methane

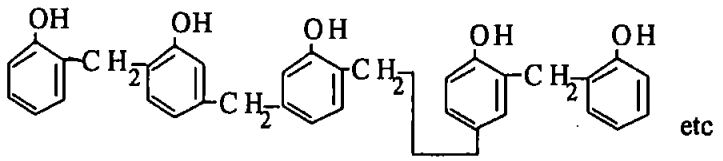

Novolac Structure.

These materials do not react further to give cross–linked resins but require a reaction with more formaldehyde to raise the mole ratio with phenol to above unity, usually 1 mole of phenol to 1.5 moles of aldehyde. The cross–linked structure is as follows.

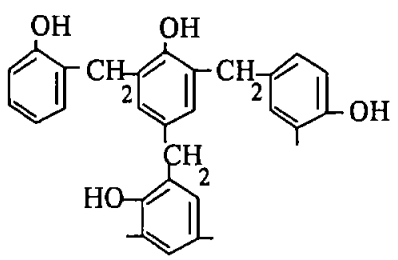

4.0. MECHANISM OF CURE

4.1. Introduction

Samples of the individual components of the MY750 resin system were analysed using NMR and IR spectroscopy.

4.2. Analysis of Components of Resin [86, 88]

4.2.1. MY750–Bisphenol A–Epichloridrin

Chemical formula:

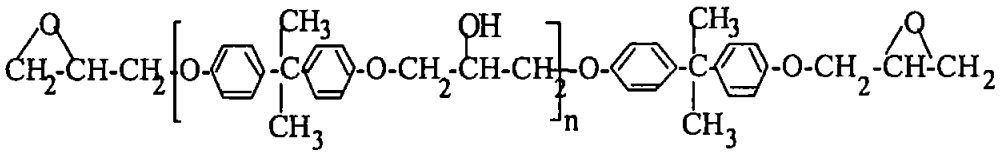

Commercial liquid epoxy resins based on the above structure have molecular weights of about 400. By the integration of the peaks on the NMR ^1H spectrum n can be estimated. This is done by taking the ratio of the epoxy end groups ($CH_2OCH–$) to the methyl groups ($CH_3–$) within the molecule (see figure 4.1.) and doing the following calculation.

i.e. $n = CH_3– : CH_2OCH–$

$CH_3– : CH_2OCH– = 4.000:2.692$

therefore, $n \approx 1$

Giving a molecular weight of approximately 400

4.2.2. HY917 – Methyltetrahydrophthalic Anhydride

Chemical formula:

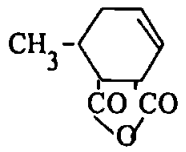

From the NMR spectrum, figure 4.2.a., it can be seen that HY917 consists of more than the anhydride. These peaks could be attributed to water ingress, since the anhydride is hydroscopic. Another reason could be that the anhydride reacts with the solvent, $CDCl_3$, which was added to gain a deuterium lock.

To clarify if there was a reaction between the solvent and the anhydride an infra–red (IR) spectrum of the anhydride alone was also taken, see figure 4.2.b. An IR spectrum does not need the presence of the solvent therefore any extra peaks could only be attributed to the hydroscopic effects of the anhydride, or that the hardener was not 100 percent pure.

Extra peaks again appeared in the anhydride FT–IR spectrum and from this the peaks were attributed to be from an amine compound, possibly a primary or secondary aliphatic amine since these are both known as cross–linking agents for an epoxy system.

An amine may have been added as the anhydride reaction can be sluggish, even so it is not usual to have more than one hardener. However, the manufacturers have given their assurance that there are only 10% impurities in the hardener and that the effect of these impurities on the cross–linking reaction is negligible.

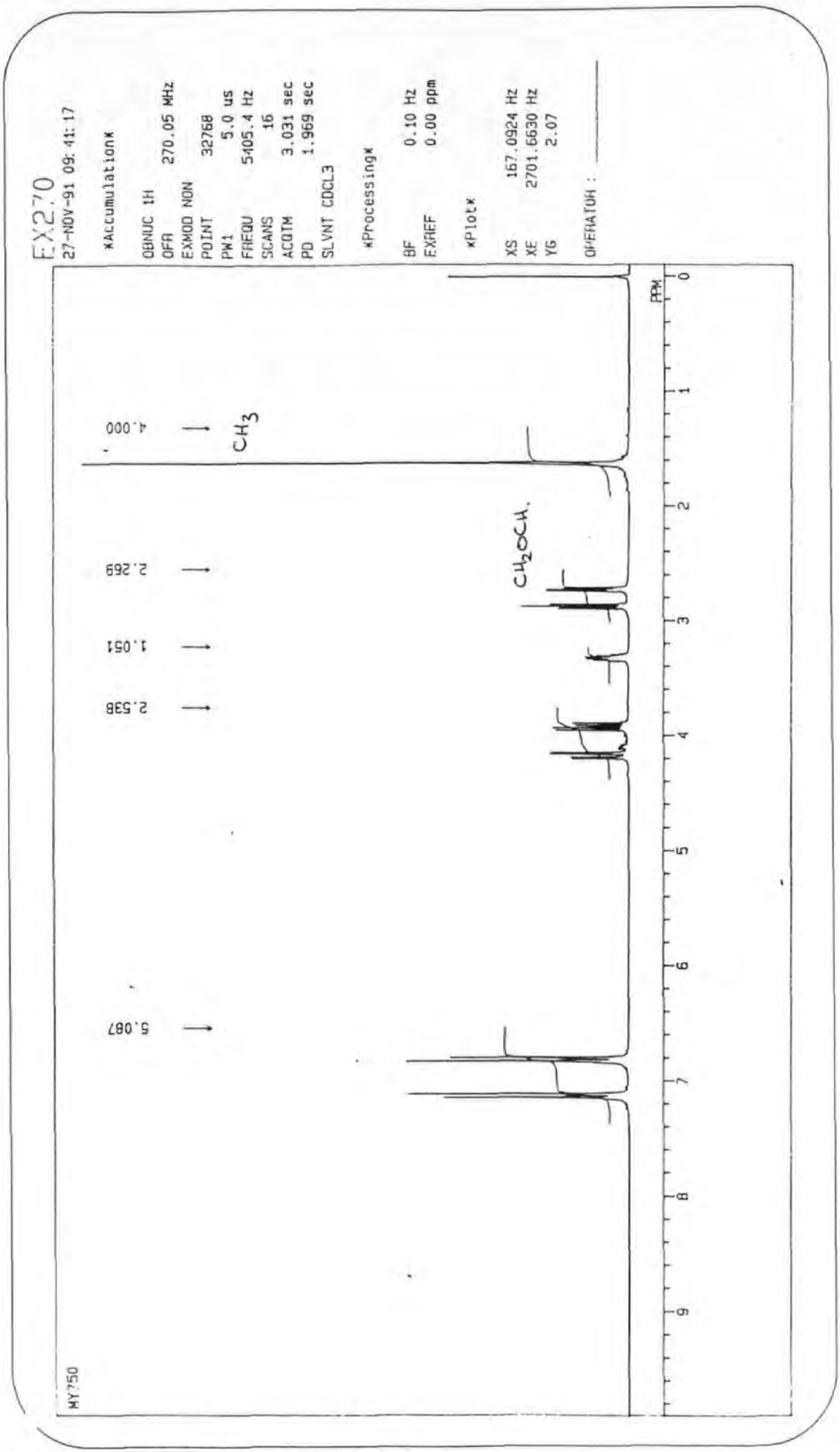

Figure 4.1. ^{1}H NMR spectrum of MY750

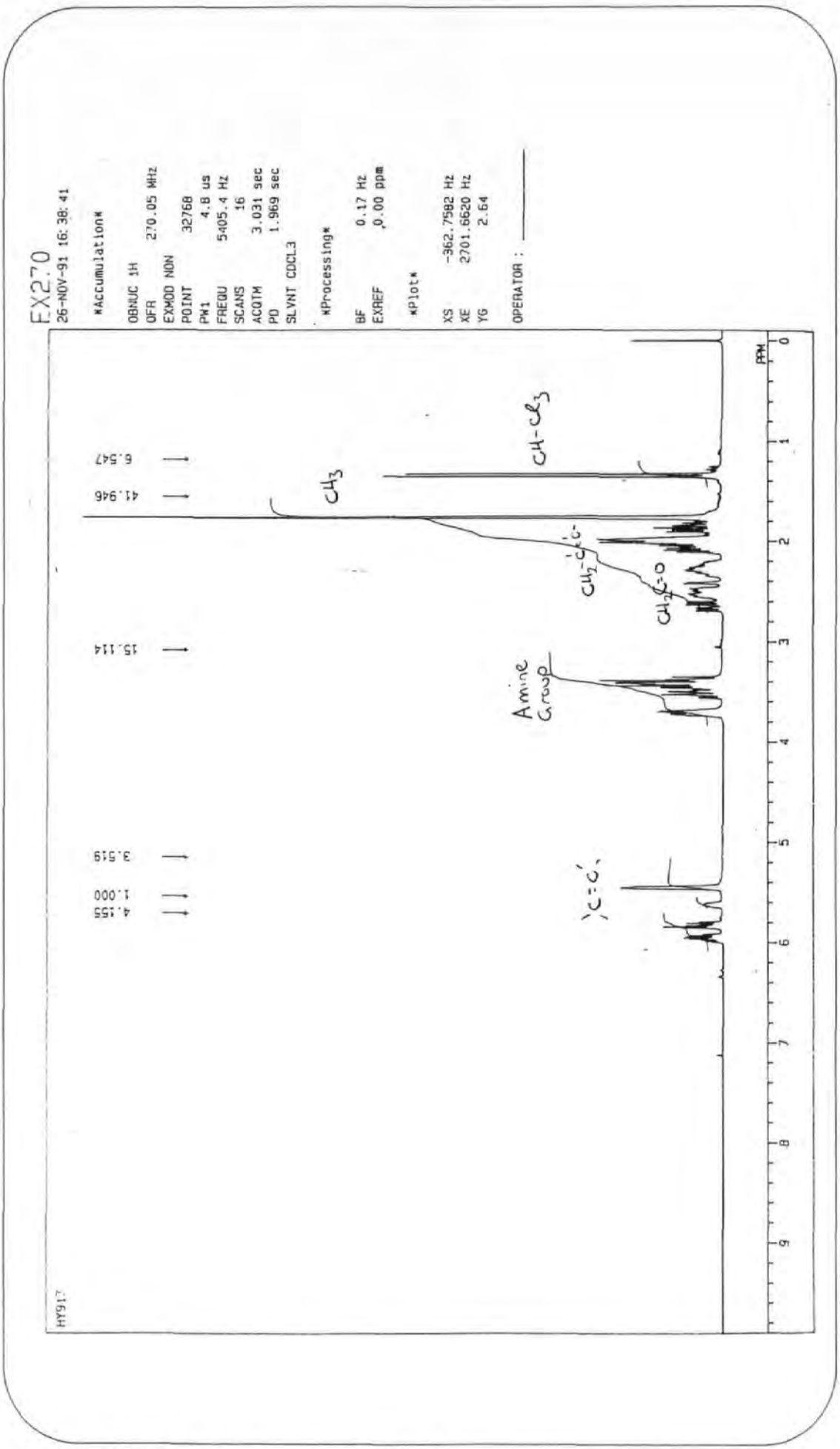

Figure 4.2.a. ^{1}H NMR spectrum of HY917

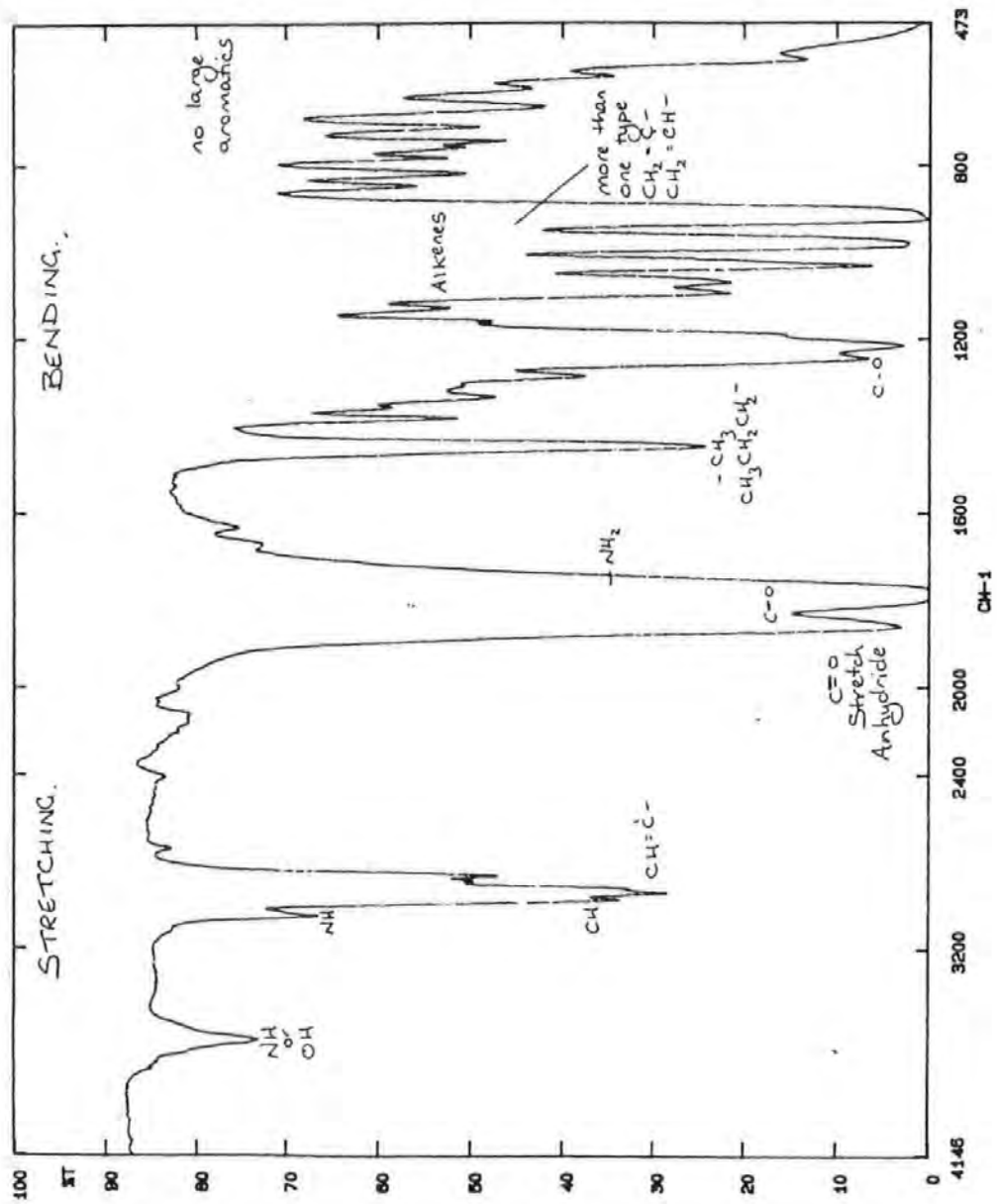

Figure 4.2.b. IR–spectrum of HY917

4.2.3. DY070 - 1-Methylimidazole

Chemical formula:

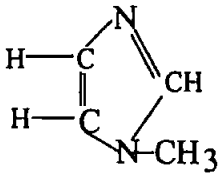

The DY070 is usually added as a catalyst, to speed up the cross-linking reaction. In this case it is can be used to adjust the balance between usable life and cure schedule.

As can be seen from figure 4.3. and the chemical structure, 1-methylimidazole is a tertiary amine and is used as a catalyst. The resin system will cure without the addition of the catalyst but it will take longer and will not have the same physical properties.

4.3. Mechanisms of Cure

The cross linking reaction that takes place during cure can be divided into two types [86]: reactions of the anhydride group and reactions of the epoxy group. For more detailed description of these reactions please refer back to chapter 3. The mechanism of epoxy-anhydride polymerisation is complex and by no means fully understood [93]. However there is more-or-less general agreement that a co-catalyst is involved for example water, alcohols, phenols, or other H-bonding agents present as contaminants in the reactants. In view of the role of co-catalysts in the reaction mechanisms, it is quite likely that contaminants such as water or low molecular acids or bases can decisively affect the reaction kinetics.

However it is possible that the previously mentioned cure scheme does not always apply since when a low molecular weight resin and a hexamethylhydrophthalic anhydride (see chemical formula 1.a.) or nadic methyl anhydride react (see chemical

formula 1.b.) there is no indication of ether formation during the reaction prior to the gel point.

1.a.

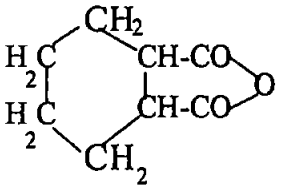

1.b.

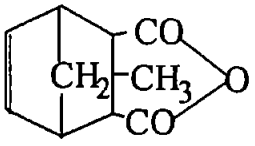

It has been suggested, on the basis of kinetic data, that the cases involve a transition state which results in the production of a diester [35].

1.c.

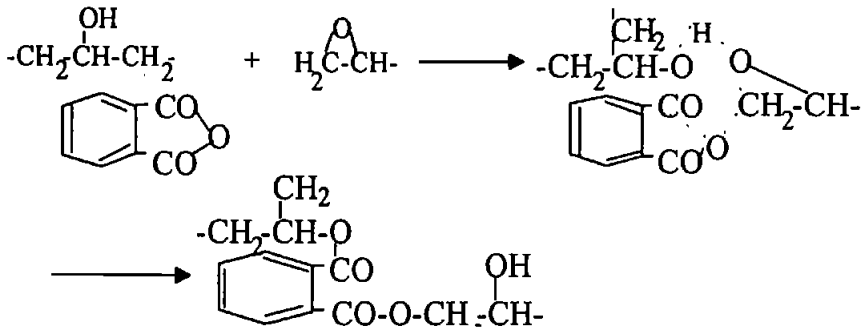

The tertiary amine acts as a catalyst by reacting preferentially with the anhydride to generate a carboxy anion. This anion opens an epoxy ring to give an alkoxide ion, which forms a second anhydride molecule and so on e.g.:

2.

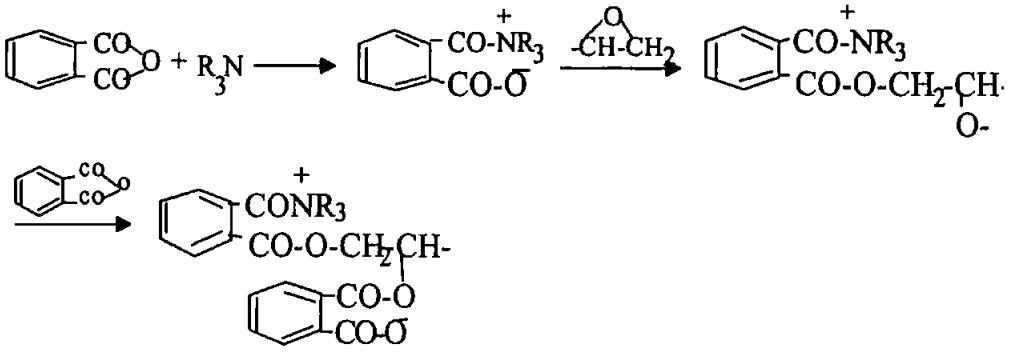

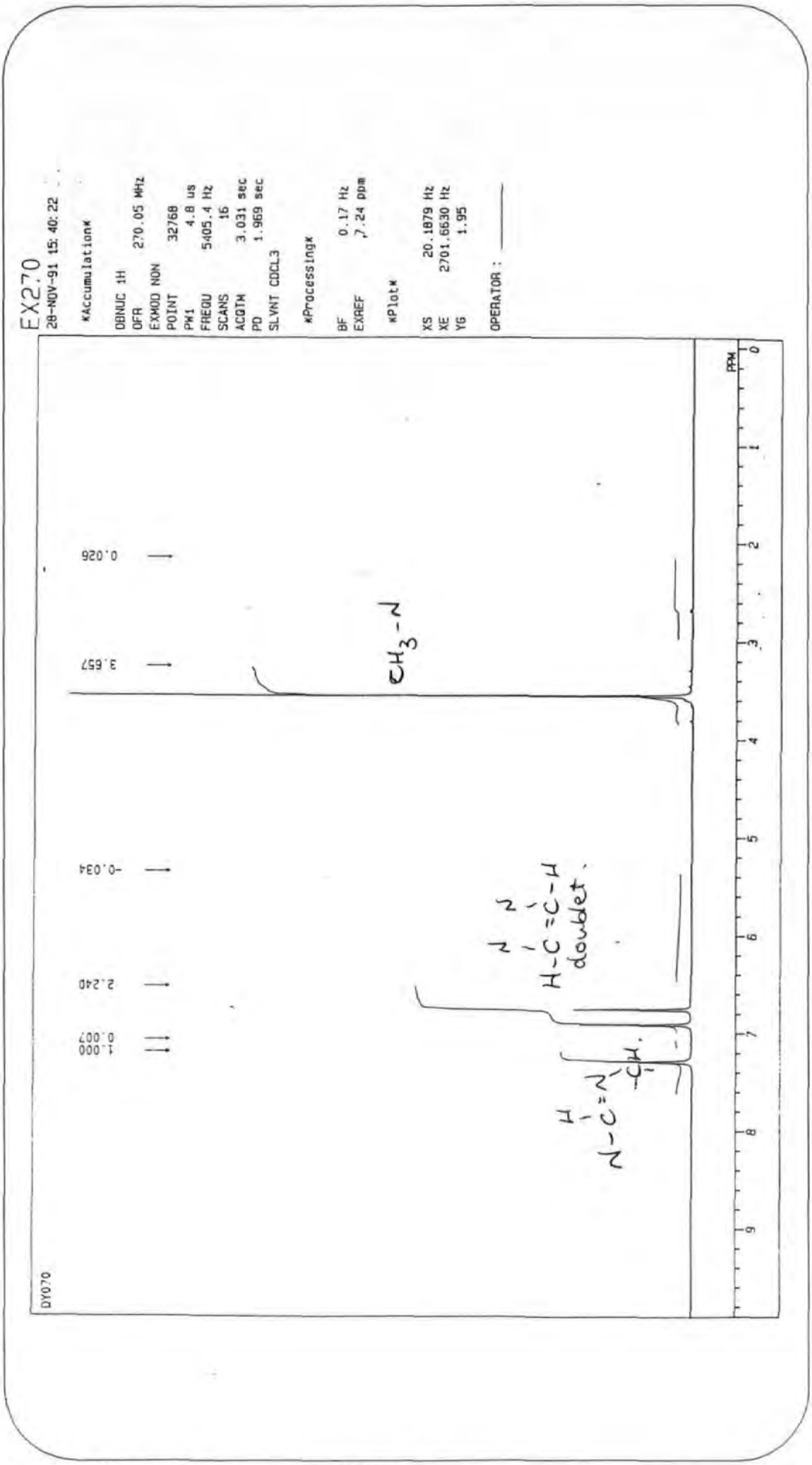

Figure 4.3. ^{1}H NMR spectrum of DY070

Therefore the cross–linked structure of the cured MY750 resin system will be of the form shown in 3. below.

3.

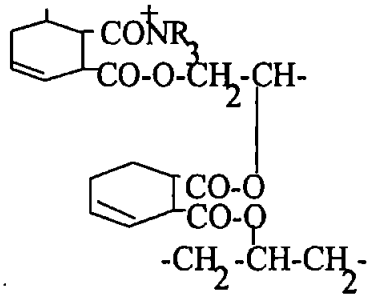

It has been assumed in this research that 100% cross–linking occurs when all the active sites within the molecular structure have been used for cross–linking. Therefore the resin is a very highly cross–linked structure.

5.0. ANALYSIS OF SPECTRA

5.1. Introduction

Samples of the MY750 resin system (100 pbw MY750, 85 pbw HY917, 2 pbw DY070) were allowed to gel and then cure at 40 °C, 60 °C, and 80 °C while being monitored by the Jeol EX270 NMR spectrometer. Data was acquired immediately the sample had reached the required temperature (and the field gradient had been re–shimmed) and at regular intervals thereafter. The interval between acquisitions was dependent on the cure schedule. To obtain a deuterium lock the deuterium oxide (D_2O) was added by use of a glass insert and therefore did not interfere with the cure reaction taking place around it. Tetramethylsilane (TMS) was not added as a reference point (taken to be at 0 ppm) since it is not soluble in D_2O. However D_2O had to be used as opposed to deuterated chloroform, $CDCl_3$, since a strong deuterium signal was required to lock the spectrometer. Acquisitions of data continued until only the solvent peak could be resolved.

5.2. Analysis of Spectra

5.2.1. 40°C Cure

The initial spectrum can be seen in figure 5.1. It can be seen that this is a combination of the MY750 and HY917 spectra which were introduced in chapter 4. On inspection of the spectrum it can be seen that the strongest peak is the methyl peak at approximately 1.5ppm. Therefore the progression of the cure can be followed by comparing the proton peak from the D_2O (termed hereafter as the D_2O peak) with the methyl peak. It was assumed that the volume of D_2O was constant, that the tubes were all the same and inserted to the same depth within the NMR tube. As the cure progresses the resin will begin to solidify, as it does so the signal due to the methyl peak will become smaller. This is due to the hydrogen environments becoming constrained. After pulsing with r.f., relaxation of the system will occur much quicker, in fact too quick for the hardware which has to change from sending

the signal to acquiring the FID. In comparison the D_2O peak will become bigger, however this is only a result of the difference between the two peaks altering, see figure 5.2. Therefore, it must be noted that this increase in strength is only with respect to the weakening of the methyl signal. In fact all differences in the spectrum must be analysed with respect to the apparent strength of the solvent peak, this is because the y–axis scale changes to give a full screen picture of the spectrum. Hence, the D_2O signal can be used as an internal standard.

After 92 minutes (figure 5.3.) it can be seen that all the peaks are broader with respect to the initial spectrum, especially for the $O–CH_2–$ and –CH=CH– signals. This indicates that cross–linking is beginning to take place (see chapter 4) due to the epoxy ring opening.

During the next hour (i.e. after 152 minutes) of cure resolution continues to be lost as the resin gels, see figure 5.4. The $CH_3–$, $CH_2–C=C–$, Amine, and $O–CH_2–$ signals broaden into one peak. Similarly there is a loss of resolution in the aromatic and –CH=CH– peaks. This broadening is an indication of the restriction in the chemical environment and so indicates the amount of cross–linking that is taking place. The number of peaks that can be identified has already diminished when this spectrum is compared to the initial spectrum of figure 5.1. Also it can be seen that the solvent peak is now half the size of the methyl peak, indicating again a loss of signal strengths.

After 214 minutes (figure 5.5) the only strong, easily resolved peak is that due to D_2O. The methyl and amine group are still distinguishable but all signals from the other hydrogen environments have been enveloped by the broadening of the peaks. There is also a substantial increase in noise on the spectrum.

A further 60 minutes (275 minutes into cure) and the spectrum has now broadened considerably, see figure 5.6. For the rest of the cure the peaks that were the methyl and aromatic signals broaden and grow smaller as their chemical environments are restricted by the cross–linking that is taking place. The decrease in their strength is indicated by the apparent growth of the solvent signal (see figure 5.7).

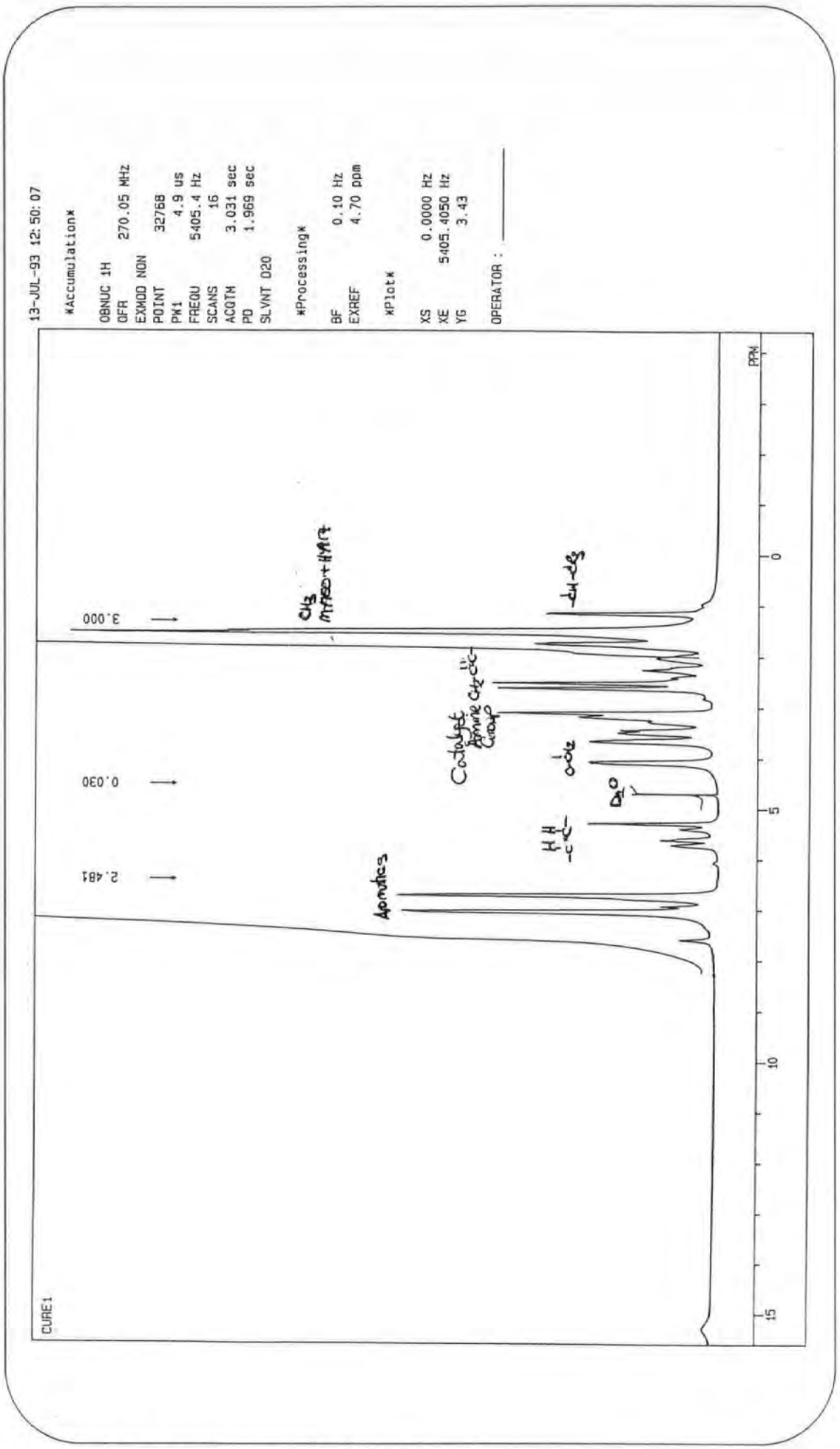

Figure 5.1. The initial spectrum for a 40 °C cure.

a) Simplification of initial spectrum, showing solvent and methyl peaks. Solvent has a constant intensity of x

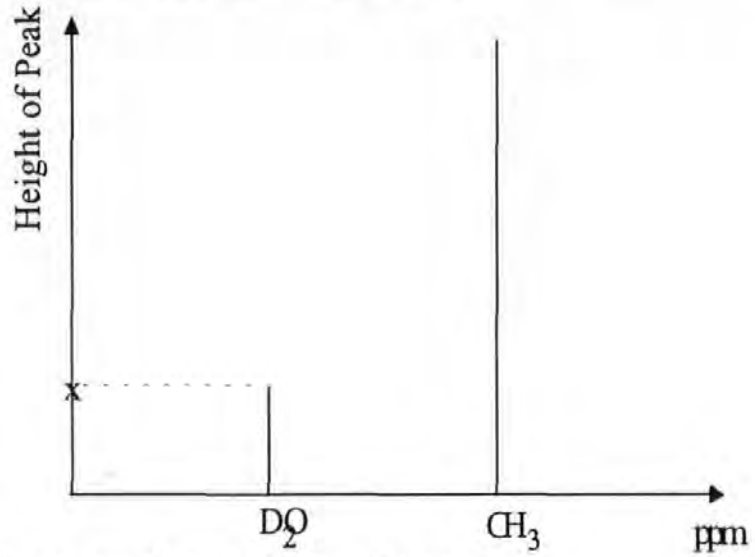

b) Spectrum after y minutes of cure.

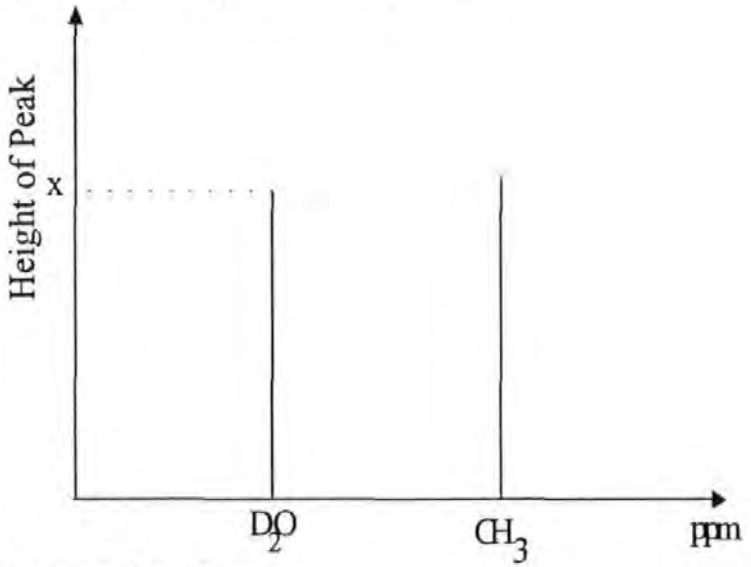

c) Spectrum later in cure.

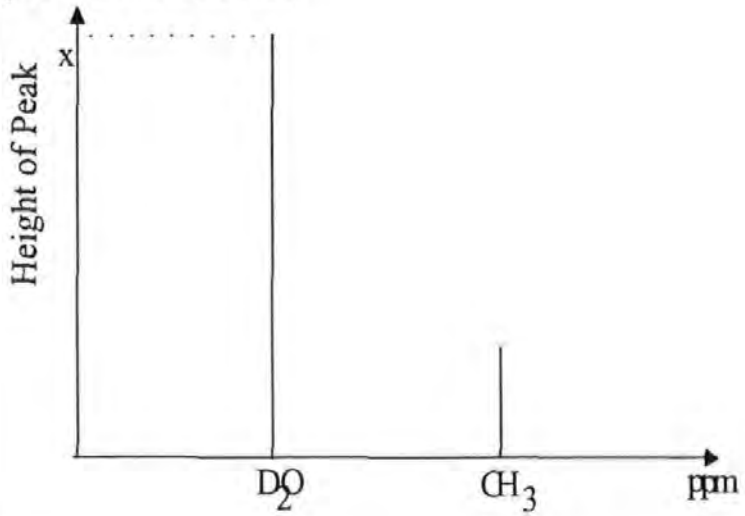

Figure 5.2. Spectral changes as resin cures.

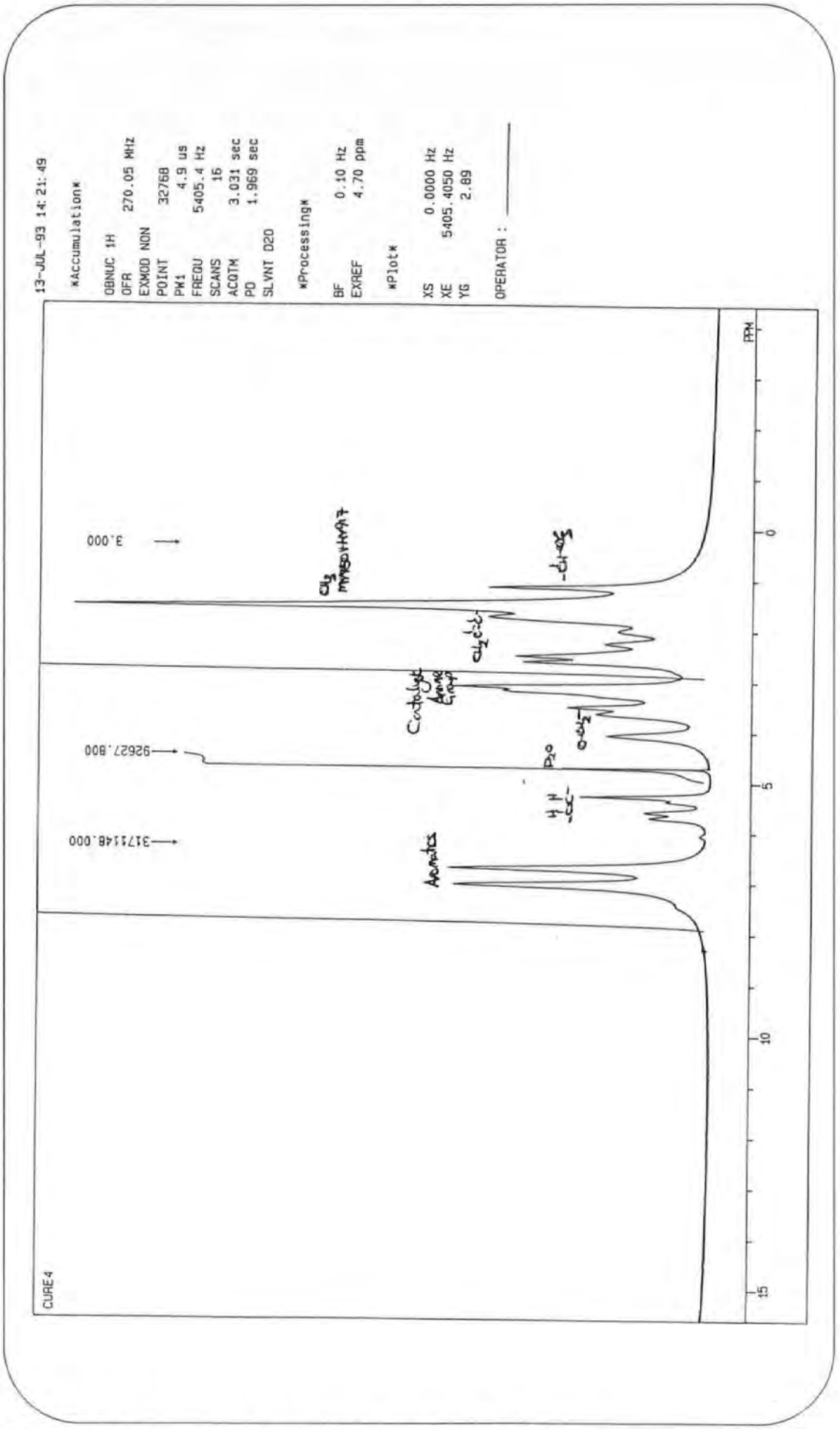

Figure 5.3. The spectrum for the 40 °C cure after 92 minutes.

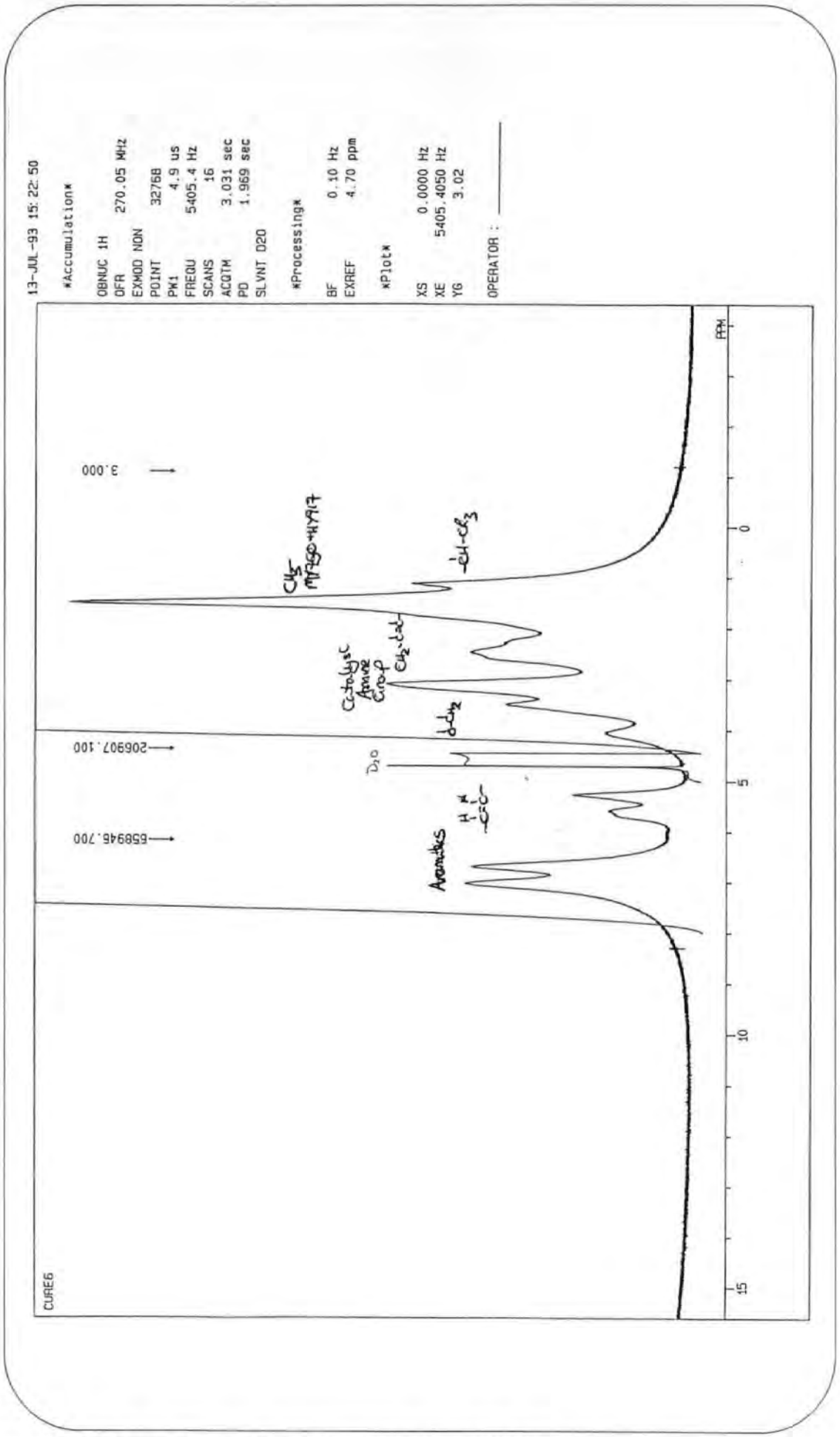

Figure 5.4. The spectrum after 152 minutes for a 40 °C cure.

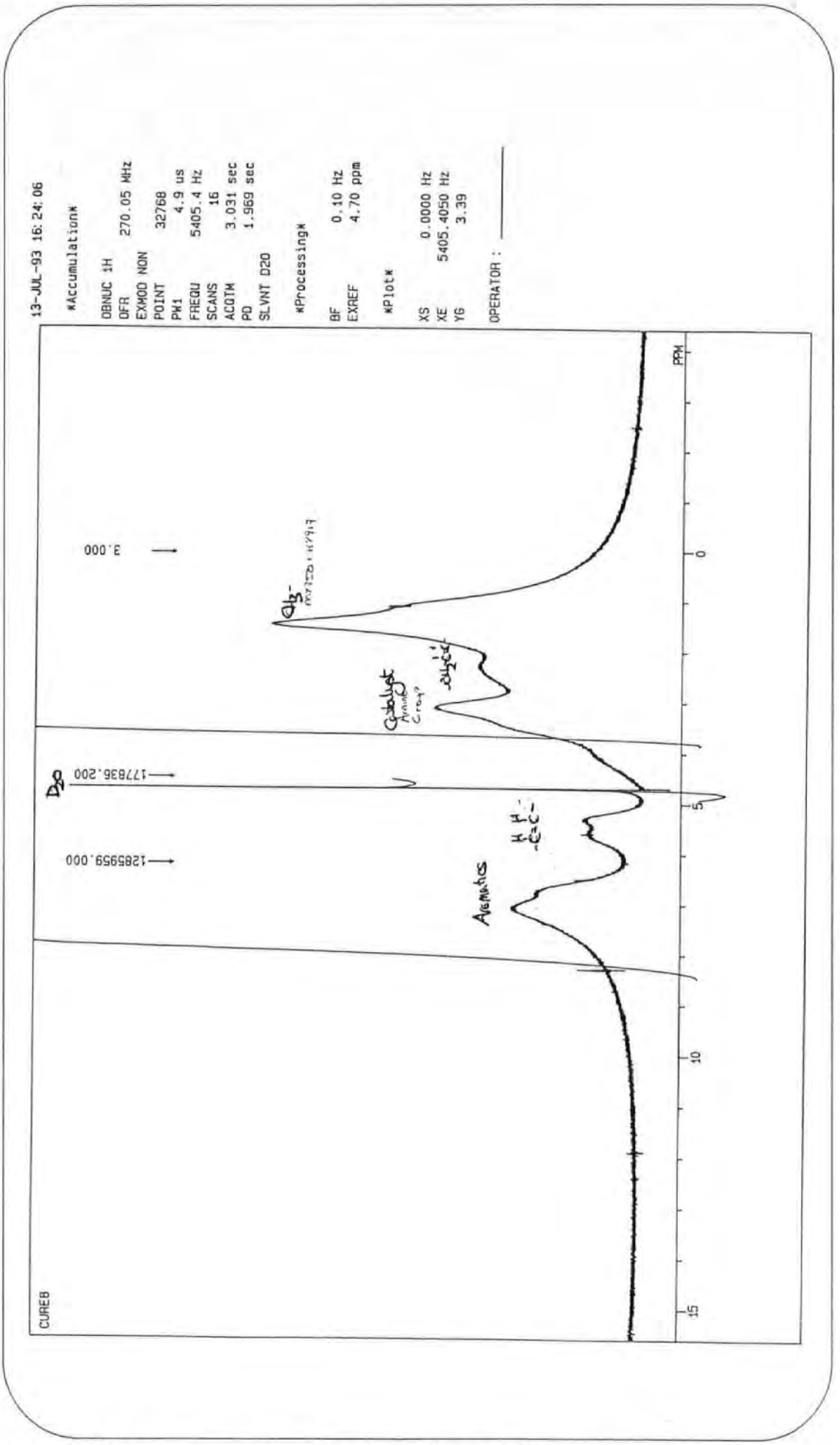

Figure 5.5. The spectrum after 214 minutes for a 40 °C cure.

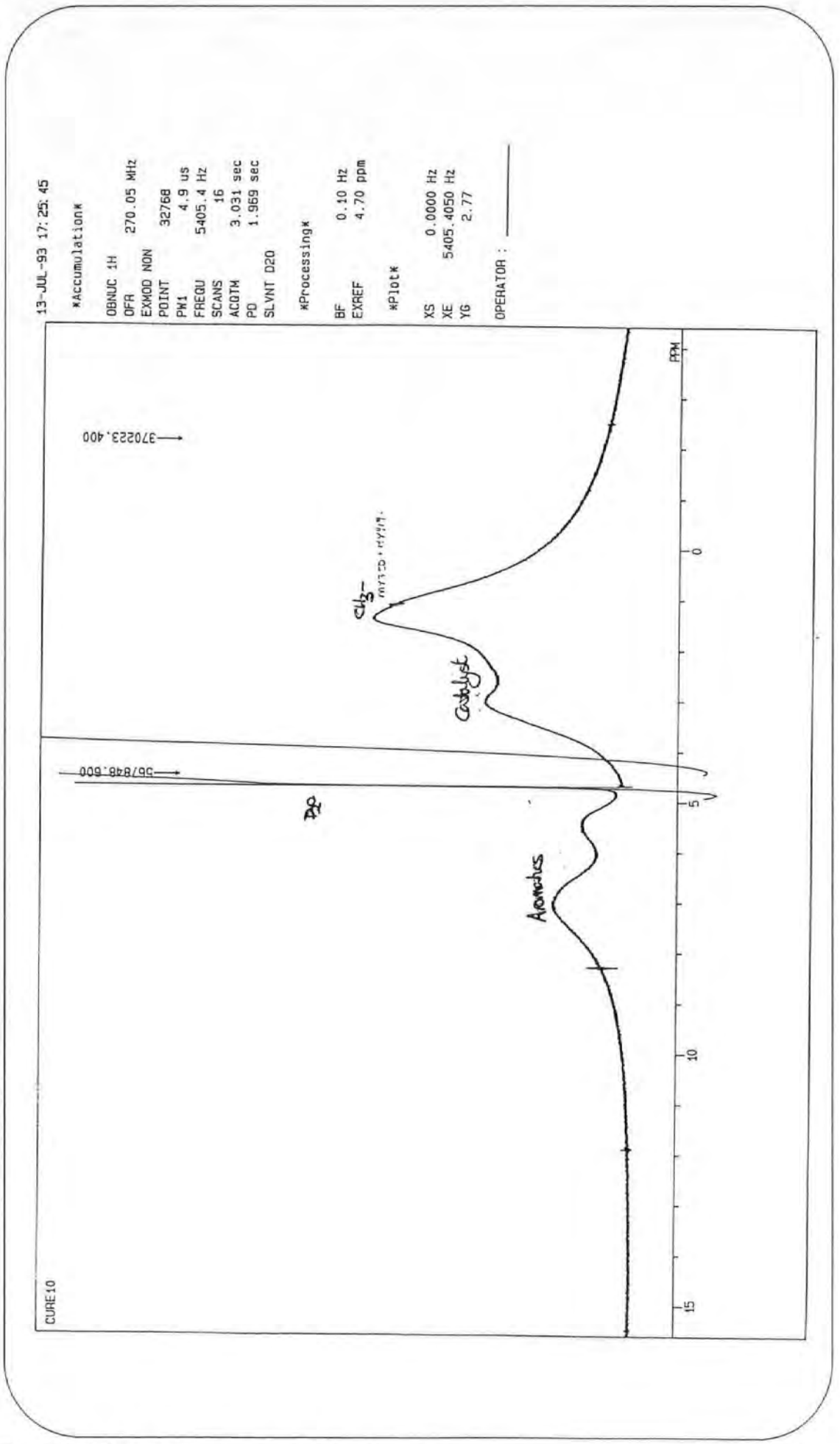

Figure 5.6. The spectrum after 275 minutes.

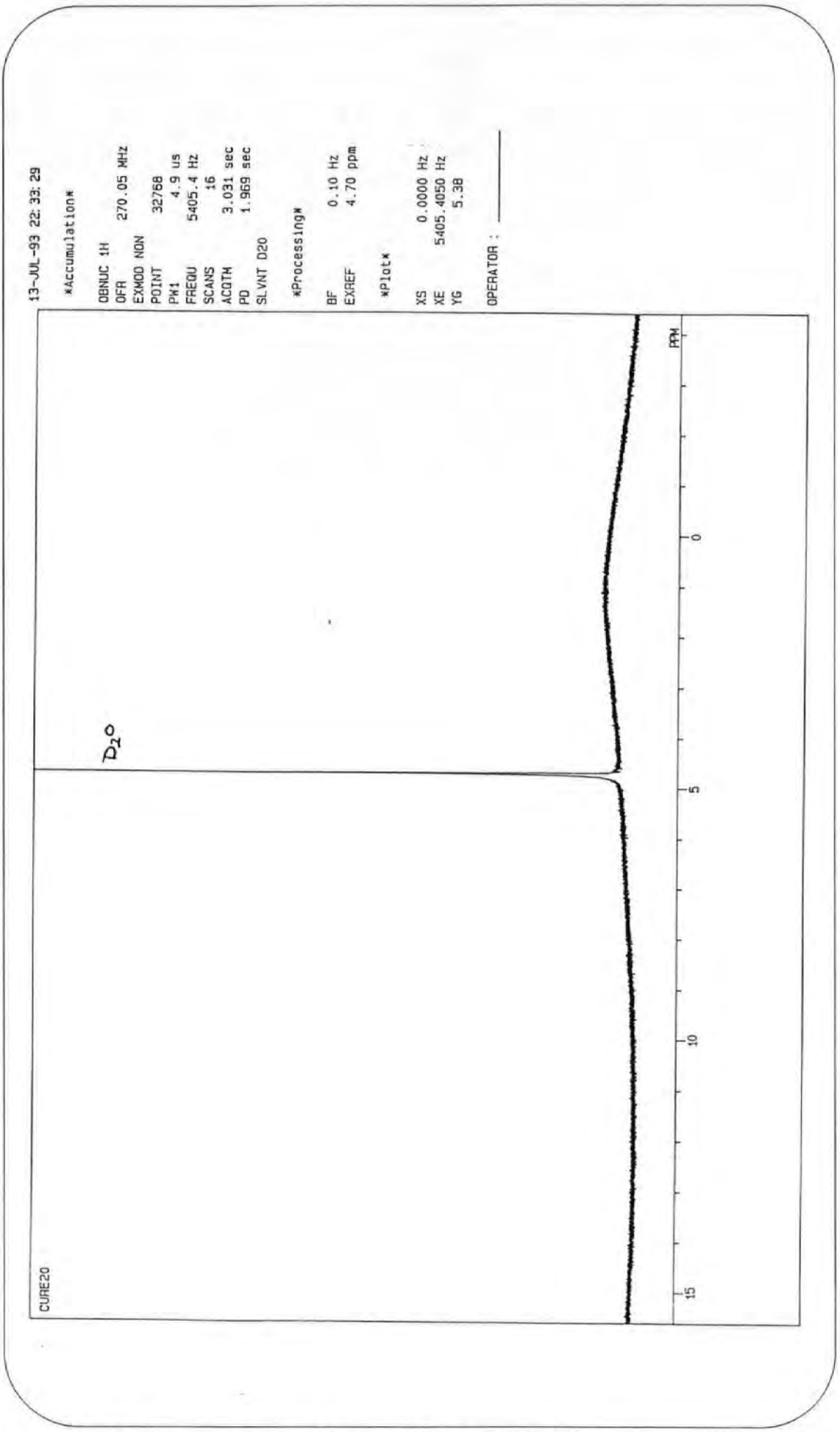

Figure 5.7. The spectrum after 583 minutes for a 40 °C cure.

5.2.2. 60 °C Cure

The initial spectrum for the 60 °C cure is slightly better resolved (there is more distinction between the peaks, this can be seen particularly for the CH_2–O– and aromatic peaks) than the initial spectrum for the 40 °C cure. This is a temperature effect, the hydrogen environments are less restricted at 60 °C than they were at 40 °C, i.e. the resin is less viscous. All of the resin peaks also appear to be stronger at 60 °C than they were at 40 °C this is indicated by the apparent "small" size of the D_2O peak. The initial spectrum can be seen in figure 5.8. Also to be noted is that although the solvent peak is at the same ppm all other peaks have shifted up by 0.25ppm, see figure 5.9. However this is due to the spectrum being referenced from the D_2O peak which was wrongly assumed to be stable. It is in fact, due to its water content affected by temperature.

After 37 minutes of cure the spectrum can be seen to be broadening and to be losing resolution. The CH–C=C– and the CH_2O– signals are already beginning to be lost to the broadening effect, as cross–linking takes place at the epoxy ring. See figure 5.10.

A further 37 minutes (i.e. 74 minutes into the cure) and the spectrum is very broad. The peaks that can be seen are the methyl, amine, aromatic and –C=C– peaks. The D_2O is still easily resolved. See figure 5.11.

As the resin continues to cure the remaining resin peaks continue to broaden while the solvent peak remains resolved. After 168 minutes only the D_2O peak remains. See figure 5.12. The resin is now too cross–linked for useful information to be gained due to the hydrogen environments being restrained.

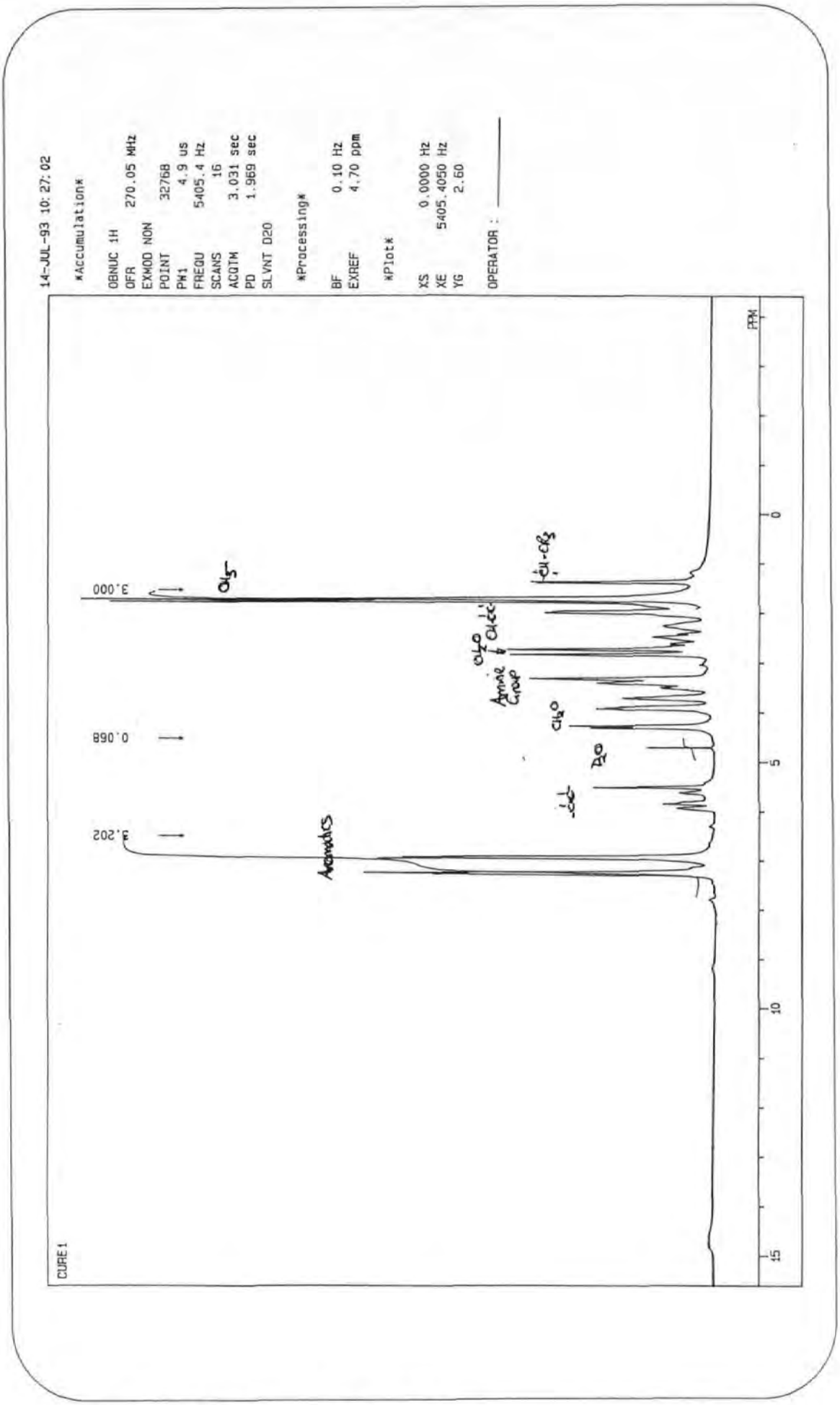

Figure 5.8. The initial spectrum for the 60 °C cure.

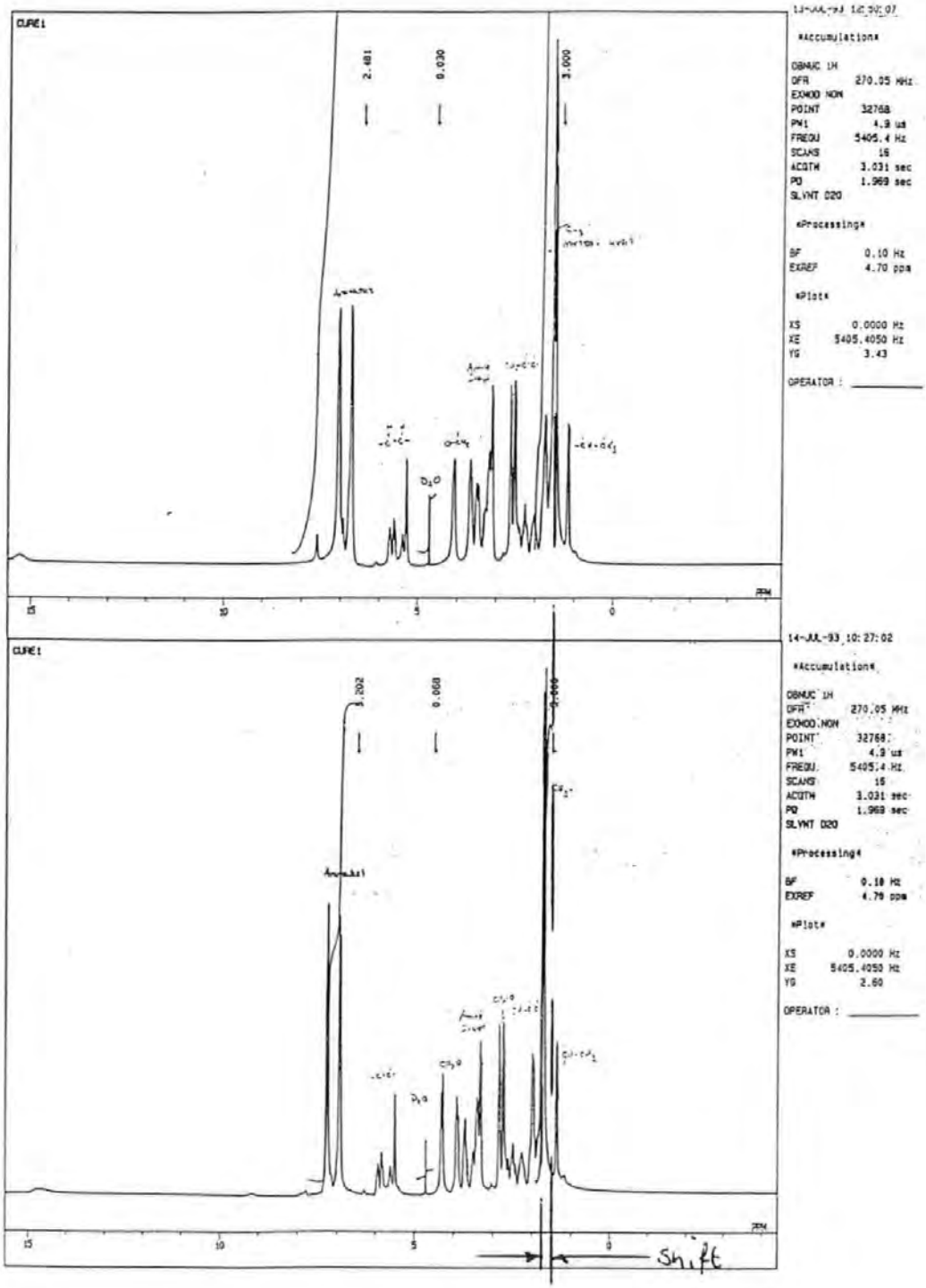

Figure 5.9. Comparison of 40 °C and 60 °C initial spectra.

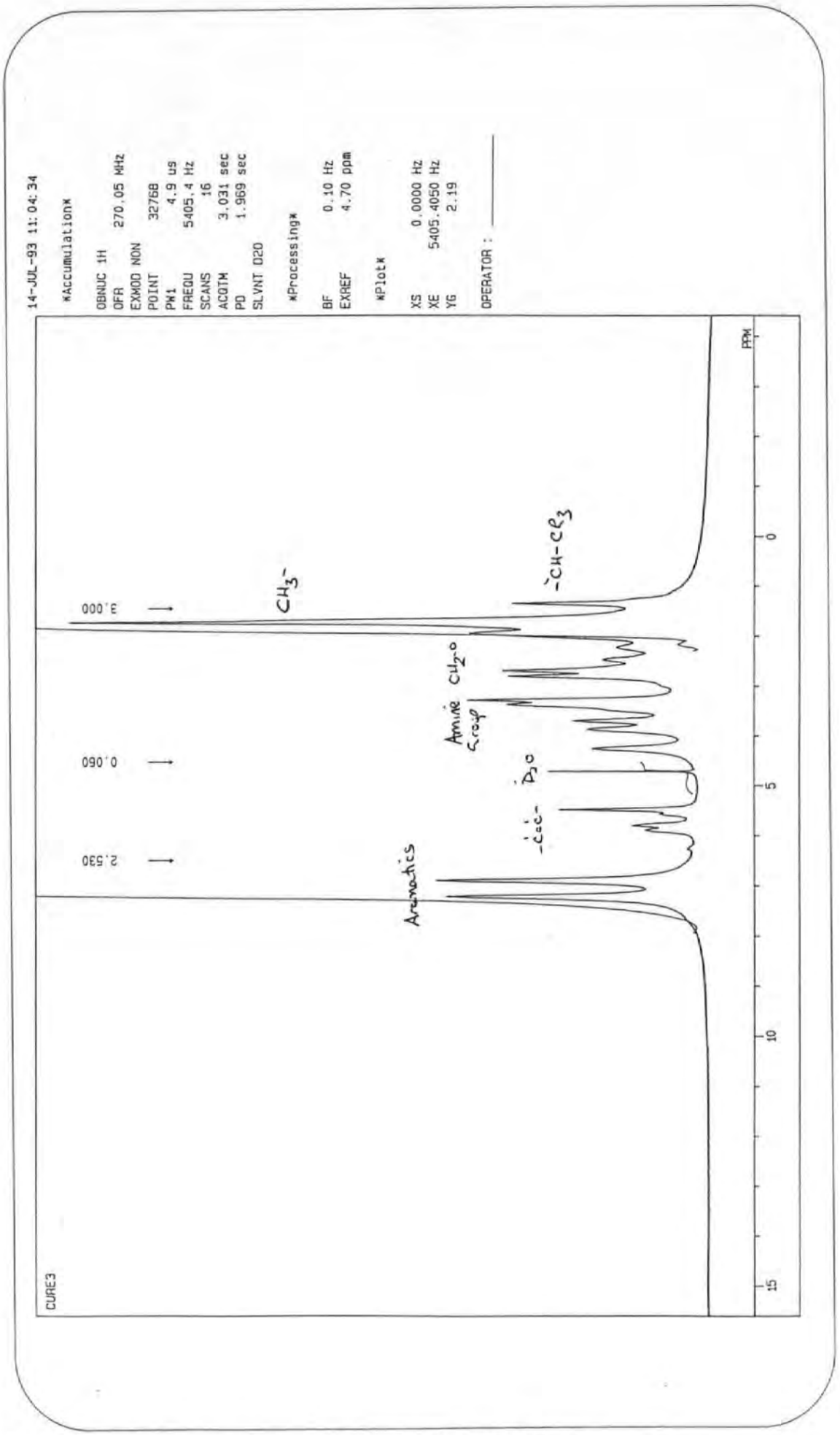

Figure 5.10. The spectrum after 37 minutes of a 60 °C cure.

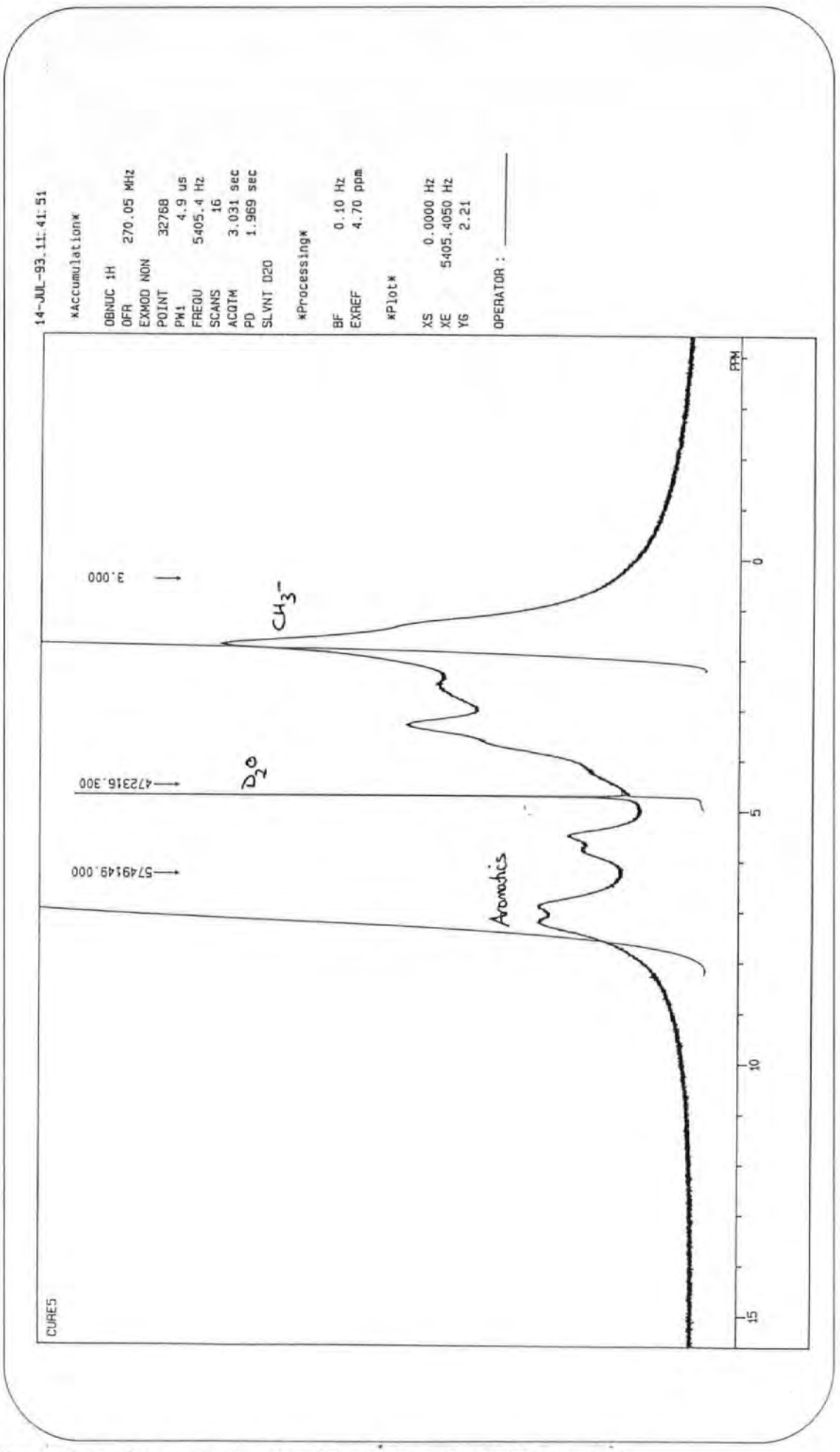

Figure 5.11. The spectrum after 74 minutes of a 60 °C cure cycle.

Figure 5.12 The spectrum after 168 minutes of a 60 °C cure cycle

5.2.3. 80 °C Cure

The first spectra (see figure 5.13) taken after the Jeol EX270 had settled at 80 °C and re-shimmed can be seen to be much more resolved with sharp spectral peaks than those taken at this stage in the cure for the 40 °C and 60 °C cure schedules. The spectrum has also shifted up by 0.417 ppm from the 40°C initial spectrum and by 0.167 ppm from the 60°C initial spectrum, see figure 5.14. Again this is due to the temperature having an effect on the D_2O.

After the resin has cured for 15 minutes the peaks are again beginning to broaden as can be seen in figure 5.15. Broadening can be seen in the methyl and aromatic peaks. The D_2O peak is still small in comparison with the resin spectrum.

After a further 15 minutes (30 minutes into the cure) the spectrum has broadened considerably, see figure 5.16. The methyl peak is still strong compared to the D_2O peak. The $-CH_2\ O-$ and $=CH-CR_3$ peaks are now being lost within the general broadening effect.

After 45 minutes into the cure the spectrum is now very broad and only the D_2O peak is discernible. This is similar to the previous cure cycles. From now on the D_2O peak will become stronger in comparison with the resin spectrum.

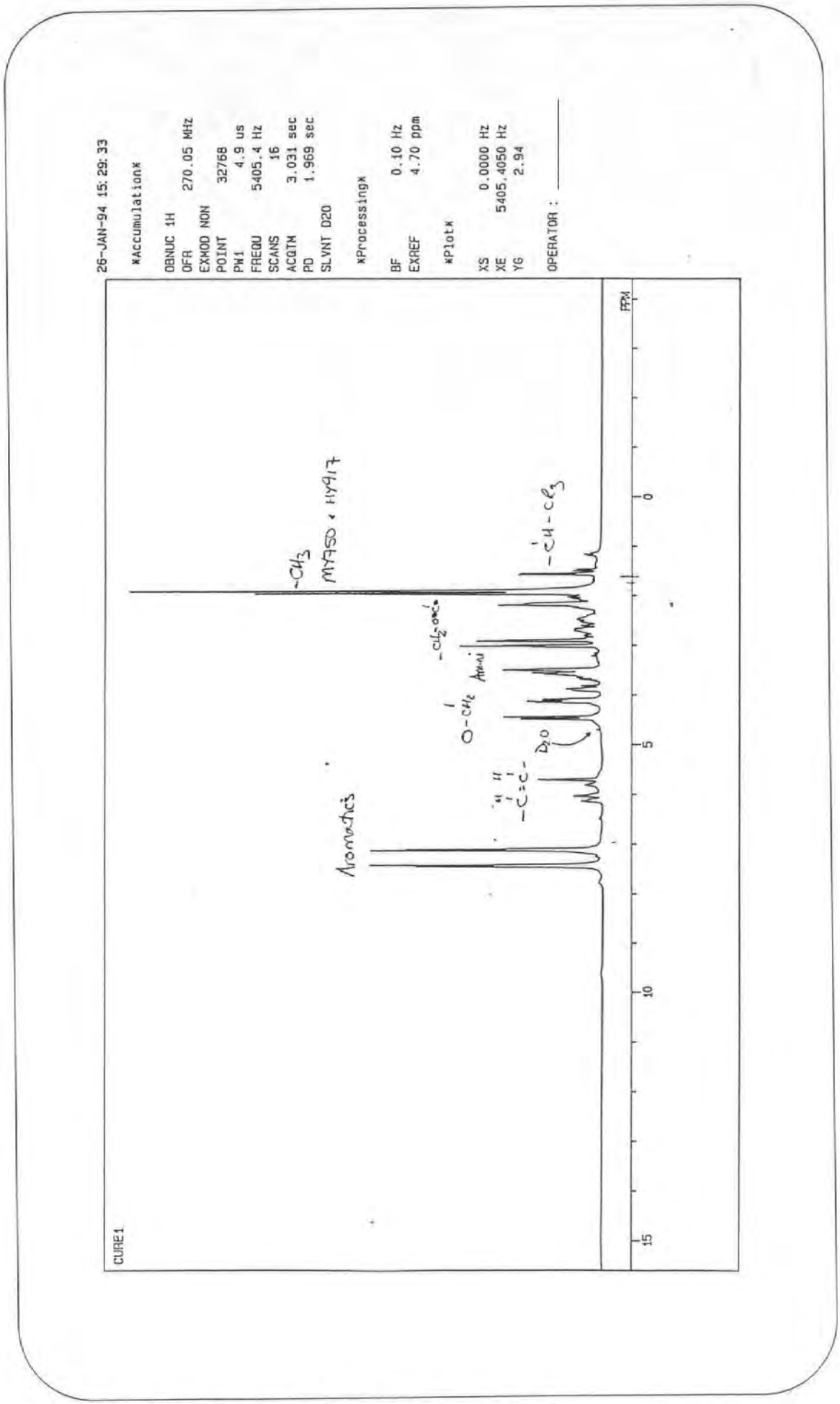

Figure 5.13. The initial spectrum for a 80 °C cure cycle.

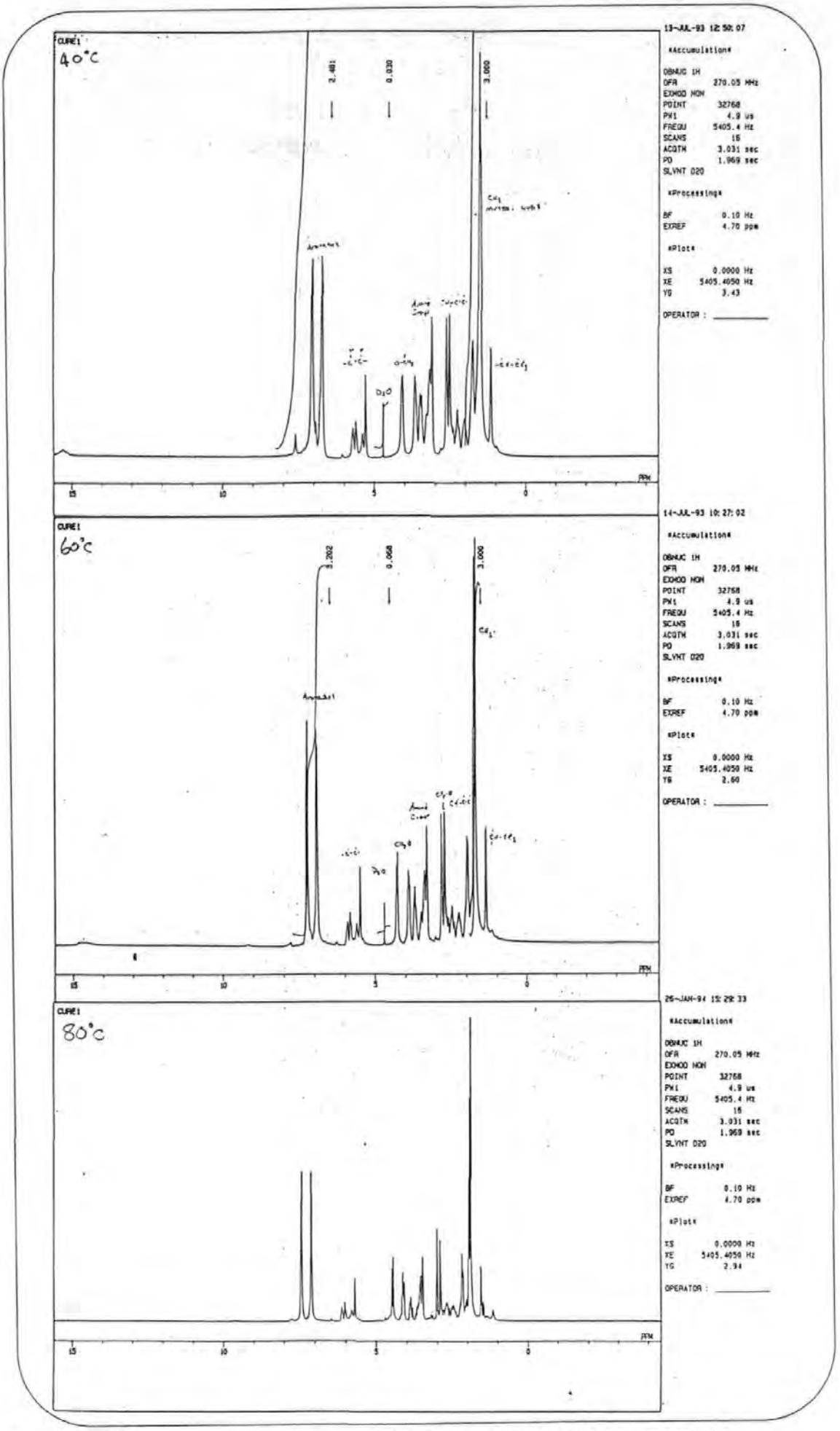

Figure 5.14. A comparison of the initial spectra at 40 °C, 60 °C and 80 °C.

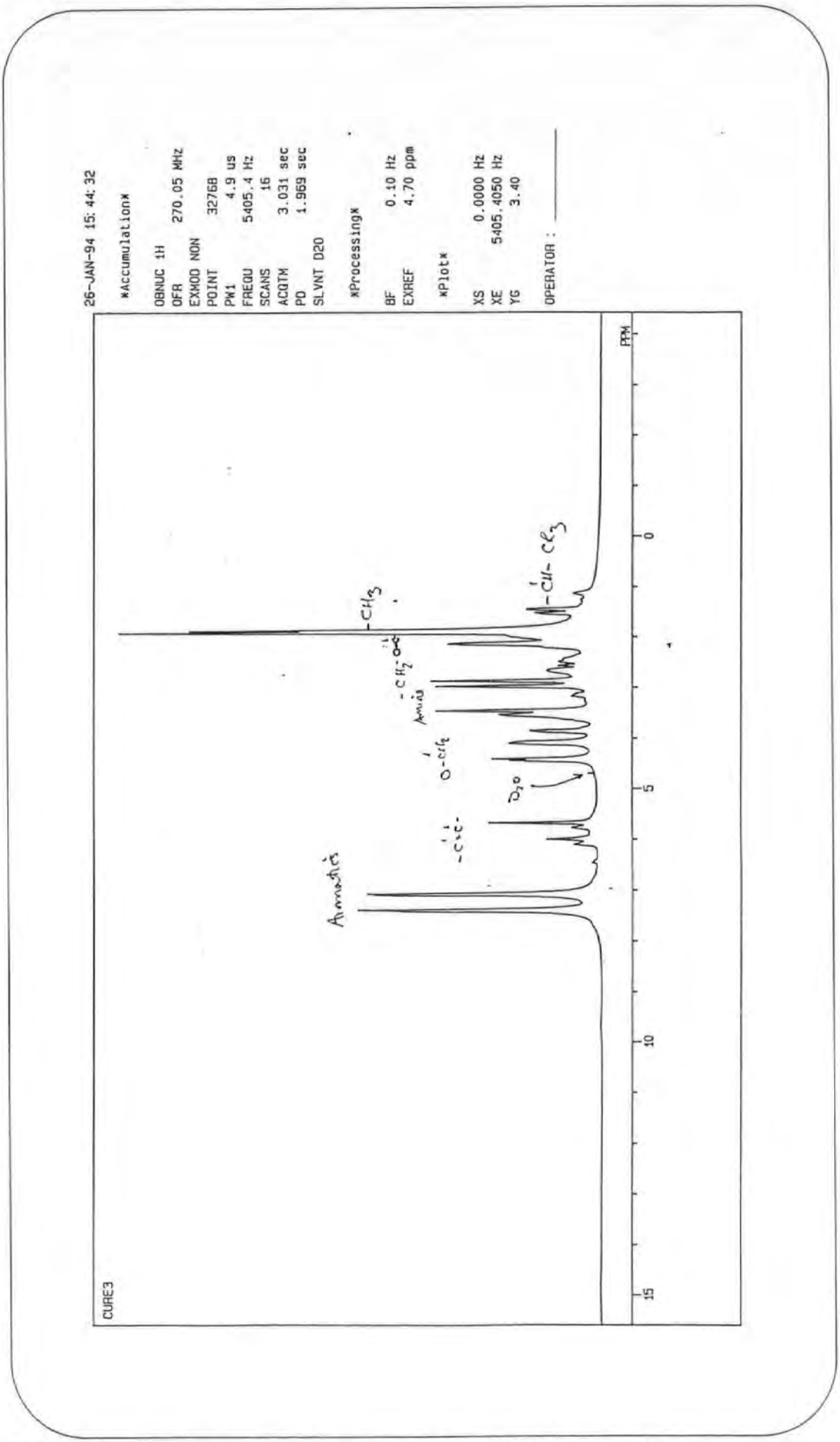

Figure 5.15. The spectrum after 15 minutes for an 80 °C cure cycle

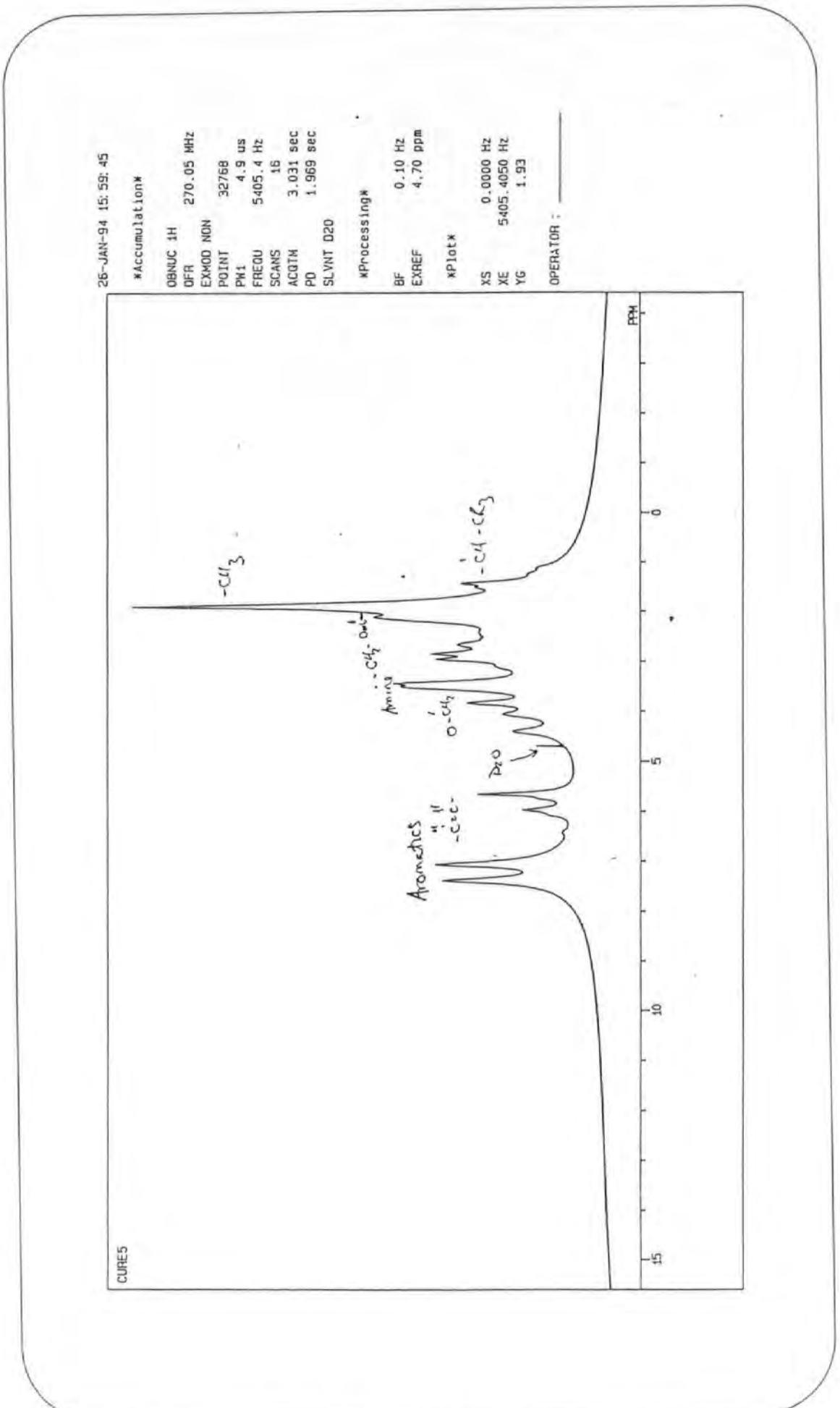

Figure 5.16 The spectrum after 30 minutes of cure

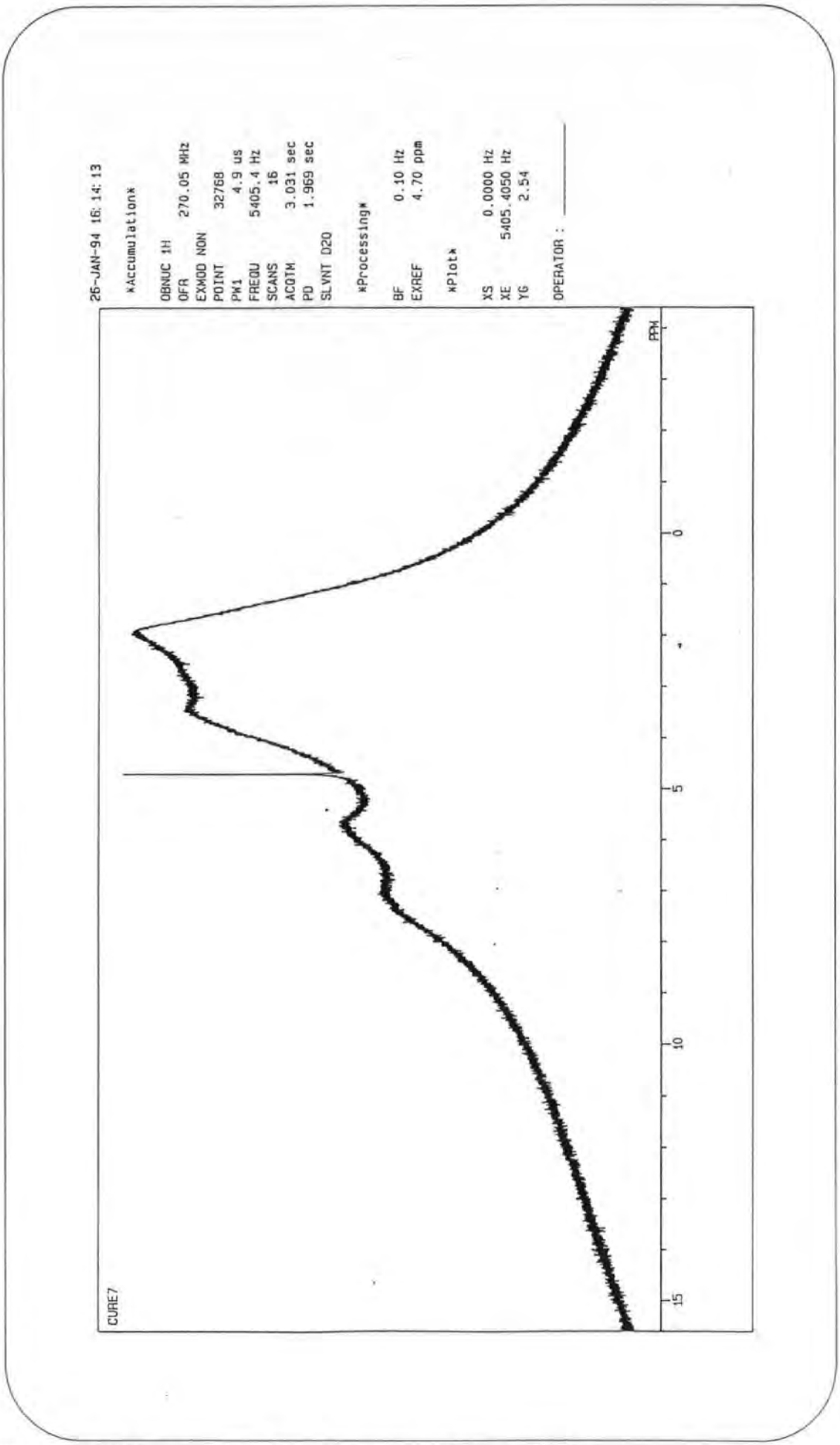

Figure 5.17 The spectrum after 45 minutes of cure at 80°C

5.3. Discussion

As the cure temperature was increased the mobility of the resin components increased and the resin mix became less viscous. The lower viscosity means that the FID can be acquired as if the sample was a liquid – the phase for which the spectrum was optimised. The higher the temperature the less viscous the resin components become, however the viscosity of the resin should only affect the sharpness of the spectrum peaks since the more viscous the liquid the broader the spectrum. At a certain cure temperature the resin components will seem to reach gelation instantaneously, this will be a factor of the decrease in viscosity at higher temperatures making the resin components more mobile and aligning themselves for cross–linking to occur more effectively.

At 40 °C the cross–linking sites on the resin, the epoxy ring and hydroxy group, may have an order of preference, e.g. the hydroxy sites are cross–linked to first and then the epoxy ring is broken for cross–linking to occur there. This would be due to differences in the activation energies of the two processes. However as the cure temperature is increased this "preference" cross–linking may not operate. At the higher temperature all cross–linking sites could be active and so the cross–linking reaction will take place quicker.Because at the higher temperature the resin components are more mobile then 100% cross–linking may be achieved thus increasing the mechanical properties of the resin.

The times for all the cure cycles to reach the point in the cure where the spectrum became so broadened only the D_2O peak can be resolved clearly is illustrated in table 5.1. This time is compared with the time to gel as given by Ciba–Geigy technical information for the Araldite MY750 resin system. As can be seen the Jeol EX270 NMR spectrometer gives broadened spectra before the gel point has been reached. These figures will be compared with the data obtained from the CPMG and FID experimentation which will be discussed in chapters 6 and 7 consecutively.

Cure Temperature °C	time to broadened spectrum (peaks still visible but not resolved) (mins)	time to gel (viscosity data) (mins)
40	275	300
60	74	105.4
80	45	90

Table 5.1. A comparison of the time for the spectra to broaden versus recommended gel time.

6.0. TRANSVERSE RELAXATION TIME MEASUREMENTS

6.1. Introduction

Transverse relaxation time (T_2) data was acquired by the CP acquisition sequence on the Jeol EX270 NMR high-resolution liquid-state spectrometer (a pre-programmed facility) and by the updated CPMG acquisition sequence on the Oxford QP NMR analyser. The CP and CPMG sequences are discussed in section 1.2.3. where there is an explanation as to the benefits of the CPMG acquisition sequence as opposed to the CP acquisition sequence.

6.2. Analysis of Epoxy Cure

6.2.1. Theory of Relaxation Time Measurements

For each cure cycle a set of decay curves were obtained initially after mixing and then at regular intervals throughout the cure. Each curve was then re-plotted using a natural logarithmic (ln) axis for the signal strength. The signal strength is related to T_2 by the following equation:

$$\text{signal strength} \propto e^{-t/T_2}$$

therefore:

$$\ln(\text{signal strength}) \propto -t/T_2$$

i.e. a plot of ln(signal) versus time for acquisition has a gradient equal to $-1/T_2$ thus giving T_2 in microseconds.

From the relaxation time data (whether acquired by the CP or CPMG pulse sequence) a graph of T_2 against duration of cure can be derived, this also decays

exponentially therefore a straight line graph of $\ln(T_2)$ against time of cure can be obtained.

6.2.2. Analysis of 40°C Cure

6.2.2.1. Analysis of MY750 Cure – Jeol EX270

A sample of resin (100 pbw MY750, 85 pbw HY917, 2pbw DY070) was cured in the NMR spectrometer at 40 °C. Acquisitions began when the sample reached the cure temperature and then every ten minutes for the duration of the experiment. The experiment was ended when only the lock signal could be resolved.

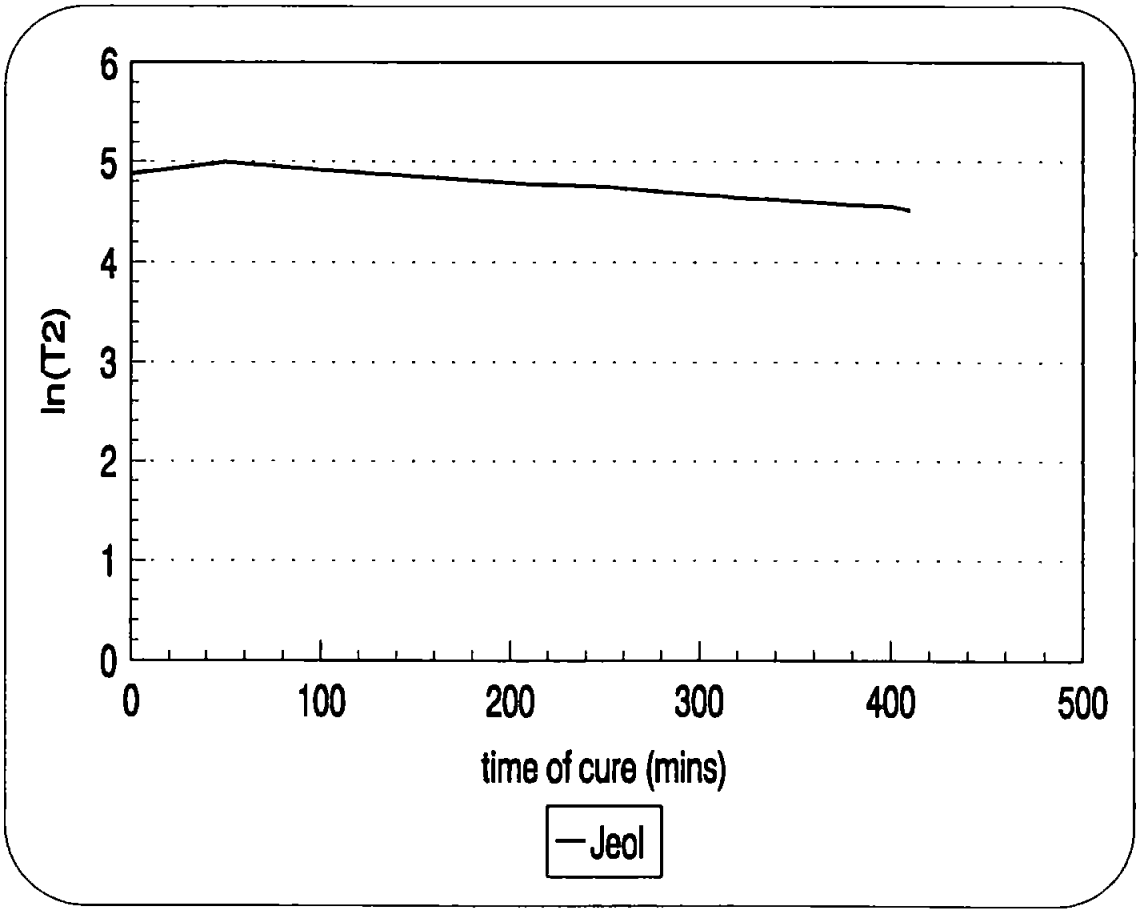

Figure 6.1. The natural log of the transverse relaxation data for the methyl peak versus time of cure. Acquisition taken at 40°C on the Jeol EX270 NMR spectrometer.

The Jeol EX270 being a standard research instrument acquires relaxation time data for each individual hydrogen environment. For this purpose only the stronger methyl data was used for the calculations for the $\ln(T_2)$ versus time of cure graph. A graph of the CH_3– relaxation time data versus time of cure can be seen in figure 6.1. Note that shortly after the gel point the methyl peak could no longer be resolved, approximately 400 minutes into the cure. This was due to the hydrogen environments becoming too restrictive and so the characteristic signal decayed too rapidly for the Jeol EX270 to acquire data. This shows clearly a major limitation of conventional liquid–state NMR technology.

6.2.2.2. Analysis of MY750 Cure – Oxford QP NMR Analyser

Again a sample of resin (100 pbw MY750, 85 pbw HY917, 2pbw DY070) was cured at 40°C. As stated previously (see chapter 2) the Oxford QP acquires average data for the sample and no chemical environment data can be obtained. From the CPMG data obtained by this method a straight line graph of $\ln(T_2)$ versus time of cure can be obtained as shown in figure 6.2. sample 1 and 2. The error limits for the data (2σ) can be seen as error1 for sample 1 and error2 for sample 2. These error limits for the relaxation data increase due to fewer data points being used to calculate T_2 as the resin cures. This is because as the resin cures the relaxation takes place quicker, therefore the exponential decay is quicker. As can be seen there is not much difference between the two data sets, demonstrating the reproducibility of the experimental technique.

From figure 6.2. it can be seen that at approximately 400 minutes, (about 6.66 hours), there is a change in gradient for $\ln(T_2)$, this change corresponds to the gel point as can be seen from the viscosity data in figure 6.3. From the viscosity data it can be seen that at approximately 6 hours the viscosity begins to rise severely. Further cure monitoring data was to be obtained by use of the VNC. This is discussed in chapter 8.

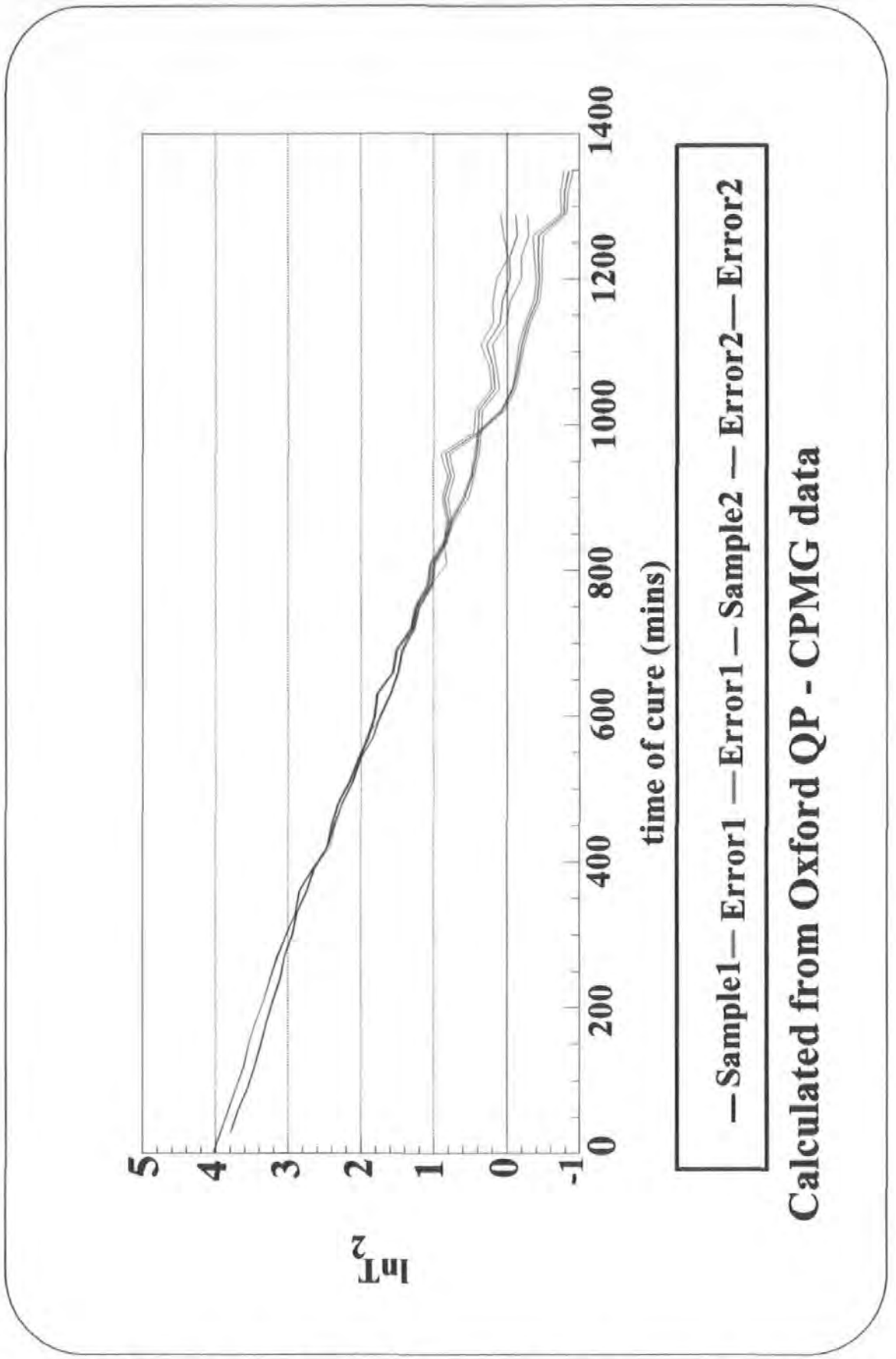

Figure 6.2 Comparison of the natural logarithm of the transverse relaxation time data versus time of cure for two samples. Acquisition for the MY750 resin system during a 40°C cure cycle. Sample1 and Sample2 being the CPMG acquisitions while error1 and error2 are the error limits.

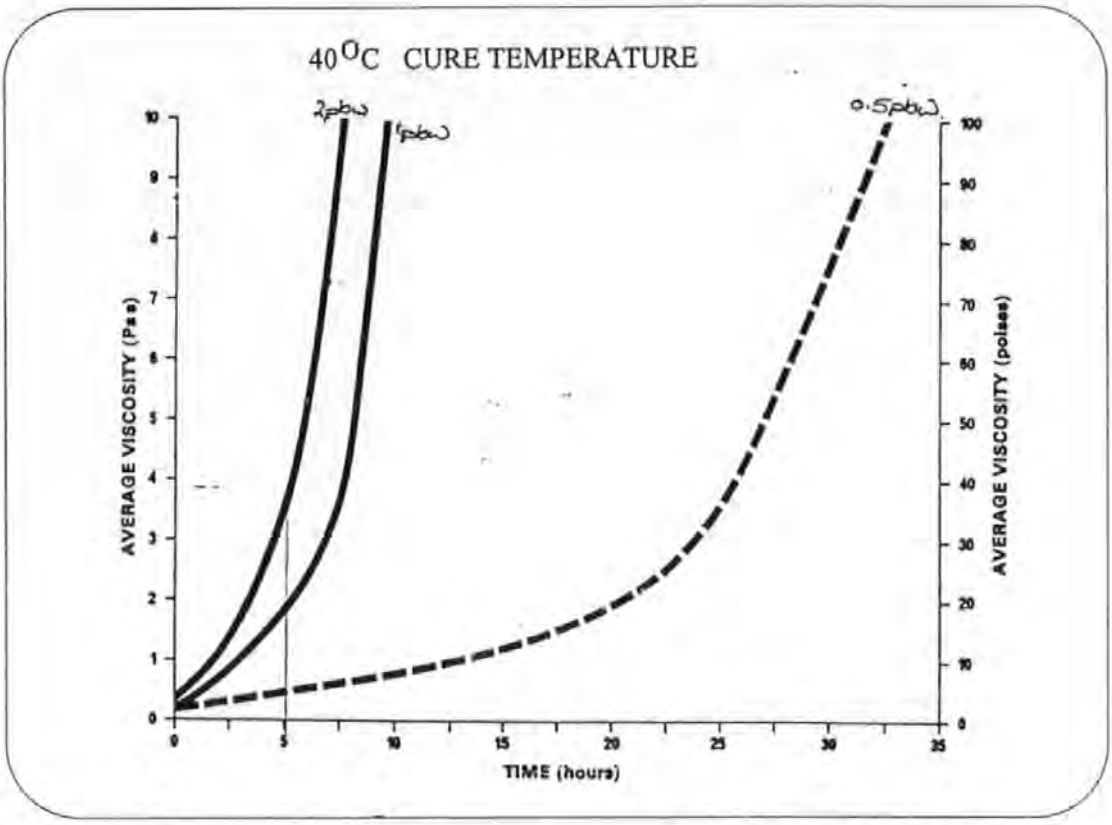

Figure 6.3. Viscosity versus time of cure. Extract from Ciba–Geigy Araldite product range technical information.

The Jeol and QP data are compared in figure 6.4. As can be seen the Oxford QP monitored the cure for far longer than the liquid–state NMR spectrometer. Since the Oxford QP monitored the average signal from the resin rather than the signal from each hydrogen environment it would be expected that this method of data acquisition would be more beneficial. Another thing to note is that the Oxford QP used the more up–to–date and accurate CPMG acquisition sequence as opposed to the Carr–Purcell sequence used by the Jeol EX270 NMR high–resolution spectrometer. The difference between these two acquisition sequences and the benefits of the CPMG sequence are discussed in chapter 1.

The results of the 40°C experimental programme is summarised in Table 6.1. This includes a comparison of the time to loss of resolution in the spectral analysis at the same cure temperature.

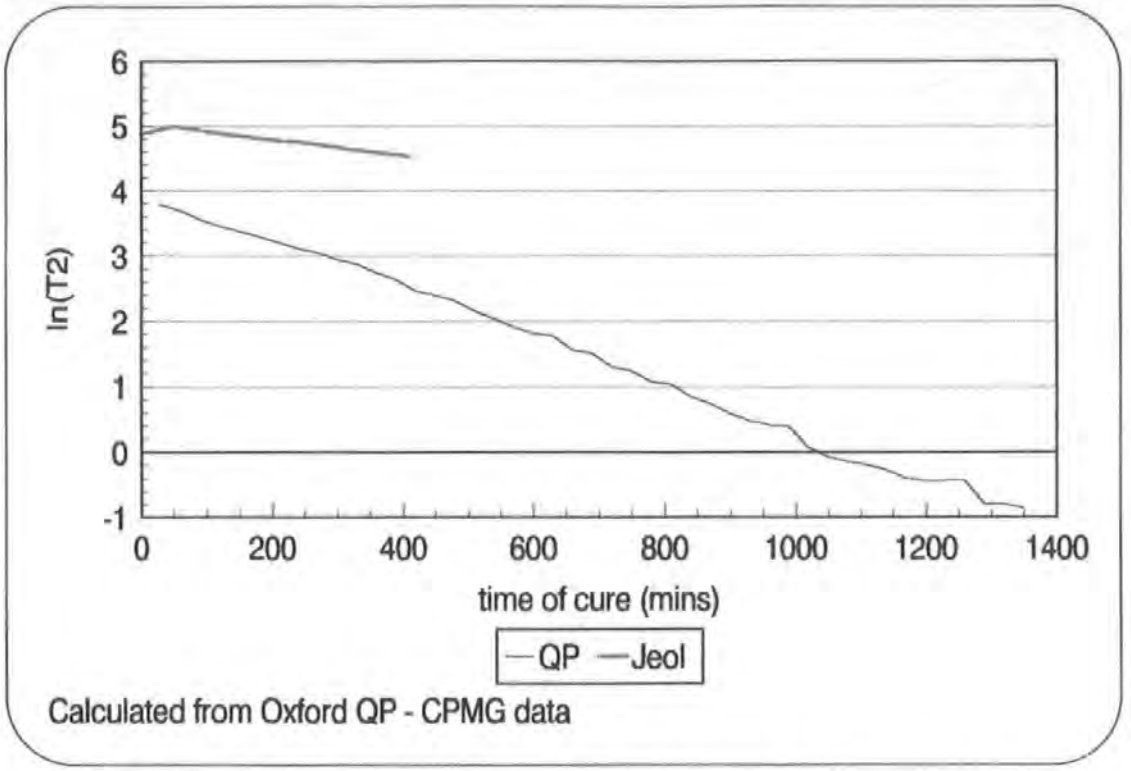

Figure 6.4. The natural log of the transverse relaxation data versus time of cure. Comparison of QP and Jeol acquisitions for the MY750 resin system during a 40 °C cure.

Method of analysis	gelation time (mins)	time to end of data acquisition (mins)
Jeol CP data	-	400
Oxford QP CPMG data	400	1,250
Jeol spectral data	275	-
Viscosity data	480	-

Table 6.1. A comparison of data obtained by the Jeol and Oxford QP relaxation time data acquisitions with the spectral analysis at 40°C and known viscosity data.

6.3. Higher Temperature Acquisitions

Higher temperature cures were attempted on the Oxford QP. The cure temperatures being 60°C, 80°C, and 100°C. Unfortunately, not enough data points, in most cases this was six data points, were acquired before the data became too noisy because of the signal amplitude reducing with respect to the noise level (see figure 6.5.). In addition the oven temperature was not consistent due to the door being repeatedly opened to allow access to samples to carry out testing (see chapter 2). The working temperature of the Oxford QP magnet assembly is set at 40°C. The resin samples were heated in an oven and then transferred to the QP for the data acquisition to take place. This meant that the sample had at least one minute when the cure temperature began to fall. It is not known whether the sample being at a higher temperature than the magnet coil would have affected the homogeneity of the field. If the sample had been monitored for longer than one minute or at more regular intervals than once every ten minutes then the magnetic coil itself may have started to rise in temperature and so affect the results.

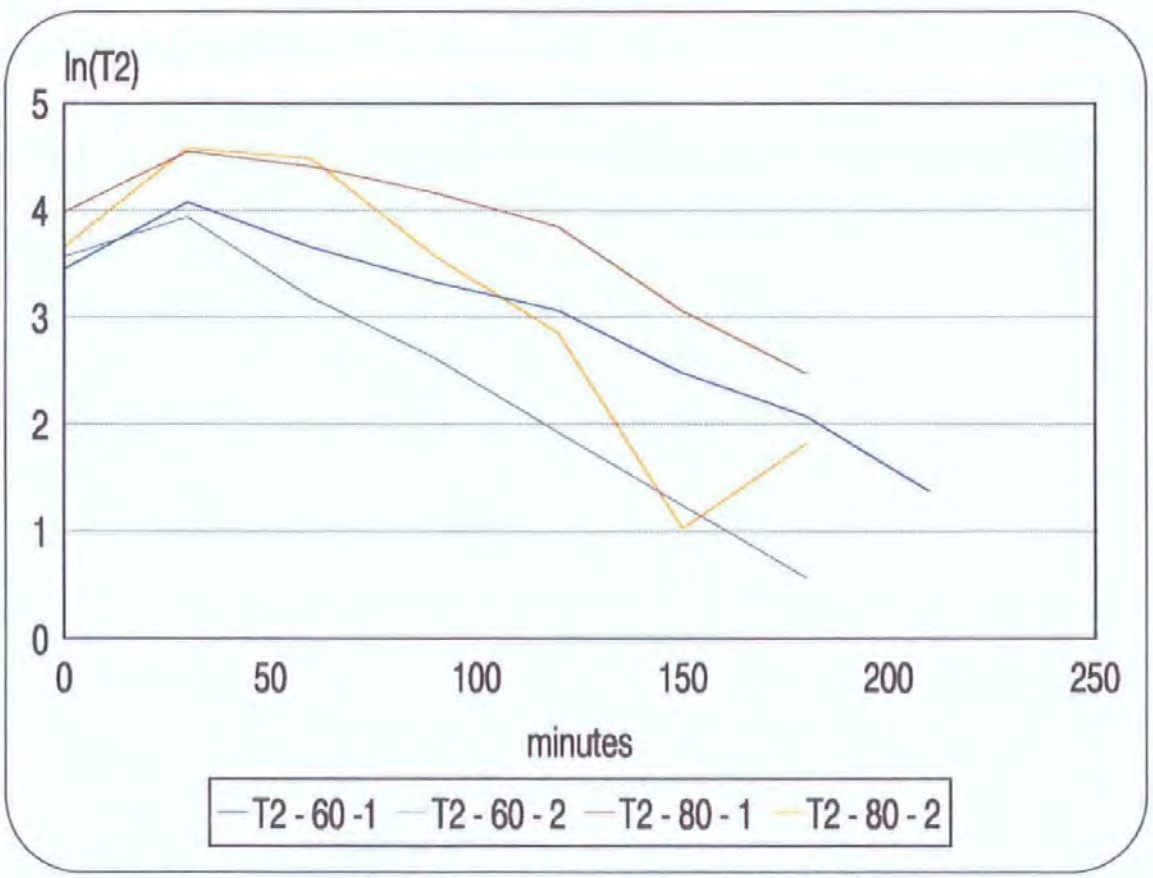

Figure 6.5. Transverse relaxation time data for an MY750 resin system curing at 60°C and 80°C

At 100°C acquisitions were taken every 10 minutes but only two data points could be obtained from each decay curve. However, the temperature gradient established in the sample when transferring to and from the QP was too high for the test–tubes which exploded after a half hour of testing. Hence, data at this temperature is unreliable and has not been presented.

6.4. Discussion

It can be seen that at higher temperatures there is more scatter between experiments carried out at the same cure temperature. This could be due to a number of reasons:

1. that temperature gradients are set up in the sample while it is being monitored (taking one minute) in the QP, which is set at a lower working temperature;
2. that the homogeneity of the magnet could be affected by the high temperature of the sample i.e. the magnet coil is being heated.

For each individual experiment, an increase in scatter did not significantly occur until after the start of gelation, the change from liquid–state to solid–state behaviour. This is due to each experimental decay curve becoming shorter and therefore the transverse relaxation time calculations were undertaken on progressively fewer data points.

There is also a difference in the pulse sequence employed by the Jeol EX270 high–resolution NMR spectrometer and the Oxford QP NMR analyser. The difference is essentially the direction of the application of the π–pulse. On the Jeol the Carr–Purcell pulse sequence is used, this applies the π–pulse along the x' direction whereas the Oxford QP is programmed for the CPMG sequence (see section 1.2.3.) which applies the π–pulse along the y' direction. Meiboom and Gill updated the CP sequence to avoid cumulative errors in the pulse sequence and therefore both sequences should acquire a signal for approximately the same length

of time, the difference being that the CPMG sequence is more accurate (see section 1.2.3.).

The difference in results between the Jeol and the Oxford QP is due to the magnetic fields that each employ. The Jeol is a high resolution spectrometer and hence uses a high magnetic field. This enables analysis of each individual chemical environment of whichever nucleus is under investigation. The disadvantage of this is that although this enables an analysis of how the cross-linking takes place it also means that this cross-linking will also restrict the extent of cure that is capable of being monitored. Therefore the Jeol can only monitor the cure until shortly after gelation. However the Oxford QP uses a much lower magnetic field and is used to investigate all the chemical environments for protons averaged into one signal. This means that it does not give any detailed analysis into the chemical changes i.e. where cross-linking is taking place, but it gives very good prolonged analysis of the overall bulk effect. Even so, relaxation techniques cannot be used to follow the whole of the cure due to the signal becoming too noisy, resulting in progressively fewer data points for analysis and hence increasing the error limits.

By using the CP data acquisition on the Jeol EX270 high-resolution NMR spectrometer, cure can be monitored until 400 minutes into the cure at 40 °C but by using the Oxford QP NMR analyser data can be acquired up to approximately 1200 minutes into the cure at the same temperature. The Oxford QP NMR analyser data appears less reliable after approximately 800 minutes, after this point too much cross-linking may have taken place and so the liquid-state acquisition pulses may not have been able to acquire the "solid" signal. At 400 minutes there is a change in the slope of the $\ln(T_2)$ versus time graph for the Oxford QP acquisitions (figure 6.2.). The Jeol acquisitions also show a drop just before 400 minutes. However it is not as clear since data acquisition of the resin signal becomes difficult to resolve due to the relative strength of the lock signal after 400 minutes. If this data is then re-plotted as a rate of change of $\ln(T_2)$ versus time of cure graph then the change in gradient at 400 minutes and the reliability of the data after 800 minutes is displayed. The $d(\ln T_2)/dt$ values were calculated over a range of three data values and plotted on the middle time of cure value. See figure 6.6 for the results.

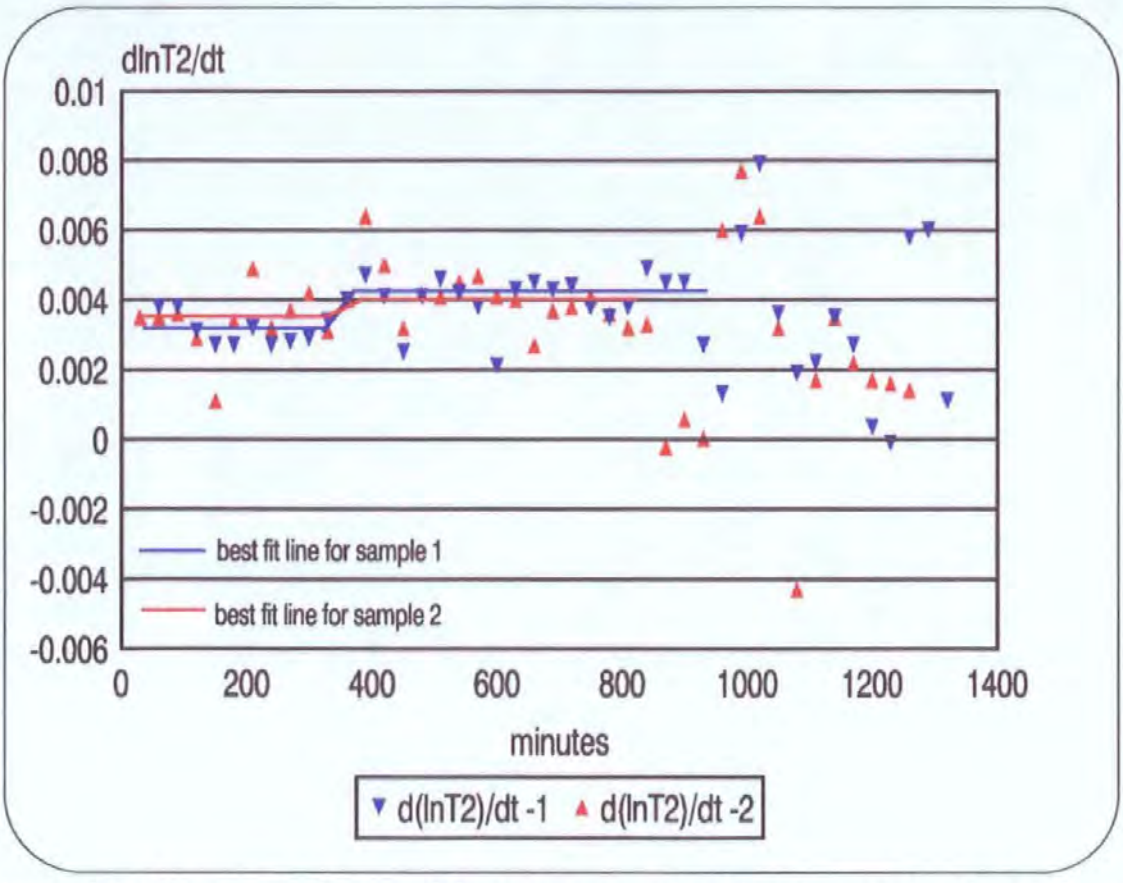

Figure 6.6. The rate of change of the transverse relaxation time during the 40°C cure for samples 1 and 2.

For sample 1 there can be seen a distinct change in gradient resulting in a step as seen in figure 6.6 (the blue line demonstrates the best fit line for sample 1). Sample 2 does not show such a large difference in gradients but even so there is still a change as depicted by the best fit line which is drawn in red. The change in gradient for both samples happens over the same time scale. After about 800 minutes it can be seen that for both samples the data becomes scattered and uncorrelated.

For sample 2 there can be seen to be more scatter between data points (depicted in red in figure 6.6), however the trends first noticed in sample 1 are followed for sample 2 thus showing the repeatibility of the experiment. In figure 6.2. it can be seen that although there is still a change in gradient at 400 minutes the change is not as pronounced as in sample 1 therefore a large step in the $d(\ln T_2)/dt$ graph cannot be expected.

From figure 6.6 there can be no question that after 400 minutes there is a change in gradient which corresponds to the gel point from the viscosity data shown in figure 6.3. These changes will now be examined further by an FID data analysis on the Oxford QP analyser (in chapter 7) and with a curemeter (in chapter 8).

7.0. FREE INDUCTION DECAY INVESTIGATIONS

7.1. Introduction

Free induction decay (FID) data was acquired on the Oxford QP for cure temperatures of 40 °C, 60 °C, 80 °C and 100 °C. As discussed in section 1.2.2, by examining the shape of the FID envelope the different phases can be distinguished. The purpose of these experiments was to see if this feature of the FID could be used to give the solid and liquid percentages of the resin as it cured and give the point of 100% solid.

Bloch [94] showed that it is sufficient to focus attention on the net macroscopic nuclear magnetisation obtained by taking the ensemble average over all the spins. This macroscopic magnetisation obeys the laws of classical mechanics in its interaction with the applied static and radio-frequency fields, while the effects of spin-spin and spin-lattice relaxation may be accounted for phenomenologically by the introduction of simple damping terms into the Bloch equations [21]. The transient Bloch equations take on a simpler form when described in a reference frame rotating with the radio-frequency frame B_1.

Most of the observed NMR phenomena can be accounted for on the assumption that each individual resonance in the high-resolution spectrum can be represented by a vector M with a characteristic intensity and a characteristic precession frequency. Each such vector M is assumed to obey the Bloch equations.

For a spin system that has been allowed to reach Boltzmann equilibrium, all these vectors are aligned along the z axis of the rotating frame, and a 90° r.f. pulse rotates them about the x' axis, leaving them along the y' axis. It is convenient to assume that the pulse is 'perfect' in that it affects all parts of the effective sample volume uniformly, and that the action is independent of the offset of a given line from the transmitter frequency. The reference phase of the receiver is usually taken to be such as to detect the y' magnetisation in the phase. Thus the signal intensity immediately after the pulse is at its maximum value. In fact, this first ordinate of the free

induction decay represents the integral of the total intensity in the absorption spectrum [94]. Therefore since the intensity is defined as the strength or amount of a quantity, as of electric field, current, magnetisation, radiation or radio-frequency [95] i.e. intensity is proportional to the number of equivalent spins per unit volume, then the area under the envelope of the decay curve is proportional to the volume of the sample.

The envelope of the free induction decays with time, in many cases falling to a negligible level before acquisition is stopped. This is a result of spin-spin relaxation and the mutual interference between macroscopic signals from different regions of the sample due to the inhomogeneity of the B_0 field. Residual instabilities in the field / frequency regulation may also contribute to this decay, particularly if several sequential free induction decays are being summed together.

Therefore, from the initial ordinate (termed in future the initial amplitude of the signal intensity) the percentages of the solid and liquid components of the FID can be determined. The signal intensity of the solid component is therefore proportional to the number of equivalent spins per unit volume of the solid phase. Therefore the proportions of solid phase to liquid phase can be monitored throughout the curing process.

7.2. Analysis of FID

For each cure FID acquisitions were taken at regular intervals. Consider the cure of MY750 resin system at 100 °C (see figure 7.1.), acquisitions being taken every ten minutes. In figure 7.1. the different shapes of the FID envelope can clearly be seen as the resin cures. At t=0, the resin is predominantly liquid in character (since the resin is very viscous some minor solid effects may be present in the FID envelope) giving a standard liquid curve. At t=30 (and for the rest of the cure time) the resin is predominantly solid as shown by the standard solid curve. Between t=0 and t=30

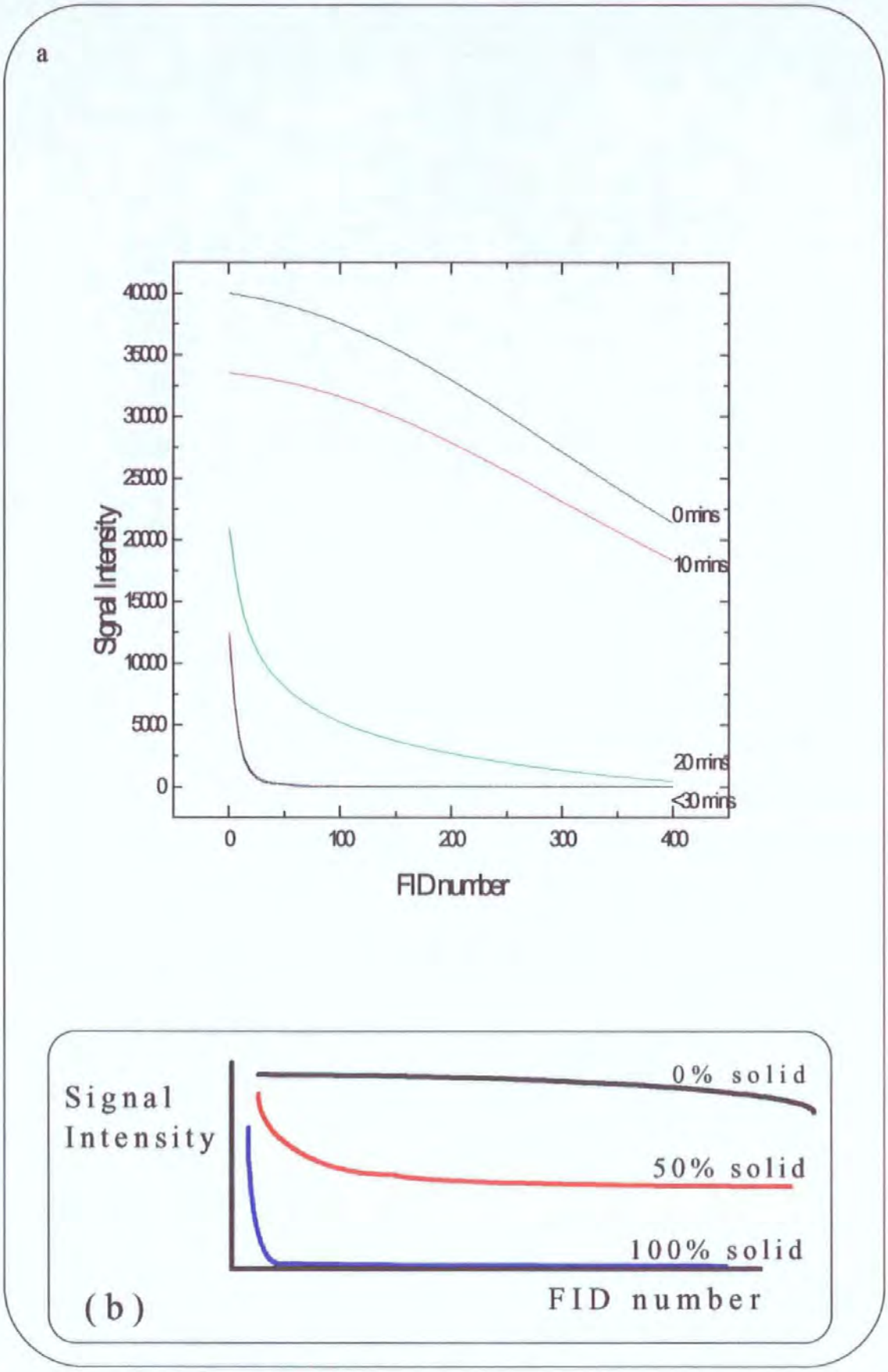

Figure 7.1. Signal Intensities versus FID number for MY750 resin system cured at 100 °C. FID data was acquired for 90 minutes into the cure. Inset (b) is a sketch of curve characteristics. Where FID number is the number of data points per acquisition.

the FID envelope can be seen to change from predominantly liquid in character to predominantly solid.

This data was then analysed by fitting it to two exponential curves (the total curve being the superposition of the solid and liquid curves) and the initial amplitude of the signal intensity was calculated for each phase. The initial amplitude of the liquid intensity is dependent on the amount of hydrogen present that still has some degree of movement called here 'free hydrogen'. As the resin cures the amount of 'free hydrogen' reduces as cross-linking takes place therefore the liquid amplitude decreases as the cure progresses. However, the initial amplitude of the solid intensity is dependent on the amount of hydrogen that has no degree of freedom called here the 'fixed hydrogen'. As the cure progresses the amount of fixed hydrogen increases due to cross-linking taking place and therefore the solid initial amplitude increases. From these initial amplitudes the percentage liquid and solid phases in the sample could be established, i.e.:

proportion of solid = initial amplitude of solid signal ÷ Sum of initial amplitudes
Intensity(A_1) ($A_1 + A_2$)

where A_2 = initial amplitude of liquid signal intensity.

therefore, $\%_{sol} = \frac{A_1}{A_1+A_2}$ x100 while, $\%_{liq} = \frac{A_2}{A_1+A_2}$ x100

As discussed earlier in this chapter, the percentage is calculated using the sum of the initial signal intensities because it is the sum of the liquid and solid phases in the sample i.e. the whole sample.

The initial amplitudes of the solid and liquid intensities change as the resin cures. For the solid phase the amplitude increases as the resin becomes predominantly solid while for the liquid phase the amplitude steadily decreases. Therefore at 50%

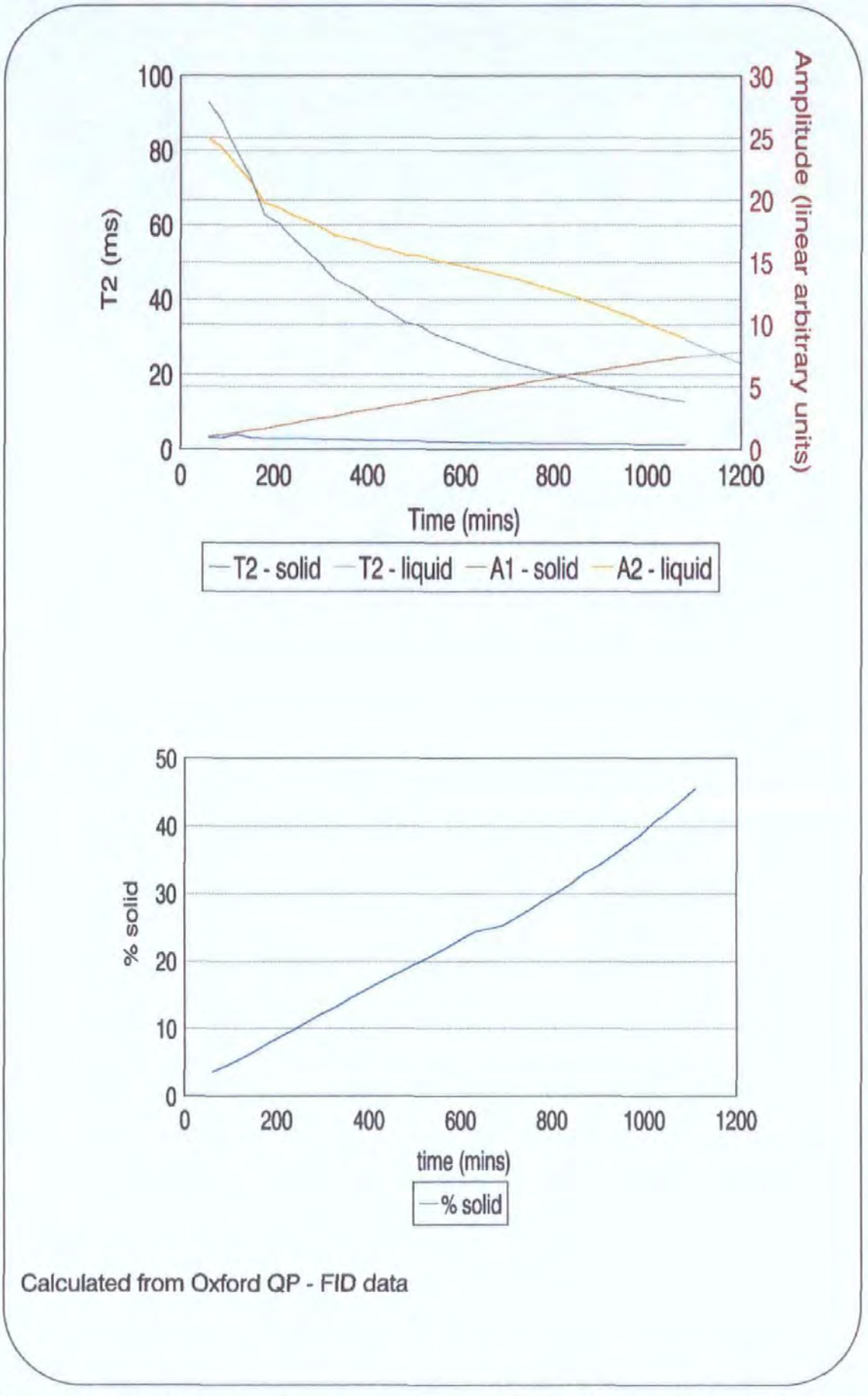

Figure 7.2. Free induction decay analysis at 40 °C. The top graph demonstrates the change in solid and liquid amplitudes as the resin cures. The bottom graph is of the calculated percentage solid versus time of cure.

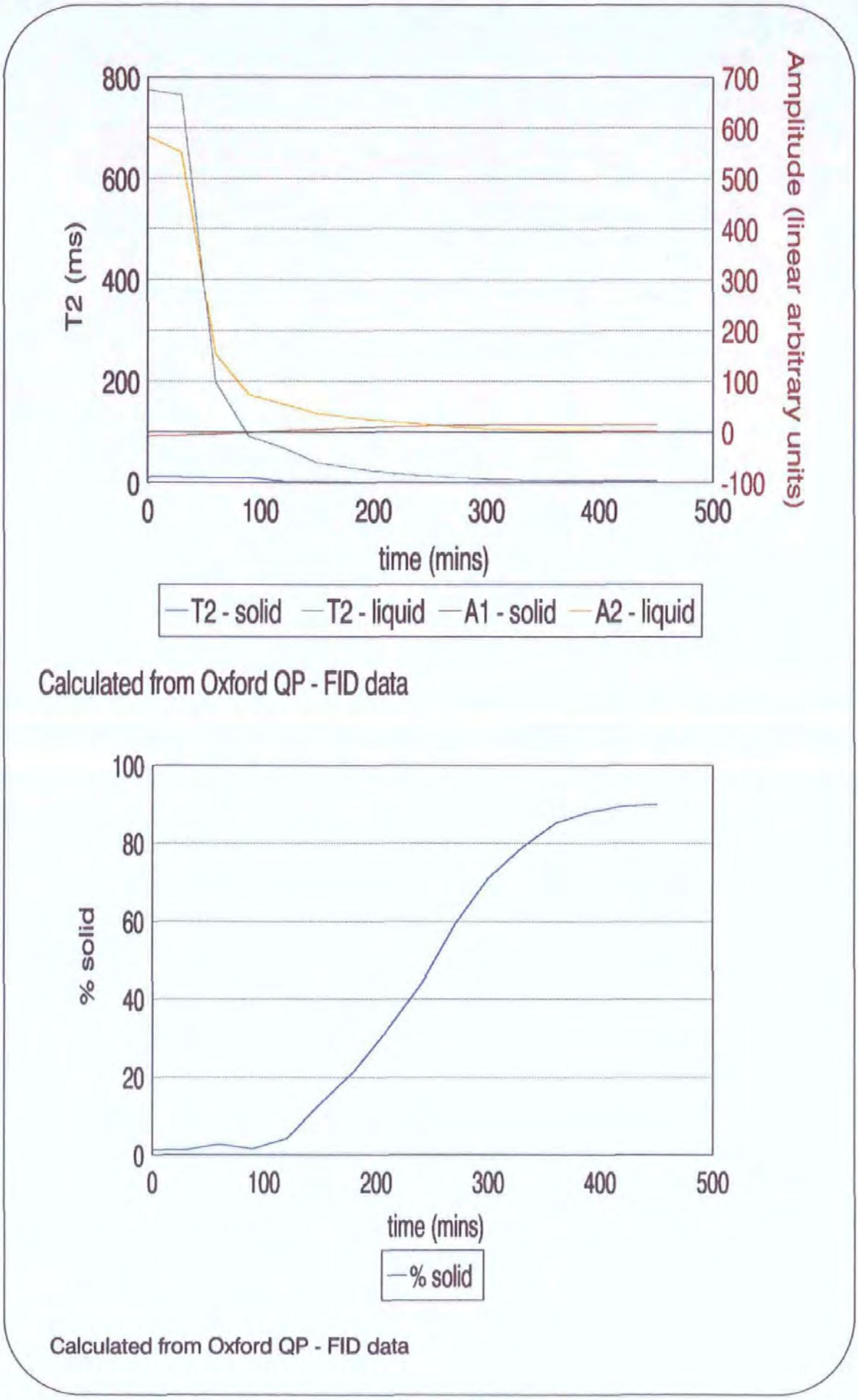

Figure 7.3. Free induction decay analysis at 60°C

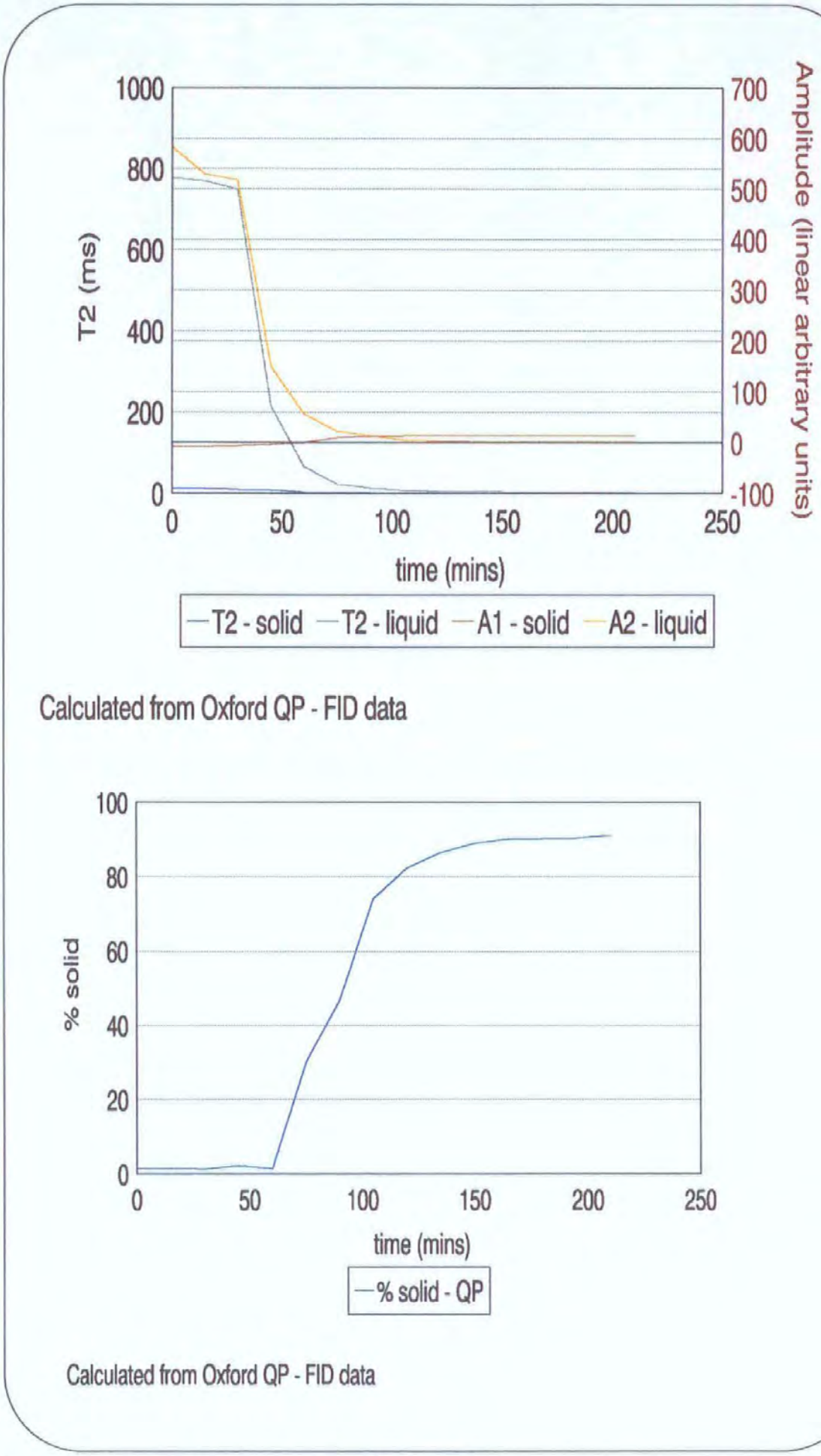

Figure 7.4. Free induction decay analysis at 80°C

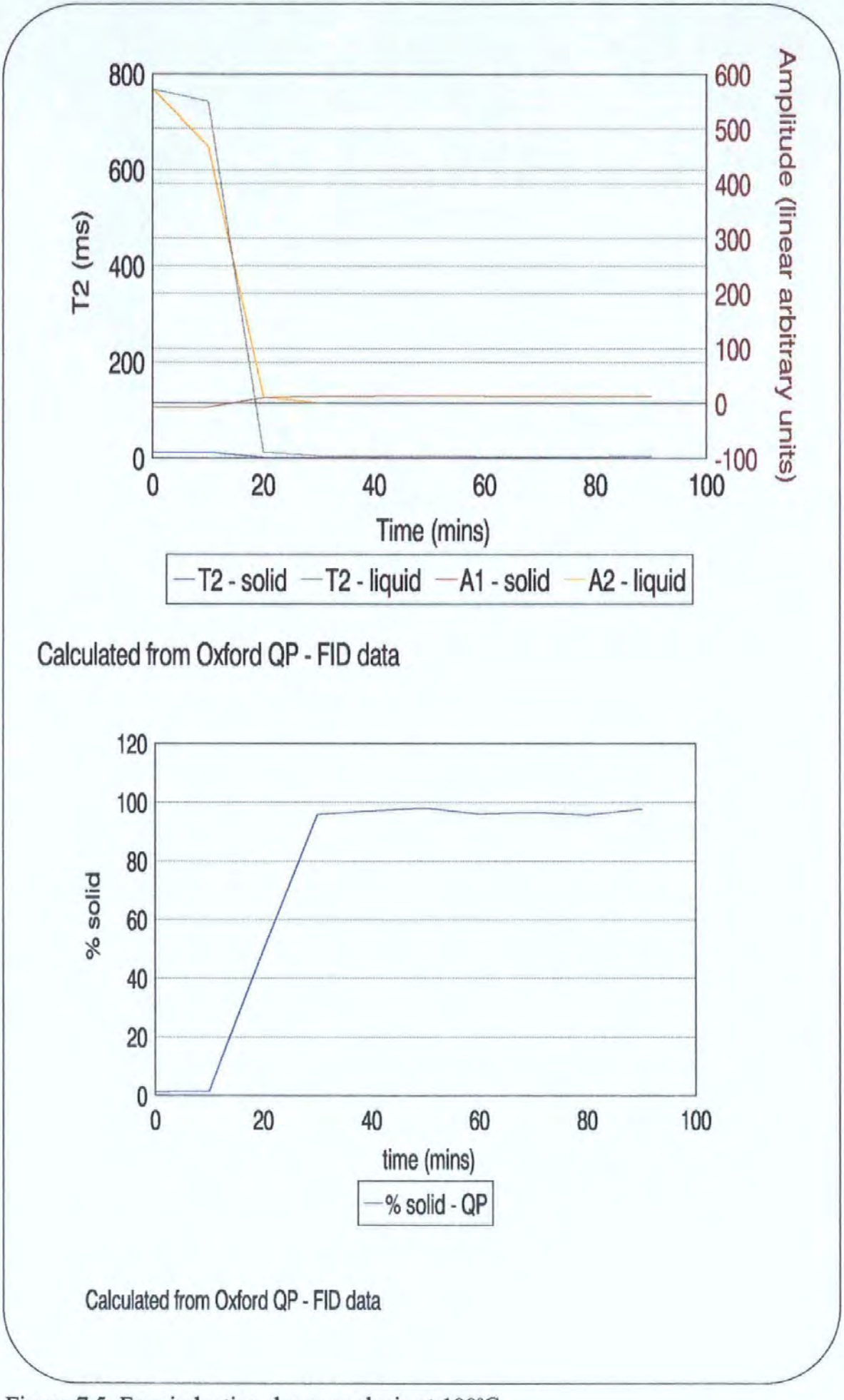

Figure 7.5. Free induction decay analysis at 100°C

cure (i.e. 50:50 liquid phase : solid phase) the initial amplitudes of the solid and liquid phases will be equal since the initial ordinate represents the integral of the total intensity in the absorption spectrum.

For each cure temperature graphs of initial amplitude and percentage solid versus time of cure were produced (see figures 7.2. to 7.5.). From these it can be seen that the cross over point of the amplitudes corresponds with 50% solid. Only the 40 °C cure temperature graph shows some difference (40 minutes) at this point, this is because the length of time the experiment takes requires that only the initial forty percent of the cure is recorded and then the data extrapolated, as illustrated in figure 7.2a. For the 40°C and 60°C analysis the data points are 30 minutes apart, 15 minutes apart in the 80°C analysis and 10 minutes apart for the 100°C analysis. Therefore, the curves are based on a limited number of data points and so are only an interpretation of the effects obtained. Especially in the case of the 100°C cure since the sample was nearly 100% solid after four data points.

7.3. Effects of Fibres on the FID

For cure temperatures of 40°C, 60°C and 80°C the FID experiment was repeated with the addition of approximately 10%, 20% and 30% volume fraction, V_f, of glass fibre. As previously the data was analysed bi-exponentially and the initial amplitude of the signal intensity was calculated for each phase. The percentage of solid and liquid phases throughout the cure could then be calculated as previously. Due to the size of the sample-tubes it was difficult to attain exact volume fractions with the chopped glass-fibre mat, therefore burn-off tests were carried out on the samples to determine the experimental volume fraction, V_{f-expt} (see chapter 2).

7.3.1. Effect of Fibres on Solid Component

In figure 7.6 there can be seen the effect of cure temperature on the solid component of the transverse relaxation time (T_2 -solid). As can be seen the initial T_2 -solid at all temperatures is approximately the same (except at 40°C where data acquisition did not start until one hour into the cure). It can also be seen that as the cure temperature increases the curves decay more rapidly. On addition of fibres it can be seen that the initial T_2 -solid falls from between 3 and 4ms, see figures 7.7 to 7.9. To determine the repeatability two experiments were completed for each volume fraction, V_f and these two experiments are termed V_f-1 or V_f-2 for the two 10% volume fraction experiments, V_f-3 and V_f-4 for the two 20% volume fraction experiments and V_f-5 and V_f-6 for the two 30% volume fraction experiments as can be seen in figures 7.7 to 7.9. To determine the exact volume fraction used for each experiment a burn-off test as described in chapter 2 was employed for actual volume fractions used (see table 7.1). In figures 7.7. to 7.9. the actual volume fraction is given.

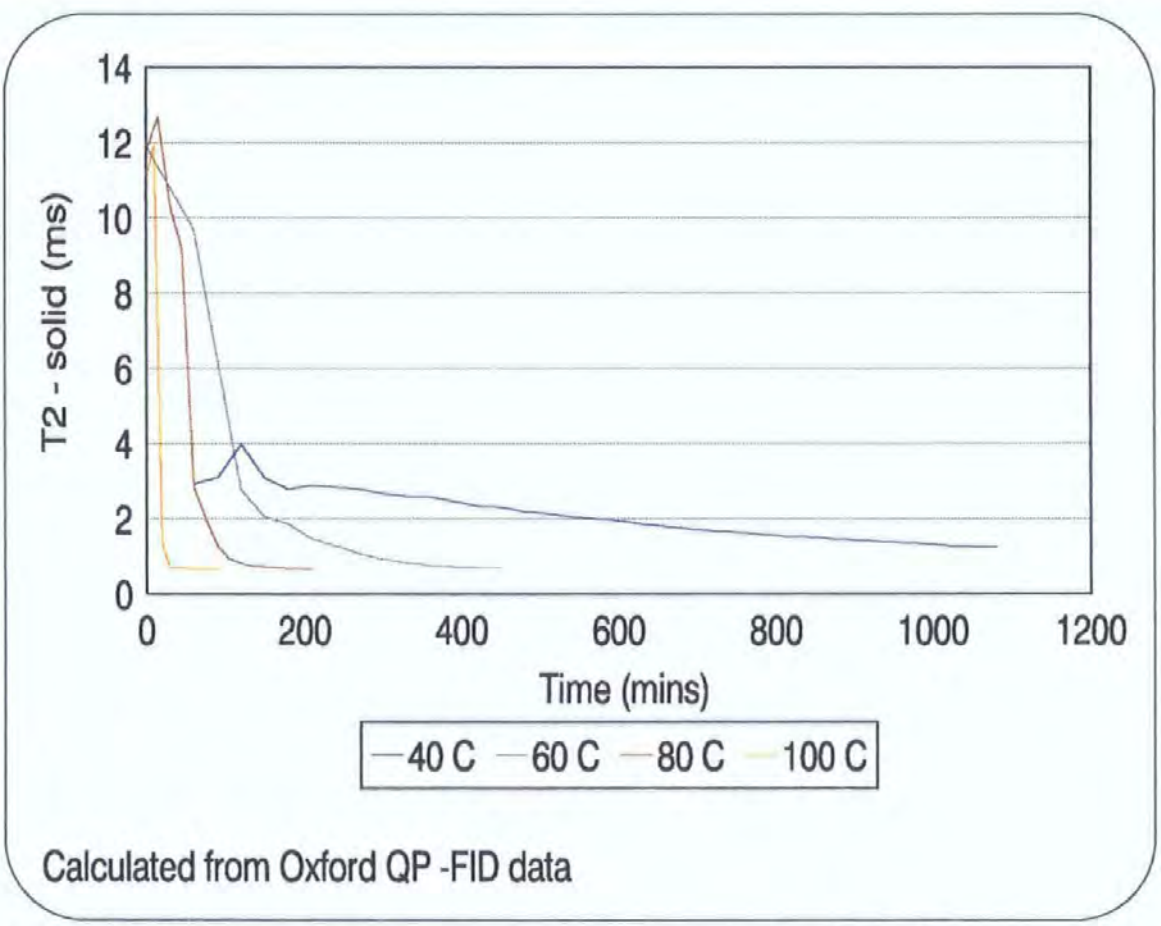

Figure 7.6. Effect of cure temperature on T_2 solid component - no fibres.

Volume fraction		Sample number	Cross of amplitudes (mins)	50% solid (mins)	Actual volume fraction, v_{f-expt}
40 °C	0		1,151.90	1,157.80	
	10	1.00	1,396.30	1,408.50	9.00
	10	2.00	1,364.40	1,363.80	5.90
	20	3.00	1,356.40	1,344.50	18.10
	20	4.00	1,340.40	1,326.20	15.70
	30	5.00	1,300.50	1,307.90	22.40
	30	6.00	1,273.20	1,262.20	22.80
60 °C	0		250.50	247.20	
	10	1.00	346.30	341.50	8.60
	10	2.00	342.60	341.50	7.10
	20	3.00	316.80	315.90	24.70
	20	4.00	326.80	324.40	16.90
	30	5.00	324.20	320.10	23.60
	30	6.00	318.30	312.20	20.43
80 °C	0		92.20	92.10	
	10	1.00	101.10	93.90	10.21
	10	2.00	104.30	98.20	8.60
	20	3.00	98.70	98.20	17.30
	20	4.00	85.60	72.60	16.50
	30	5.00	93.10	76.80	23.90
	30	6.00	73.70	67.90	21.20

Table 7.1. The effect of addition of fibres to the 50% cure point.

At 40°C it can be seen that there appears to be little repeatability between samples of the same volume fraction however the results from the burn-off test will determine which samples should show a similar trend, results of which are shown in table 7.1. As expected from the transverse relaxation time data in figure 7.6. the curves decay more rapidly at higher temperatures regardless of volume fraction. For each cure cycle all the curves 'bottom-out' at the same time and T_2 value as the 0% volume fraction curve does (figure 7.6). The repeatability of these tests will be discussed in the discussion section at the end of this chapter.

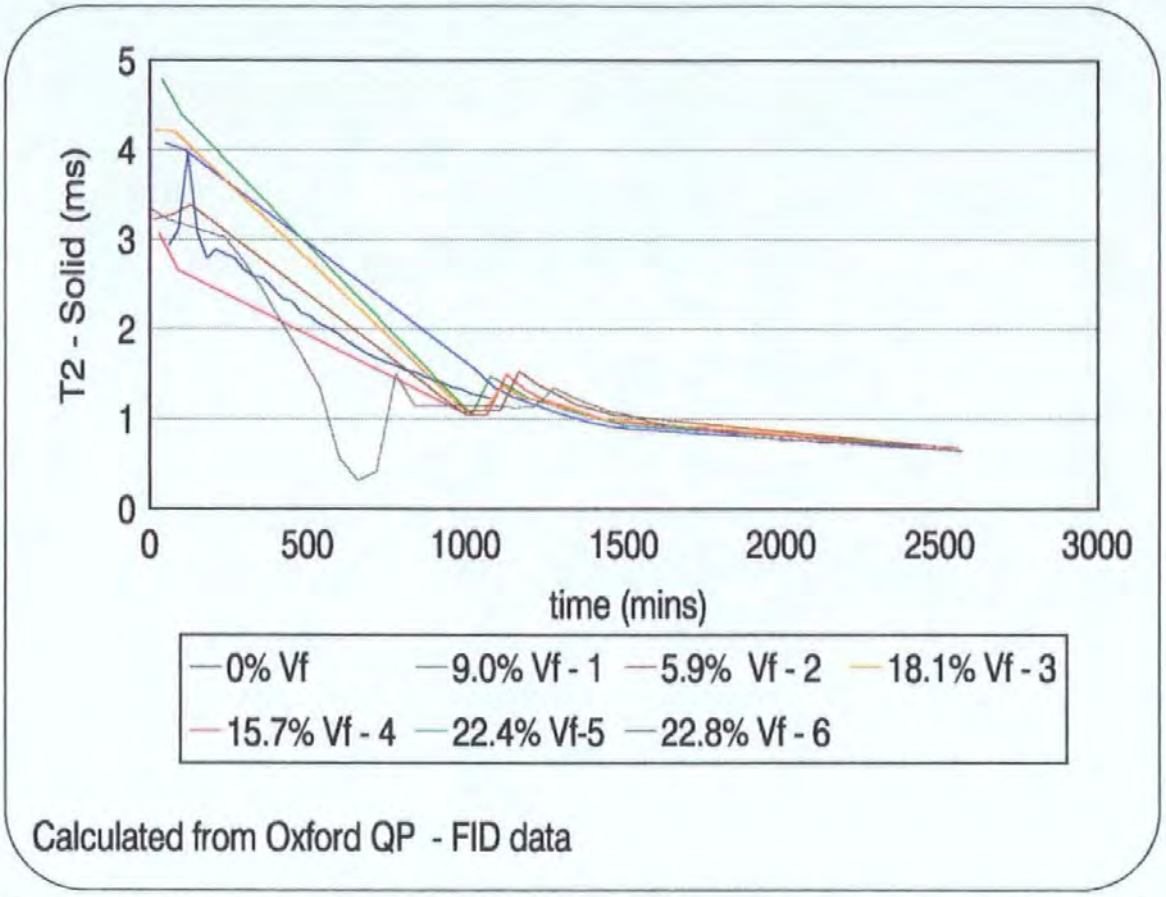

Figure 7.7. Effect upon T_2 -solid on addition of fibres at a cure temperature of 40°C

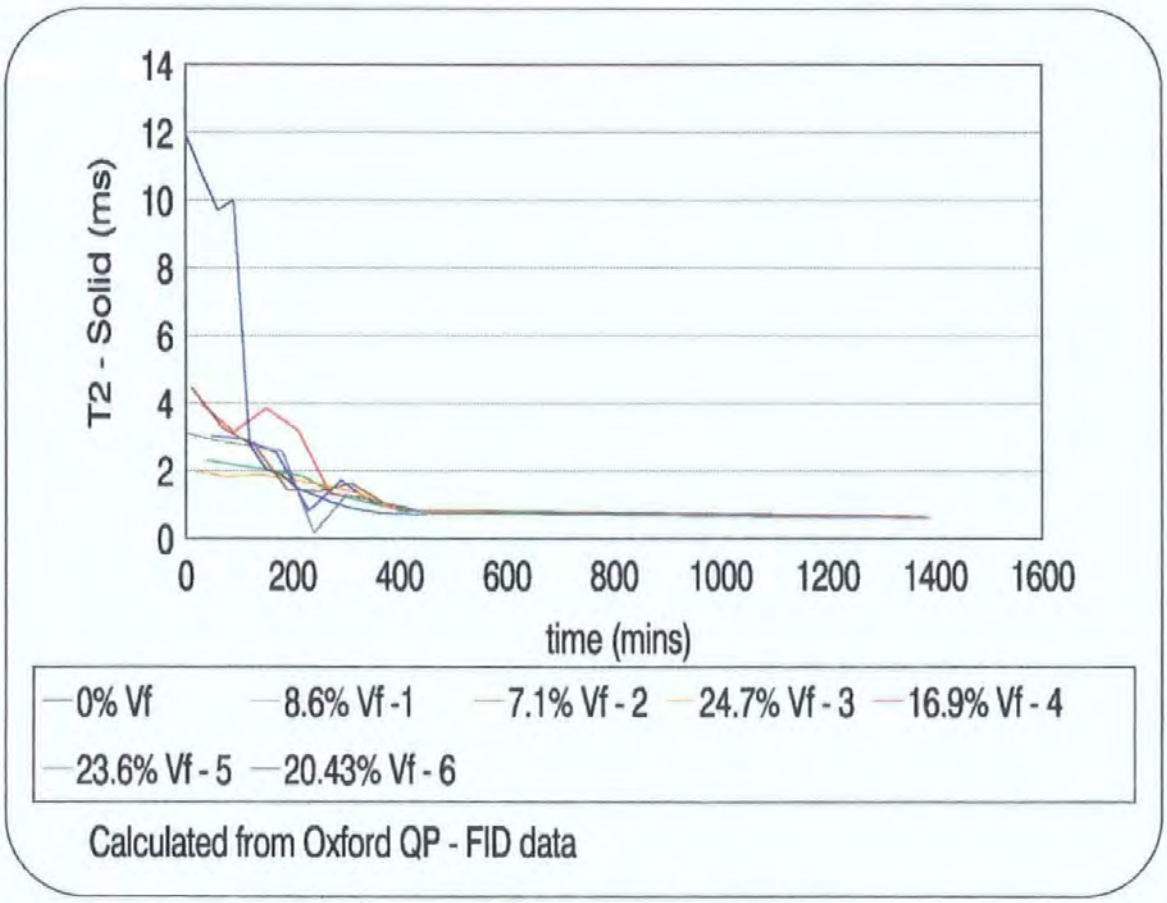

Figure 7.8. Effect upon T_2 -solid on addition of fibres at a cure temperature of 60°C

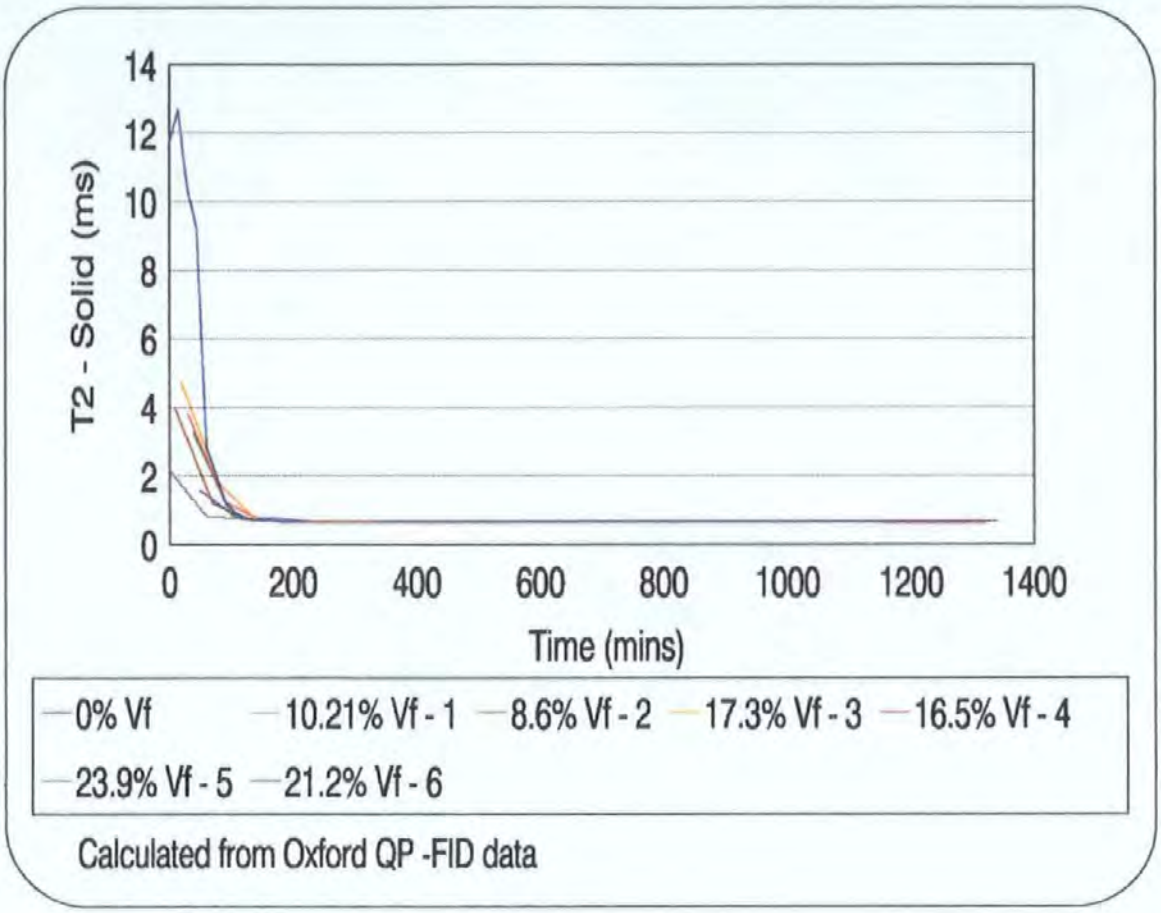

Figure 7.9. Effect upon T_2 -solid on addition of fibres at a cure temperature of 80°C

7.3.2. Effect of Fibres on the Liquid Component

On the addition of fibres the initial T_2 - liquid can be seen to drop from approximately 800ms to between 25 and 15ms see figures 7.11 to 7.13. This could be due to one of two reasons:

1. The glass fibres are obscuring the signal strength, or
2. The glass fibre restricts the freedom of the liquid-state hydrogen.

Although the glass fibre contains no hydrogen within the fibre itself it may be coated with an agent to enhance the chemical interface that is required between the fibre and resin to make the component structurally sound. Any such coating will be a hydrocarbon and hence contain hydrogen which may be in a more restricted environment than the uncured resin.

The cure temperature has little effect on the initial T_2 values as can be seen in figure 7.10. However, as the cure temperature increases the curves can be seen to decay more rapidly.

These results were taken from the same experiments as previously mentioned in section 7.3.1. therefore the experiments undertaken for each volume fraction, V_f are referred to as follows, experiment 1 and 2 for 10% volume fraction, 3 and 4 for 20% volume fraction and 5 and 6 for 30% volume fraction. As previously stated the exact volume fractions, $V_{f\text{-}expt}$ were determined by a burn–off test the results of which are presented in table 7.1. In figures 7.11 to 7.13 the actual volume fractions are given in brackets after the theoretical value.

As mentioned in the previous section for the T_2 –solid analysis, the effect of adding fibres to the resin is to greatly reduce the first T_2 –liquid value. However, as before, for each cure cycle the curves for all volume fractions 'bottom–out' at the same time and T_2 value. The data presented in this section will be discussed further in the discussion at the end of this chapter.

7.3.3. The Effect of Addition of Fibres on Solid and Liquid Amplitudes.

As discussed in part 7.2. the percentage solid at any moment during the cure cycle of the resin can be calculated from the initial solid and liquid amplitudes of the FID. At 40 °C and 60 °C the volume fraction increases the time to 50% solid (i.e. when the liquid and solid components cross). The time to 50% solid then decreases as the volume fraction increases. However at 80°C the same trend is seen through the 10 to 30% volume fractions however the 0% V_f sample has a time to 50% solid in the middle of this effect rather than before it. See figure 7.14 and table 7.1. For diagrams of amplitudes and % solid these figures were derived from please see appendix 3.

The cure temperature has little effect on the initial T_2 values as can be seen in figure 7.10. However, as the cure temperature increases the curves can be seen to decay more rapidly.

These results were taken from the same experiments as previously mentioned in section 7.3.1. therefore the experiments undertaken for each volume fraction, V_f are referred to as follows, experiment 1 and 2 for 10% volume fraction, 3 and 4 for 20% volume fraction and 5 and 6 for 30% volume fraction. As previously stated the exact volume fractions, V_{f-expt} were determined by a burn–off test the results of which are presented in table 7.1. In figures 7.11 to 7.13 the actual volume fractions are given in brackets after the theoretical value.

As mentioned in the previous section for the T_2 –solid analysis, the effect of adding fibres to the resin is to greatly reduce the first T_2 –liquid value. However, as before, for each cure cycle the curves for all volume fractions 'bottom–out' at the same time and T_2 value. The data presented in this section will be discussed further in the discussion at the end of this chapter.

7.3.3. The Effect of Addition of Fibres on Solid and Liquid Amplitudes.

As discussed in part 7.2. the percentage solid at any moment during the cure cycle of the resin can be calculated from the initial solid and liquid amplitudes of the FID. At 40 °C and 60 °C the volume fraction increases the time to 50% solid (i.e. when the liquid and solid components cross). The time to 50% solid then decreases as the volume fraction increases. However at 80°C the same trend is seen through the 10 to 30% volume fractions however the 0% V_f sample has a time to 50% solid in the middle of this effect rather than before it. See figure 7.14 and table 7.1. For diagrams of amplitudes and % solid these figures were derived from please see appendix 3.

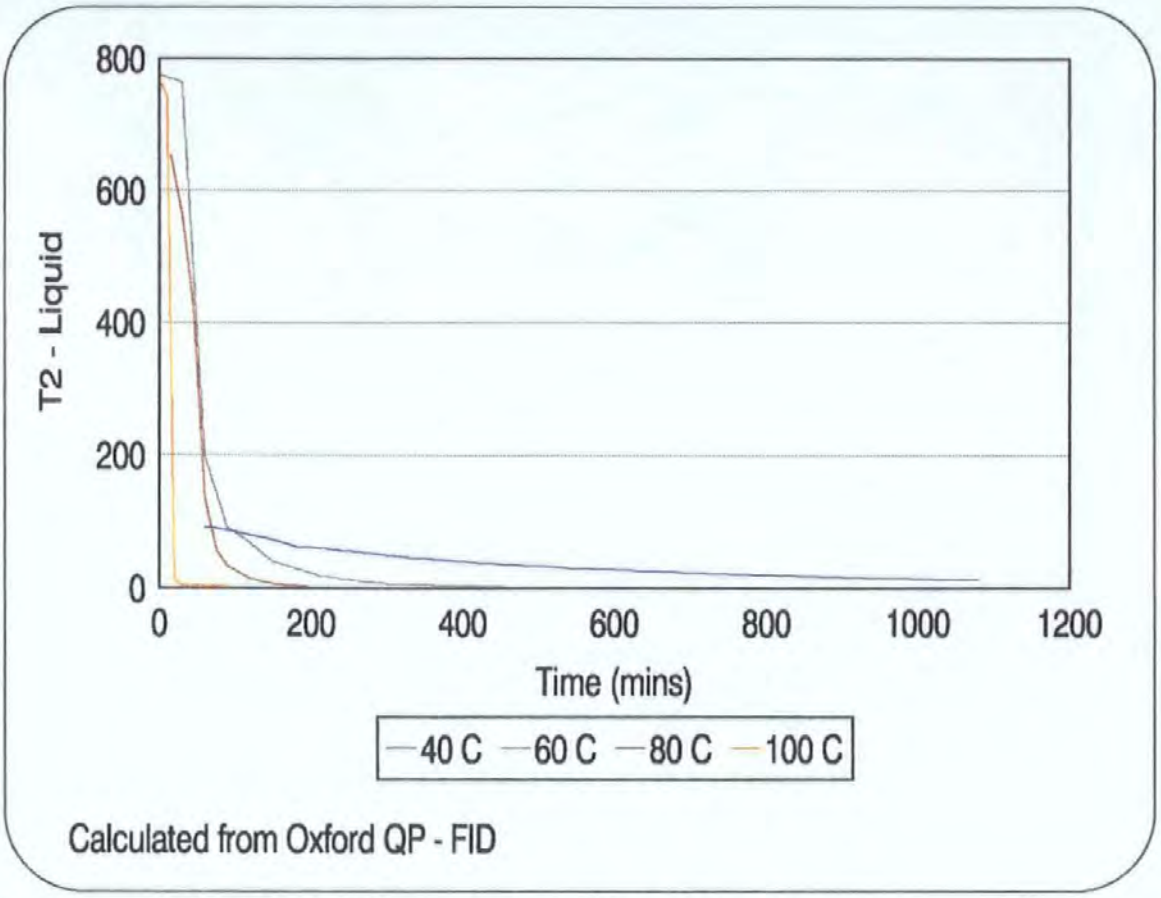

Figure 7.10. The effects of temperature on T_2 -liquid, no fibres.

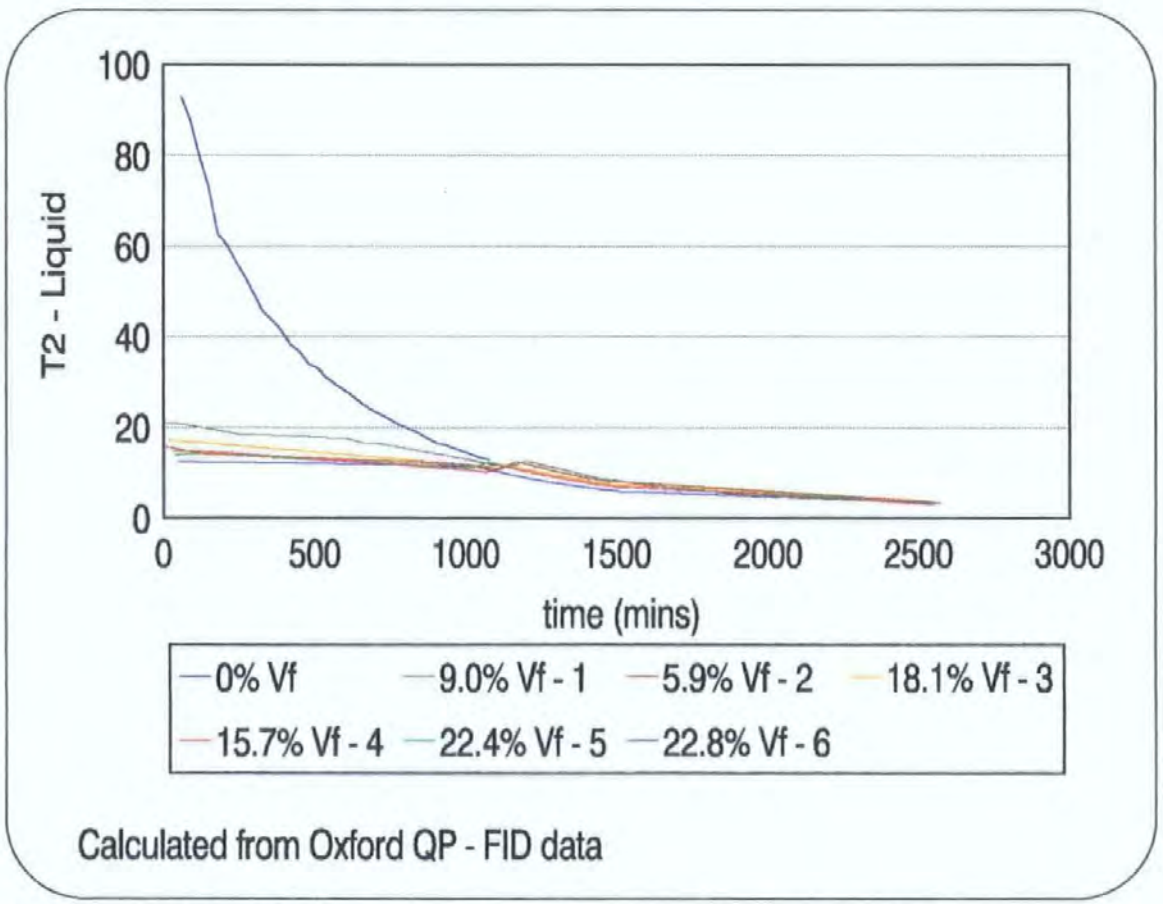

Figure 7.11. The effect of the addition of fibres on T_2 -liquid at 40°C.

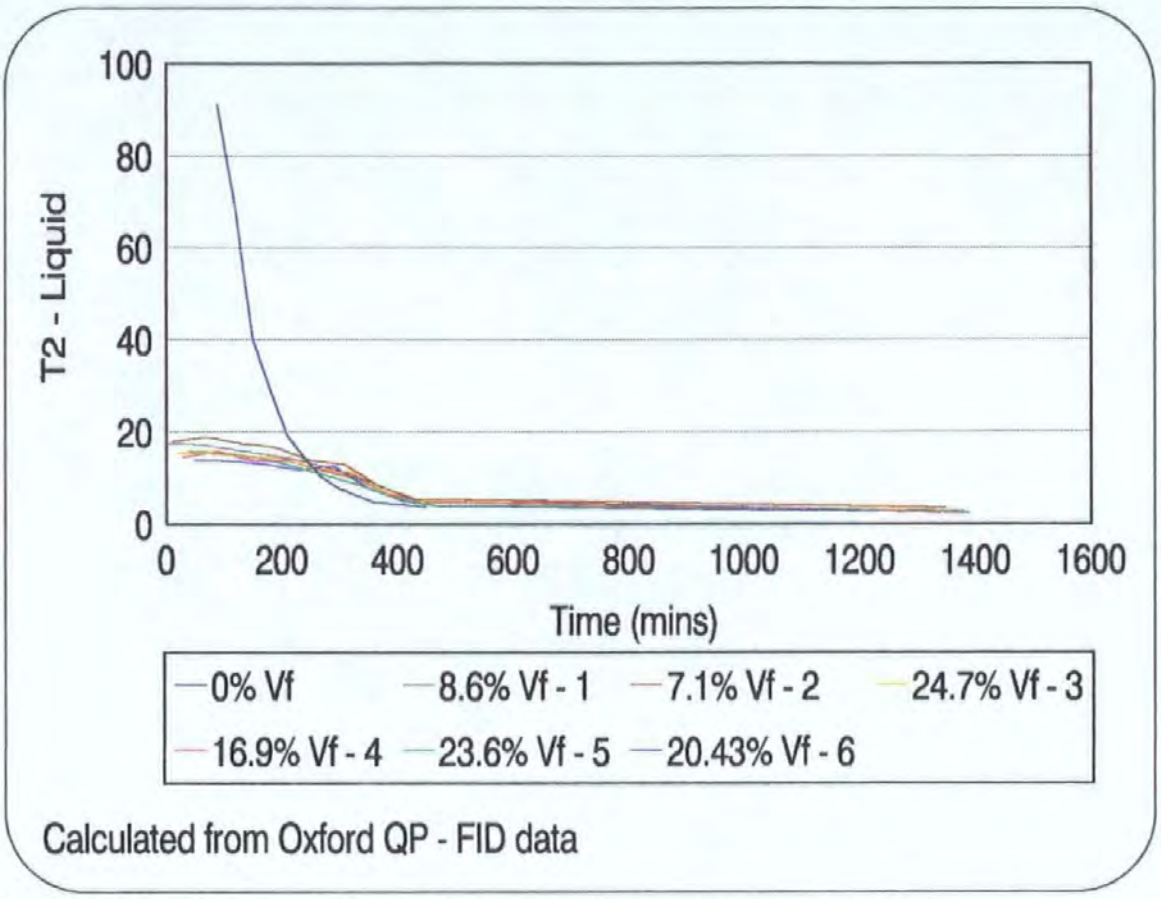

Figure 7.12. The effect of the addition of fibres on T_2 -liquid at 60°C.

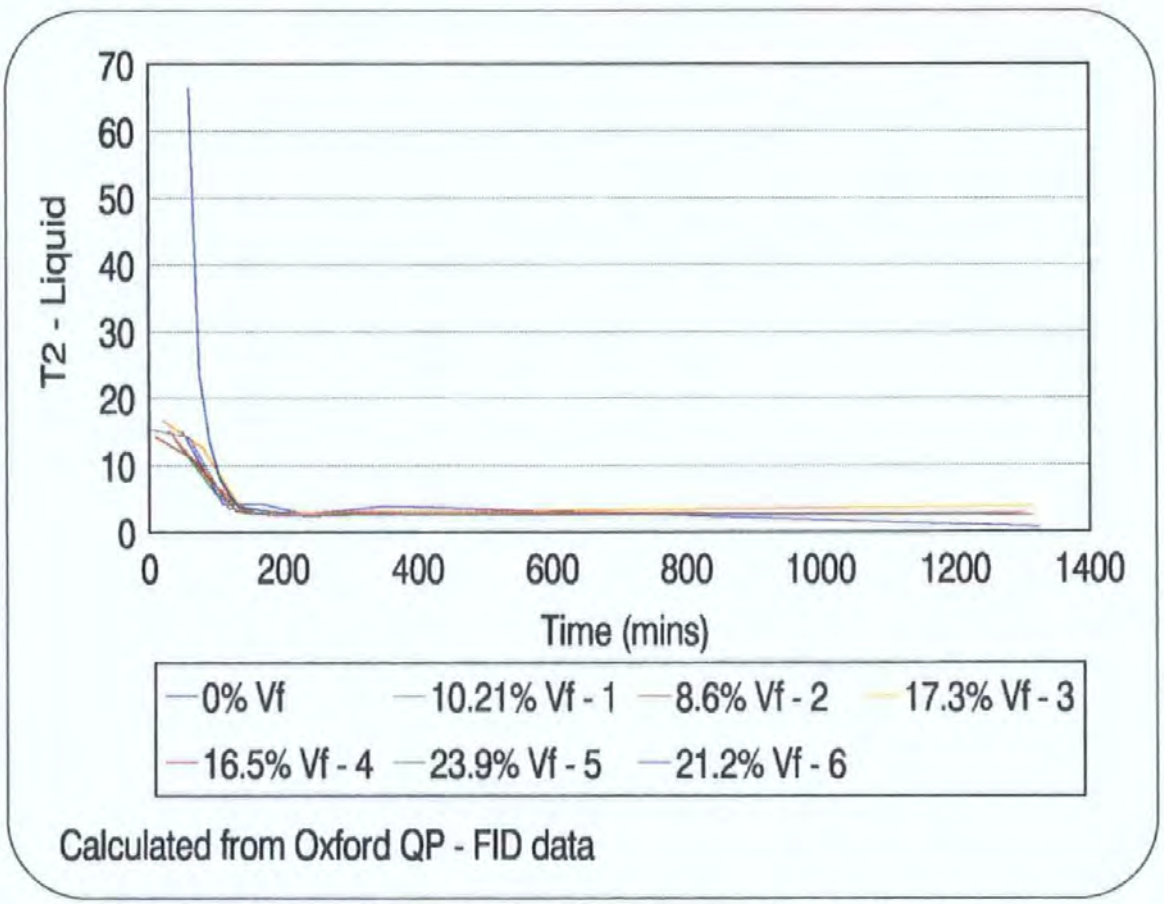

Figure 7.13. The effect of the addition of fibres on T_2 -liquid at 80°C.

7.4. Discussion

Throughout this chapter % solid has been referred to rather than % cure, this is because the validity of this method for cure monitoring is still under investigation. It is unknown yet whether this method will show the point of complete cross-linking or if there is a limit to the amount of cross-linking this method can monitor. Therefore, although this method can monitor the % solid of the resin sample can it monitor the % cure?

By analysing the envelope of the FID curves using the first ordinate to determine the percentages of the solid and liquid phases the cure can be monitored for longer into the cure than with the CPMG method discussed in chapter 6.

Since the signal intensity is proportional to the number of equivalent spins per unit volume then from the initial ordinate of the FID the volume of the solid and liquid phases can be determined. This could be taken further to determine the volume fraction of the resin when fibres are present.

The analysis of the liquid and solid components of the transverse relaxation time data shows how the initial amplitude drops on addition of fibres regardless of volume fraction and cure temperature. As shown in the previous chapter T_2 (solid or liquid) gives little information towards the end of the cure regardless of acquisition method (i.e. CP, CPMG or FID acquisitions).

The liquid amplitude of the signal intensity drops severely on addition of fibres from between 600 and 800 to 20 or 40 with fibres added independent of volume fraction. The solid amplitude of the signal intensity is not affected by volume fraction. Since the signal intensity is proportional to the number of equivalent spins per unit volume then the reduction in the initial amplitude for the liquid phase could be a result of there being less resin present when fibres are added.

The applicability of the Oxford QP as a curemeter will be examined with reference the vibrating needle curemeter (VNC) and a Barcol hardness investigation on

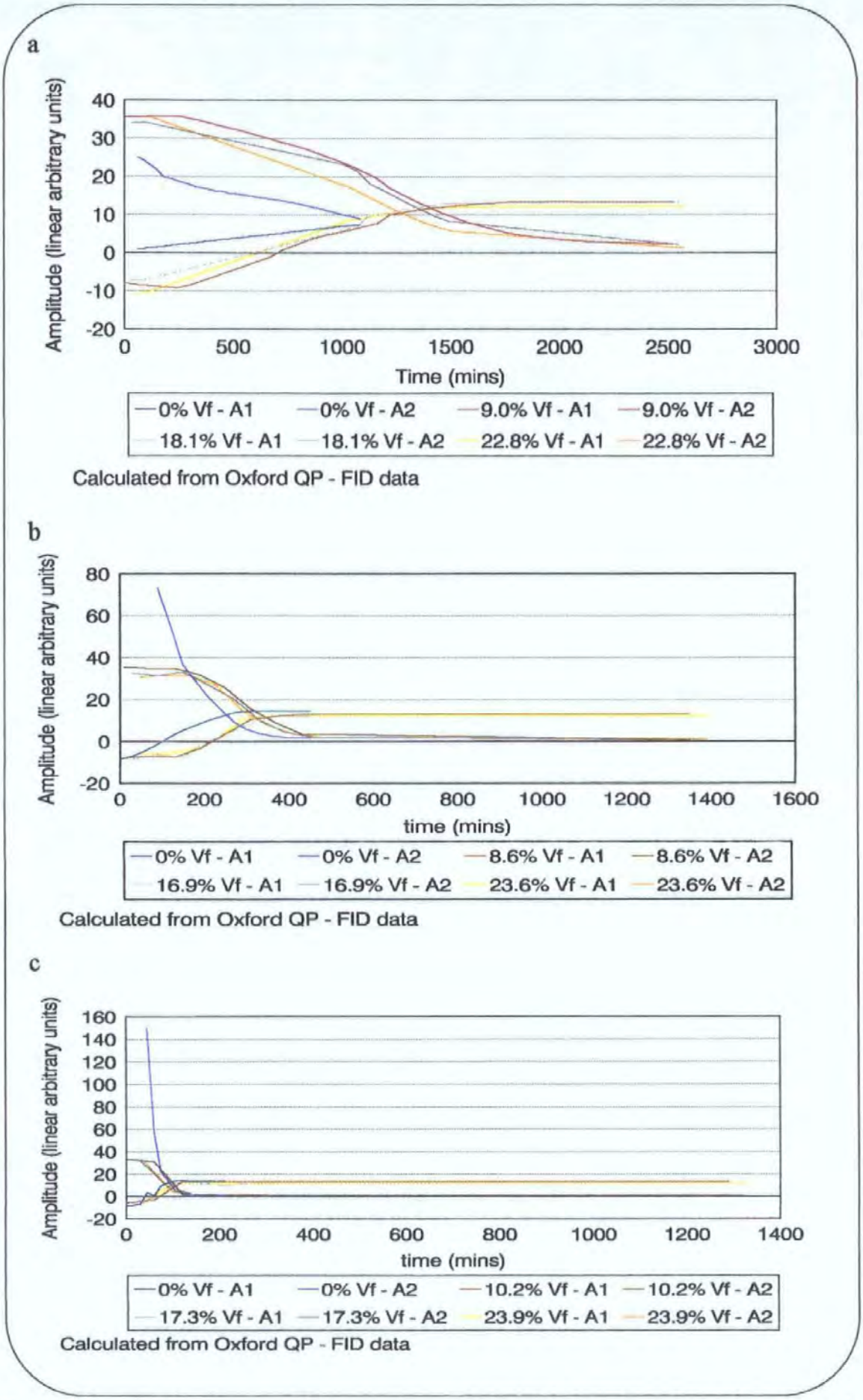

Figure 7.14. The effects of fibres on the solid and liquid amplitudes at a: 40°C, b: 60°C and c: 80°C.

similar size and geometry samples. These investigations will be presented in chapters 8 and 9 consecutively.

8.0. CUREMETER INVESTIGATIONS

8.1. Introduction

The Rapra vibrating needle curemeter (VNC) monitors the increase of viscosity before gelation, but in addition subsequent changes in the stiffness of the solidifying resin can also be measured. This is achieved by suspending a needle into the formulation (by 4 mm) and vibrating the needle vertically, see section 2.3.1. It is the resistance of the resin to the movement of the needle that results in the cure profile as a plot of voltage versus time of cure. Once the whole cure profile is monitored the software can then determine the potential at 10% and 95% solid termed V10 and V95 respectively, the corresponding times and the times for 80% and 100% solid (termed T10, T95, T80 and T100 respectively). Further details are discussed in chapter 2.

8.2. Analysis of Cure Profiles

Samples of resin with and without glass fibre reinforcement were cured under constant temperature conditions for 40 °C, 60 °C, 80 °C and 100 °C cure cycles. The samples for the VNC were the same geometry as the samples used in the QP tests to allow for consistency. Also each experiment was performed three times in order to ensure reproducibility. The samples were heated by a hot plate and a heating coil which was wrapped around the mould. The needle was suspended by approximately 4 mm into the resin. A typical cure profile can be seen in figure 8.1. As can be seen as the cure proceeds the voltage drops due to the resin decreasing the needle displacement. This can either be virtually instantaneous as in the case of the 100 °C cure or can take place over a period of time.

The cure monitoring was then repeated with 10%, 20% and 30% volume fraction (V_f) glass fibre. The glass fibre was a standard E–glass matting which was chopped to allow ease of fill of the mould. Again each cure profile was repeated three times

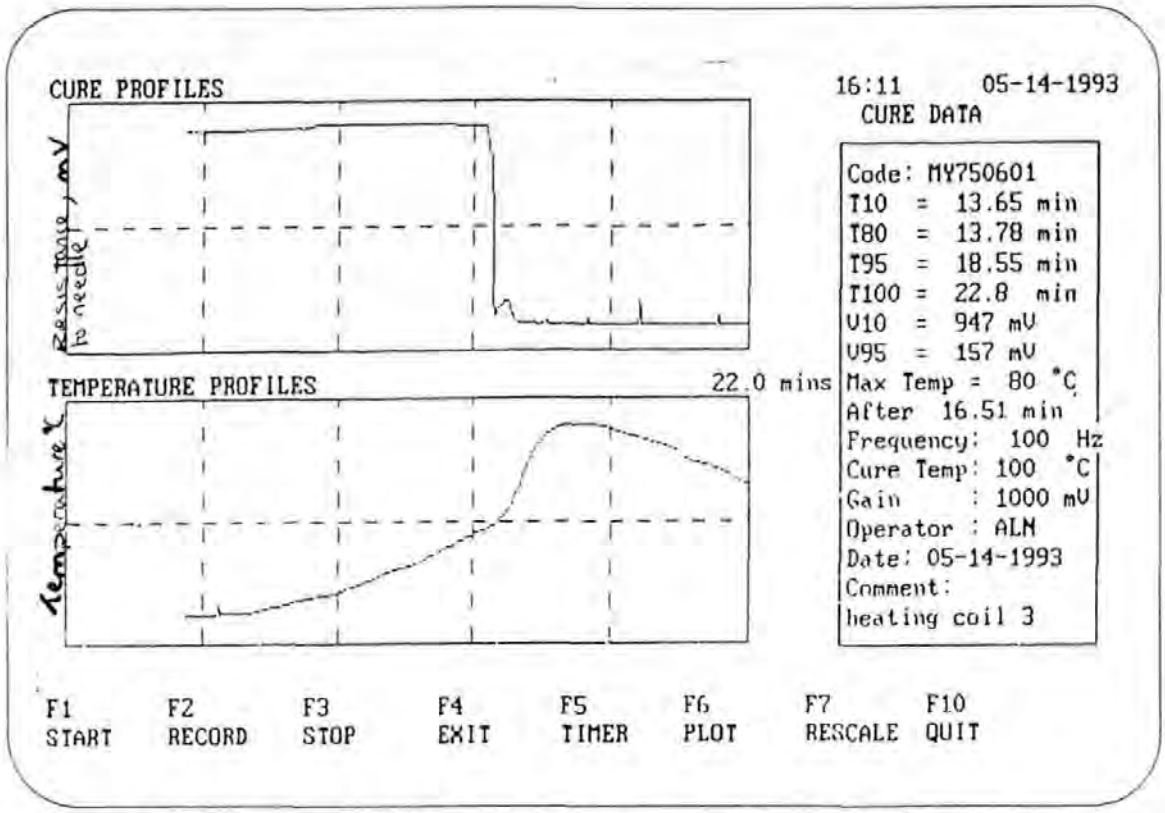

Figure 8.1. Cure profile for MY750 resin system during a 100 °C cure cycle – no fibres.

in order to ensure repeatability. For all cure profiles the initial voltage and frequency were 1000 mV and 100 Hz respectively.

To ensure the VNC follows the true cure profile the fibres must be evenly distributed. Fibres directly under the needle will restrict the movement of the needle giving the impression the resin is curing quicker than it actually is. Therefore again an average of three cure profiles is required and the average of the voltage and time measurements were used as a comparison with the data obtained from the Jeol EX270 high–resolution NMR spectrometer and Oxford QP NMR analysis.

An analysis of the above results is given in table 8.1 and it can be seen that as the temperature increases, the times for 10%, 80%, 95% and 100% solid decrease as would be expected.

On the addition of fibres the time to 10% solid decreases as the volume fraction increases. This indicates the restriction the fibres are putting on the needle as it vibrates. Fibres directly under the needle would stop the needle from vibrating freely and so give the impression that the sample was cured. The presence of the fibres has also influenced the time to 80%, 95% and 100% solid. Ten percent volume fraction gives times longer than 0% volume fraction. However these times decrease as would be expected when more fibres are added. As the resin cures the fibres can do one of two things: draw the resin away from the needle; or restrict the movement of the resin and so keep it by the needle. This was demonstrated by the ease with which the needle was withdrawn from some samples upon completion of the cure.

The VNC takes the point of 100% solid when the rate of change in voltage reaches a negligible level. However, the rate of change in voltage will be different for a 40°C cure cycle than a 100°C cure cycle, therefore the VNC cure profiles give different points for 100% solid at different cure temperatures. This point is demonstrated by the voltages for ten percent solid with no fibres present, the higher the cure temperature the higher the voltage. This point is illustrated further by the fact that as the resin cures the voltage for 95% solid decreases as the cure temperature increases. Therefore the VNC can only be used to compare resin samples curing at the same cure cycle and not across different temperature cycles.

Cure temp (°C)	Volume fraction, (v_f)	T10 (mins)	T80 (mins)	T95 (mins)	T100 (mins)	V10 (mV)	V95 (mV)
40.00	0.00	663.10	1,361.20	1,632.80	2,699.50	900.00	118.00
	10.00	444.10	1,339.90	2,824.60	2,867.30	884.00	120.00
	20.00	213.40	844.70	2,637.40	2,918.80	798.00	116.00
	30.00	88.30	942.10	1,125.70	1,415.60	510.00	122.00
60.00	0.00	213.00	366.50	588.80	666.50	922.00	110.00
80.00	0.00	36.80	38.10	77.80	93.70	939.00	107.00
100.00	0.00	13.70	14.50	18.30	23.00	960.00	103.00

Table 8.1. Results of temperature and voltage calculations for curemeter analysis.

Table 8.1. Results of temperature and voltage calculations for curemeter analysis.

The times obtained for T10, T80, T95 and T100 were assumed to represent the times for 10%, 80%, 95% and 100% solid for each cure cycle. (As previously stated in chapter 7 it is not known whether cure monitoring by this method or the QP can determine the point of 100% cross-linking). This data can now be compared with the % solid calculations determined in chapter 7 to ascertain if the Oxford QP gives a good indication to the % solid for the specified volume sample. See figures 8.2 to 8.5.

There were a number of experimental differences introduced into the VNC experiments because of the existence of a temperature gradient in the top 4 mm of the sample. This lead to difficulty in keeping the top 4 mm of the sample at the cure temperature (the VNC only penetrating the top 4 mm with the needle). The top of the sample was measured to be (in the worst case) 20 °C lower than the rest of the sample even with the addition of the heating coil. Even so during the 100 °C cure cycles the VNC sample exothermed considerably for two of the repetitions reaching a maximum temperature of 195 °C. Unfortunately it was not possible to monitor the exotherm temperature of the QP samples, but it was noticed that the

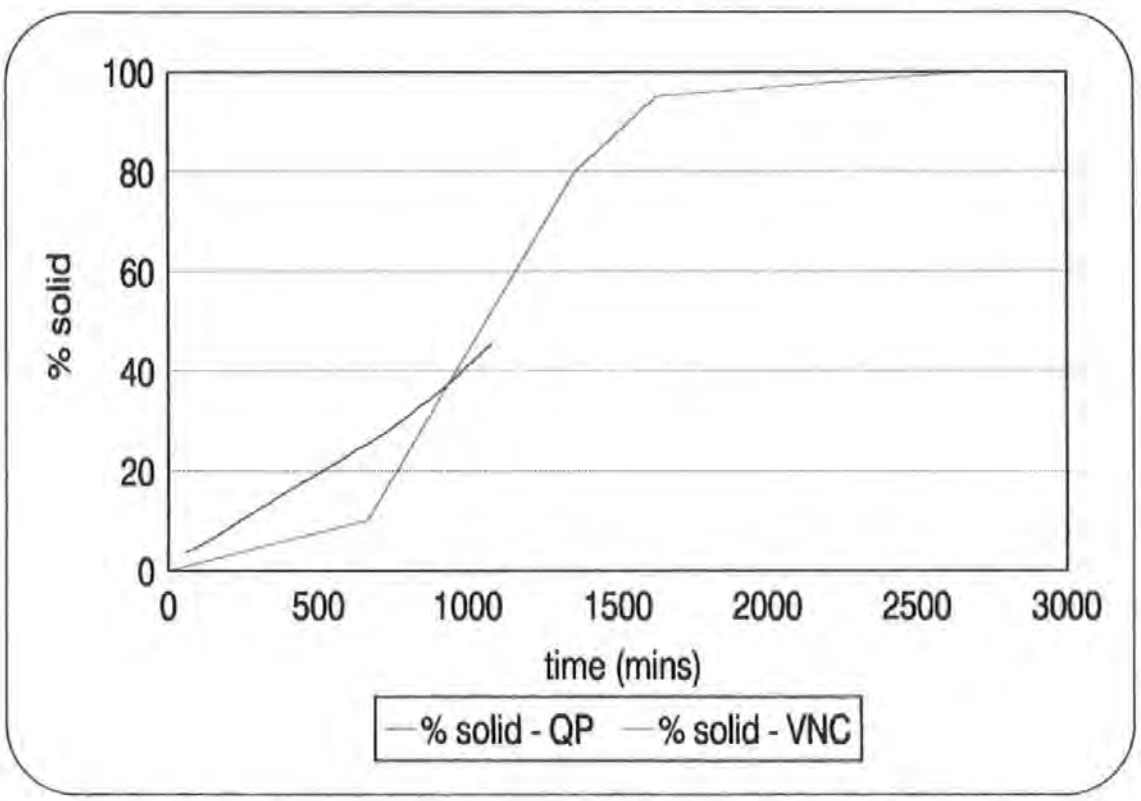

Figure 8.2. Comparison of % solid as calculated by the QP and the VNC at 40 °C.

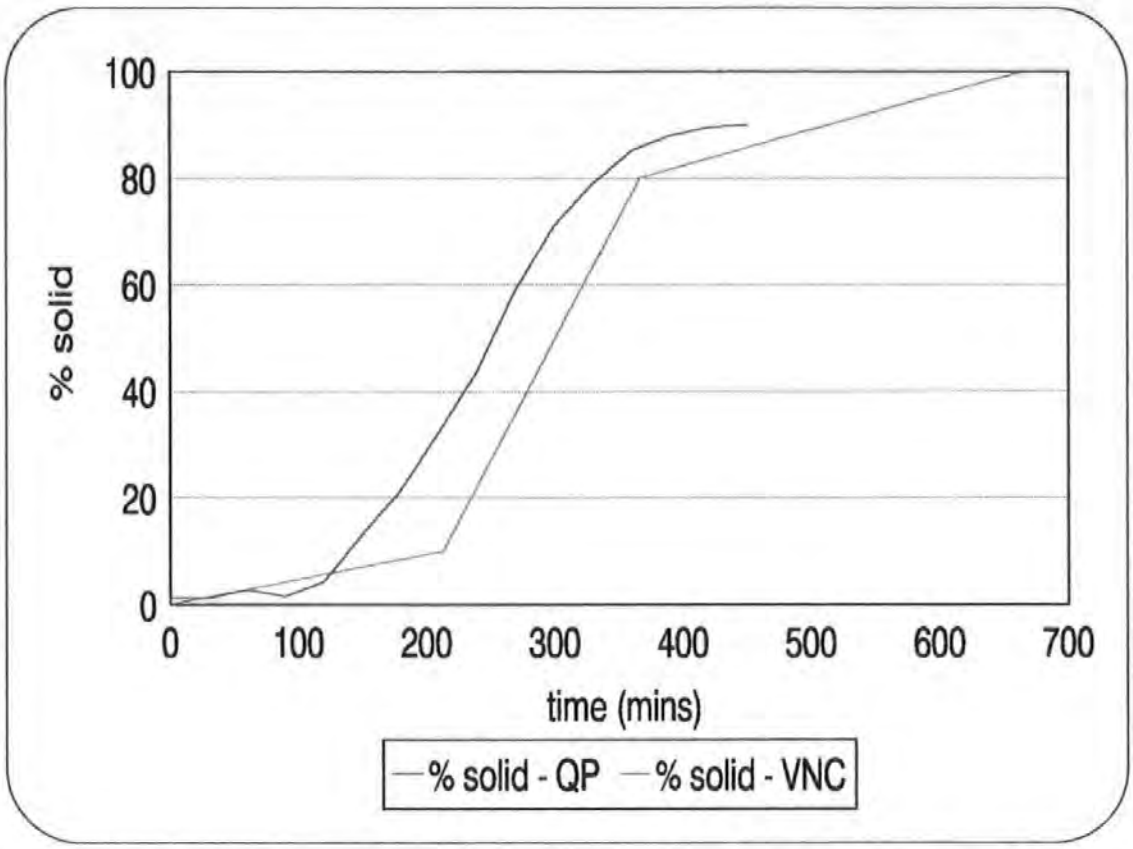

Figure 8.3. Comparison of % solid as calculated by the QP and VNC at 60 °C

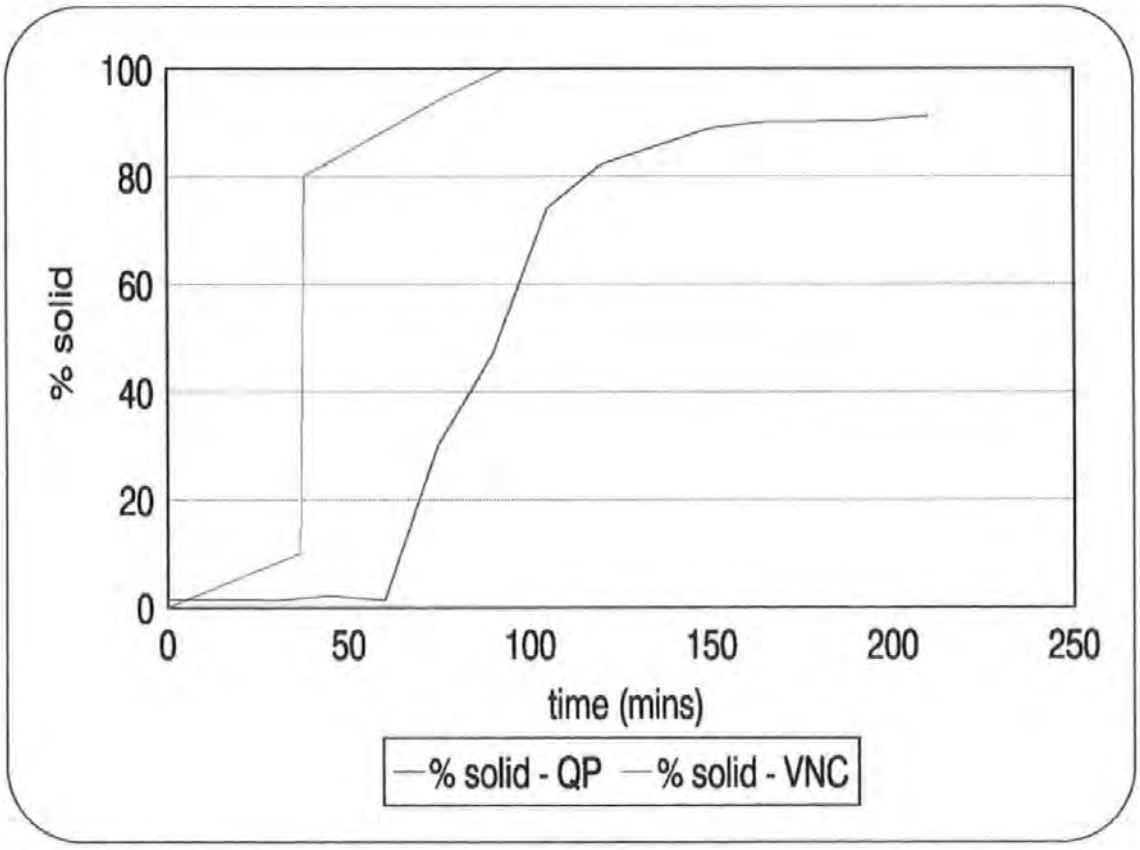

Figure 8.4. Comparison of % solid as calculated by the QP and VNC at 80 °C

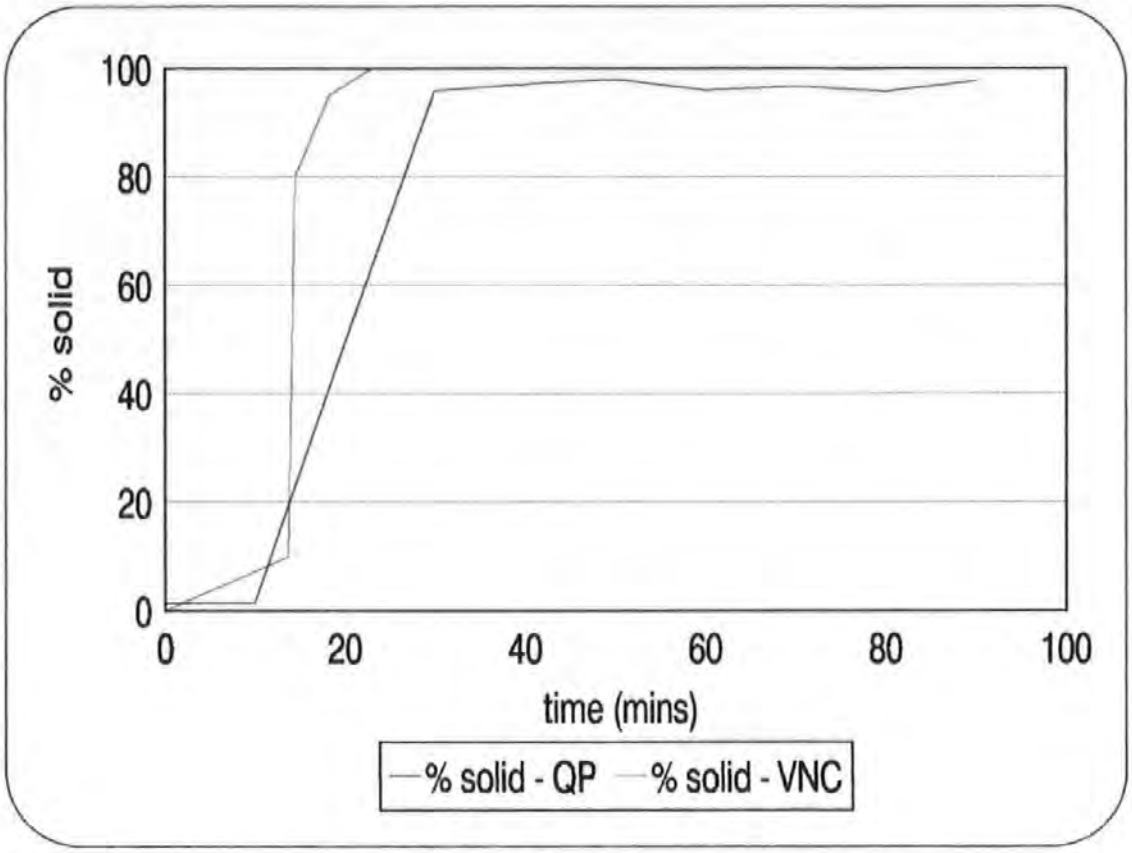

Figure 8.5. Comparison of % solid by the QP and VNC at 100 °C.

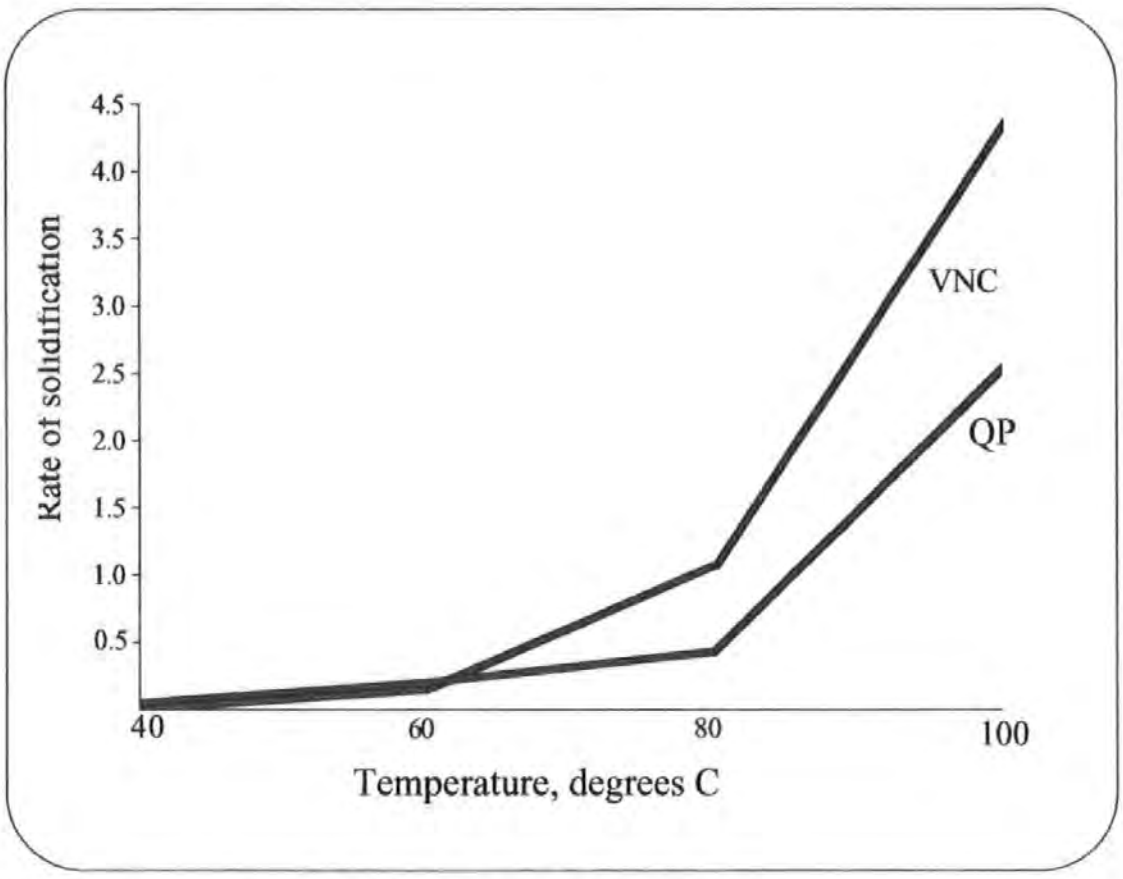

Figure 8.6. Rate of solidification for the QP and VNC.

resin changed colour and increased in volume. Such a high exotherm temperature with the QP sample would have been unlikely due to the fact that the oven door was being opened every 10 minutes to allow samples to be placed in the QP, there was an oven temperature difference of ±5 °C every time a sample was removed from the oven.

A better way to compare the two techniques for cure monitoring is to analyse the rate of solidification (i.e. the time for the VNC cure data to reach 100% solid and for the QP data to reach its maximum % solid) for each cure temperature, see figure 8.6. There is good correlation between the two techniques over the 40 and 60 °C cure cycles after this the VNC monitored samples have a higher rate of solidification than those samples monitored by the Oxford QP NMR analyser. As can be seen in figures 8.4 and 8.5 the VNC has determined the resin is solid far earlier than with the same sample geometry and resin mix with the Oxford QP NMR analyser.

Cure temperature °C	volume fraction v_f	time to 10% solid –VNC (mins)	time to 10% solid– QP (mins)
40.00	0.00	633.10	221.70
40.00	10.00	444.10	–
40.00	20.00	213.40	–
40.00	30.00	88.30	–
60.00	0.00	213.00	138.70
80.00	0.00	36.80	66.10
100.00	0.00	13.70	11.78

Table 8.2. The time to 10% solid as obtained by the QP and the VNC cure monitoring techniques.

On the addition of fibres at 40 °C the time to 10% solid as monitored by the VNC decreases substantially as the volume fraction increases (see table 8.2.) (This may also be due to the fibres interfering with the movement of the needle, fibres directly under the needle thereby stopping it vibrating fully will give the impression that the resin is gelling). However once fibres were added to the QP samples the minimum % solid obtained was approximately 20%. The QP volume fraction data can be seen in appendix 4.0.

8.3. Discussion

As can be seen from the data presented in this chapter the VNC and Oxford QP give very different cure profiles. At the two lower temperatures the VNC lags behind the QP whereas at the higher two cure temperatures the VNC gives a far higher rate of solidification. As stated in chapter two the resin mix was accurate to ±2% therefore, this does not account for the difference in cure profiles.

The main difference between the VNC and the Oxford QP are their methods of monitoring the cure. The VNC monitors the cure mechanically by vibrating a needle in the top 4 mm of the sample. As the solidification progresses the resin resists the movement of the needle, therefore the VNC is monitoring the resilience of the top 4 mm of the resin, whereas the Oxford QP monitors the restricting hydrogen environments throughout the whole sample. It therefore takes into consideration the fact that the resin will solidify outside in and that the top surface of the resin is in contact with the air which may alter the rate of solidification.

Finally both techniques monitor the cure to their experimental limits. These limits for the QP or VNC may not be the point when the resin has achieved 100% cross-linking. In fact the point of 100% solid may be different for each of the two techniques. These results from the two cure monitoring techniques will now be compared with hardness data obtained by using the Barcol impressor, see chapter 9.

9.0. BARCOL HARDNESS ANALYSIS

9.1. Introduction

Samples of resin of the same volume and geometry as the Oxford QP NMR specimens were cured at the 40 °C, 60 °C and 80 °C cure cycles. Once the resin had gelled a sample was taken from the oven and sanded down along the length of the specimen to give a flat surface. Four Barcol hardness measurements were then taken along this length. The average of these readings was assumed to represent the overall hardness of the sample. This procedure was carried out at regular intervals throughout the rest of the cure cycle. The sample is considered fully cured when the hardness readings remain constant.

The hardness tests were carried out to assess the cure of the resin and to ascertain a time when the specimens could be said to be fully cured, this will vary with each temperature. As the temperature increases the time to full cure decreases as illustrated in previous chapters with the QP and VNC data. Also by comparing the results with those obtained from the NMR and VNC analysis the percentage cure that is required before the resin is "hard" enough for a hardness test to be successfully completed was ascertained.

An analysis of the topography of the indentations in the samples caused by the Barcol hardness indentor indicated changes in the stages of cure. The phrase "stages of cure" is taken to mean the percentage of cross-linking that has taken place to give these particular physical properties. Therefore, 100% cured (i.e. a completely cross-linked structure) will have the ultimate physical properties.

9.2. 40 °C Cure Cycle.

Barcol Hardness readings were taken once an hour after gelation. In order to check the reproducibility of the results, two separate experiments were performed, both at 40°C. These results were identified as cure1 and cure2, see table 9.1. However

gelation at 40 °C did not render the resin "hard" enough for readings to be taken until the resin had cured for approximately 24 hours and 38 minutes. Comparing this to the VNC data this point is approximately 95% solid.

For cure 1, photographs of the indentations were taken as part of the test procedure. For sample 18A it can be seen that the resin was very soft so that the resin effectively flowed away from the indentor when pressure was applied, see figure 9.1. After a further two hours the resin had cured enough to support the weight of the indentor, but under hand pressure the resin was still soft. Figure 9.2. shows clearly the concentric rings caused by the support column. There is also a ring around the indentation caused by the top of the indentor. Therefore, at this point in the cure the resin was very ductile.

Figure 9.3. (sample 15A) shows a sample that was cured for a further hour. As can be seen the ring from the top of the indentor can no longer be seen but there are still the concentric circle markings caused by the support column. After a further two hours (sample 19A) the support column markings become less pronounced, see figure 9.4.

In figure 9.5, (sample 3A) a further hour into the cure, the markings are only just visible. Hardness readings at this point begin to register on the scale of the hardness tester.

Cure 2 was taken further in to the cure as can be seen in Table 9.1. After 2490 minutes (equivalent to 99.2% solid from the VNC data) the resin is solid according to the curemeter and Oxford QP data, however subsequent Barcol hardness readings increased. The corresponding indentation can be seen in figure 9.6.

As the cure is continued past the point of 100% cured (as determined by the VNC) the resin becomes harder i.e. more brittle. Therefore over–cure can be seen to make the resin brittle (figure 9.7 illustrates the effect of the brittle hardness test on the epoxy resin).

Cure 1			Cure 2		
Time into cure (mins)	Sample number	Average Barcol Hardness reading	Time into cure (mins)	Sample number	Average Barcol Hardness reading
1,058.00	18A	0.00	1,050.00	15A	0.00
1,178.00	17A	0.00	1,110.00	8A	0.00
1,238.00	15A	0.00	1,170.00	5A	0.00
1,358.00	7A	0.00	1,230.00	12A	0.00
1,418.00	19A	0.00	1,290.00	3A	0.00
1,478.00	3A	0.50	1,350.00	2A	0.00
1,538.00	1A	6.75	1,410.00	1A	0.00
			1,470.00	4A	4.50
			1,530.00	6A	4.75
			2,490.00	11A	13.25

Table 9.1. Barcol hardness readings for a 40 °C cure.

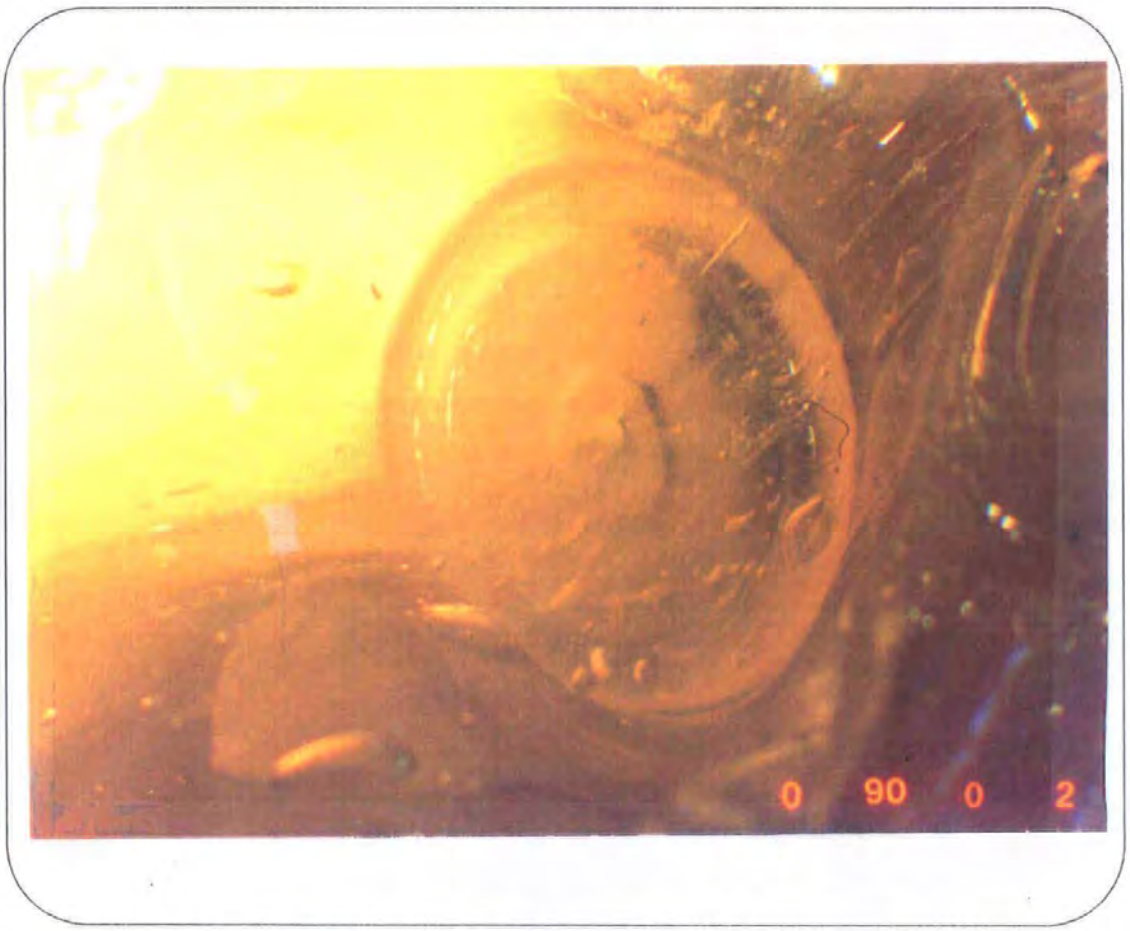

Figure 9.1. The indentation caused at 1058 minutes into the cure.

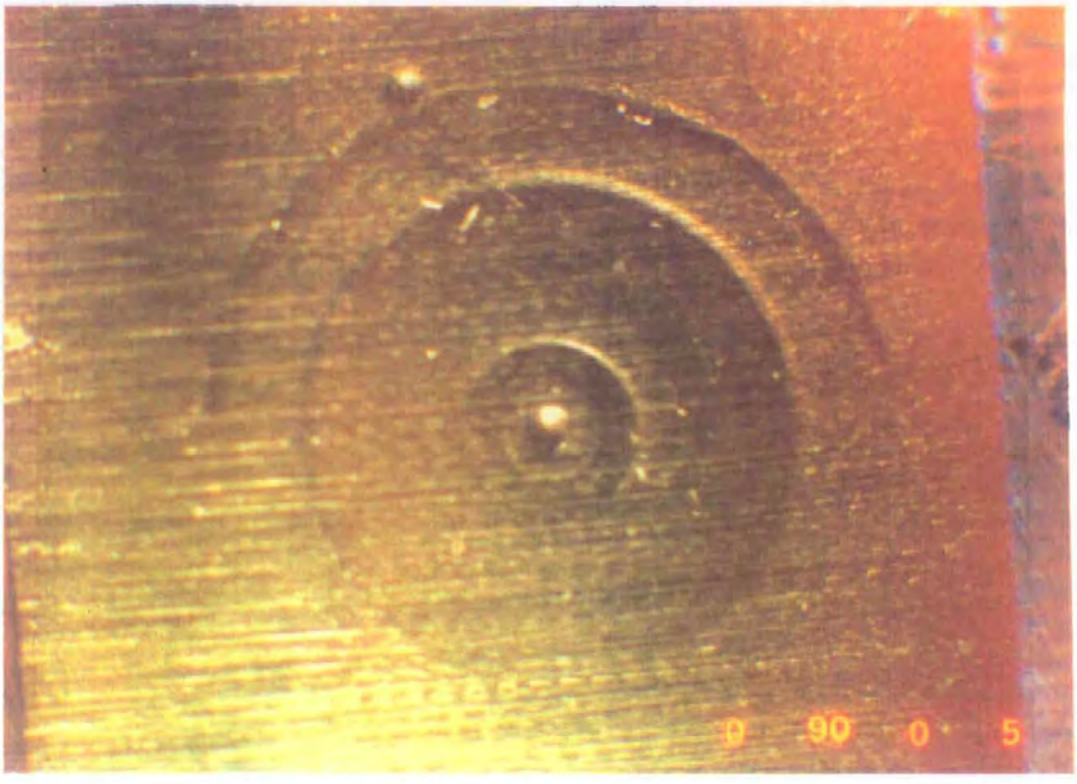

Figure 9.2. 1178 minutes into the cure.

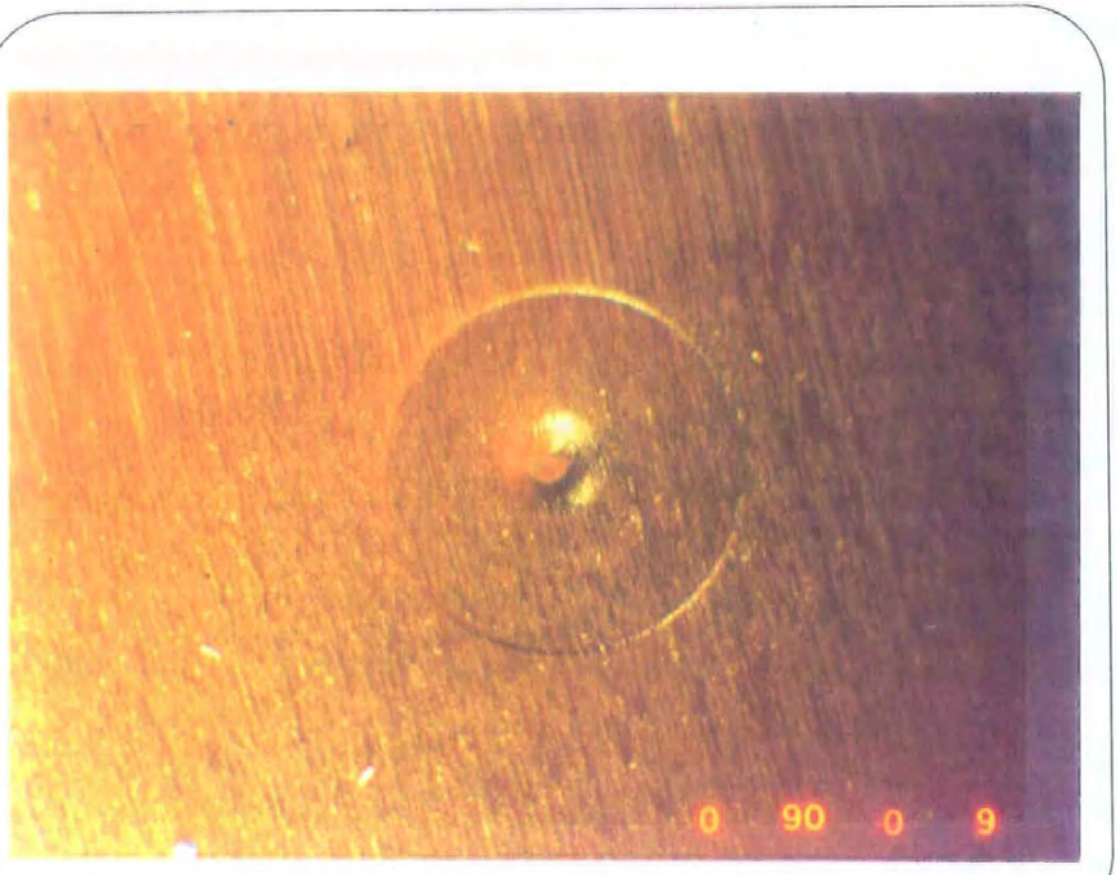

Figure 9.3. 1238 minutes into the cure.

Figure 9.4. 1418 minutes into the cure.

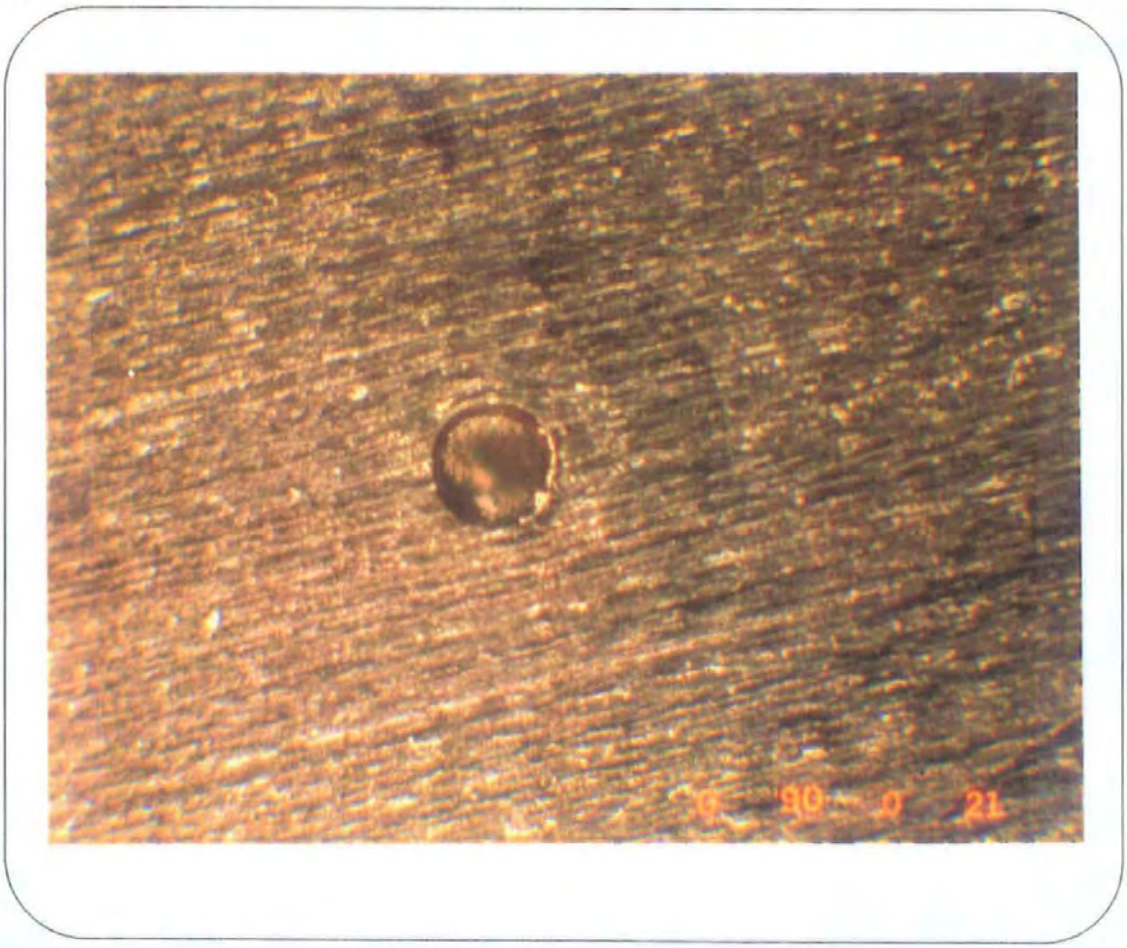

Figure 9.5. 1478 minutes into the cure.

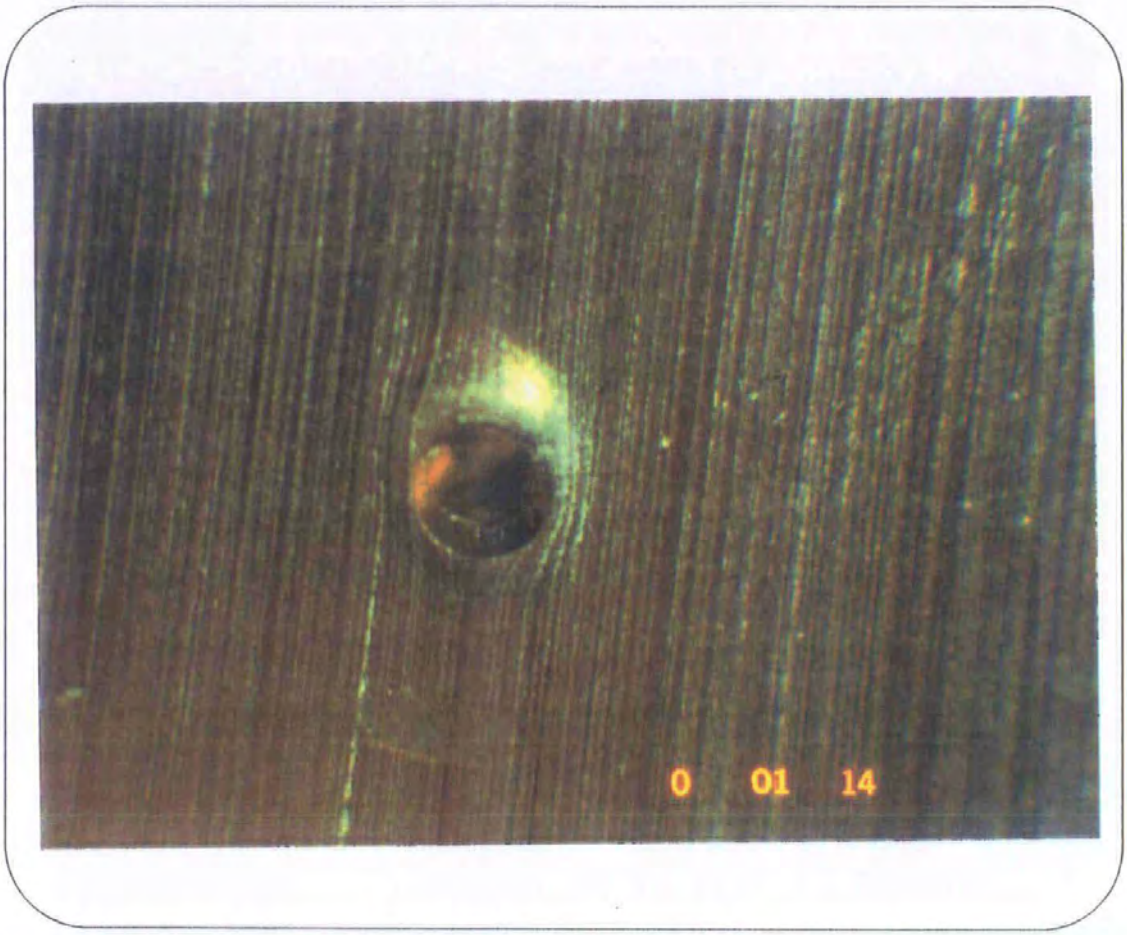

Figure 9.6. 2,490 minutes into cure 2.

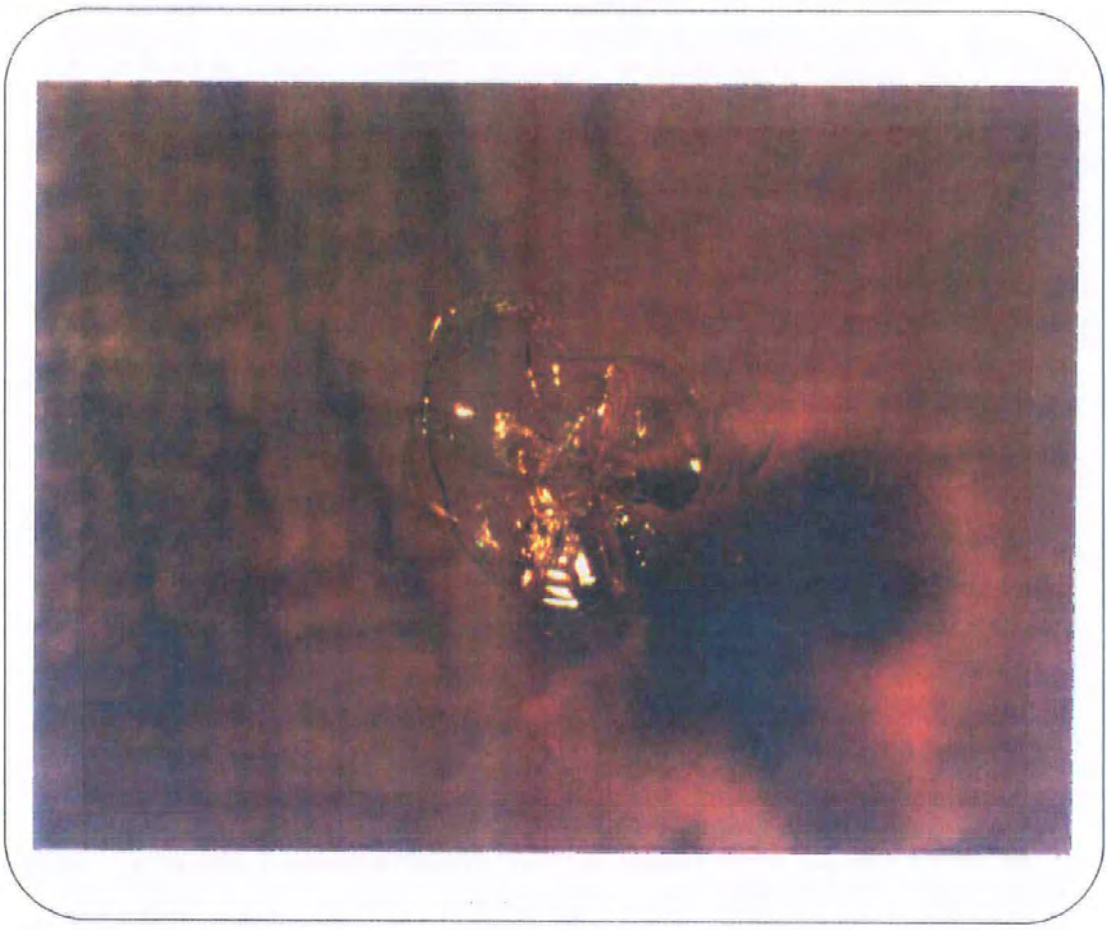

Figure 9.7. A brittle indentation in epoxy resin after 2700 minutes of a 40°C cure.

9.3. 60 °C Cure Cycle

Hardness tests were carried out on samples undergoing a cure schedule at 60 °C. Again, in order to check the reproducibility of the results two separate experiments were performed. These results were identified as cure3 and cure4, see table 9.2. No photographs were taken of the indentations during these cure cycles. As can be seen from the table, hardness readings started after 300 minutes of cure. From the VNC cure analysis it can be seen that this is approximately 55% solid. Readings were continued until 680 minutes into the cure which corresponds to 100% solid from the VNC analysis. It was stated earlier in this chapter that the resin is termed fully cured once the Barcol hardness values remain constant. However since the resin becomes brittle into the later stages of the cure this will affect the hardness readings i.e. they will be lower because the brittle solid has less resistance than a ductile solid. As can be seen from table 9.2 – cure3 the readings reached a maximum 575 minutes into the cure and then began to decline in value. From the VNC analysis 575 minutes into the cure corresponds to 93.8% solid. These results will be discussed further in the discussion section at the end of this chapter.

Cure 3			Cure 4		
Time into cure (mins)	Sample number	Average Barcol Hardness reading	Time into cure (mins)	Sample number	Average Barcol Hardness reading
440.00	1.00	39.00	240.00	1.00	0.00
470.00	2.00	45.25	270.00	2.00	0.00
500.00	3.00	46.00	300.00	3.00	8.00
530.00	4.00	46.25	339.00	4.00	19.25
545.00	5.00	40.40	360.00	5.00	25.50
560.00	6.00	43.50	390.00	6.00	33.00
575.00	7.00	48.75	420.00	7.00	31.50
590.00	8.00	48.25	450.00	8.00	37.00
605.00	9.00	40.25	480.00	9.00	32.75
620.00	10.00	46.25	510.00	10.00	41.25
635.00	11.00	47.00	540.00	11.00	43.50
650.00	12.00	45.25	570.00	12.00	42.25
665.00	13.00	43.75	600.00	13.00	35.50
680.00	14.00	44.50			

Table 9.2. Barcol hardness readings for a 60 °C cure cycle.

9.4. 80 °C Cure Cycle.

Hardness tests were carried out on samples undergoing a cure schedule at 80 °C. Again in order to check the reproducibility of the results, two separate experiments were performed. These results were identified as cure5 and cure6, see table 9.3. As can be seen it would have been advantageous to begin testing after 30 minutes of cure. The hardness values reached a maximum 105 minutes into the cure which corresponds to 100% solid from the VNC analysis but the QP analysis showed this to be 75% solid. After this point the hardness readings decrease in value but do not reach a constant value. The Oxford QP did not give a reading of 95% solid until after 200 minutes into the cure, at this point cure6 reaches its maximum. The results of these experiments will be discussed further in the discussion section at the end of this chapter.

Cure 5			Cure 6		
Time into cure (mins)	Sample number	Average Barcol Hardness reading	Time into cure (mins)	Sample number	Average Barcol Hardness reading
90.00	1.00	49.50	90.00	1.00	42.75
105.00	2.00	54.75	120.00	2.00	43.00
120.00	3.00	50.34	150.00	3.00	42.00
135.00	4.00	54.25	180.00	4.00	39.50
150.00	5.00	51.75	210.00	5.00	53.50
165.00	6.00	41.00	240.00	6.00	48.50
180.00	7.00	46.75			
195.00	8.00	48.00			
210.00	9.00	51.00			
225.00	10.00	46.25			
240.00	11.00	48.75			
255.00	12.00	49.75			
270.00	13.00	42.50			
285.00	14.00	48.00			
300.00	15.00	51.75			
315.00	16.00	45.00			

Table 9.3. Barcol hardness readings for an 80 °C cure cycle.

9.5. Discussion

The Barcol hardness tester must be used on a flat surface. This surface is produced using wet glass paper. In order for the specimens to remain in the right position while undergoing testing a flat base required grinding. This was not possible, therefore the specimen was kept upright in a bed of plasticine, the specimen being pushed in as far as possible so as not to effect the readings. However, any tilt on the specimen would have caused a low reading.

The Barcol Hardness tester is a hand held instrument operated under hand pressure. The supporting column is designed so that the indentor only moves the same distance into the specimen, however the speed and pressure of the indentation may change the results slightly.

From the indentation topography it can be seen that once the resin has gelled it passes through three distinct types of behaviour. The first suggests the behaviour of a high viscosity Bingham fluid, next the resin behaves as a ductile material and finally when the resin is nearing '100% cured' the resin behaves as a brittle solid. It is this transition from one mode of behaviour to another that could account for the discontinuities in the hardness readings. As can be seen in tables 9.2 and 9.3 and figure 9.8 the hardness readings begin to drop as cure time increases. This was not expected since it is generally believed that the resin will increase in hardness as the cure time increases. However, in the cases where brittle failure has occurred around the indentor the hardness numbers will decrease in value because there is less resistance. Figures 9.9. and 9.10 illustrate how the Barcol hardness number varies with time in comparison with the QP and VNC % solid curves. As can be seen, the Barcol hardness readings are only relevant near the end of the cure, however in both cure cycles the hardness values did not remain constant once 100% solid had been reached. This could be due to the fact that since the geometry of the samples (which had been dictated by the Oxford QP, see chapter 2) was required to be small, approximately 40 mm in length with an 18 mm diameter, only four hardness tests could be carried out per sample.

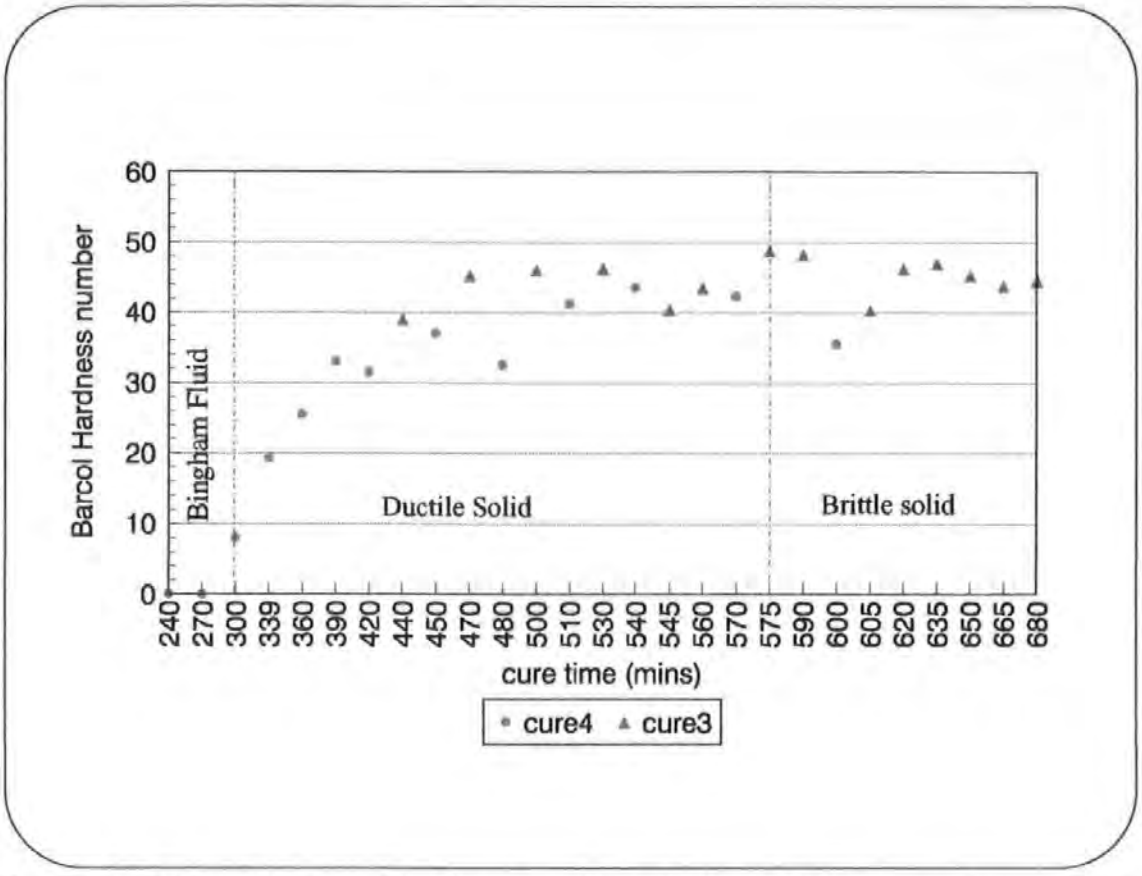

Figure 9.8. Change in Barcol hardness readings during a 60°C cure cycle.

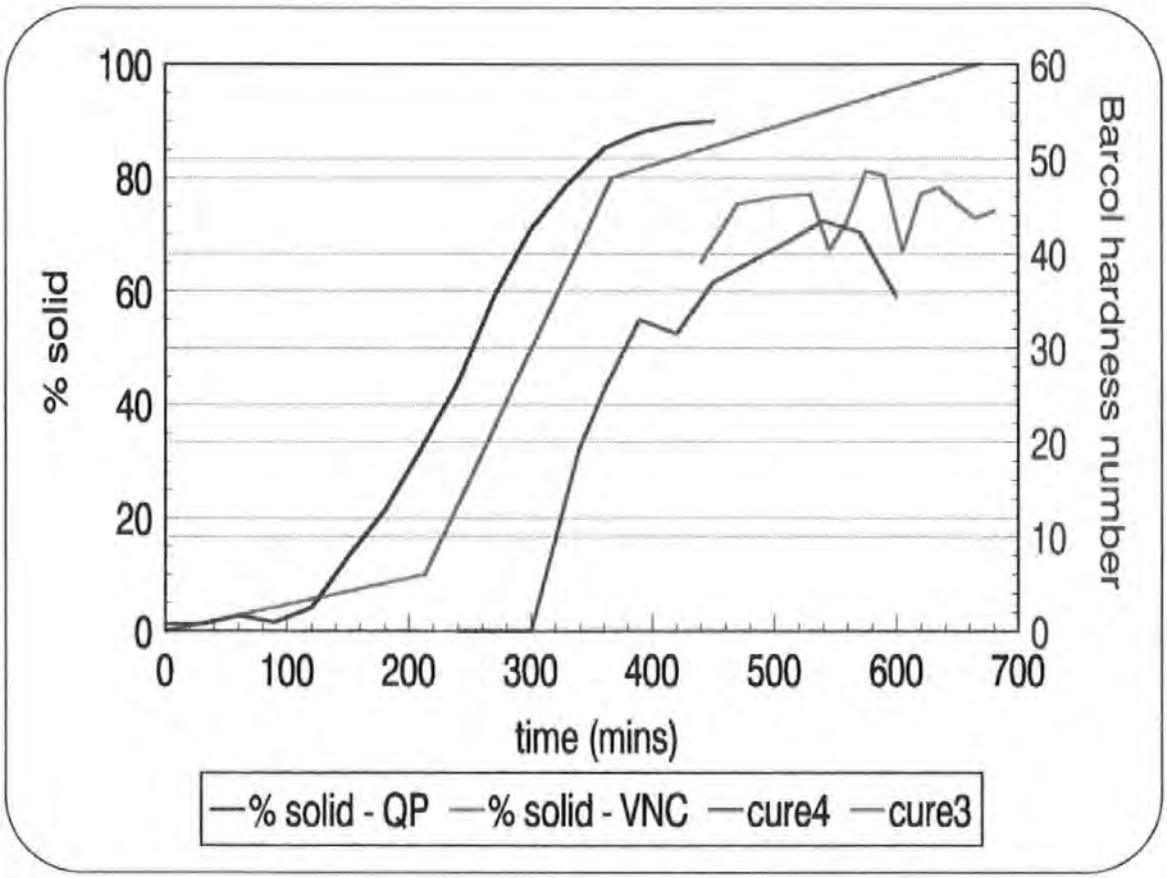

Figure 9.9. Comparison of VNC and QP % solid curves with the Barcol hardness readings for a 60°C cure cycle.

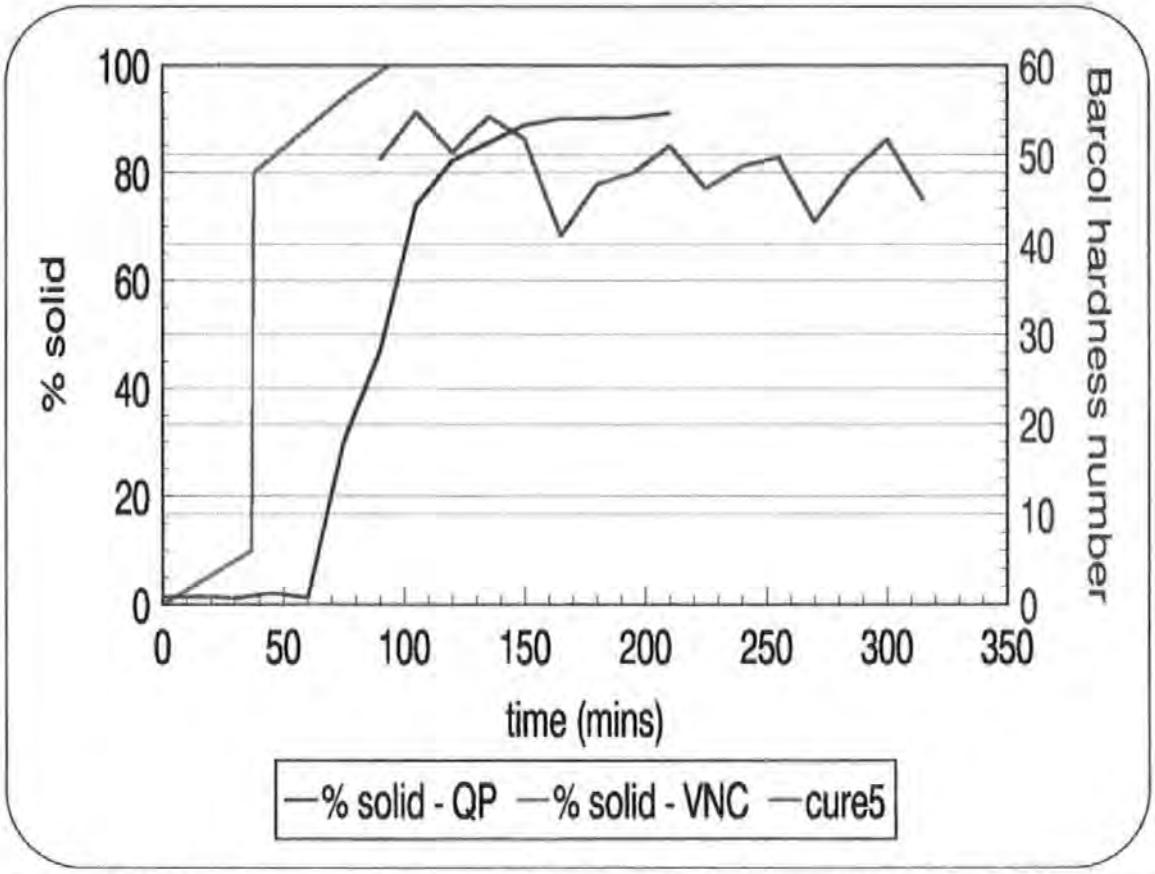

Figure 9.10. Comparison of VNC and QP % solid curves with the Barcol hardness readings for an 80°C cure cycle.

The American Society for Testing and Materials [96] recommends an average of 7 to 8 readings to be taken on homogeneous materials with a Barcol hardness of between 30 and 40. This gives a reading variance of 1.93 and 2.20 consecutively. Since only half the recommended number of readings could be taken then the data will give a low correlation.

As the resin nears 100 % cured, the resin behaves in a brittle fashion, as discussed earlier, resulting in a lower Barcol hardness reading. Therefore the nearer to fully cured the resin becomes the more readings are needed to gain a better approximation to the true hardness. However, since brittle failure does occur is the Barcol hardness the best method to determine 100% cured? The results of this section will be discussed more fully in comparison with the previous experimental chapters in the next chapter.

10.0 DISCUSSION

The purpose of the investigations was to determine the applicability of nuclear magnetic resonance for cure monitoring of resin fibre composites. This was achieved by comparing an NMR analyser, the Oxford QP, with a standard high-resolution NMR spectrometer designed for liquid-state investigations. The results obtained were then compared with a standard industrial / research curemeter, the vibrating needle curemeter, VNC, and physical property testing using a handheld hardness tester, the Barcol hardness tester.

Present research into the use of NMR with composites has dealt mainly with investigations into imaging or spectroscopy using solid-state techniques which are both expensive and not applicable to industrial usage due to size restraints.

Lizak investigated the applicability of NMR for the non-destructive examination of epoxy / graphite composites with the aim of removing improperly cured materials from the production process [80]. NMR relaxation times were exploited to observe the curing epoxy. It was found that the NMR monitors not only properties of the curing material, but also changes in the prepreg chemistry as well as oven performance.

The relaxation times monitored by Lizak [80] were T_2^* and T_{1D} (relaxation time for dipolar order) which is sensitive to ultra-slow motions. It was found that T_2^* reduces until the material becomes more rigid and motions are sufficiently reduced in rate that T_2^* reaches a constant value. This is known as the Rigid Lattice Limit. However T_{1D} will still increase with further increases in rigidity. The T_{1D} is measured with the Jeener Broekhaert pulse which can be represented diagrammatically as follows:

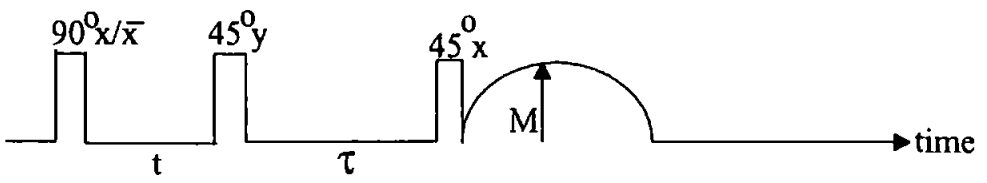

where t is fixed and τ is incremented through several values.

T_{1D} can then be extracted from the variation of the signal amplitude M with τ i.e.

$$M=M_0 e^{\frac{-\tau}{T_{1D}}}$$

where M_o = initial signal amplitude.

Neither T_2^* or T_{1D} are sensitive to pulse errors or the inhomogeneity of the static field therefore the measurement of relaxation times to monitor curing can be easily transported, says Lizak, from the laboratory to the factory setting.

Lizak uses the above theory to test graphite / epoxy prepreg and found that the relaxation times T_2 and T_2^* are good indicators of cure state. It is believed that T_2 can be used to indicate time of minimum viscosity as well as the actual value of the minimum viscosity. For the latter part of the cure cycle T_{1D} is used.

Lizak concluded that the technique could be taken into an industrial setting by using surface coils [64]. In which case with the carbon fibres being conductive, only a limited depth δ could be analysed. Or alternatively the coil could be buried within the composite to give cure monitoring and be used to determine structural integrity once a component is in service.

Haw [77] used ^{13}C NMR spectroscopy to study formation of thermosetting resins. Haw's study demonstrated that magic angle spinning (MAS) could be used throughout the entire curing process, without loss of material or rotor instabilities. With such a strategy, progression of resin from a 'solution' to a 'solid' may be compensated for (in part) by a switch from NMR excitation techniques suitable for solutions to techniques appropriate for the study of solid samples, for example, cross polarisation (CP) see chapter 1.

However, in the vicinity of the gel point it was found to be impossible to obtain a ^{13}C spectrum by either CP or single–pulse excitation. Rothwell and Waugh [89] have shown that stochastic averaging of dipole – dipole couplings due to random molecular motions can defeat all attempts at coherent averaging of such couplings by, for example, proton decoupling, if the time scales of the two averaging processes

are similar. This effect results in short T_2 values (especially for protonated carbons), and has been demonstrated experimentally for plastic crystals and proposed as a complication in NMR studies of macromolecules in solution. Thus, the gel region of this curing process (in which significant molecular motion is occurring in the mid–kilohertz frequency region) is not available for study by methods used in Haws investigation.

As the resin solidifies, the amplitude of the molecular motions decreases and it becomes possible to obtain ^{13}C spectra using cross polarisation.

Haw made several observations from this study the most significant being that ^{13}C NMR with magic angle spinning (MAS) can be used to study the formation of thermosetting epoxy resins in situ. Haw encountered no difficulty in spinning freshly prepared liquid solutions of epoxides and curing agents, and physical and chemical changes during polymerisation were manifested in the NMR properties. MAS may be of some use in obtaining spectra at short reaction times because the chemical shift anisotropy contributions to the line widths will be averaged. Unfortunately, molecular motion of the same time scale of the decoupling greatly hampers attempts at obtaining spectra during an important phase of the reaction. A possible solution to this problem is to shift the frequency distribution of molecular motions, either by reducing the temperature prior to spectral acquisitions and quenching much of the motion (as well as the reaction) or by raising the temperature with a concomitant increase in reaction rate. Haw found that the spectra obtained in this preliminary study provided little, if any, insight into the curing process, largely due to inadequate resolution and signal–to–noise ratio per unit time. Haw suggested that the obvious solution to this problem was to specifically enrich the epoxy and / or curing agent with ^{13}C or ^{15}N at one or more important sites and observe only those signals that are due to functional groups produced or consumed in the curing process.

Cholli et al [31] also used ^{13}C CP/MAS (cross–polarisation / magic angle spinning) NMR spectroscopy for the diglycidyl ether of bisphenol A with 2% dimethylbenzylamine. The spectra of the cured system were compared with similar spectra under solution spectrometry conditions. The CP/MAS technique results in

sufficiently high resolution to resolve the methyl, epoxide ring, and aromatic carbons.

Jackson [74] used NMR imaging to monitor the cure of carbon reinforced epoxy by investigating the temperature dependence of T_2. He also found that the T_2 measurements could be used to monitor the change in the polymer viscosity. It was found that by raising the measurement temperature from 20 °C to 100 °C , the transverse relaxation time (T_2) increased from 160μs to 25.9ms. Jackson found that by performing T_2 experiments in the first 5 minutes after reaching the appropriate temperature, it is possible to neglect the influence of reactive cross–linking as a result. During this early part of the cure cycle, the polymer viscosity is determined only by the temperature of the sample, and the increasing T_2 reflects the decreasing viscosity of the sample as the temperature is raised. Jackson used an echo time of 5ms and found it was possible to obtain images from the mobile epoxy at all temperatures above 55°C. By relating the transverse relaxation time at a specific temperature to the viscosity obtainable at that temperature (again the contribution made by the cross–linking to viscosity was neglected), T_2 could be directly related to the polymer viscosity. Since the image signal observed depends on the echo time used and the T_2 of the polymer, Jackson then went on to further calibrate the curves for polymer viscosity against image signal for each experimental echo time used, with the image signal in terms of the percentage of the total available signal. These curves now enable:

a). the optimum imaging conditions to be used at a particular temperature given the knowledge of T_2 values;

b). the calibration of any temperature inhomogeneity across the sample during the early stages of a cure cycle by knowledge of the relationship between the image signal obtained at a particular location and the temperature; and

c). the calibration of local viscosity changes within the sample due to cross–linking after thermal equilibrium has been reached by knowledge of the relationship between image signal and viscosity.

The maximum viscosity accessible to the imaging experiment is currently limited by the length of echo time used. Jackson found that by performing experiments at shorter echo times, it should be possible to measure internal viscosities in excess of 2000 poise. The use of more rapid imaging schemes would allow much faster curing mechanisms to be investigated, offering the potential to obtain images in less than 1 second.

Jackson hoped to develop further the principles outlined in his paper so that the temperatures and conditions found in commercial cure cycles could be duplicated and analysed further. This would include the use of temperatures up to 200°C, and pressures up to $5kgcm^{-2}$. It was also hoped to increase the sample size to approximately 20cm x 10cm x 0.5cm by using wide–bore magnet technology. Jackson concluded that with this technique it was possible to obtain images from the system which can give detailed information on important cure characteristics in a non–invasive, non–destructive fashion.

All of the above techniques use technology that is very expensive, therefore for NMR to succeed as a cure monitoring technique it must offer something that is not currently available and be cost effective. It must also be capable of monitoring components within moulds and autoclaves. But most importantly it must impose no restrictions on the component size or geometry.

At present there is a restriction on the size of specimen that can be accommodated by NMR if the field is to surround the sample (one sided techniques were discussed early in this chapter). For large solid samples a large r.f field strength is required but this can be difficult with respect to transmitter output power. The alternative is to use a surface coil to generate a large r.f field in a small region of the sample being imaged. However with one–sided techniques there is still a restriction on the thickness of the specimen that can be analysed and still give an adequate spatial resolution [64]. This situation can be improved by using a more efficient pulse train (i.e. fewer pulses) to excite the spin system. However even with these improved pulse trains the sensitivity of selective detection can be poor.

The NMR investigations during this research have been to determine the relevance of NMR for cure monitoring using both spectra analysis and relaxation time monitoring with both the FID and CPMG acquisitions.

The Jeol EX270 high–resolution liquid–state spectrometer was used to analyse the spectral changes that occurred as the resin gelled and solidified. At 40°C the cure was followed for 583 minutes at which point only the D_2O (lock signal) peak could be resolved. As can be seen in figure 6.3 the viscosity data shows that gelation occurs between 178 minutes and approximately 400 minutes, therefore at 40°C the spectral changes were followed past the gel point using the liquid–state pulses and spectrometer.

On analysis of the spectra during the 40°C cure cycles it can be seen that the methyl peak is the strongest at the beginning of the cure. The chemical structure of MY750 and HY917 are as follows:

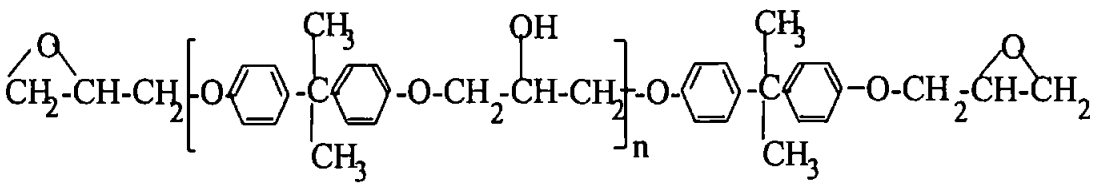

MY750

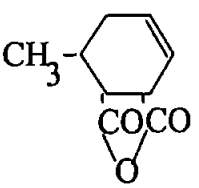

HY917

In the presence of the catalyst the resin forms a cross–linked structure:

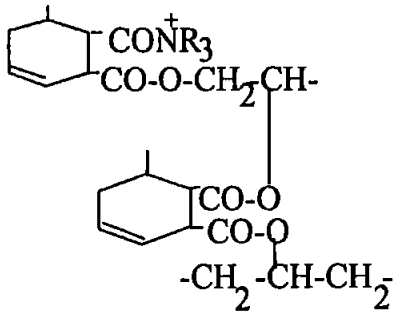

As can be seen the methyl groups play no part in the cross-linking reaction and are unaffected except that for the fact that the chemical environment will become more restricted as more cross-linking takes place. Therefore by monitoring the spectra one can determine the point when the methyl groups become restricted. For a 40°C cure temperature the spectra can no longer be resolved after 583 minutes into the cure. From the VNC experiment the resin reached 10% cured after approximately 10.6 hours (636 minutes) therefore the spectra can be used to monitor the cure until the resin reaches 9.2% solid for the 40°C cure cycle.

For the 60°C cure cycle the spectra can be resolved until 168 minutes into the cure. From the VNC data 10% cured is reached after 213 minutes therefore the liquid-state spectrometer has resolved spectra until the resin is 7.9% solid.

At 60°C the spectral changes were followed for 168 minutes into the cure. Again from the viscosity data in figure 2.3 it can be seen that gelation occurs between 69 and 124 minutes, therefore as in the 40°C cure cycle the spectral changes were followed past the gel point.

For the 80°C cure the spectra were only resolved until approximately 15 minutes into the cure and from the VNC data this corresponded to 1.6% solid.

It was also noticed that an increase in the cure temperature not only increased the cure rate but also modified the initial spectrum, moving the spectra up-field as the temperature increased. It has been noted that when the cure temperature is increased the resin mix initially becomes less viscous before gelation, this is shown quite markedly in chapter 8 (curemeter investigations). This decrease in viscosity could be

the cause of the chemical shift in the initial spectrum. As discussed earlier in this chapter Jackson [74] proposed the use of NMR T_2 measurements to monitor the viscosity of a polymer sample. Therefore if the transverse relaxation time is dependent on cure temperature then a simple spectrum acquisition will show the same effect. The chemical shift the resin undergoes as the temperature is increased could therefore be used to monitor the resin viscosity. The resin viscosity is important for resin transfer moulding (RTM) where a low viscosity is required for injection into the mould but the resin is required to be viscous enough to wet out the fibres and not just flow straight through the mould. The same is true for vacuum bagging techniques, the resin is required to be viscous to wet out the fibres but not to be "pushed" away from the fibres when pressure is applied. This is also true for a hot press.

Using the Oxford QP NMR analyser the change in the transverse relaxation time, T_2, could be calculated easily and for 40°C a plot of $\ln T_2$ versus time of cure could be attained, see figure 6.1. On this graph a change in the gradient indicated the point of gelation i.e. once the resin had gelled the rate of change of the transverse relaxation time increased. However as shown by the increase in the error bars, after approximately 800 minutes the data becomes unreliable, even so this means the Oxford QP has monitored the resin for 400 minutes (6 hours 40 minutes) after gelation has occurred. The cure profiles obtained for this cure cycle indicated that the resin became 10% solid after 10.6 hours and 80% solid after approximately 21.2 hours, therefore since the QP monitored the resin for 800 minutes (13.3 hours) into the cure, the resin was approximately 20% solid.

At higher cure temperatures the resin became "too solid" too quickly and only a few data points could be acquired. The graph in figure 6.5 shows how for 60°C and 80°C the transverse relaxation time increases as the viscosity decreases. This fact was the topic of Jackson's research [64].

By analysing the cure using the FID the changes in T_2 for the solid and liquid components of the resin during the cure and the initial amplitudes of the solid and liquid components could be acquired. The initial liquid amplitude is dependent on

the amount of hydrogen present that still has some degree of movement (referred to earlier in chapter 7 as 'free hydrogen'). As the resin cures the amount of free hydrogen reduces as cross-linking takes place therefore the liquid initial amplitude decreases as the cure progresses. Similarly the hydrogen now 'fixed' due to cross linking gives the solid signal and this signal increases in strength as more cross-linking takes place, therefore the solid initial amplitude increases. From these initial amplitudes the percentage solid and liquid components of the resin could be established.

From the graphs (figure 7.2 onwards) it can be seen that as the cure takes place the solid and liquid amplitudes cross over. This has been assumed to be the point of 50% cure. It can also be seen that in most cases the experiments were terminated before the resin reached 100% solid. At 40 and 60°C it can be seen that the liquid amplitude slowly decreases; however at 80 and 100°C it can be seen that initially the liquid amplitude increases before decreasing as the resin solidifies. This initial rise is because of the viscosity decreasing due to the cure temperature – this is well documented [74]. The percentage cured graphs that were derived from the FID data were then compared with the same data gained from the VNC.

The VNC only gave the times for 10%, 80%, 95% and 100% solid giving no indication as to whether the slope (on the % solid vs time graph) would be a straight line or exponential curve. When these were compared with the FID % solid graphs it could be seen that the FID experiments were stopped before cure was complete; this was subsequently shown to be the case by the VNC results especially for the 40°C profile. There is consistency in the profile of the curves (see figure 8.2 to 8.5). However, there is a time displacement between tests. The time is dependent on the way each technique measures the % cure.

This is explained by the way the cure monitoring process takes place. For the VNC the % cure is measured at a discrete position in the sample and it measures the change in voltage resulting from a change in the vibrating needle displacement as the resin solidifies. The needle is inserted by 4 mm into the resin and so is really only monitoring the cure at the surface level of the sample, where the speed of cure

will be affected by the temperature gradient in the sample, caused by differential heat transfer from the surface of the container and ambient.

The temperature differences due to the cure cycle are more significant at higher temperatures and so the agreement at the low temperature cure cycles is not surprising as the cure rate is less sample dependent.

The Oxford QP FID experiments monitored the cure throughout the whole of the sample and give an average result. Therefore the surface effect is taken into account as much as the slower cure that will take place in the centre of the sample. Therefore the QP FID results are more representative of the way cure actually occurs than the VNC and the discrepancies in the results are due to the way in which the cure is monitored.

The Barcol hardness tests that were carried out on samples of the same dimensions and geometry as the Oxford QP and VNC experiments gave an insight into how 'hard' the resin was when the two cure monitoring techniques assumed the resin was fully cured. At 100% cured as defined by the NMR and VNC experimentation the resin is still ductile while if left longer in the oven i.e. "post-cured" the Barcol hardness increased and the resin became more brittle .

As has been shown by the previous experimentation, at 100% cured (according to NMR and VNC techniques) the resin is still ductile but 'hard' enough to take a load from the Barcol hardness indentor without brittle fracture occurring, these are the optimum conditions. An examination of the Barcol hardness indentation showed a transition from a wholly ductile deformation for 100% cured and partially brittle (evidence of cracking) after post-cure. The later phenomenon indicated a reduction in hardness reading due to fracture.

In this work 100% solid is defined as the point at which all the cross-linking has taken place (i.e. the theoretical end of cure), however if the hardness reading is still continuing to rise after the QP and VNC has indicated 100% cure then further cross-linking must still be taking place (it is known that it takes many days

post–cure to reach a stable hardness reading). Therefore the resin must reach a point of cure when further cross–linking will have a negligible effect upon the curemeter readings; this could be due to the resin becoming more plastic as opposed to visco–elastic or elastic. Since the Barcol hardness impressor measures plastic properties then a further change in readings is expected with this means of measurement even though this is not indicated by the curemeter techniques. It was noticed that as the resin became brittle and so unsuitable for structural purposes in the unreinforced state because of chances of brittle failure, however the addition of fibre–reinforcement adds toughness to the brittle resin.

Thus, 100% cured is defined as 'cured to optimum conditions' and not that all possible cross–links have been formed. This difference between 'optimum' and 'absolute' 100% cure could cause problems when relating the results of one experimental technique to another. However, it has been shown that both VNC and NMR relaxation techniques yield the same point as 100% cured.

11.0 CONCLUSIONS

11.1 Concluding Remarks

Nuclear magnetic resonance (NMR) has been used for obtaining medical images for a number of years but it has not been extensively used for industrial purposes. This research programme has highlighted the advantages and disadvantages of NMR for use with composite components and carried out investigations into improving the existing applications and furthering its usage. As has been indicated in the literature survey, NMR spectroscopy and imaging have a great potential for many applications including cure monitoring, viscosity monitoring and non-destructive examination. The method of analysis of the sample within either spectroscopy or imaging has the potential to give considerable information concerning the matrix, fibres, voids and contaminants. However due to size restraints of the hardware, cost and lack of user friendliness it has not had wide usage within industry.

NMR for cure monitoring has the potential to be a useful quality assurance tool within industry. The Oxford QP can be programmed to give a user friendly interface making NMR less daunting for the user who does not have a great NMR background. This would remove one obstacle stopping NMR from becoming more generally used outside the research laboratory. Since the Oxford QP gives results for the sample as a whole rather than each individual chemical environment therefore it can be used for quality control by a semi-skilled operator.

It has been shown that by using the Oxford QP NMR analyser the test can obtain results far longer into the cure than with a conventional liquid-state NMR spectrometer. This was the case for both CPMG and FID studies. It was also shown that the % cure figures obtained by the Oxford QP FID experiment were comparable to the VNC curemeter cure profiles even though the mechanics of the two techniques were different, the first measuring molecular freedom the other measuring continuum freedom. However, both curemeter techniques indicated that the resin was 100% solid before the Barcol hardness had reached a maximum value.

Both of the curemeter techniques measure the degree of cure of the resin to the point where further cross-linking results in such negligible changes in the chemical behaviour that the NMR can no longer resolve these differences. The limitation and strengths of the VNC and its agreement with the NMR analysis indicates that this technique does not follow the last stages of the cure and assumes 100% cure prematurely. Using the FID method of analysing the data as opposed to the CPMG technique the resin can be monitored far longer into the cure than previous NMR techniques. The following can be concluded from the NMR investigations:

1. The CPMG data acquisition gives a good indication of the gel point of the resin,

2. The transverse relaxation time (T_2) obtained by both the CPMG and FID acquisitions gives a good indication of the viscosity with respect to the initial viscosity of the resin mix,

3. The FID % cure calculations give comparable results to existing curemeter techniques,

4. The FID curemeter method can be used on a resin/glass fibre mix to give a cure profile comparable with those obtained for a zero volume fraction.

Therefore nuclear magnetic resonance has the potential to be used as a curemeter in the low-field configuration (Oxford QP NMR analyser) used in this work. It will give readings throughout the cure as well as an indication of the viscosity of the resin. However due to the physical size (constraints on the size of the internal bore of the magnet) the Oxford QP may only be used as a research tool rather than being used as an on-line quality control tool within the composites industry. To be an effective tool the NMR hardware needs to be developed from the conventional form of the sample being surrounded by the magnetic field and move towards one-sided NMR technology.

11.2 Further Work

The following is suggested as further work to make nuclear magnetic resonance a more viable process control technique.

1. Investigate one-sided NMR techniques to understand the advantages and restraints imposed by the magnet and r.f. coil configurations,

2. To analyse the use of NMR curemeter techniques with different resins (for example phenolic and polyester resins),

3. To analyse further the effects on the NMR readings of the addition of fibres both glass, carbon and Kevlar,

4. Correlate NMR measurements made with the Oxford QP with regard to viscosity measurements. In this way the NMR can assist by monitoring resin viscosity and resin flow and hence indicate gel point. Also, if resin flow is monitored then dry areas in the mould could be detected.

5. Create a user-friendly signal analysis interface so that all that is required is the input of the sample type (resin, fibre and volume fraction used) and what information is required e.g. viscosity monitoring, gel point or % solid and all calculations will be carried out within the software, to provide the data required without further analysis or interpretation being needed.

However this will only find a place in the market place if the price is competitive with existing curemeters.

APPENDIX 1.0

1.1. Oxford QP Specification

QP Specification

Magnet	
Construction	Permanent magnet, thermally stabilised
Field	0.47 Tesla (20MHz proton)
Adjustment range	± 10G (automatic or manual)
Pole diameter:	125mm
Air gap	25mm
Homogeneity:	Better than 40mG (170Hz) over 30mm x 10mm diameter volume FWHHM
RF Probes	
Sample sizes:	2ml or 8.5ml. Automatic sample-in detector
Tuning:	Pre-set tune and match
90° pulse time:	Nominal 2μS (2ml ratio probe), nominal 5μS (8.5ml absolute probe)
Total dead time	9μS (2ml probe)
Detection	
Type	Dual channel phase sensitive detector (quadrature), with programmable low-pass filter
Offset correction:	Automatic
Data acquisition rate:	Programmable; maximum 1MHz per pair of points
Receiver gain:	Auto/manual selection
Pulse generator	
Phases:	0, 90, 180, 270 transmit and receive
Phase accuracy:	Better than 3°
Event resolution:	100nS
Shortest event:	200nS
Interfaces	40 column, 2 colour dot matrix printer with dot addressable graphics. 256 x 64 dot LCD screen with dot addressable graphics. Alphanumeric keypad. RS232/Digital balance interface. Real time clock (date and time).
Weights & dimensions	
Console:	45lb (20kg), 22" x 18" x 11" (56 x 46 x 28cm)
Magnet:	200lb (89kg), 21" x 21" x 11" (54 x 54 x 28cm)
Power requirements	100/110/120/220/240V AC, 50/60Hz, 700W

1.2 Specifications

Listed hereunder are the specifications related to the handling of spectrometers and the requirements for installation.

1.2.1 Basic Performance

Item	EX270/EX270W	EX400
Nuclei to be measured	H, ^{13}C	
Reference magnetic field	6.34 tesla	9.4 tesla
Reference frequency	^{1}H : 270 MHz ^{13}C : 68 MHz	^{1}H : 400 MHz ^{13}C : 100 MHz
Resolution Sensitivity Variable temperature range	Depends on the probe in use.	

1.2.2 Spectrometer

Item	EX270/EX270W	EX400
NMR lock	^{2}H internal lock (Auto lock)	
Observation frequency	270MHz/68MHz	400MHz/100MHz
	Offset range : 0 ~ 250 kHz (at 0.1 Hz steps)	
Irradiation frequency	270 MHz	400 MHz
	Offset range : 0 ~ 250 kHz (at 0.1 Hz steps)	
Decoupling mode	Hetero decoupling mode : ^{13}C -{^{1}H} Wide band noise decoupling, CW, Gated NOE, Waugh sequence decoupling, Gated NNE, Selective NOE Homo spin decoupling : ^{1}H-{^{1}H} Gated homo spin decoupling Extention mode	
Room temperature shim	X, Y, Z^{1}, Z^{2}, Z^{3} Z^{4}, etc.	
Pulser	Programmable multi pulser	

1.2.3 Data system

■ Host computer: DEC LSI11/73, RSX-11M operating system

Memory capacity : 1MB (16bits + parity check)

■ Data processing

computer : JEC32

Memory capacity : EX270 : 12MB (3MW)
EX400 : 20MB (5MW) (32bits + auto correction bit)

Fourier transformation time : Approx. 5 seconds for 8KW data

Cycle time : 250ns

■ AD converter: 12-bits/100kHz, 2 channels

Sampling time : Minimum 10 μs (frequency range : 100kHz)

■ Hard disk

Capacity : 171MB (unformatted)
138MB (formatted)

■ 3.5-inch floppy disk drive

capacity : 1.47MB × 2

■ Color graphic display

Size : 14 inches

Graphic : 640 × 480 dots

Number of planes : 4 + character 1

Provided with a joy-disk, a magnetic-shielded case and a keyboard.

■ High speed plotter

Pen speed : 80cm/s

Step size : 0.025mm

Plotting range : A4 (210mm × 297mm) and A3 (297mm × 420mm) sizes

Color pen : 8

Auto-feeding of chart paper is possible.

■ Dot-matrix printer

Printing speed : 120 characters/s

1.2.4 Software

- A variety of pulse sequences for one-dimensional and two-dimensional NMR
- Inputs of parameters by keys, function keys and knobs
- Alphanumeric display on color CRT
- Real-time FT
- Auto receiver gain
- 32-bit time domain accumulation
- Help function (English : standard : Japanese : option)
- Various sets of time window functions (expontial, trapizoidal, sinebell, Gaussian, etc.)
- FFT (Fast Fourier transformation)
- Phase correction (auto and manual)
- Baseline drift correction (auto and manual)
- Integration (whole, partial, auto and manual, normalization and display of integrated values)
- Multi-view function (whole, partial, data manipulation on CRT)
- Multi-spectrum CRT display and plotting
- Plotting (A3, A4, auto, manual)
- Scale (units of ppm, Hz and kHz, auto-scale)
- Data reduction (auto, manual, plotting, CRT display)
- One-point reduction
- Data saving, loading and manipulation (Winchester disk)
- Data saving, loading and manipulation (floppy disk)
- File management of measurement conditions (menu files)
- File management of shim values (shim files)
- Auto T_1 and auto T_2 measurements
- Auto plotting of T_1 and T_2
- CRT display of T_1 and T_2 (relaxation curves)
- Auto calculation of T_1 and T_2
- Automatic calculation of signal half-width
- Data addition and subtraction (time-domain and frequency-domain)
- Moving and exchanging data block (s)
- Smoothing
- Power spectrum
- Print-out of Parameters
- Reference set (auto, manual, conversion of chemical shift)
- Control of sawtooth generation and NER lock monitor)
- Control of programable multi-pulser
- Auto zero-filling
- Control of observation frequency offset and observation power
- Control of irradiation frequency offset and irradiation power
- Setting temperature
- Interactive GLG
- Auto stacking (Multi-mode, automatic successive measurement)
- Single user, multi-task (Multiple, parallel processings)

1.3. VNC Specification

THE VIBRATING NEEDLE CUREMETER

A unique instrument for monitoring liquid polymer cures

by Keith W. Scott

SUMMARY

Simple instrumentation has been developed, which is able to provide a convenient basis for comparison of the cure of liquid systems. This instrument, the Vibrating Needle Curemeter (VNC), offers the following benefits to its users:

- Produces a continuous trace of the cure (analogous to that obtained with a Monsanto rheometer, for solid rubbers).
- Can be 'tuned' to give increased sensitivity to any chosen stage of the cure.
- Unique ability to take the instrument to the sample.
- Can monitor the cure of a wide range of liquid systems, including polyurethanes, unsaturated polyester resins, silicones, phenolics and epoxides.

For more information about the VNC please contact:

Keith Scott
Rapra Technology Limited,
Shawbury,
Shrewsbury,
Shropshire, SY4 4NR,
England.

Telephone: (0939)250383 Telex: 35134 Fax: (0939)251118

INTRODUCTION

The ability to monitor the curing characteristics of liquid polymer formulations is vital to the needs of quality control, trouble-shooting and product development. Of course one technique which is widely used is the measurement of gel time. This is simple to perform and supplies numerical data so that comparisons between systems can be made. However, such single point data may be of little value outside routine quality control: the method may serve to indicate that two cures are different but provides little further to distinguish what the differences are. Closer monitoring of the physical properties of a curing formulation provides more information about the curing characteristics of the formulation.

Viscosity is probably the physical property most widely monitored, in the study of the cure of mixes which are initially free-flowing. However it should be recognised that a curing liquid mix develops elasticity as the molecular network builds up. Thus a simple viscometer cannot monitor reliably beyond the earliest stages of the cure.

The limitation of such measurements to non-elastic systems is a serious one. Undoubtedly the technologist would like to produce a complete cure profile, as can be accomplished for conventional solid rubber vulcanisations. In the latter case rheometers or curometers are used, but most of these appear to be wholly unsuited to handling a free-flowing liquid mix. Even when such an instrument, (a Wallace-Shawbury curometer), was modified to retain a free-flowing liquid, the monitoring responses of the instrument proved inadequate for study of the early, i.e. viscous, stages of the cure[1].

Such problems were recognised at Rapra in the late 1970's and initiated the development of an entirely new instrumental technique. This instrument in its earliest guise[2] has been used extensively in Rapra's own developments on cure control, and to support other consultancy work on liquid polymer cures. The principle by which this operates allows the instrument to be taken to the cure, rather than vice versa, and in its latest guise[3] is commercially available. This is the Rapra Vibrating Needle Curemeter (VNC), which is capable of producing complete cure profiles of many different types of formulation (e.g. polyurethanes, liquid polysulphides and unsaturated polyester resins).

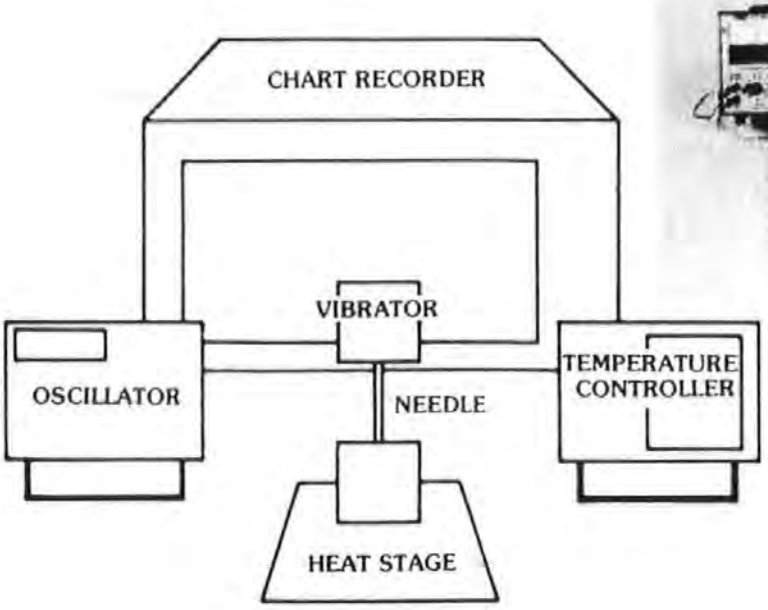

Figure 1 The Vibrating Needle Curemeter

THE INSTRUMENT

The Vibrating Needle Curemeter (VNC) monitors the increase in the viscosity of curing formulations before gelation: however subsequent changes in the stiffness of the gelled formulation are also measured. This is achieved by suspending a steel needle in the formulation. This needle is vibrated vertically by a small electrodynamic vibrator driven by a low power amplifier/oscillator (see Figure 1): resistance to its movement is ultimately recorded on a chart recorder. This allows the instrument to be unattended during the monitoring of a cure. A cure trace analogous to a Monsanto Rheometer cure trace for solid rubber, can be obtained.

The VNC can be operated with the needle vibrating at a wide variety of frequencies. The shape of the VNC trace obtained is dependent on this frequency. By way of an example, Figure 2 shows cure traces for a polyurethane formulation, which gelled after 8 minutes, obtained using the VNC operating at various frequencies. The formulation being monitored was: Diorez 520; 100 parts. DBTL; 0.2 parts and Hyperlast Isocyanate 2875/000; 15.4 parts. It can be seen that changes in the early stages of the cure are more closely monitored at lower frequencies (e.g. 60 Hz), with more sensitivity to changes in the later stages of the cure being achieved, when monitoring at higher frequencies (e.g. 150 Hz). In effect the instrument can be tuned to suit the type of cure and the requirements of the operator.

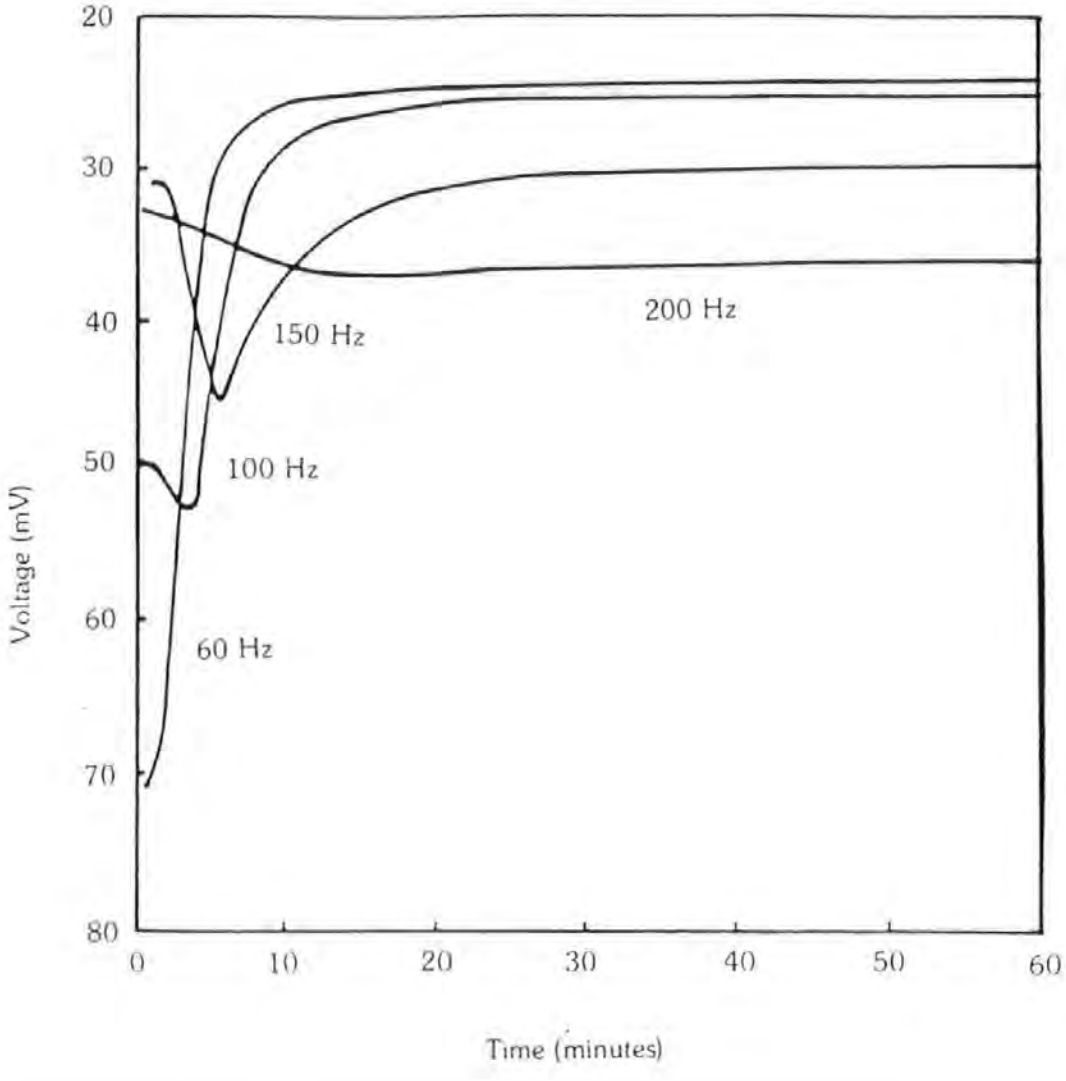

Figure 2 Cure traces, for a PU formulation, obtained at different frequencies

Numerical data can be derived from the VNC traces. Figure 3 shows how such data can be obtained from a cure trace obtained with the VNC operating at 80 Hz. The cure being monitored was that of Diorez 520 (100 parts) with Hyperlast Isocyanate 2875/000 (15.4 parts), in the presence of dibutyltin dilaurate (0.25 parts). The cure was repeated several times and the numerical data obtained from each cure are listed in Table 1.

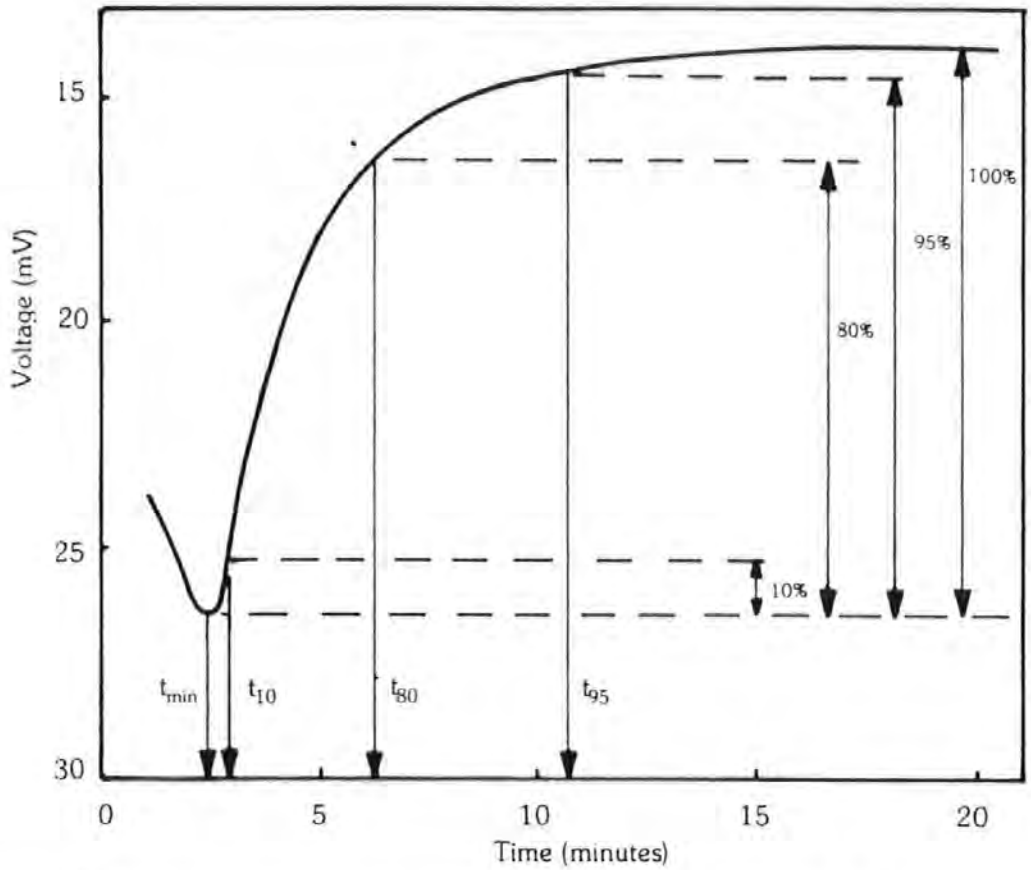

Figure 3 VNC trace of cure, when monitored with the VNC operating at 80 Hz

Table 1 VNC data for cures monitored at 80 Hz

Cure	t_{min}(mins)	t_{10}(mins)	t_{80}(mins)	t_{95}(mins)	t_{100}(mins)
1	2.4	3.0	6.0	10	30
2	2.4	3.1	6.0	11	30
3	2.4	2.8	6.2	13	30
4	2.8	3.3	7.5	14	30
5	3.0	3.6	8.2	15	30
mean	2.6	3.1	6.8	12.6	
standard deviation	0.25	0.29	0.9	1.9	

These data demonstrate the reproducibility of the VNC, the standard deviation of the results being around 10% of the mean.

As mentioned previously, the progress of a cure can be monitored using a Brookfield Viscometer. Figure 4 compares the build-up in viscosity with the cure trace obtained with the VNC operating at 40 Hz. of a polyurethane formulation (Diorez PR1, 100 parts; Hyperlast Isocyanate 2875/000; 21.5 parts and tributyltin oleate, 0.2 parts). This shows that the VNC can monitor cure well beyond the gel time, even when operating at 40 Hz. Monitoring with a Brookfield Visometer is not possible after gelation.

By offering the facility to monitor through the gel point, the VNC brings a new dimension to liquid cure monitoring. The whole process of cure, from liquid through to solid, is presented on a single trace. That single trace can provide information on pot life, application time, cure time, etc., and a convenient format for rapid comparison between samples.

The monitoring of liquid polymer cures is important to those involved with cast elastomers, sealants, adhesives, paints and resins. All these systems have proved amenable to monitoring with the VNC, and its applicability will be demonstrated in this review by reference to a variety of examples.

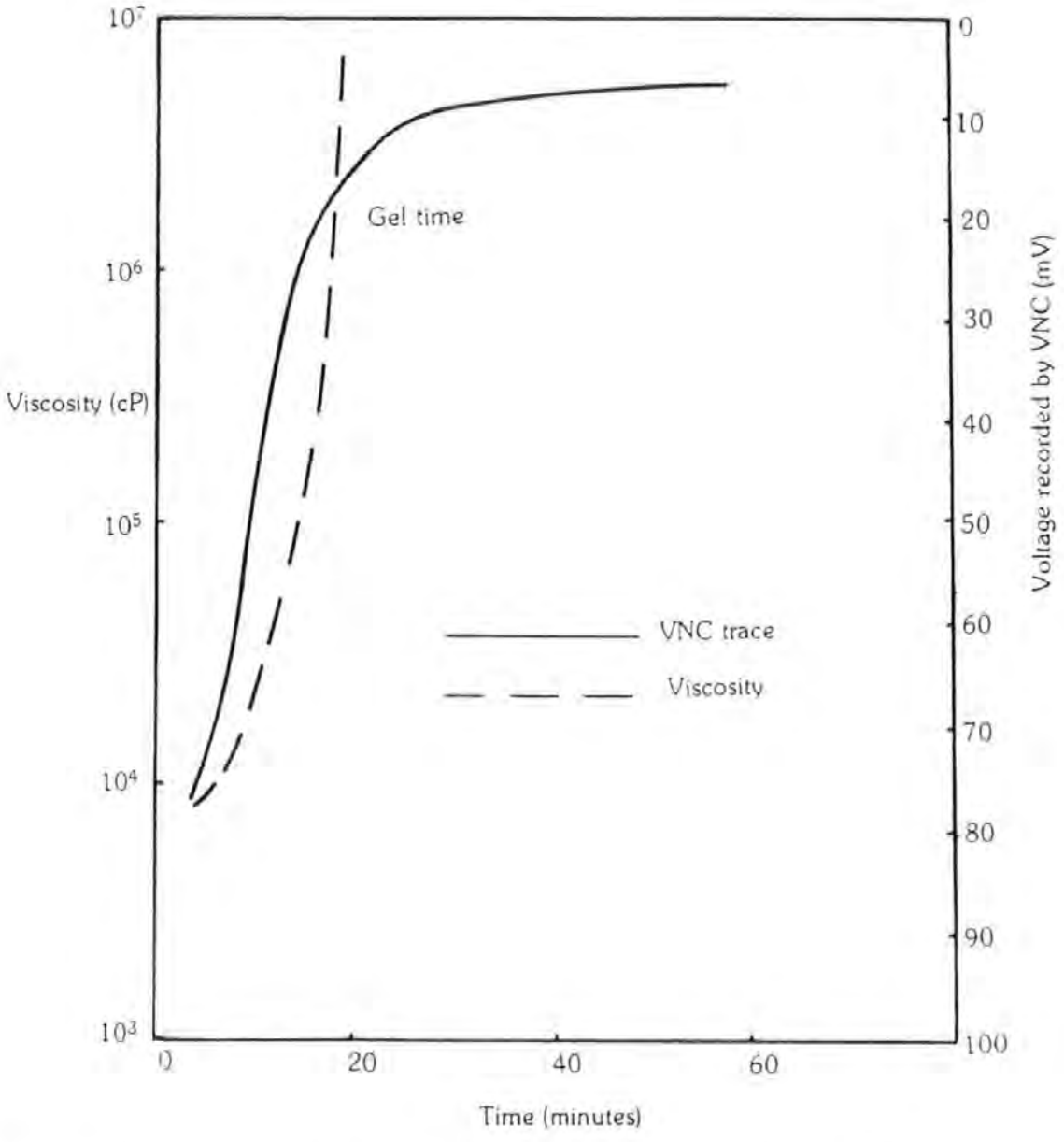

Figure 4 VNC trace and increase in Viscosity of a PU formulation at room temperature

BARBER COLMAN COMPANY

Product Information

1260/DB 10

(CONFORMS TO BRITISH STANDARD BS 2782)

THE IMPRESSOR: A Hand-Held Portable Hardness Tester

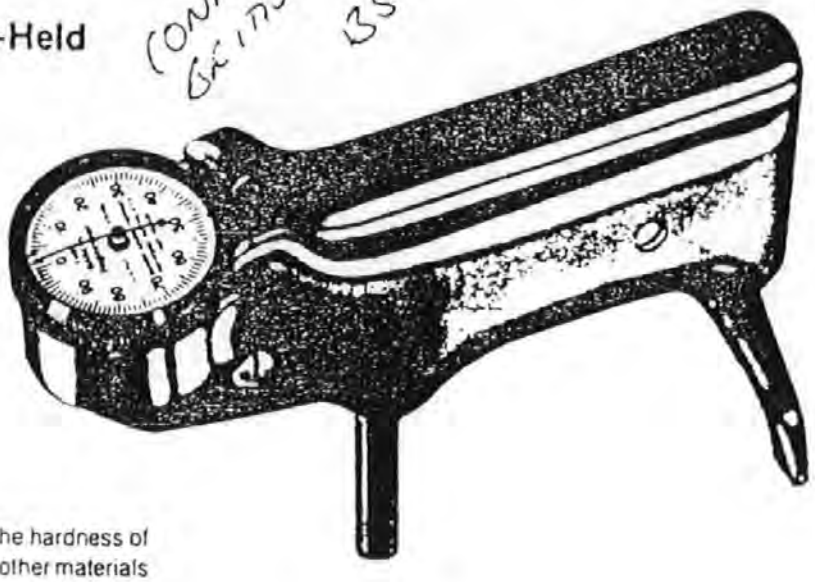

Applications for:

- Aluminum
- Aluminum Alloys
- Soft Metals
- Plastics
- Fiberglass

Portable

The Impressor is a convenient tool for testing the hardness of aluminum, aluminum alloys, copper, brass and other materials including plastics and fiberglass. The instrument is designed for use on fabricated parts and assemblies as well as on raw stock.

Easy to Use

No experience required, can be used in any position and in any space that will allow for the operator's hand. The hardness reading is instantly indicated on the dial, which is divided into one hundred graduations. No waiting, preloading or separate measurements.

Lightweight

The Impressor weighs only 1 lb. 2 oz. and comes complete with carrying case, adjusting wrench and two spare indenter points, 2 lb. 8 oz.

Three Models Available

GYZJ 934-1 for soft metals such as aluminum and its alloys, brass, copper, and some of the harder plastics and fiberglass. Approximate range 25 to 150 Brinell (10MM ball 500 KG load). This unit meets American Society for Testing and Materials (ASTM) Standard D-2583.

GYZJ 935 for the softer plastics and very soft metals.

GYZJ 936 for extremely soft materials such as lead, linoleum and leather.

Barber-Colman engineers will be glad to recommend the most suitable model upon receipt of sample materials.

Testing Instructions

The Impressor is best suited for testing homogeneous materials. Materials of granular, fibrous or coarse structure will produce a wide variation in hardness readings because of the small diameter of the indenter point.

For accurate readings, material should be at least 1/32" (0.79mm) thick and large enough for a minimum distance of 1/8" in any direction from the indenter point to the edge of the specimen. The testing area should be smooth and free from mechanical damage.

Simply exert a light pressure against the instrument to drive the spring-loaded indenter point into the material. The indenter point must be perpendicular to the surface being tested.

On very soft metals, the highest reading should be used since cold flow permits the spring-loaded indenter point to continue penetration.

Note: Physical characteristics of very soft materials are such that uniform correlation between different hardness measuring systems cannot be established. For this reason, no conversion curves are offered for the 935 and 936 models. We recommend that Impressor hardness limits for each material be established by test.

Recommended Sample Sizes to Equalize the Variance of the Average

Hardness Scale GYZJ 934-1	Reading Variance	No. of Readings	Variance of Average
	— Homogeneous Material —		
20	2.47	9	0.27
30	2.20	8	0.28
40	1.93	7	0.27
50	1.66	6	0.28
60	1.39	5	0.28
70	1.12	4	0.28
80	0.85	3	0.28
	— Reinforced Plastics —		
30	22.4	29	0.77
40	17.2	22	0.78
50	12.0	16	0.75
60	7.8	10	0.78
70	3.6	5	0.75

Typical Impressor Readings of Aluminum Alloys

Alloy and Temper	1100-0	3003-0	3003H14	2024-0	5052-0	5052H14	2024T3
GYZJ 934-1	35	42	56	60	62	75	85

Approximate Conversion Curves for GYZJ 934-1

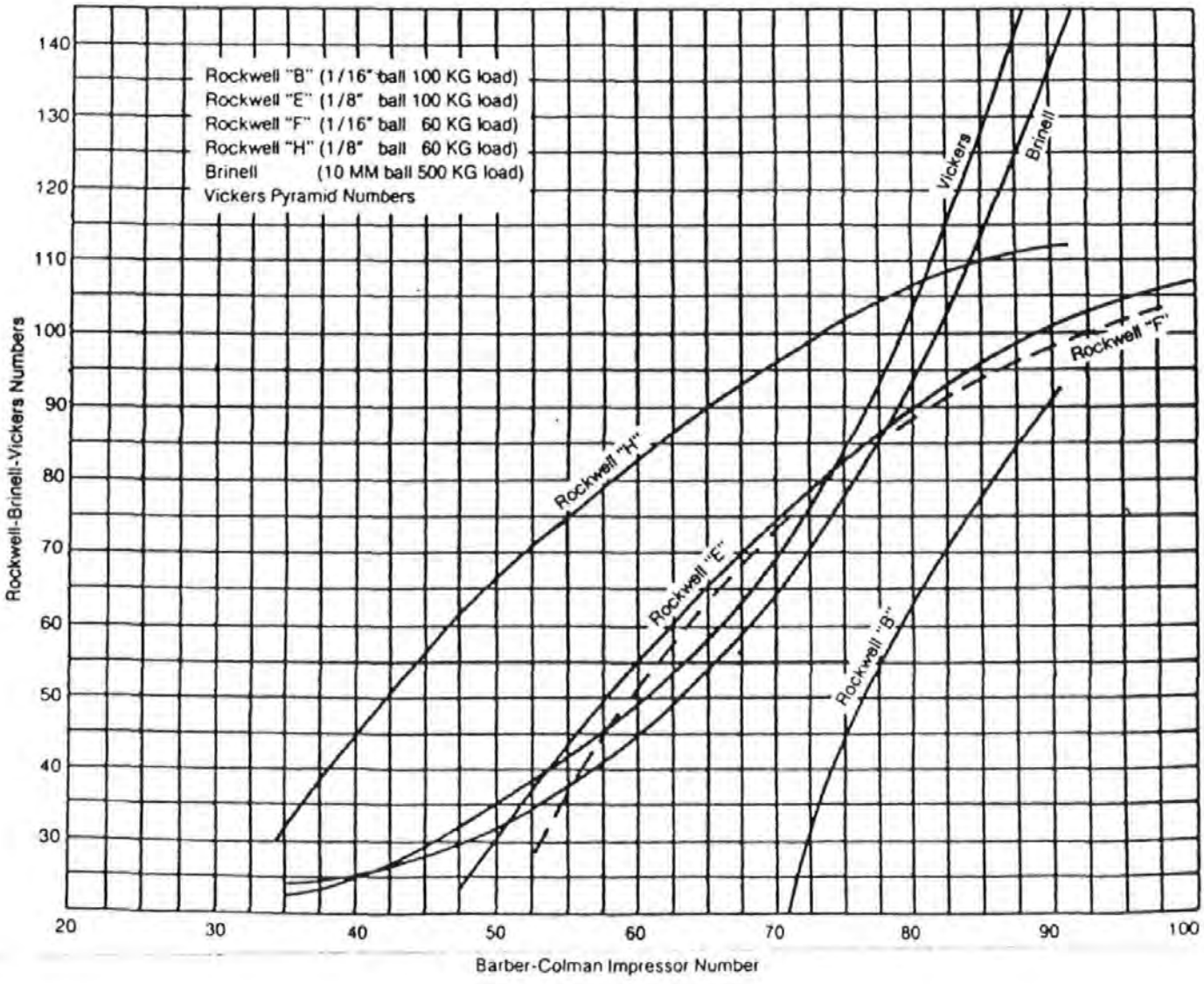

Approximate Conversion Chart for GYZJ 934-1

934-1	Brinell	Vickers	Rockwell B	Rockwell E	Rockwell F	Rockwell H
35		23				32
36		23				33
37		24				37
38		24				40
39		25				43
40	25	25				45
41	26	26				47
42	26	27				49
43	27	27				52
44	27	28				54
45	27	29				56
46	28	30				58
47	29	32		24		61
48	30	33		25		63
49	31	34		28		64
50	32	35		30		66
51	33	36		33		68
52	34	38		36		70
53	35	39		39	29	72
54	37	41		42	33	73
55	38	42		44	38	75
56	39	44		46	40	76
57	40	45		48	43	78
58	42	47		51	47	80
59	44	48		53	49	81
60	45	49		55	51	83
61	47	51		57	54	84
62	48	53		59	56	86
63	50	55		62	58	88
64	52	57		64	61	89
65	54	58		65	63	90
66	55	60		67	65	91
67	58	62		69	67	92
68	60	64		71	69	94
69	62	67		73	71	95
70	64	69	18	74	73	96
71	67	72	19	76	75	98
72	69	74	28	77	77	99
73	71	76	33	79	79	100
74	73	81	39	81	81	101
75	76	85	45	83	83	102
76	80	88	48	84	84	103
77	84	92	52	86	86	104
78	87	95	56	88	87	105
79	90	99	60	89	88	106
80	94	103	63	90	89	107
81	97	108	65	91	90	108
82	100	111	69	92	91	108
83	105	116	72	94	92	109
84	109	122	75	95	93	109
85	113	127	77	96	94	110
86	117	133	80	97	95	111
87	122	137	83	98	96	111
88	126	142	86	99	97	112
89	131		89	100	97	112
90	135		91	101	98	113
91	139			102	99	113
92	145			103	100	
93				103	101	
94				104	101	
95				104	102	
96				105	102	
97				106	103	
98				107		
99				108		
100				108		

PLASTICS MACHINERY CONTROL

From the very beginning of the plastics industry, Barber-Colman has provided reliable temperature control equipment. Today, Barber-Colman offers the most complete line of control equipment for the plastics industry — equipment that includes sensors, temperature controllers, data loggers and recorders; plus complete control systems for plastics forming machines and plant-wide plastics processing information and control systems.

For further information on any of the quality plastics processing control products offered by Barber-Colman, call or write your local Barber-Colman Sales and Service Office or our central office in Loves Park, Illinois.

Albuquerque 505/255-1638 Williams Assoc.
Appleton 414/739-4247 Pyro-Matic, Inc.
Atlanta 404/451-0125
Baton Rouge 504/567-3633 ASKCO-LA.
Birmingham 205/988-5842 M & W Controls, Inc.
Boston 617/828-9496
Buffalo 716/693-6400
Calgary, AL 403/255-3448 Instrument Service Labs
Charlotte 704/372-5492
Chicago 312/676-4052
Cincinnati 513/791-0900
Cleveland 216/461-2480
Denver 303/289-5647 Williams Assoc.
Detroit 313/476-9060 Applied Inst.
Edmonton, AL 403/463-7488 Instrument Service Labs
Florida 813/461-7706 J. J. Galleher Co.
Fort Worth 817/921-5188
Grand Rapids 616/744-1381 Applied Inst.
Hackensack 201/489-8050
Houston 713/472-3688 ASKCO Instrument Co.
Indianapolis 317/872-2571 Robinson Equip.
Kansas City 913/381-9330 Parker & Foster, Inc.
Los Angeles 213/327-3282 Instrument Lab
Memphis 901/795-4200 Industrial Process Controls
Milwaukee 414/453-1171 Pyro-Matic, Inc.
Minneapolis/St. Paul 612/540-0192 Pyro-Matic, Inc.
Montreal 514/631-9064
New York City Toll Free 800/631-0795
Omaha 402/734-2434 Process Measurement
Philadelphia 215/647-4650
Phoenix 602/947-4297 Williams Assoc.
Pittsburgh 412/344-1500 Weiss Inst.
Richmond 804/272-7270 Indamation Co.
Rock Island 309/788-1275 Carlin Automation
St. Louis 314/968-5242 Temtron
Salt Lake City 801/364-6425 Control Systems, Inc.
San Francisco 415/328-1040 Instrument Labs
Scottsdale 602/947-4297 Williams Associates
Seattle 206/883-4999 Sales and Engineering Assoc.
Shreveport 318/865-2393 JDJ Sales Co.
South Bend 219/299-0190 Robinson Equipment
Syracuse 315/437-7052 Ossman Instrument
Toronto 416/742-6210
Vancouver, B.C. 604/278-4511 Instrument Service Labs
Vancouver, WA 206/573-5161 Sales & Engineering Assoc.

Barber-Colman Company
World Headquarters
Rockford, Illinois, U.S.A.

European Headquarters
Hofheim/Ts. West Germany

Canadian Headquarters
Toronto, Canada

Japan Headquarters
Tokyo, Japan

For complete information, contact:

Barber-Colman Company
INDUSTRIAL INSTRUMENTS DIVISION

1354 Clifford Avenue
P.O. Box 2940
Loves Park, IL U.S.A. 61132-2940

Phone: (815) 877-0241
Telex: 6871476 Barber

January, 1985

LITHO IN U.S.A.

APPENDIX 2.0

2.1. Oxford OP Programme

```
CONST
  Transfer_Type = 2   ! MA602
  Rec_Phase     = "0213"
  TX90_Phase    = "0213"
  TX180_Phase   = "1320"

VAR
   i  = 0[0:32767]
  v2  = 0[0:32767]
  v3  = 0[0:32767]
  v4  = 0[0:32767]
  v5  = 0[0:32767]
  v6  = 0[0:32767]
  fname = ""
  P90=2[0:20]
  P180=4[0:40]
  RD=2[0:200]
  DWELL=1[1:1000]
  DEAD1=20[0:1000]
  DEAD2=3[0:1000]
  FID_POINTS= 600[1:16384]
  ECHO_POINTS= 9[1:16384]
  TAU=100[5:1E6]
  NUM_ECHO= 600[1:3192]
  NS=16[1:32767]
  Delay        = 10[10:1E6]
  NO_ZERO      =  1[-1:3]
  Scale_Msg    = "Scale = 1/"
  Prev_Scan    = -1[-1:32767]
  POINTS         = 1[0:16384]
  Rec_Phase    = "0213"
  TX90_Phase   = "0213"
  TX180_Phase= "1320"
  EXP_NO       = 1[0:120]
  EXP_ID       = 1[0:120]
  Run          = FALSE[FALSE:TRUE]

BEGIN
form1:=10
form2:=2

LOAD "FIELD.ADJ"
 FIELD
ENDLOAD

Option:=1
WHILE Option<>6                          ! Uses menus to allow parameters
                                         ! to be changed.
  MENU 6
  0 "Other Page              "
  V "P90          = ",P90,0,2
  V "P180         = ",P180,0,2
  V "REP DELAY    = ",RD,0,3
  V "DWELL        = ",DWELL,0,0
  0 "Continue                "
  ENDMENU
```

```
    IF Option=1
      MENU 1
      0 "Other Page          "
      V "Dead1        = ",dead1,0,2
      V "Dead2        = ",dead2,0,2
      V "FID  POINTS = ",FID_POINTS,0,0
      V "ECHO POINTS = ",ECHO_POINTS,0,0
      ENDMENU
    ENDIF
    IF Option=1
      MENU 1
      0 "Other Page          "
      V "TAU          = ",TAU,0,0
      V "NUM ECHOS    = ",NUM_ECHO,0,0
      V "NUM SCANS    = ",NS,0,0
      V "Filter freq  = ",filter,7,0
      ENDMENU
    ENDIF

  IF Option=1
      MENU 1
      0 "Other Page          "
      V "GAIN             = ",REC_GAIN,0,1
      V "FIELD            = ",FIELD,0,0
      V "No. of Expts.    = ",exp_no,0,0
      ENDMENU
    ENDIF
  WEND

  CLS
  exp_id := 1
  ! *** main loop of time base
  WHILE exp_id < (exp_no + 1)

    ! *** wait for time trigger ***
    CLS
    Locate 10,10
    PRINT "Waiting for experiment "
    PRINT exp_id

    ! *** wait for minutes to change to 30 or 00
    RUN := FALSE
    WHILE Run = FALSE
    TIME v1, v2, v3, v4, v5, v6
    IF v5 = 29
      RUN := TRUE
      WHILE v5 <> 30
        TIME v1, v2, v3, v4, v5, v6
      WEND
    ENDIF
    IF v5 = 59
      RUN := TRUE
      WHILE v5 <> 00
        TIME v1, v2, v3, v4, v5, v6
      WEND
    ENDIF
    WEND

    ! *** run pulse sequence ***
    CLS
    Delay:=Tau-(Echo_Points*Dwell/2)
    POINTS:=FID_POINTS+(ECHO_POINTS*NUM_ECHO)
    SEQUENCE NS
```

```
    P90*US                  RF:TX90_Phase
    Dead1*us
    Dead2*us                REC
    DO Fid_points
      Dwell*US              ADC:Rec_Phase REC
    LOOP
    (TAU-Dead1-Dead2-(Fid_points*Dwell))*US
    DO Num_Echo
      P180*US               RF:TX180_Phase
      Delay/2*US
      Delay/2*US            REC
      DO Echo_Points

        Dwell*US            ADC:Rec_Phase REC
      LOOP
      Delay*US
    LOOP
    60*S
    NEXT TX90_Phase
    NEXT TX180_Phase
    NEXT Rec_Phase
  ENDSEQUENCE
  CALL Foreground NS

  ! *** set up file extension ***
  ITOA exp_id, fname
  IF exp_id < 10
    fname := "00" + fname
  ELSE
    IF exp_id < 100
      fname := "0" + fname
    ENDIF
  ENDIF
  fname := "FID_ECHO." + fname

  ! *** output file data ***
  CLS
  LOCATE 10,10
  PRINT "TRANSFERRING DATA"
  XFER 1, POINTS, MAG32, fname
  CLS

  ! *** increment experiment if for next expt.
  exp_id := exp_id + 1
WEND

XFER 1,1,TERMINATE,""

END
```

FID DATA ACQUISITION

CPMG ACQUISITION SEQUENCE

APPENDIX 3.0

3.1. Free Induction Decay Analysis at 40°C with fibres

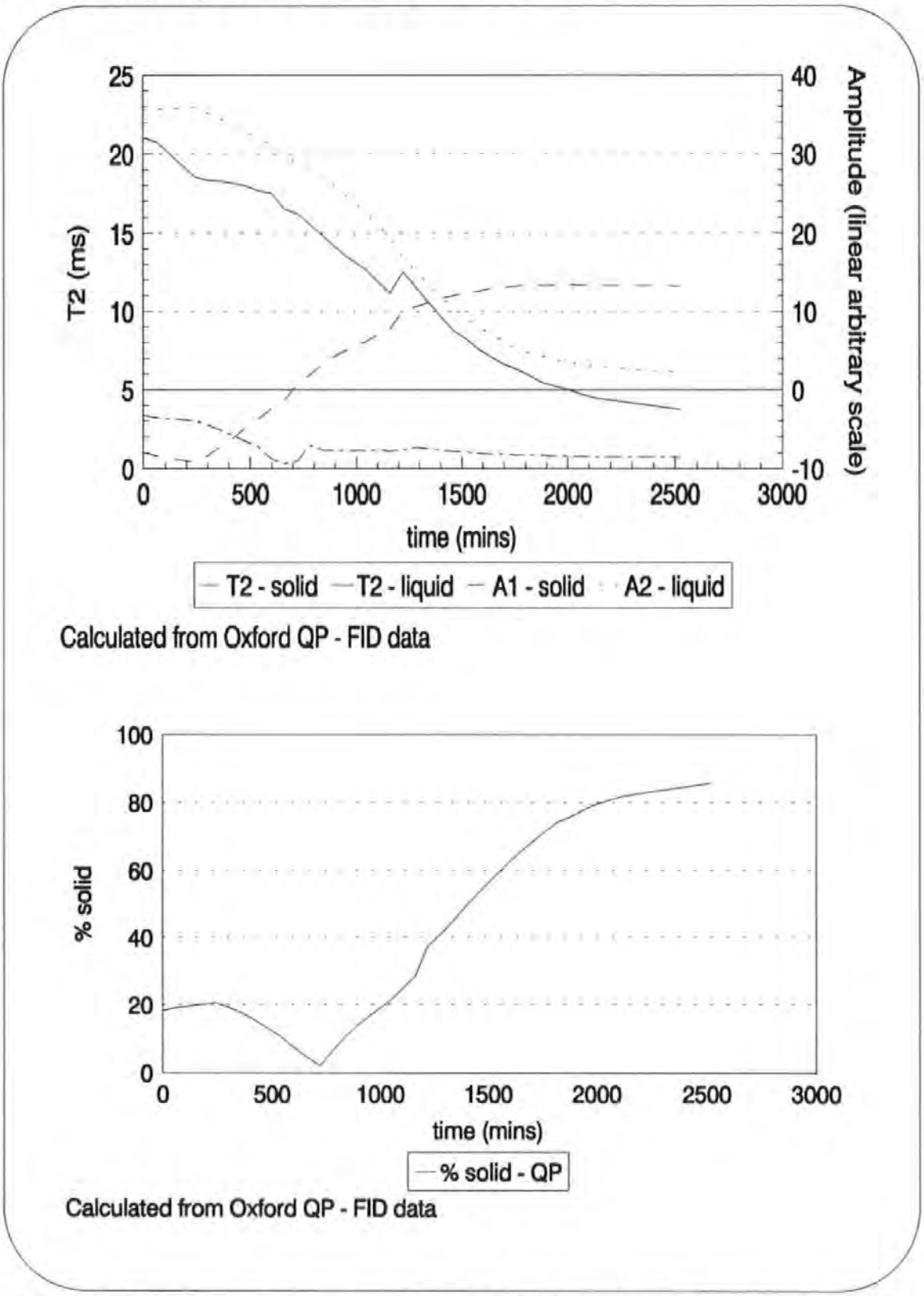

Figure A3.1. FID analysis at 40°C with 9.0% volume fraction. Top graph demonstrates the change in liquid and solid amplitudes as resin cures. The bottom graph is of the calculated solid versus time of cure.

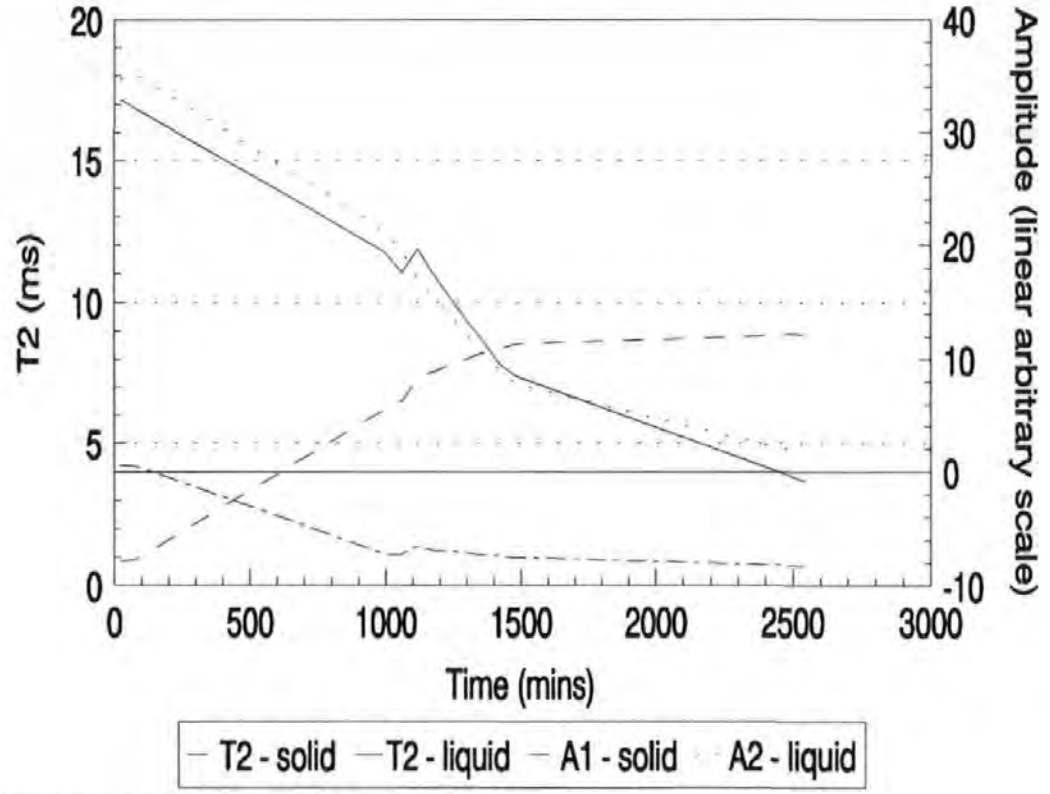

Calculated from Oxford QP - FID data

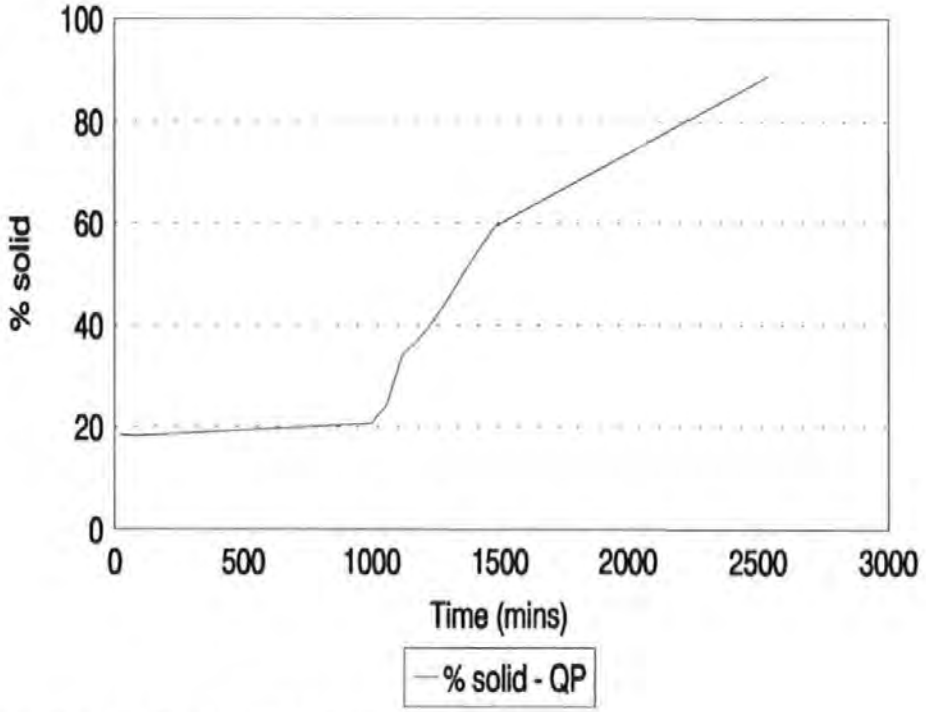

Calculated from Oxford QP - FID data

Figure A3.2. FID at 40°C with 18.1% V_t.

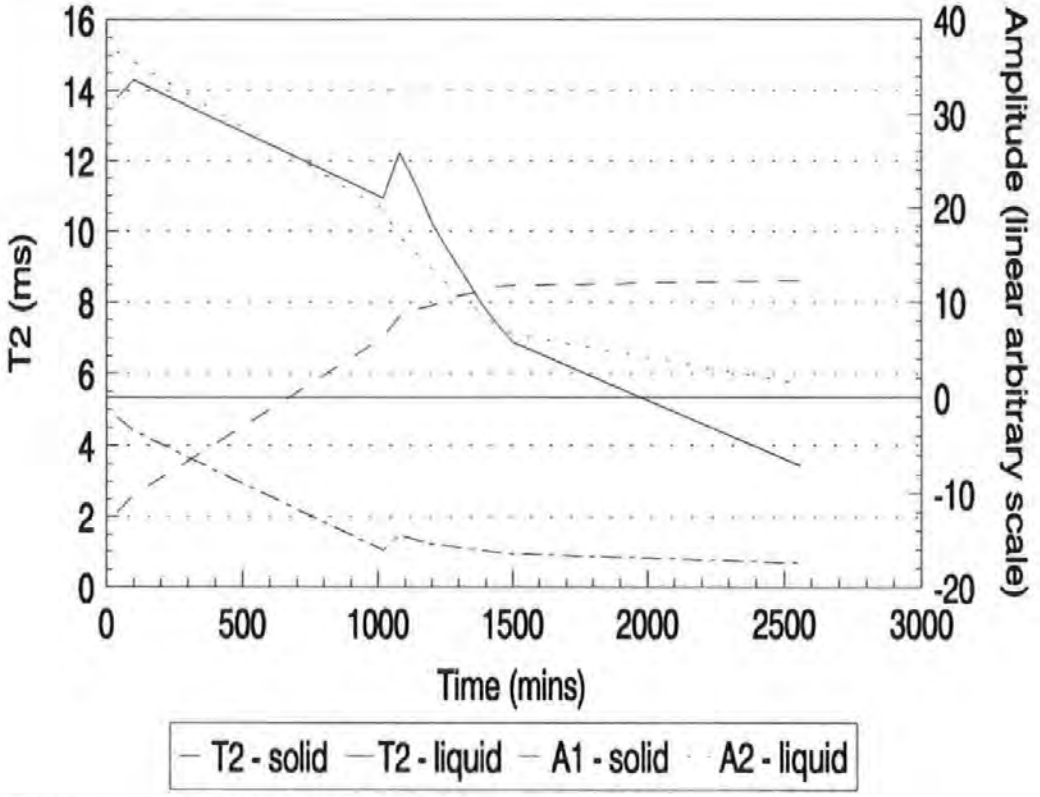

Calculated from Oxford QP - FID data

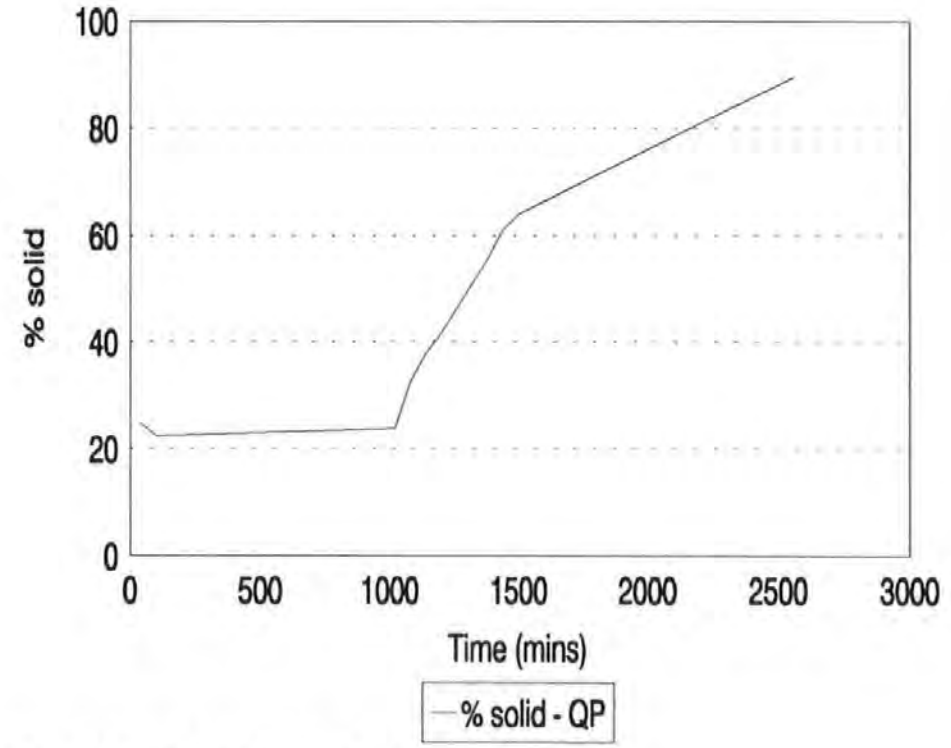

Calculated from Oxford QP - FID data

Figure A3.3. FID at 40°C with 22.8% V_f.

APPENDIX 4.0

4.1. Comparison of QP and VNC volume fraction experiments

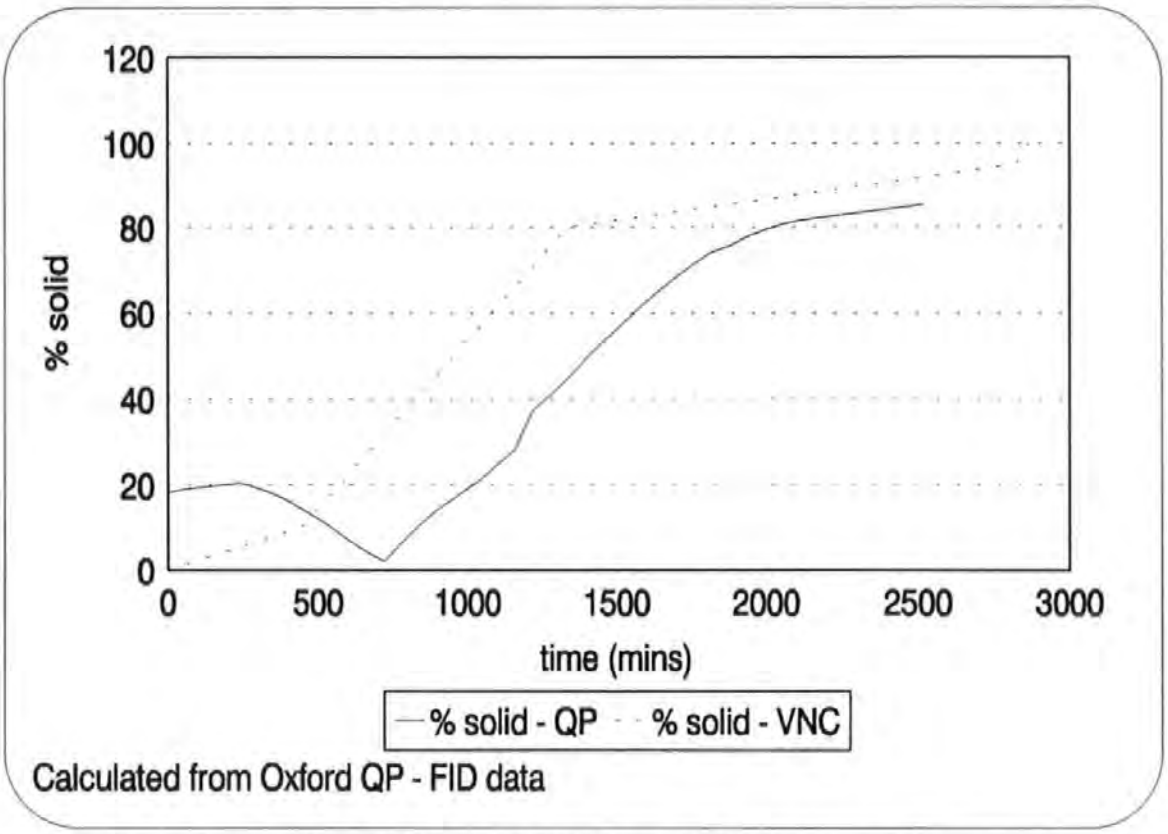

Figure A4.1. Comparison of QP and VNC data with 9.0% V_f at 40°C.

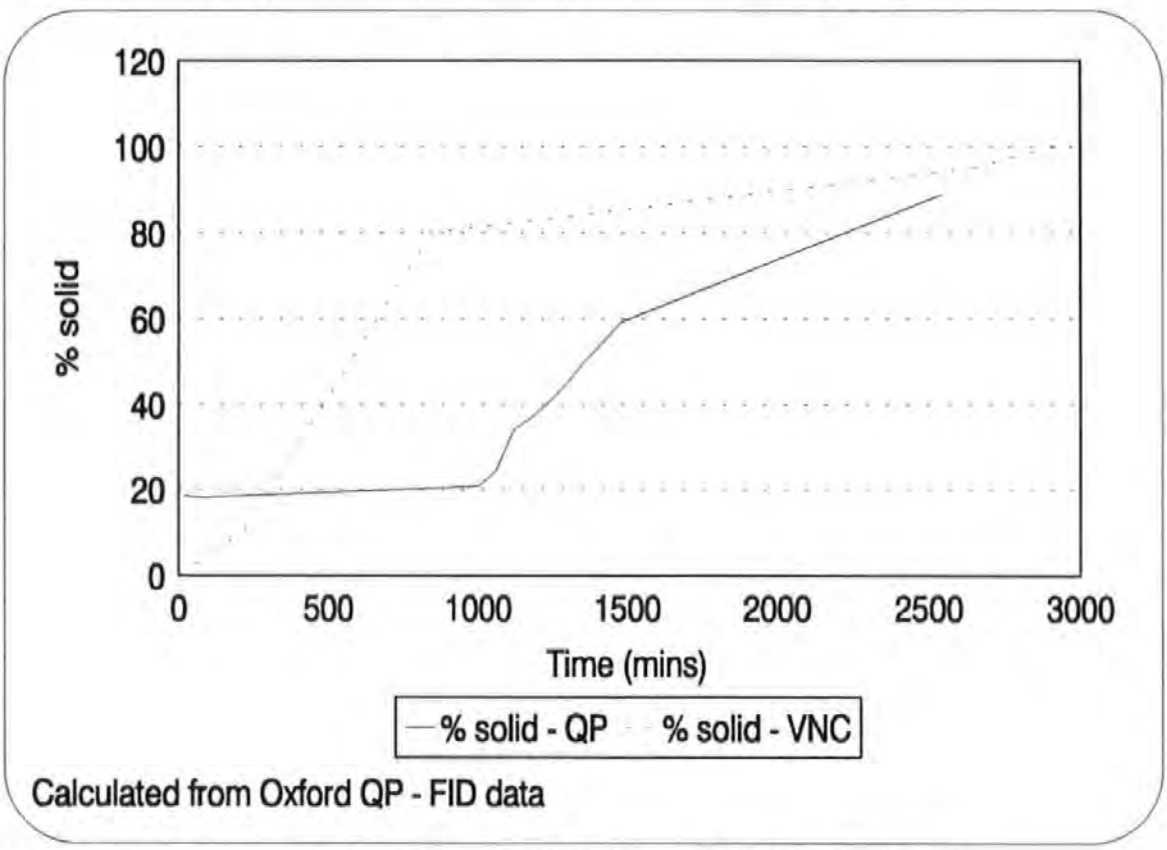

Figure A4.2. Comparison of QP and VNC data with 18.1% V_f at 40°C.

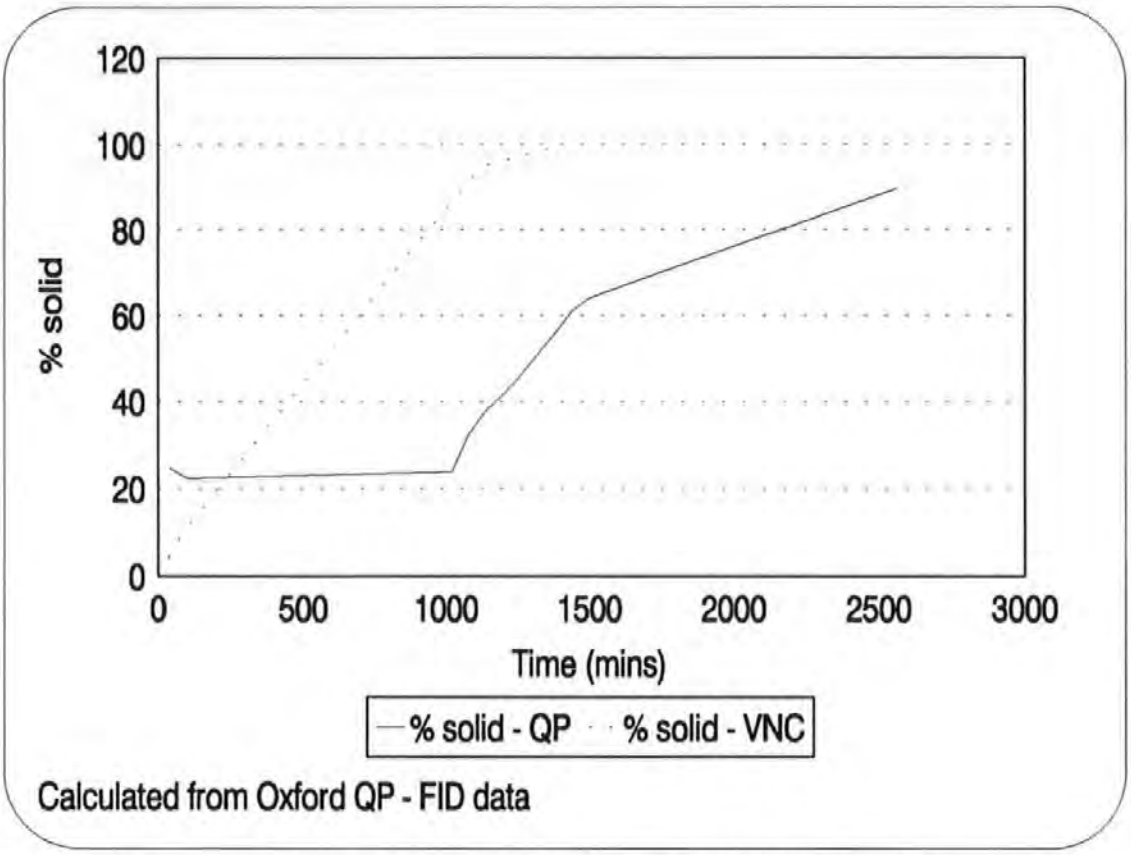

Figure A4.3. Comparison of QP and VNC data with 22.8% V_f at 40°C.

APPENDIX 5

INDUSTRIAL INSPECTION OF FIBRE-REINFORCED COMPOSITES

Angela L. Newbury
Advanced Composites Manufacturing Centre,
School of Manufacturing, Materials and Mechanical Engineering,
Polytechnic South West,
Plymouth. PL4 8AA.

Tel: 0752 232650
Fax: 0752 232293
Telex: 45423 pswas g

ABSTRACT

Fibre-reinforced composite materials are being used in an increasing number of applications but in common with other structural materials, they may suffer from some loss of integrity. Therefore non-destructive examination (NDE) techniques are being developed to cater for composite materials. Current attitudes in industry towards NDE techniques may limit the potential use of composites. This paper attempts to address the problem by use of a survey of industrial attitudes towards and the implementation of NDE techniques. It was found that there is no one NDE technique where the results can be reliably interpreted to establish the defect and its cause.

INTRODUCTION

Fibre-reinforced composite materials have highly attractive physical properties which justify the present rapid increase in applications in the aerospace and other industries.

However, composite materials suffer, like every structural material, from a failure to achieve their design properties which can arise from:

-defects or flaws initiated during production and revealed at the final quality inspection.

-local damage in-service, due to excess loading by mishap or from environmental hazards.

The present technology of non-destructive examination (NDE) enables a wide range of defects to be detected. However, the knowledge which would allow a decision on the type and extent of defects that can be accepted is scarce. What are the consequences on the load transfer capacity or on the continued resistance to the environment of the affected components [1].

Pipes [1] stated, "the present attitude to NDE techniques is to attempt to elude the problem by exercising a policy of severity, leading to discard or rejection of any suspected component, often far below the level of reasonable risk."

To ascertain whether this view of the use of NDE techniques within industry is current a survey was conducted of a small sample from shipbuilding, aerospace, automotive and general industries in the U.K., Europe and the U.S.A. A total of twenty one companies were approached and a seventy one percent response was obtained. The following section summarises the response.

TECHNICAL SURVEY

1. What NDE Techniques Do You Use With Regard To Fibre-Reinforced Plastic Composite Components

Shipbuilding

Ultrasonic - thickness measurement
Visual Inspection / Transmitted Light
- void / inclusion content
Cure Monitoring - Barcol hardness
Stiffness, Deflection Testing
Weight and Density Measurement

Aerospace and Space Systems
Military Aircraft

Computer Controlled C-scan Systems - water jet and immersion tanks
Manual Control A-scan
Radiographic Facility
Acoustic Flaw Detection
Ultrasonic Thru Transmission
Ultrasonic Pulse Echo
Thermal Imaging (I/red)

Helicopters

Radiographic Facilities
Acoustic Flaw Detector
A-scan and C-scan Ultrasonics

Civil Aircraft

Visual Inspection
Coin Tap Method
Ultrasonic Techniques

Automotive

Visual Inspection (translucent mouldings for detailed inspection)
Audio-sonic, manual
Ultrasonic High Resolution and Impedance Plane - portable scanning device

General

Natural Frequency
Real-Time Radiographic Examination

2. What Process Defects Are Investigated? (Please Give An Indication To The Size/Content Of Each Defect Which Is Used In An Accept/reject Criteria

Shipbuilding

Voids (3.18-6.35mm diam) or (>2% content)
Inclusions
Lay-up errors / thickness deficiencies (tolerance +0/-1 mm)
Glass / Resin Ratios
Excessive Exotherm Damage
Overall Dimensional Tolerances / Alignment
Shrinkage / Warpage and Any Associated Cracking
Uncured Resin

Aerospace
Military and Civil Aircraft

Wavy fibres
Disbonds (honeycomb sandwich >1 cell)
Delamination, caused by Retention of

Backing Film
Dry Fibres
Voids

Helicopters

Disbonds
Delaminations (4x4 mm^2)
Porosity
Resin / Moisture Content
Cracks

Automotive

Inclusions
Delaminations
Skin/Core Disbonds
Core Crushing
Migration (of moisture or reinforcement)
Under Cured Resin

General

All process and gross structural variations from control limits.

3. What In-Service Loads Are The Components Designed To Withstand? What Minimum Size/Content Of Defect(s) Would Cause A Highly Stressed Component To Fail

Shipbuilding

Shock
Buckling (panel stiffness)
Local Deflections
Small Circular Voids, Bolted Joints
Stress Riser of 4 or 5 i.e. Notch, Sharp Void or Load Transition
Folds In Laminate Plies

Aerospace
Military Aircraft

Fatigue
Environmental Degradation
Impact Resistance
Thermal Shock

Helicopters

Fatigue and Environmental Ageing - moisture uptake
Impact - bird strike
Lightning Strike

Civil Aircraft

Minor Impact Damage (depends on size, location, type of defects and stress level)

Automotive

Hot /Wet Factors

General

Environment, Moisture
Fatigue
Creep

4.Further Comments

Shipbuilding

Refer to standards as described in NES (Naval Engineering Standards) 140 and 701. "Any failures in shear are seen to be due to the difference in material expansion of the core. This is due to moisture or temperature and can create critical defects, flaws and stresses."

Aerospace

"Defect allowables will vary from project to project, however on highly stressed structures the NDE system / techniques used must be able to detect defects in the order of 4x4 mm's."

"The assessment of defect sizing varies with the NDE method applied. For instance X-ray will find minute traces of metallic inclusions but will not find delaminar defects of any size. Ultrasonic through transmission will detect dry areas and delamination with a reflective area of 12.7mm^2 and greater. Smaller areas of delamination can be revealed in solid composite sections by application of the ultrasonic through transmission equipment. The resolving of defects when applying the above techniques is (for an experienced technician) relatively easy, the difficulty comes in the interpretation. What type of defect do we have, compare dry fibres and delamination, the ultrasonic signal is the same. Experience and knowledge of the make-up of

the composite generally determines our interpretation of the defect type, and hence the cause".

"We believe that quite accurate assessment of discontinuities and their size / location is normal. It is often necessary to employ more than one technique to establish accurate size and location of these. Automatic systems are largely used to achieve recording of many data points in scanning modes. For good repeatability, data archives and post analysis is required."

Space Systems: "Composite materials are normally only permitted dry coupled NDE to prevent ingress of fluid that may cause delamination or disbonding on launch."

Helicopters: "...using ultrasonics as an example, a representative part will be manufactured containing artificial defects of the size stated by the consumer. This test standard will then be scanned and test parameters adjusted until the artificial defects are clearly resolved. Inspection of the component then takes place. This method of "mocking-up" the inspection area with artificial defects is often used in the aerospace industry and can be done for other NDE methods as well."

Civil: One company stated, "...damage that is not visible is acceptable. If any surface damage is noticed then ultrasonic inspection should be performed."

General

"...programme of work was carried out to investigate the process variables and structural faults. Frequency windows were then set to qualify the technique. A fast on-line process is required to monitor one tube every minute."

DISCUSSION

Non-destructive examination (NDE) techniques of fibre-reinforced plastic composites can range from a simple visual inspection to very elaborate techniques which, as has been stated, require interpretation by an experienced technician. No single technique can detect all defect forms. The cost of the equipment currently used varies considerably, from a few pounds for a simple technique to £100K plus for ultrasonics or radiography. The areas where NDE techniques are utilised the most are the aerospace and shipbuilding industries.

The process defects investigated include voids, delaminations, dimensional tolerances, uncured resin and dry fibres. Typical accept / reject criteria are of the type: voids of 3.18 - 6.35 mm diameter and or $\geq$ 2% content; thickness deficiencies of the type +0/-1 mm; honeycomb damage of one cell or more; delaminations of 4X4 mm's.

The in-service loads that the components are designed to withstand include: shock; buckling; deflections; fatigue; environmental degradation; impact damage.

From the comments made by industry it can be seen that the techniques used may be easy to apply but the difficulty arises in the interpretation. Dry fibres and delaminations look the same when using an ultrasound technique. It was also stated that it is not unusual to cut specimens up to determine defect types, the technique therefore is no longer non-destructive (however it could be useful if the component has already been rejected).

Ultrasonics is not a popular technique for certain applications since the ingress of fluid may cause delaminations or disbonds. Therefore this narrows down the range of techniques that can be used since it is often necessary to employ more than one technique to establish accurate size and location of defects.

CONCLUSION

An experienced person will be able to examine non-destructively a component using more than one technique to justify his decisions concerning the defect. However it may still be necessary to cut up the component to establish the true nature of the defect. Therefore, there is currently no one NDE technique where the results can be reliably interpreted to establish the defect and cause. If the company uses radiography and ultrasonics the cost can be 100K for each technique. In this case there is a potential market for an NDE technique that does not need an experienced technician to operate, that the results can be interpreted easily and reliably and that is of reasonable cost.

REFERENCES

1. R.B. Pipes (Ed),"NDE and Flaw Criticality for Composite Materials." ASTM STP 696, (1979)

ACKNOWLEDGEMENT

The author is grateful for the replies to questionnaires submitted by several companies.

REFERENCES

1. R. J. Shuford, T. J. Murray, Y. L. Hinton, R. H. Brockelman; "Advanced NDE Techniques for Composites"; Society of Manufacturing Engineers, EM85–113.
2. B. Fanconi, F. Wang, D. Hunston, F. Mopsik; "Cure Monitoring for Polymer Matrix Composites", Sagamore Army Research Materials Research Conference Proceedings, 31st. (1986).
3. S. N. Chatterjee, K. W. Buesking, B. W. Rosen, W. R. Scott; "Assessment of Defects in Laminated Composites", Review of PONDE, (1984), V4B, pp1189–1201.
4. S. Bishop; "The Significance of Defects on the Failure of Fibre Composites. (A review of Research in the United Kingdom)", Agard Report No. 690.
5. A. L. Newbury , J. Summerscales; "NMR for Non–Destructive Examination of Composites"; Third International Conference on Automated Composites. The Hague 15–17 October 1991. (Poster Presentation).
6. J. Summerscales; "NDT of Advanced Composites – an Overview of the Possibilities", British Journal of NDT, (1990), V32, n11, pp568–577.
7. W. Roye; "The Reliability of Nondestructive Techniques within the Field of Modern Composite Materials", British Journal of NDT, (1991), V33, n11, pp549–550.
8. J. H. Williams, Jnr, S. S. Lee; "Promising Quantitative NDE Techniques for Composite Materials", Materials Evaluation, (1985), V43, pp561–565.
9. P. Cawley; "Low Frequency NDT Techniques for the Detection of Disbonds and Delaminations", British Journal of NDT, (1990), V32, n9, pp454–461.
10. F. Chau, S. L. Toh, C. J. Tay, H. M. Shang; "Some Examples of Nondestructive Flaw Detection by Shear–ography", Journal of NDE (USA), (1989), V8, n4, pp225–234.
11. P. De Meester, M . G. Wevers; "Non–Destructive Techniques for Composites", 4th European Conference on NDT, pp98–117.
12. O. J. Lokberg, J. T. Malmo; "Detection of Defects in Composite Materials by T. V. Holography", NDT International, (1988), V21, n4, pp223–228.
13. J. Gotro, M. Yandrasits; "Simultaneous Dielectric and Dynamic Mechanical Analysis"; Polymer Engineering and Science, (1989), V29, n5, pp278–284.

14.W. W. Bidstrup, S. D. Senturia; "Monitoring the Cure of a Composite Matrix Resin with Micro-dielectrometry"; Polymer Engineering and Science, (1989), V29, n5, pp290- 294.

15.K.Scott; "The Vibrating Needle Curemeter. A Unique Instrument for Monitoring Cures"; Rapra Technology Ltd.

16.K.Scott; "Giving Good Vibrations. A New Examination of Viscosity"; Urethanes Technology, (1983), V5, n4, pp61-63.

17.R.F.Pryde; "Analysis of Composite Materials by DSC and DMTA"; ACMC Short Course Notes, December 10-12, (1990).

18.C. Gramelt, G. E. Owen, Jr; "Use of Thermal Analysis to Determine the Extent of Cure in Fibreglass Reinforced Plastics"; Society of Plastics Engineers, 44th Annual Technical Conference, (1986), V32, pp415-418.

19.A. L. Newbury; "Industrial Inspection of Fibre-Reinforced Composites"; Unpublished (1991). See appendix 5

20.R. B. Pipes; "Non-Destructive Examination and Flaw Criticallity for Composite Materials"; ASTM STP 696, (1979).

21.F. A. Bovey; "Nuclear Magnetic Resonance Spectroscopy"; Academic Press, (1988).

22.W. Kemp; "NMR in Chemistry. A Multinuclear Introduction"; Macmillan, (1986).

23.A. E. Derome; "Modern NMR Techniques for Chemistry Research"; Organic Chemistry Series, Perganon Press, (1990), V6.

24.J. Attard, L. Hall, N. Harrod, S. Duce; "Materials Mapped by NMR"; Physics World, (1991), V4, n7, pp41-45.

25.M. L. Martin, J. J. Delpeuch, G. J. Martin; "Practical NMR Spectroscopy"; Heyden and Son Ltd., (1980).

26.J. B. Miller, A. N. Garroway; "Multinuclear NMR Imaging of Solids"; Review of Progress in Quantitative NDE, (1989), V8A, pp567-574.

27.G. A. Matzkanin; "Applications of Spacially Localised NMR to Non-Destructive Examination"; 11th World Conference on NDT, (1985), V3. pp1607-1614.

28.P. Jackson, J. A. BArnes, N. A. Clayden, T. A. Carpenter, L. D. Hall, P. Jezzard; "Defect Detection in Carbon Fibre Composite Structures using Nuclear Magnetic Resonance"; Journal of Materials Science Letters, (1990), V9, pp1165-1168.

29.T. L. Weeding, W. S. Veeman, L. W. Jenneskens, H. Angad Guar, H. E. C. Schuurs, W. G. B. Huysmanns; "^{13}C and ^{29}Si NMR Investigations of Glass–Filled Polymer Composites"; Macromolecules, (1987), V22, pp706–714.

30.T. L. Weeding, W. S. Veeman, H. Angad Guar, W. G. B. Huysmanns; "Structural Investigations of Polyamide–6 and Polyamide–6 Composite using CP/MAS NMR"; Macromolecules, (1988), V21, n7, pp2028– 2032.

31.A.Cholli, A. M. Zaper, J. L. Koenig; "Applications of Solid–State Magic–Angle NMR Spectroscopy to Fibre–Reinforced Composites"; National ACS Meeting, (1983), pp215–216.

32.J. Summerscales, Ed; "Non–Destructive Testing of Fibre–Reinforced Plastic Composites"; Elesvier Applied Science, (1987), V1.

33.E. Koller, G. Dobmann, W. Kuhn; "Nondestructive Characteristics of Prepreg Ageing Using NMR Techniques", Res. Nondestructive Evaluation, (1990), V2, pp187–194.

34.R. F. Pryde; "Dielectric Analysis – Theory and Application"; ACMC Short Course Notes; 10–12 December, (1990).

35.R. E.Wetton, A. M. Rowe, M. R. Morton; "Epoxy Resin Cure Followed by DMTA and DETA Measurements"; 32nd International Sampe Symposium, April 6–9, V32, (1987).
pp1084–1091.

36.J. Gotro, M. Yandrasits; "Cure Monitoring using Dielectric and Dynamic Mechanical Analysis" Annual Technical Conference – Society of Plastics Engineers, (1987), pp1039–1042.

37.D. R. Day, D. D. Shepard; "Sensor Development for PMR15 Cure Monitoring and Control"; 32nd International SAMPE Symposium, April 6–9, (1987), V32, pp 1472–1479.

38.K. A. Nass, J. C. Seferis; "Analysis of the Dielectric Response of Thermosets During Isothermal Cure"; Polymer Engineering and Science, (1989), V29, n5, pp315–324.

39.S. A. Bidstrup, N. F. Sheppard, Jr., S. A. Senturia; "Dielectric Analysis of the Cure of Thermosetting Epoxy / Amine Systems"; Polymer Engineering and Science, (1989), V32, n5, pp325–328.

40.D. R. Day; "Dielectric Determination of Cure State During Non–Isothermal

Cure"; Polymer Engineering and Science, (1989), V32, n5, pp334–338.

41.J. W. Lane, R. K. Khattak, M. R. Dusi; "Evaluation of Dielectric Cure Models for an Epoxy–Amine Resin System"; Polymer Engineering and Science, (1989), V32, n5, pp339–346.

42.A. Vasudev, T. Wei Lee; "Thick Laminate Monitoring"; 35th International SAMPE Symposium, April 2–5, (1990), Bk 2, pp1265–1279.

43.M.Ungarish, R. Joseph, J. Vittoser, S. Kenig; "Cure Cycle Optimisation of Composites"; Israel Journal of Technology, (1988), V24, pp375–380.

44.D. E. Kranbuehl, S. E. Delos, M. S. Hoff, L. W. Weller, P. D. Haverty, J. A. Seeley, B. A.Whitham; "Monitoring Processing Properties of High Performance Thermo–plastics using Frequency Dependent Electromagnetic Sensing"; 32nd International SAMPE Symposium, April 6–9, (1987), V32, pp338–348.

45.D. E. Kranbuehl; "Electrical Methods of Characterising Cure Processes in Resins"; Dev. Reinf. Plast. 5: Process and Fabrication, (1986), V5, pp181–204.

46.N. Arrington; "Accoustic Emission and Acousto–Ultrasonics as Methods of Monitoring Composite Manufacture"; ACMC Short Course Notes, December 10–12, (1990).

47.S. A. Saliba, T. E. Saliba, J. F. Lanzafame; "Aoustic Monitoring of Composite Materials During the Cure Cycle"; 34th International SAMPE Symposium, May 8–11, (1989), pp397–406.

48.J. A. Sezna; "Correlation of Results from Different Designs"; Rubber World, (1992), V205, n4, pp21–27.

49.K. Scott; "Polyurethane Applications for the Vibrating Needle Curemeter"; Rubber World, (1990), V202, n6, pp19–22.

50.A. Davies, M.Ohn, K. Liu, R. Measures; "A Study of an Opto–Ultrasonic Technique for Cure Monitoring"; SPIE (1991), V1588, Fibre Optic Smart Structures and Skins IV, pp264–274.

51.K. Liu, A. Davies, M. Ohn, B. Park, R. Measures; "Embedded Optical Fibre Sensors for Damage Detection and Cure Monitoring;" ADPA / AIAA / SPIE, (1991), Active Materials and Adaptive Structures, pp395–398.

52.R. L. Levey, S. D. Schwab; "Monitoring the Composite Curing Process with a Fluorescence– Based Fibre–Optic Sensor"; 47th Annual Technical Conference – Society of Plastics Engineers, (1989), pp1530–1533.

53.F. W. Wang, R. E. Lowry, B. M. Fanconi; "Novel Fluorescence Method for Cure Monitoring of Epoxy Resins"; Polymer, (1986), V27, n10, pp1529–1532.

54.A. Stroeks, M. Shmorhun, A. M. Jamieson, R. Simha; "Cure Monitoring of Epoxy Resins by Excimer Fluorescence"; Polymer, (1988), V29, n3, pp467–470.

55.R. J. Shuford, T. J. Murray, Jr., M. T. Bostic, R. H. Brockelman, Y. L. Hinton; "Evaluation of NDE Techniques for Detecting Moisture in Composites"; 11th World Conference on NDT, (1985), V2. pp1366 –1373

56.G. A. Matzkanin; "Applications of NMR to the Non–Destructive Examination of Composites", 14th Symposium on NDE Applications, (1983) pp270–286.

57.G. A. Matzkanin; "NDE of Composites Using Pulsed NMR"; Society of Plastics Engineers, 45th Annual Technical Conference, (1987), pp1060–1063.

58.G. A. Matzkanin; "Investigation of the Effect of Moisture on the Mechanical Properties of Organic Matrix Composite Material Using Nuclear Magnetic Resonance"; SWR1–15–5607–807, USAARADOM–TR–81–F–5, AD A100 426.

59.P. Jackson, N. J. Clayden, J. A. Barnes, T. A. Carpenter, L. D. Hall, P. Jezzard; "New Analytical Techniques for Advanced Polymer Composites"; Proceedings of 12th International European Chapter Conference of SAMPE, Maastricht, The Netherlands, MAy 28–30, (1991).

60.P. Jezzard, T. A. Carpenter, L. D. Hall, P. Jackson, N. J. Clayden; "Simple NMR Imaging of Solid Polymers at Elevated Temperatures"; Polymer Communications, (1991), V32, n3, pp74–76.

61.F. De Luca; "Magic–Angle NMR Imaging"; Journal of Magnetic Resonance, (1986), V67, pp169–172.

62.D. G. Cory, A. M. Reichwein, J. W. Van Os, W. S. Veeman; "NMR Images of Rotating Solids"; Journal of Magnetic Resonance, (1988), V67, pp543–547.

63.A. N. Garroway, J. Baum, M. G. Munowitz, A. Pines; "NMR Imaging by Multiple–Quantum Resonance"; Journal of Magnetic Resonance, (1984), V60, pp337–341.

64.J. B. Miller, A. N. Garroway; "NMR Imaging of Solids with a Surface Coil"; Journal of Magnetic Resonance, (1988), V77, pp187–191.

65.T. A. Carpenter, L. D. HAll. P. Jezzard; "Proton Magnetic Resonance Imaging of Solid Polymers Using Instrumentatiôn Designed for the Liquid State";

Journal of Magnetic Resonance , (1989), V84, pp383–387.

66.J. K.Saunders; "Modern NMR Spectroscopy. A Guide for Chemists"; Oxford University Press. (1987).

67.R. L. Ward, J. A. Happe, J. W. Pyper; "Bound and Free Moisture Studies of Solid Materials by FT–NMR"; Proceedings of 1985 Symposium on Moisture and Humidity, Washington D.C., April 15–18, (!985).

68.I. G. Matis, G. M. Kerch, A. N. Aniskevich; "Investigation of the State of Water Sorbed by an Organic Polymer by High–Resolution ^{1}H NMR and Differential Thermal Analysis"; Mech. Compos. Mater. (USA), (1990), V26, n2, pp259–262.

69.N. K. Batra, T. P. Graham; "Measurement of moisture in Hydrothermally Degraded Fibre–Reinforced Epoxy Composites by Continuous Wave (CW) NMR"; British Journal of NDT, (1983), V25, n1, pp21–23.

70.E. Jeong, M. S. Conradi, K. Cueman, L. J. Thomas, III; "NMR as a Probe of Absorbed Water in Graphite–Reinforced Plastic"; Review of Progress in Quantitative Non–Destructive Evaluation, (1990), V9B, pp1449–1455.

71.D. L. Tzou, P. Desai, A. S. Abhiraman, T–H Huang; "NMR Studies of Structural Development of High–Speed Melt–Spun Poly(Ethylene Terephthalate) Fibres"; Journal of Polymer Science, PtB: Polymer Physics, (1991), V9, pp49–56.

72.L. W. Jelinski, J. J. Dumais, A. K. Engel; "Solid–State NMR Studies of Molecular Motions in Polymers"; Annual Technical Conference – Society of Plastics Engineers, 41st Antec 1983.

73.Ye. R. Gavilova, N. P. Kotelyanets, E. T. Lippmaa, M. Ya. Magi, L. S. Semenova, V. A. Shevelev; "NMR Study of the Phase Structure and Relaxational Properties of Epoxide Composites"; Polymer Science USSR, (1987), V29, n6, pp1301–1310.

74.P. Jackson; "Curing of Carbon–Fibre Reinforced Epoxy Resin; Non–Invasive Viscosity Measurements by NMR Imaging"; Journal of Materials Science, (1992), V27, pp1302–1306.

75.P. Jackson, N. J. Clayden, N. J. Walton, T. A. Carpenter, L. D. Hall, P. Jezzard; "Magnetic Resonance Imaging Studies of the Polymerisation of Methyl–methacrylate"; Polymer International, (1991), V24, pp139–143.

76.P. Jackson, N. J. Clayden, J. A. Barnes, T. A. Carpenter, L. D. Hall, P. Jezzard; "New Analytical Techniques for Advanced Polymer Composites"; 12th

International European Chapter Conference of SAMPE, Maastricht, The Netherlands, May 28–30., (1991), pp277–288.

77.J. F. Haw, N. A. Johnson; "In–Situ Curing Study of an Epoxy Resin using NMR with MAS"; Analytical Chemistry, (1986), V58, pp3254–3256.

78.A. Charlesby; "The Determination of Crosslinking by NMR Spectroscopy"; PRI London Section Conference , (1982).

79.K. Bergmann, K. Demmler; "An Investigation of the Hardening Process in Unsaturated Polyester Resins with the Aid of NMR Measurements"; Colloid and Polymer Science, (1974), V252, n3, pp193–206.

80.M. J. Lizak; "Applications of NMR to NDE Advanced Materials"; PhD Thesis, Washington University, USA, (1991).

81. J. H. Strange; "Echoes and Imaging in Solids"; Phil Trans R. Soc. Lond. A., (1990), V333, pp427–439.

82.BS2782, Pt10, Method 1001, (1977), EN99.

83.W. Harper; "Statistics;" Pitman Publishing, sixth edition, (1991)

84.P. Bevington; "Data Reduction and Error Analysis for the Physical Sciences;" McGraw–Hill Book Company, (1969).

85.C. May, Y. Tanaka, Ed.; "Epoxy Resin: Chemistry and Technology", Marcel Dekker Inc., (1973)

86.K. J. Saunders; "Organic Polymer Chemistry"; Chapman and Hall, (1973).

87.F. Billmeyer, Jnr; "Textbook of Polymer Science", John Wiley and Sons, (1984).

88.W. Kemp; "Organic Spectroscopy"; Macmillan Press Ltd., (1979).

89.W. P. Rothwell et al; Journal of Chemistry and Physics, (1981), V74, pp2721–2732.

90.A. C. Lind; "NMR NDE of Composite Materials" April 1991, McDonnell Douglas Research Labs. Research Report

91.P. Jezzard, C. J. Wiggins, T. A. Carpenter, L. D. Hall, J. A. Barnes, P. Jackson, N. J. Clayden; "Demonstration of Nuclear Magnetic Resonance Imaging for Void Detection in Carbon–Fibre Reinforced Polymer Composites, and Comparison with Ultra–sound Methods" Journal of Materials Science, (1992), V27, pp6365–6370.

92.K. Lui, A. Davies, M. M. Ohn, B. Park, R. M. Measures; "Embedded Optical Fibre Sensors for Damage Detection and Cure Monitoring", ADPA/AIAA/ ASME

/SPIE Conference on Active Materials, November 1991, pp395–398.

93.P. Peyser, W. D. Bascom; "Kinetics of Epoxy Resin Polymerisation using DSC," Journal of Applied Polymer Science, *1977), V21, pp2359–2373.

94.R. Freeman; "A Handbook of NMR,"Longman Scientific and Technical (1988).

95.S. Homans; "A Dictionary of Concepts in NMR," Oxford Science Publications, (1992).

96.ASTM 2583; "Indentation Hardness of Rigid Plastics," (1981).